

Helwan University
Faculty of Engineering
Mataria - Cairo

Engineering Research Journal

(ISSN 1110-5615)

VOLUME 123

SEPTEMBER 2009

1917
No. 1000
1000

1000

1000

1000

1000

1000

Engineering Research Journal

Volume 123 September 2009

AIMS AND SCOPE

Engineering Research Journal

Is a journal devoted to the publication of research & scientific papers in all fields of and engineering related subjects in English and Arabic Language. Articles are refereed before publication.

Contributions those wishing to submit articles for publication should send three copies and a soft copy to Editor or Assistant Editor. Electronic submissions are acceptable via erj@helwan.edu.eg

Contributors should refer to the guide for authors on the inside back cover.

Engineering Research journal was established in 1985 by the Faculty of Engineering –Mataria-Helwan University.

Editor

Prof. Samir El Demerdash

Dean

Faculty of Engineering-mataria

Helwan University

E-mail samir_aldemerdash@m-eng.helwan.edu.eg

Assistant Editor

Prof. Haniaa Hamdy

Vice Dean,

Faculty of Engineering-mataria

Helwan University,

E-mail haniahamdy@helwan.edu.eg

EDITORIAL BOARD

Prof. Samira EL-Sherif, Head of Department of Mechanical Power Engineering.

Faculty of Engineering-Mataria

Helwan University,

Prof. Alaa Mohamed Ahmed El-Butch, Head of Department of Mechanical Design Engineering,

Faculty of Engineering-Mataria

Helwan University,

Prof. Randa Kamel, Head of Department of Architectural Engineering.

Faculty of Engineering-Mataria

Helwan University,

Prof. Alaa El-Din Ali El-Gendi, Head of Department of Civil Engineering

Faculty of Engineering-Mataria

Helwan University,

Prof. Randa Kamel, Head of Department of Architectural Engineering.

Faculty of Engineering-Mataria

Helwan University,

Associate Prof. Inas M. Bakr, Head of Department of Physics and Engineering Mathematics

Faculty of Engineering-Mataria

Helwan University,

Associate Prof. Ahmed Abu El-Yazeed Abed El-Hammed, Head of Department of Automotive Engineering

Faculty of Engineering-Mataria

Helwan University.

Editorial Assistance

Mrs. Nivin lotfi

The Engineering Research Journal is published by the Faculty of Engineering-Mataria-Helwan University-Masakin El Helmia

11 718 Cairo-Egypt Tel/Fax 20226333813-202632398 E-mail: erj@helwan.edu.eg



Detailed Instructions for Authors

The submitted paper should not have been submitted earlier or at the same time to any other journal in Egypt or abroad.

For multi-author papers, the corresponding author must affirm that all of the authors have read and approved the manuscript.

Those wishing to submit articles for publication should send three copies and a soft copy that must be consistent to the Editor or Assistant Editor. Electronic communications are welcomed via erj@helwan.edu.eg

Paper Format

- Page standard size A4 .High-contrast laser printed, typewritten, or photocopied on white paper. Single-sided printing only
- Maximum 12 pages (each extra page up to 25 pages will be charged additional fees).
- Margins: All the margins except the first page are 3.0 cm from the top and bottom and 2.5 cm from the right and left. The first page should have a 5 cm margin from the top.
- Text in Times New Roman 14 pt
- The text should be flushed to the right and left margins

Spacing, and Indentation: Double space throughout the manuscript with no indentation. Single spacing can be used for table titles and headings, figure captions, references, footnotes, and long quotations and for the final manuscript.

Title of paper: Centered Times New Roman 18 pt bold, upper and lower case.

Author's Names: Times New Roman 14 pt bold, upper and lower case. First name, middle initials, followed by last name

Authors' Affiliation: Arial 12 pt italic, upper and lower case

Structure: Article title, Author, Affiliation, Abstract, Keywords, Main Text, Acknowledgments, Appendices, References, Figure Captions, Tables.

Abstract: An abstract, not to exceed 350 words, is required.

Corresponding author: The name, postal address, telephone and fax number and the E mail of the corresponding author should be shown on the first page of the manuscript.

Number tables: consecutively as they appear in the text, using only whole numbers

Appendices: Label each appendix and give it a title.

For annual subscription or purchase of single copies please contact the assistant editor of the Journal

The Engineering Research Journal is published by The Faculty of Engineering-Mataria -Helwan University - Masakin El Helmia 11718 Cairo -Egypt Tel /Fax 202 26333813- 202 26332398 e-mail :erj@helwan.edu.eg



CIVIL ENGINEERING

- Estimation of Evaporation Losses from Lake Nasser
Using Remote Sensing and GIS Raster Calculator Model
Hala M. Ebaid C1-C14
- The Effect of Expanded Perlite Aggregate/Powder
on the Mechanical Properties of Concrete
Assistant Prof. Esraa Emam Ali,
Assistant Prof. Islam M. Elhabbal C15-C28

MECHANICAL ENGINEERING

- Optimization of the Drilling Cycle on Conventional
and CNC Machine Tools M1-M19
Part I- Formulation of the Optimization Model
for the Drilling Cycle
Prof. Dr. Mohamed A. El Hakim,
Dr. Wael S. Moughith & Engineer Ahmed S. Abd-Allah
- Optimization of the Drilling Cycle on Conventional
and CNC Machine Tools M20-M31
Part II - Experimental Verification of the Optimization Model
Prof. Dr. Mohamed A. El Hakim,
Dr. Wael S. Moughith & Engineer Ahmed S. Abd-Allah
- Static and Dynamic testing of Simple Structures
Produced by Rapid Prototyping Technique M32-M45
Prof. Dr. Mohamed A. El Hakim,
Dr. Atef A. Afifi & Engineer Hany F. Mokbel
- Investigation of Machine Tool Structures Behavior
Using Rapid Prototyping Models M46-M60
Prof. Dr. Mohamed A. El Hakim,
Dr. Atef A. Afifi & Engineer Hany F. Mokbel

An Experimental Investigation of the Effect
of Magnetic Fuel Treatment on SI Engine Performance
Ahmed A. Abdel-Rehim
Ramadan Abdel-Aziz, Khairy H. El-Naga
Hamdy H. Maarouf

M61-M76

PHYSICS AND ENGINEERING MATHEMATICS

Mathematical Models Simulate Scour Depth under Effect
of Gate Operating Systems [a Comparison Study]
Abdelmoez. M. Hesham and Mohamed A. Nassar

P1-P20

ARCHITECTURE ENGINEERING

Materiality in Architecture A Study on the Transformation
In the Meanings of Materials
Gabr, M., Amin, A., EL-Fiki, S. & Kattaria, T.

A1-A16

Exploring Green Architecture through Eras
Dr Zeinab El Razaz

A17-A52

نحو إعداد منظومة متكاملة لمعايير قياس التدهور في المناطق والأحياء السكنية
هايدي أحمد شلبي

AA1-AA20



ESTIMATION OF EVAPORATION LOSSES FROM LAKE NASSER USING REMOTE SENSING AND GIS RASTER CALCULATOR MODEL

Hala M. Ebaid

*Researcher, Survey Research Institute, National Water Research Center,
E-Mail:hala_sri@yahoo.com*

ABSTRACT

Remote sensing and GIS technologies with aerodynamic principles have been integrated to estimate evaporation from Lake Nasser. The Moderate Resolution Imaging Spectroradiometer (MODIS), onboard the NASA Terra Earth Observing Satellites images have been used for surface temperature determining, specifically MOD11_L2, Land surface temperature (LST) image. Also a GIS Raster Calculator model technique for processing the raster data, which applied Aerodynamic equations on 4 LST MODIS images, was used for evaporation calculation. Applying and rerunning the model on the four MODIS images showed that the evaporation rate varies from one month to the other throughout the lake, thus ranging from 5-8 mm/day in February, 9-15 mm/day in May, 17-26 mm/day in August, and 9-12 mm/day in October. As for the evaporation values that represented the 4 seasons of this same year i.e. winter, spring, autumn, summer were 1.50, 2.67, 2.86 and 4.75 billion cubic meter respectively. Hence this summed up value of 11.78 billion cubic meter per year, obtained by applying this technique was slightly higher as compared to that obtained in the year 2005(10.58 billion cubic meter), using pan evaporation method. Evaporation using satellite imagery data, GIS model, and applying Aerodynamic principle could be a promising and reliable technique which is easy to handle and capable for aiding decision making.

KEYWORDS: Remote sensing, MODIS, Raster Calculator model, lake Nasser

1. INTRODUCTION

Lake Nasser is the second largest man-made lake in the world, extending from the southern part of Egypt to the northern part of Sudan, about 500 km length, and 6000 km² surface area. The level of water oscillates between 147 to 182 meter above the sea level during a year, and from year to year. It is, the water bank of Egypt, contains about 162 billion cubic meters from fresh and renewable water. The lake is surrounded by empty flat desert where the nominal annual insolation is more than 2500 kWh/m². The water loss from the lake is one of the national problems. The evaporated water loss ranges between 10 to 16 billion cubic meter every year, which is equivalent to 20 to 30% of the Egyptian income from Nile water [1].

Many theories and formulas have been developed to obtain accurate estimates of lake evaporation. Common equations describing evaporation are the Penman, Hargreave's, and Hamon's equations. Although these methods are simple, still yet less accurate results are obtained [2]. Later, [1] used Meteosat infra-red window (10.5 – 12.5 μm) observations and the empirical models, estimated the evaporated water every day and determined the yearly water loss from the integration of daily values. Nevertheless the Bulk-Aerodynamic Method that utilizes the skin temperature of water, relative humidity, wind speed, and air temperature to estimate evaporation, from Aster images of Elephant Reservoir in New Mexico was carried out by [3] and that method shows different temperature of 1.7° Celsius, and about 1.2426 mm/day evaporation rate difference, between Aster image and measured value at certain point in December through the elephant lake which is considered as a good result. From that, one can say that remote sensing shows promising results.

The objective of this present study is to calculate evaporation loss from lake Nasser using MODIS Satellite image, and GIS spatial analyst model to process surface temperature image values of the lake by applying Bulk aerodynamic principle and automatically calculate evaporation rate per day and the yearly water loss from the integration of daily values using a chain group of raster calculator tools. By this

way advantages in use of satellite thermal data and GIS spatial model for evaporation calculation are gained.

2. METHODOLOGY

The research in this paper developed a remote sensing and GIS model to estimate evaporation loss from Lake Nasser. The model uses the energy balance principle (Aerodynamic equation) which utilizes the skin temperature of water data to measure evaporation depth (mm/day) and water loss in billion cubic meters per year. The evaporation depth has a moderate spatial resolution (1000 m by 1000 m). The model is developed in GIS spatial analyst model builder environment, and process 4 MODIS satellite images as representation for all year surface temperature (Mod11_L2 LST raster data), besides utilizing the weather stations data (Air temperature, wind speed, and humidity). The model first calibrates digital image data using raster calculator tool to obtain LST in C° and after that utilized Aerodynamic equations on LST Raster data with all necessary meteorological parameters and finally calculate evaporation rate in mm/day and then integrate daily values to get the yearly water loss, and rerun the model four times for the four months, and then calculate total evaporation in billion m³/year.

3. STUDY AREA

Lake Nasser is extending from the southern part of Egypt to the northeast part of Sudan and the research area of interest of the lake cover Egypt only. Lake Nasser area (Fig.1) extends along the eastern desert. Its length is about 500 kilometers, its maximum width is 35 kilometers. The total area surveyed is approximately 50,000 feddans. In general the geographic boundary area lies between latitude 21° and 24° 30' north and longitude 31° 30' and 33° east.

4. DATA AND APPROACHES

4.1 Satellites Data:

MOD11_L2 are stored in the Hierarchical Data Format "HDF-EOS". In each product file, the parameters are written as science Data Sets "SDS". The parameter LST are scaled to integer to reduce file size, the scale and offset values are provided as SDS attributes to convert back to actual data value, the following equation are used to convert stored values back to actual data:

Data values (calibrated) = scale factor* (stored numbers-offset)

MOD11_L2 is retrieved using a generalized split-window algorithm by MODIS land team [4]. Meteorological, hydrological, and agricultural research communities require an accuracy of 0.5-2 °C for LST retrieved from satellite observations at 1-10 km spatial resolution [5], and MOD11_L2 products have been validated in previous studies and reported to be 1°C.

In this research four scenes of MODIS images are obtained as shown in Fig.1, from MODIS products through [6] via search tool.

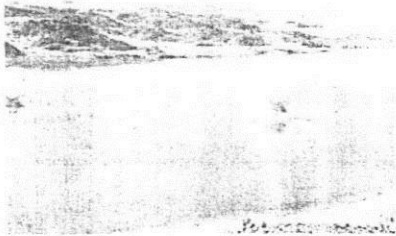


Fig. 1. Photo image for part of Lake Nasser & MOD11_L2 (LST raw data, Aug. /2006).

Table 1. Satellite images information

Image type	Acquired date	Cloud percentage	Time/DAY	Scale factor/Offset	Spatial/Temporal resolution
MOD11_L2.5	22 -2-2006	Less than 5%	9 am /D	0.02/0.0	1km at nadir /5 min.
MOD11_L2.5	6 -5- 2006	Less than 17%	9 am /D	0.02/0.0	1km /5 min.
MOD11_L2.5	4 -8-2006	Less than 10%	9 am /D	0.02/0.0	1km at /5 min.
MOD11_L2.5	6 -10-2006	Less than 4%	9 am /D	0.02/0.0	1km at /5 min.

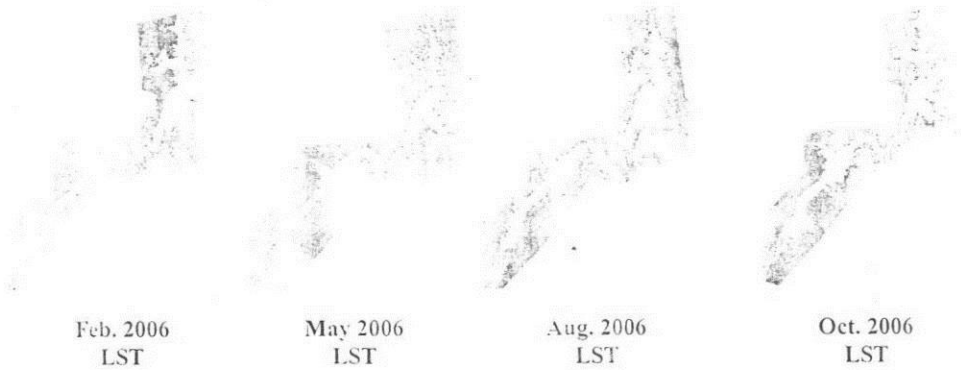


Fig. 2. MOD11_L2 (Raster LST after mask extraction process for different months)

4.2 Meteorological Stations Data

The stations are distributed and centered on the middle part of the lake as seen in Fig. 3. Average calculations per month have been made for the meteorological parameters of the stations that are utilized in the Aerodynamic equations, and have been tabulated as follows.

Table 2. Local station parameters around the lake

Date	Average air temperature (C Deg)	Average Wind speed (m/s)	Average Relative Humidity (%)	Average BP (mbar)
2-2006	21.09	3.16	31.24	922.69
5-2006	31.38	3.53	19.02	928.93
8-2006	36.06	3.80	17.75	917.45
10-2006	28.64	3.27	28.27	928.45

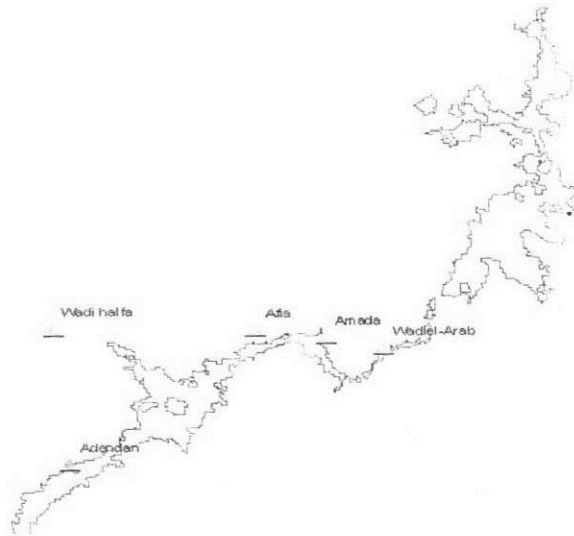


Fig. 3. Meteorological stations distribution around lake Nasser

**4.3 Applied Evaporation Method
Aerodynamic Equations:**

$$E = K_E U (e_s - e_a) (86.4 * 10^6) \tag{1}$$

$$e = e_s (R_{fj}) / (100) \tag{2}$$

Where K_E is determined as follows:

$$K_E = \frac{0.622 \rho_a \times (0.4)^2}{P \rho_w \left[\ln \left(\frac{z_m - z_d}{z_0} \right) \right]^2} \quad (3)$$

Saturation vapor pressure, e_s , of the air is a property that is dependent on temperature and was estimated by polynomial function [7]. Water surface temperature or "skin" temperature was used to determine the saturation vapor pressure at the water surface. Vapor pressure of the air was determined by multiplying relative humidity with saturated vapor pressure. In this case, saturated vapor pressure of air was determined by using the air temperature (all parameters are defined in the list of symbols paragraph).

$$e = \frac{a_0 + T(a_1 + T(a_2 + T(a_3 + T(a_4 + T(a_5 + a_6 T))))))}{10} \quad (4)$$

5. PROCESSING WORK FLOW

1- The MODIS satellite raster data are produced in HDF format which cannot be used in GIS environment so it needs a conversion tool to convert the HDF format to GIS format (Geo_TIFF) in order to process the data. The HDF-EOS to GeoTIFF Conversion tool (HEG) can be provided from the internet for free, and it needs special installation instruction to work. It has a graphical user interface, Fig. 4, which uses Java Swing technology. The main purposes of this tool are:

- a- Create files that are more useful and informative (GeoTIFF format).
- b- Reproject the image to UTM - WGS 84 projection .

The HEG tool works specifically on HDF-EOS Swath and Grid objects.

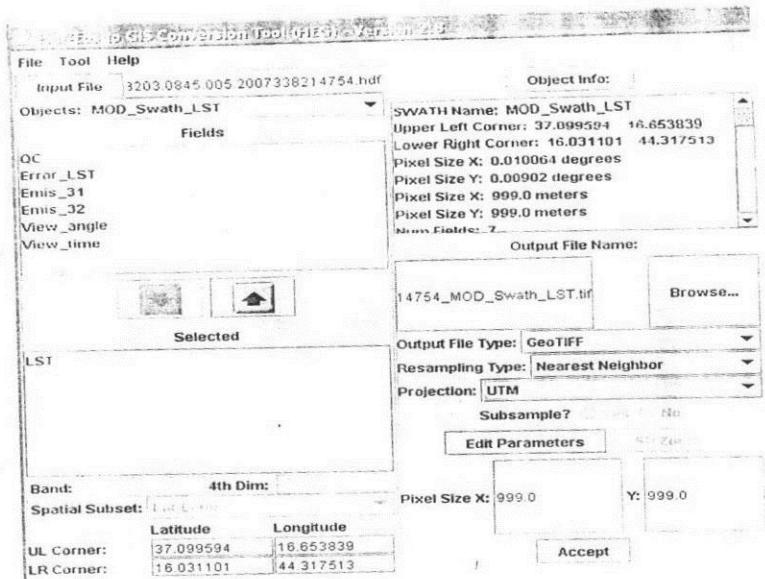


Fig.4. GUI of the HDF-EOS to GeoTIFF conversion tool (HEG).

2- Digitizing vector layers for the four raster LST scenes (August_LST, February_LST, May_LST, October_LST) which are needed for the evaporation calculation for the lake area as shown in Fig. 5.

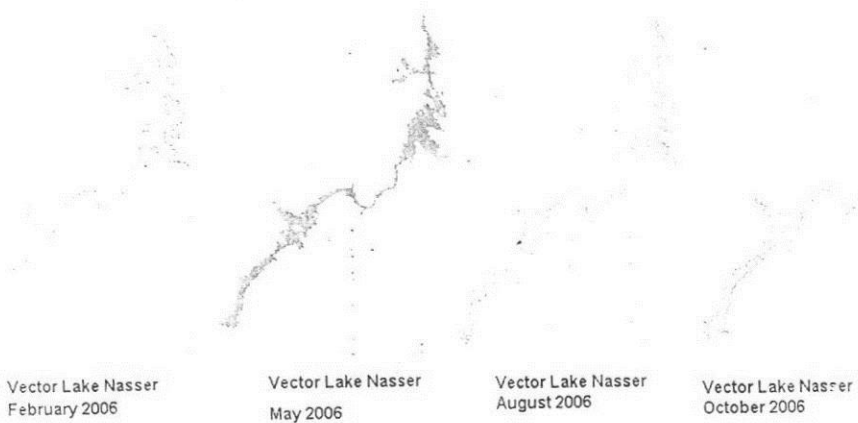


Fig. 5. Four polygons for Lake Nasser digitized from MOD LST images.

3- Preparing logical flow diagram of the GIS model, which utilizes Aerodynamic method on MOD_LST raster data that calibrate and manipulate Lake Nasser raster data from row data stage until yearly evaporated loss calculation stage.

4- Running every Raster Calculator tool inside the model builder individually to check the performance and the output raster data see Fig. 6.

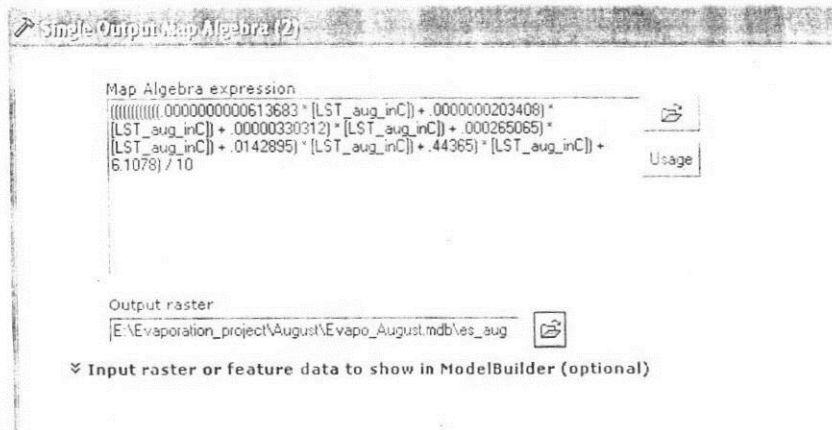


Fig. 6. Applying equation in raster calculator tool.

5- Running the spatial analyst model as one operation as shown in Fig. 7, taking into consideration that the model should be interactive, enabling decision-makers to modify the parameters and data used, and can be re-run to evaluate the new evaporation rate results regarding different months and different meteorological stations data . The entire Evaporation model runs in 3-6 minutes depending on the speed of the processor and tool complexity.

6. RESULTS AND DISCUSSIONS

From the research work the resulted approximated evaporation losses per year was 11.788 billion m³/year in 2006 which resulted by integrating the 4 season's evaporation values, the yearly evaporated losses was calculated as follows:

1-Multiply the resulted evaporation rate (which resulted by applied evaporation method Aerodynamic equations) by factor to change mm/day to m³/month (for specific season).

2- Multiply the above resulted value by Lake Nasser's specific area for specific month (lake Nasser's area change from month to month) and finally get the season losses m³/3 months (season) and integrate the 4 seasons losses to get the yearly value and this value is considered as approximated value and may be slightly bigger than the value calculated by pan method in year 2006 for the previous mention approximation. The model results for the 4 months are indicated in Table 3.

Table 3. Evaporation rate results

Month-year	Range of evaporation rate in mm/day	Evaporation in m ³ /month
5-2006	9-15	892307021
8-2006	17-26	1582514569
10-2006	9-12	953955836
2-2006	5-8	500636267.7
Evaporation/year = 11.788 billion m ³ /year		

Some aspects have been considered when calculating the evaporation for Lake Nasser:

- There are many assumptions that go into these calculations ,i.e. the wind speed used is assumed to be constant throughout the lake, which it is not, and consider wind speed at 2 m above the lake water surface which may be slight different.

- Also, we apply the monthly average value for air temperature, and relative humidity (%) which is derived from weather stations around the lake, and that is for simplicity but we have to consider the variation of air temperature and relative humidity for all day time for all month, which means that the measured bulk-aerodynamic method had many measured points at different times of the day, while MODIS image used was at only one time. Also the geographic distribution of meteorological stations, which lies on the lake center is fitting for the parameters average calculations
- Another approximation is the calculation of evaporation loss per year depends only on 4 months which represent the four seasons (spring, summer, autumn, winter) and multiply evaporation loss per specific month by 3 to get the evaporation rate per season and integrate the results of four seasons evaporation to get the evaporation loss per year.
- For Evaporation calculation for Lake Nasser area, we need to determine the exact pixels which cover the lake for digitizing for accurate processing work, and this is difficult due to: 1) low spatial resolution and 2) shortage information about local surface temperature through the lake for evaluation purpose, and this issue can be solved by careful digitizing for all closed tone colors of the pixels carrying the LST digital values as indicated in Fig. 8., depending on the fact say that the surface temperature through the lake has slight different in specific time and date as indicated in Fig. 9., Table 4.

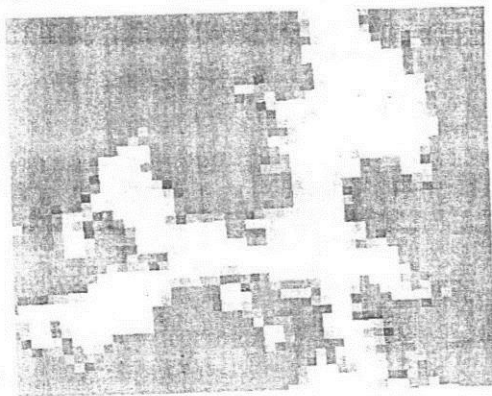


Fig. 8. Closed tone color of pixels carry LST values for August scene

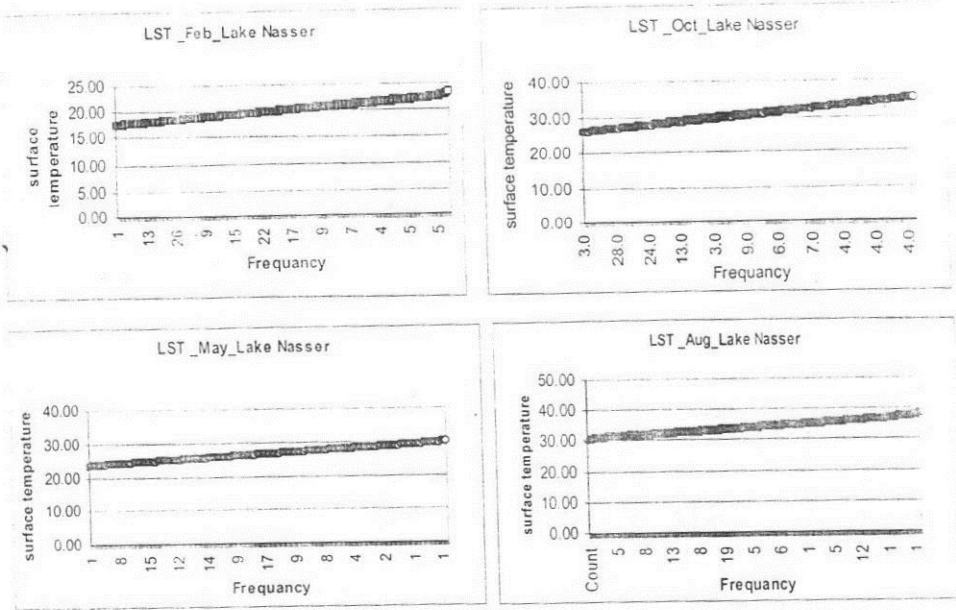


Fig.9. Surface temperature of lake Nasser in (Aug., Feb., Oct., May.)

Table 4. Land Surface Temp. Statistics of Lake Nasser for different months

Month	Minimum Surface temp. in C'	Maximum Surface temp. in C'	Mean Surface temp. In C'	Time
October	25.77	30.51	28.14	9 O'clock/Day
May	23.35	30.09	26.54	9 O'clock/Day
August	30.51	38.55	34.21	9 O'clock/Day
February	17.39	23.13	19.98	9 O'clock/Day

From the above illustration it can be deduced that evaporation estimates are very useful for practical applications and research. The bulk-aerodynamic method is very promising, and seems to also be the best fit for estimating evaporation using satellite imagery. Further research and data collection are recommended to continue with the progress that has been made and all previous approximation can be manipulated and treated with more investigation and gathering more data.

REFERANCES

1. Shaltout, M. and El-Hosary ,T. N., "Estimating the evaporation over Nasser lake in the upper Egypt from Meteosat observations", *Advances Space Research*, Vol.19, pp. 515-518,1997.
2. Salas , J. D., "Notes on Evaporation and Evapotranspiration" , CE Report 322, department of Civil and Environmental Engineering ,Colorado State University,2004.
3. Herting ,et.al., "Mapping of the Evaporative loss from Elephant Butte Reservoir Using Remote Sensing and GIS Technology", NMSU Report, New Mexico state university,Mexico,2004.
4. Wan, Z. and Dozier, J. "A generalized split-window algorithm for retrieving land-surface temperature from space", *IEEE Transactions on Geosciences and Remote Sensing*, Vol.34, pp. 892-905,1996.
5. GCOS, "Systematic observation requirements for satellite-based products for climate-supplemental details to the satellite" GCOS Report 107, The Global Climate Observation system, USA ,2006.
6. http://ladsweb.nascom.nasa.gov/browse_images/l3_browser.html
7. Lowe, P.R. , "An approximating polynomial for the computation of saturation vapor pressure" ,*Journal of Applied Meteorology*, Vol. 16, pp. 100-103,1977.

LIST OF SYMBOLS

E = evaporation rate [mm day^{-1}]

K_E = coefficient [kPa^{-1}]

u = wind speed measured at 2 m above the surface as standard [m s^{-1}]

e_s = saturation vapor pressure at the water surface [kPa]

e_a = vapor pressure of the air above the water surface [kPa]

K_E = coefficient of efficiency of vertical transport of water vapor by eddies of the wind [kPa^{-1}]

ρ_a = density of air [1.220 kg m^{-3}]

ρ_w = density of water [1000 kg m^{-3}]

P = atmospheric pressure [kPa]

Z_m = height at which wind speed and air vapor pressure are measured [m]

Z_d = zero-place displacement [m]; $Z_d = 0$ over typical water surfaces

Z_o = roughness height of the surface [m]; $Z_o = 2.30 \times 10^{-4} \text{ m}$ over typical water surfaces

e_s = saturation vapor pressure [kPa]

T = temperature [$^{\circ}\text{C}$]

THE EFFECT OF EXPANDED PERLITE AGGREGATE/POWDER ON THE MECHANICAL PROPERTIES OF CONCRETE

Assistant Prof. Esraa Emam Ali,
Housing and Building National Research Center-Dokki-Cairo
** Assistant Prof. Islam M. Elhabbal,
Higher Technological Institute, 6-of October City-Cairo

ABSTRACT

Expanded perlite aggregate (EPA) is a heat and sound insulator. Moreover it characterized as a lightweight material which ensures economical benefits in constructions. This paper investigates the properties of concrete containing expanded perlite aggregate/powder considering cement type (CEM I 42.5R), dosages (350 and 450 Kg/m³) and replacement ratios (0, 15, 30, and 50%) from cement or fine aggregate, and the effect of using silica fume with expanded perlite aggregate on the mechanical properties of concrete. The tests were conducted on fresh and hardened concrete. Cubes with nominal size 150x150x150mm were used for determining compressive strength and permeability, while cylinders with dimension Φ 150mmx300mm were used for determining splitting tensile strength at the end of 28 days. The results showed that the minimum unit weight of concrete mixture was 1900 kg/m³ at cement content of 350 kg/m³, and compressive strengths of EPAC (expanded perlite aggregate concrete) ranged from 22.8 to 31.2 MPa at cement content 350 and 450 Kg/m³, respectively, at the replacement ratios of 30%. This proved that EPAC can be used as structural lightweight concrete with adequate replacement ratios, despite some losses in mechanical properties.

KEYWORDS: Expanded perlite aggregates, lightweight concrete, compressive strength, permeability.

1. INTRODUCTION

Perlite is obtained from pumice, which is a glassy form of rhyolitic or dacitic magma. It contains 2–5% water [1]. Upon rapid heating, perlite transforms into a cellular material of low bulk-density. As the chemical water held within the perlite boils (at temperatures of 900–1100 °C), the resultant steam forms bubbles within the softened rock to produce a frothy-like structure. The formation of these bubbles allows perlite to expand up to 15–20 times of its original volume Expanded perlite aggregate (EPA) has been used in constructional elements such as brick, plaster, pipe, wall and floor block; however has not been industrially used in concrete yet approximately, 4.5 billion tonnes of the total 6.6 billion tonnes of perlite reserve is located in Turkey. Besides, other reserves are located in Greece, USA, Japan, Philippines, Russia, Hungary, Mexico and Italy The economical benefits of lightweight concrete are the low-heat conductivity and unit weight Today, lightweight property of concrete has been still desirable in constructional elements In most cases, high buildings have been affected during earthquakes due to the higher unit weight of concrete; however, replacement of EPA in concrete may be a solution for reducing damages of earthquakes owing to lightweight property Otherwise, EPA bricks may be used in buildings to reduce the weight of walls which is mentioned in a recent study In most studies, EPA has been used as admixture in cement or directly in concrete as aggregate. In concrete, EPA is used instead of fine aggregate with various replacement ratios depending on required strength. In cement, perlite is easier to be ground than the Portland cement clinkers; therefore they result in less energy requirement to produce blended cements by grinding clinker and perlite together. However, blended cements with perlite may cause strength losses at early ages compared to Portland cement, then the strength is improved by pozzolanic reactions lately The strength of EPA-based concrete is explained with the bonds between cement and perlite aggregate Generally, admixtures such as silica fume and fly ash has been used in concrete to improve mechanical properties (hydration, alkali silica reaction and permeability) Nonetheless, EPA is an alternative material to these admixtures; however unit weight and compressive strength are decreased with replacement of EPA in concrete mixtures. As is known, the effect of EPA on concrete is increased with increasing cure periods [2]. Furthermore, the natural perlite powder has a significant pozzolanic effect and is a good active mineral admixture for concrete, it has also

high-freeze-thaw resistance and fire protection capability [3]. Moreover, EPA contains some microcrystalline quartz and has a matrix that is mainly composed of chalcedony, which is potentially susceptible for alkali silica reaction [4]. Hence, there has been an increasing interest in EPA-based concrete.

There are a number of methods to produce lightweight concrete (LWC). In one method, the fine portion of the total concrete aggregate is omitted, which is called 'no-fines'. Another way of producing LWC is to introduce stable air bubbles inside concrete by using chemical admixtures and mechanical foaming. This type of concrete is known as aerated, cellular or gas concrete. The most popular way of LWC production is by using lightweight aggregate. Such aggregates, natural or artificial, are available in many parts of the world and can be used in producing concrete in a wide range of unit weights and suitable strength values for different fields of applications. The concrete strength and other properties heavily depend on its microstructure. The microstructure of concrete depends upon a number of parameters such as type, amount, and structure of constituent materials, etc. [5]. Constituent materials for concrete include fine as well as coarse aggregates (traditional or lightweight aggregates), and hydrated cement paste as a binder resulting from hydration or pozzolanic reaction of cementitious materials with water. Lightweight aggregate, made up of lightweight aggregates, have superior properties such as lightness, thermal isolation, freeze-thaw resistance, and fire protection but have the disadvantage of having low mechanical properties. Most lightweight aggregates used today such as expanded clay, the expanded perlite aggregate (EPA), and silicafume have been manufactured at a fringe temperature of approximately 1200 °C or above [6]. Such a high fringe temperature may have an influence on the pozzolanic reactivity of the aggregate. Therefore, an experimental investigation related to the effect of using expanded perlite aggregate/powder on the mechanical properties was carried out and the results reported.

2. EXPERIMENTAL STUDY

2.1. Materials

2.1.1. Expanded perlite aggregate (EPA)

Perlite contains 70–75% silicon dioxide and 12–16% alumina. Other components are sodium oxide, potassium oxide, ferro oxide, manganese

oxide, titan oxide and sulfide The physical properties of EPA are given in Table (1).The unit weight of EPA depends on gradation and expansion.

2.1.2. Cement

The cement used in this investigation was "El-Suez Cement Company (El Suez Plant)" Type CEM I 42.5 N, which is manufactured locally and complies with the standard specifications. The mechanical properties of the used cement as determined by laboratory tests showed its suitability for concrete work. The properties of the cement used in this investigation are given Table (2).

2.1.3. Aggregate

Local dolomite and sand from natural sources were used in experimental work. Dolomite used had a nominal maximum size of 10 mm. The properties of dolomite and sand used in this experimental work are indicated in Table (3).

2.1.4. Silica fume

Silica fume has been used in high strength concrete. It is a by product resulting from the reduction of high purity quartz with coal in electrical core furnaces in the production of silicon, the fume which has a high content of amorphous silicon dioxide and consists of very fine spherical particles, is collected from the gases escaping from the furnaces, Table (4) shows the physical properties and chemical analysis of silica fume.

2.1.5. Mixing water

Tap water free from impurities was used for mixing.

2.1.6 Super plasticizers

It is a powerful water reducing agent in concrete mixture. The super-plasticizer used was ADDICRETE BVF, which is a product of Chemical for Modern Building Company.

2.2. Mix constituents

The concrete mixes were prepared in the laboratory of Housing and Building National Research Center in countercurrent mixer for total of 5 min. hand compaction was used, precautions were taken to ensure from homogeneity and full compaction. for each mix nine specimens 150x150x150mm and six cylinders Φ 150x300mm were prepared and cured at $20\pm 3^{\circ}\text{C}$ for compressive strength, permeability tests and splitting tensile strength tests respectively, the mixes constituents were given in Tables (5 and 6).

Table (1) Physical properties of perlite: Table (2): Mechanical properties of cement

Components	Weight Ratio (%)
SiO ₂	71.0-75.0
Al ₂ O ₃	12.5-16.0
Na ₂ O	2.90-4.00
K ₂ O	4.00-5.00
CaO	0.20-0.50
Fe ₂ O ₃	0.50-1.45
H ₂ O	3.05-5.16
MgO	0.03-0.50
TiO ₂	0.03-0.20
MnO ₂	0.00-0.10
Cr	0.00-0.10
Ba	0.00-0.05
PbO	0.00-0.30
S	0.02-0.04

Properties	Measured values	
Soundness (Le Chatelier) mm	1.2	
Initial Setting Time (mins)	120	
Initial Setting Time (mins)	165	
Compressive strength (MPa)	2 days	21.8
	28 days	50.5

Table (3): Properties of dolomite and sand

Test	dolomite	sand
Specific gravity	2.6	2.5
Unit weight and voids	1.62	1.71
Materials finer than no 200 sieve	1.12	2.8
Abrasion (Los Anglos)	14.62	-
Absorption	1.23	-
Crushing	20.5	-
Impact	11.6	-

Table (4) Properties of silica fume

Properties	item	value
Physical properties	color	Light grey
	Specific weight	2.2
	Bulk density	350
	Specific area	16.7
Chemical properties	% SiO ₂	97
	% C total	0.5
	% Fe ₂ O ₃	0.5
	% Al ₂ O ₃	0.2
	% CaO	0.2
	% MgO	0.5
	% K ₂ O	0.5
	% Na ₂ O	0.2
	% SO ₃	0.15
	% Cl	0.01
% H ₂ O	0.5	

Table (5) Mix constituents for cement content 350 Kg/m³

Perlite replace.	As cement replacement				As fine aggregate replacement			
	0%	15%	30%	50%	0%	15%	30%	50%
Cement kg/m ³	350	297.5	245	175	350	350	350	350
Coarse agg kg/m ³	1190	1190	1190	1190	1190	1190	1190	1190
Sand kg/m ³	595	595	595	595	595	505.75	416.5	297.5
Perlite kg/m ³	0	3.848	7.7	12.83	0	16.06	32.2	53.6
water liter/m ³	175	175	175	175	175	175	175	175

Table (6) Mix constituents for cement content 450 Kg/m³

Perlite replace.	As cement replacement				As fine aggregate replacement			
	0%	15%	30%	50%	0%	15%	30%	50%
Cement kg/m ³	450	382.5	315	225	450	450	450	450
Coarse agg kg/m ³	1054	1054	1054	1054	1054	1054	1054	1054
Sand kg/m ³	527	527	527	527	527	448	368.9	263.5
Perlite kg/m ³	0	4.94	9.9	16.5	0	14.23	28.45	47.43
water liter/m ³	225	225	225	225	225	225	225	225

Table (7) Mix constituents for cement content 350 and 450 Kg/m³ with silica fume

Perlite replace.	As cement replacement 350 Kg/m ³			As cement replacement 450 Kg/m ³		
	0%	15%	15%sf+15%perl.	0%	15%	15%sf+15%perl.
Cement kg/m ³	350	297.5	252.85	450	382.5	325.1
Coarse agg kg/m ³	1190	1190	1190	1054	1054	1054
Sand kg/m ³	595	595	595	527	527	527
Perlite kg/m ³	0	0	3.272	0	0	4.2
Silica fume kg/m ³	0	52.5	52.5	0	67.5	67.5
water liter/m ³	175	175	175	225	225	225

3. RESULT AND DISCUSSION

3.1 Unit weight and slump

According to the obtained data, it was observed that unit weights of 28-day hardened concrete decreased with increasing EPA in the mixtures, because the specific gravity of EPA is lower than that of normal

aggregate. SF used in replacement of PC also lowered the unit weight of samples a little. The values of unit weights decreased with increasing

EPA ratio in the mixes. The lowest value was 1900 kg/m^3 at 50% EPA. The other samples unit weights changed between 2300 and 1900 kg/m^3 . The slumps of concrete mixtures were observed between 70 and 120 mm. The concrete mixtures with lower unit weight had higher slump values, due to their porous structures, it was observed that the slump values of concretes with cement content 350 Kg/m^3 were higher than the concrete mixtures with cement content 450 Kg/m^3 .

3.2 Effect of expanded perlite aggregate/powder on the compressive strength of concrete

Tables (8 and 9) shows the hardened concrete test results of concrete mixtures containing expanded perlite aggregates. The concrete specimens were grouped as 350 and 450 Kg/m^3 as shown in figures (1 and 2) considering the dosages of perlite. It was observed the compressive strength was decreased by (15, 30 and 60%) compared to conventional concrete when using the expanded perlite aggregate as a cement replacement while it decreased by (16, 20 and 26.5%) compared to conventional concrete when using the expanded perlite aggregate as a fine aggregate replacement at cement content 350 Kg/m^3 , while it decreased by (13.3, 38.3 and 50%) compared to conventional concrete when using the expanded perlite aggregate as a cement replacement and by (7, 10 and 13%) compared to conventional concrete when using the expanded perlite aggregate as a fine aggregate replacement at cement content 450 Kg/m^3 , it was observed that as the cement content increase the loss in the compressive strength decreased compared to conventional concrete as using expanded perlite aggregates as fine aggregate replacement. While the compressive strength of concretes containing expanded perlite aggregates lose more than 50% of its strength when using it as cement replacement at different cement contents. The compressive strength of concretes containing 30% expanded perlite aggregates were decreased by (20 and 10%) at cement contents (350 and 450 Kg/m^3) respectively compared to the conventional concretes which indicates that at higher dosages of perlite, there are an adequate loss of the mechanical properties of the concrete with improving the lightweight property.

3.3 Effect of expanded perlite aggregate/powder on the splitting tensile strength of concrete

Tables (8 and 9) shows the hardened concrete test results of concrete mixtures containing expanded perlite aggregates. The concrete specimens were grouped as 350 and 450 Kg/m³ as shown in figures (3 and 4) considering the dosages of perlite. It was observed the splitting tensile strength was decreased by (54.3, 65 and 68.3%) compared to conventional concrete when using the expanded perlite aggregate as a cement replacement while it decreased by (52.5, 56.9 and 63.3%) compared to conventional concrete when using the expanded perlite aggregate as a fine aggregate replacement at cement content 350 Kg/m³, while it decreased by (61.5, 65.4 and 73.3%) compared to conventional concrete when using the expanded perlite aggregate as a cement replacement and by (58.2, 64.8 and 70%) compared to conventional concrete when using the expanded perlite aggregate as a fine aggregate replacement at cement content 450 Kg/m³, it was observed that the splitting tensile strength lose more than 50% of its strength when the dosage of perlite increased.

According to results, the optimum strengths for lightweight concrete were obtained between 15% and 30% ratios at the dosage of 350 Kg/m³ and 450 Kg/m³ furthermore, results have shown that higher replacement of expanded perlite aggregate at 50% negatively affects both compressive and splitting strengths of concrete specimens, but positively affects the lightweight property.

3.4 Effect of expanded perlite aggregate/powder on the permeability of concrete

As shown in fig(5 and 6), the permeability increased in the concrete mixtures as the percentage of EPA replacement increased (as a cement replacement) by (1.5,2.1 and 2.5 times) and (2.7,3.67 and 4 times) at cement contents (350 Kg/m³ and 450 Kg/m³) respectively compared to conventional mixes, and by (2,4 and 4.8 times) and (3.2,5.8 and 7 times) at cement contents (350 Kg/m³ and 450 Kg/m³) respectively compared to conventional mixes (as a sand replacement). It was observed that as the cement content increased the permeability increased with the increase of EPA replacement ratios this was attributed to the very high absorption effect of the EPA.

3.5 Effect of expanded perlite and silica fume on the mechanical properties of concrete

As shown in fig(7 and 8), the compressive strength of mixtures containing silica fume and EPA increased by (2.12% and 1.44%) compared to conventional mixes for mixes containing 15%SF and 15%EPA at cement contents (350 Kg/m^3 and 450 Kg/m^3) respectively, while the compressive strength increased by (1.3% and 1.9%) for mixes containing 15% SF only compared to conventional concrete at cement contents (350 Kg/m^3 and 450 Kg/m^3) respectively, it was observed that there was a positively effect of the combined addition of silica fume and EPA due to the high reactivity of silica fume and its famous micro filler effect.

Table (8) Mechanical properties of concrete with cement content 350 Kg/m^3

Perlite replace.	As cement replacement				As fine aggregate replacement			
	0%	15%	30%	50%	0%	15%	30%	50%
Comp. strength (kg/cm ²)	286	183	158	115	286	240	228	210
Tensile strength (kg/cm ²)	24.65	11.3	8.6	7.8	24.65	11.7	10.6	8.9
Permeability $\times 10^{-8}$	0.6	0.9	1.26	1.5	0.6	1.25	2.4	2.92

Table (9) Mechanical properties of concrete with cement content 450 Kg/m^3

Perlite replace.	As cement replacement				As fine aggregate replacement			
	0%	15%	30%	50%	0%	15%	30%	50%
Comp. strength (kg/cm ²)	347	301	214	174	347	320	312	302
Tensile strength (kg/cm ²)	35.6	13.7	12.3	9.5	35.6	14.9	12.5	10.8
Permeability $\times 10^{-8}$	0.45	1.25	1.65	1.8	0.45	1.45	2.62	3.2

Table (10) Mechanical properties of concrete with cement contents 350 and 450 Kg/m³ with silica fume

Perlite replace.	As cement replacement 350 Kg/m ³			As cement replacement 450 Kg/m ³		
	0%	15sf%	15%sf+15%perl.	0%	15sf%	15%sf+15%perl.
Comp. strength (MPa)	286	370	412	347	660	737
Tensile. strength (MPa)	24.65	28.3	36.7	35.6	39.6	42.7
Permeability *10 ⁻⁸	0.6	0.3	0.45	0.45	0	0

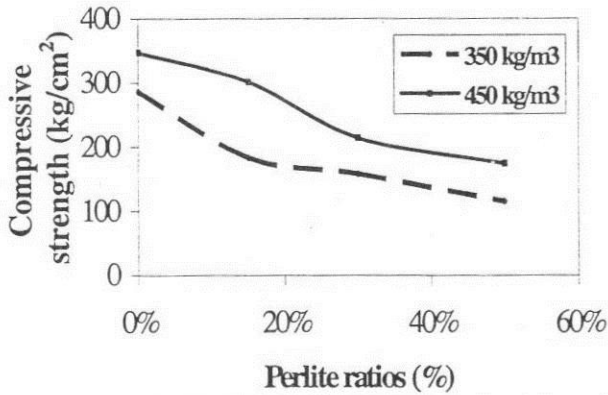


Fig (1) Effect of perlite ratios on the compressive strength of concrete as a cement replacement

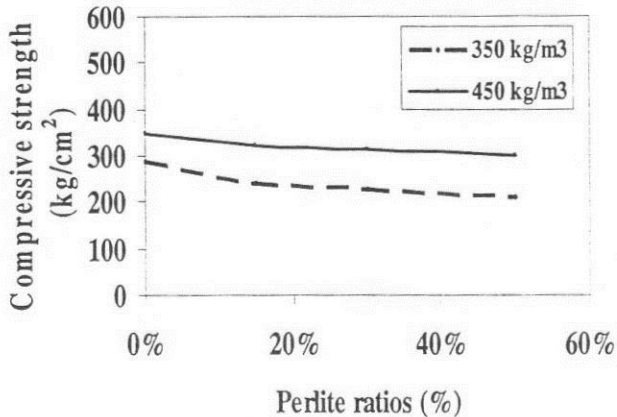


Fig (2) Effect of perlite ratios on the compressive strength of concrete as a sand replacement

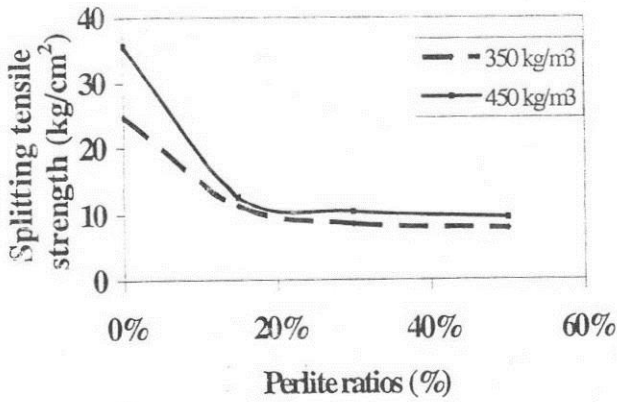


Fig (3) Effect of perlite ratios on the splitting tensile strength of concrete as a cement replacement

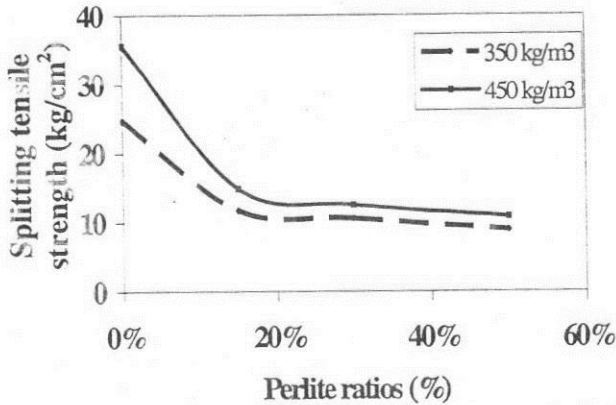


Fig (4) Effect of perlite ratios on the splitting strength of concrete as a sand replacement

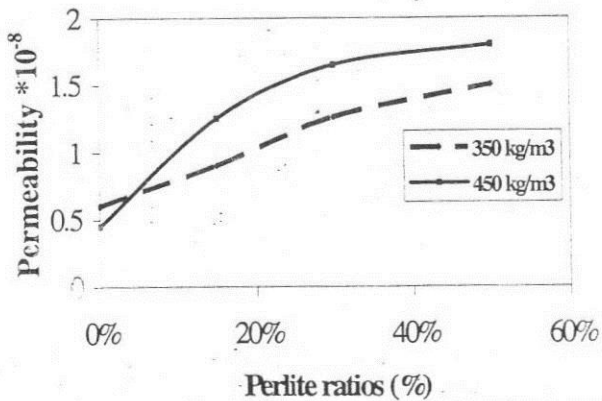


Fig (5) Effect of perlite ratios on the permeability of concrete as a cement replacement

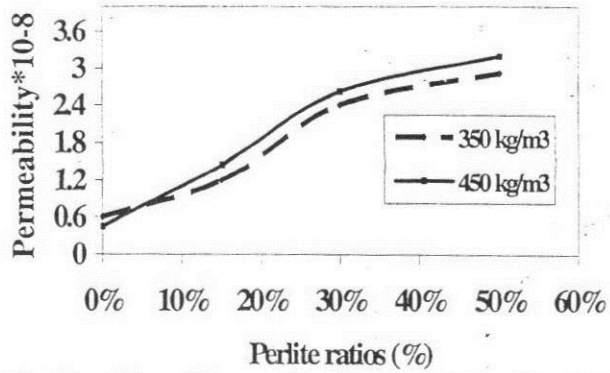


Fig (6) Effect of perlite ratios on the permeability of concrete as a sand replacement

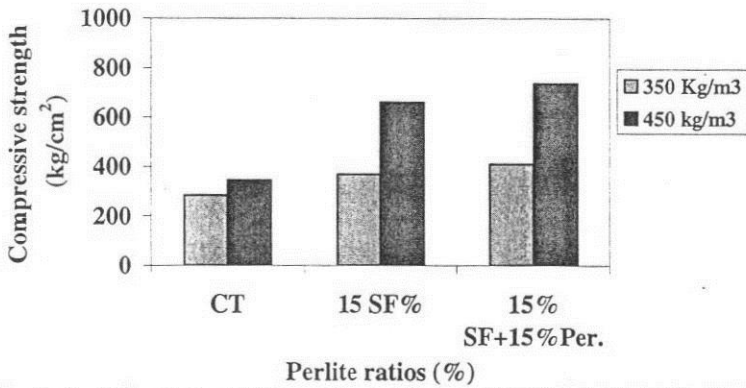


Fig (7) Effect of silica fume and perlite ratios on the compressive strength at cement content 350 Kg/m³ and 450 Kg/m³

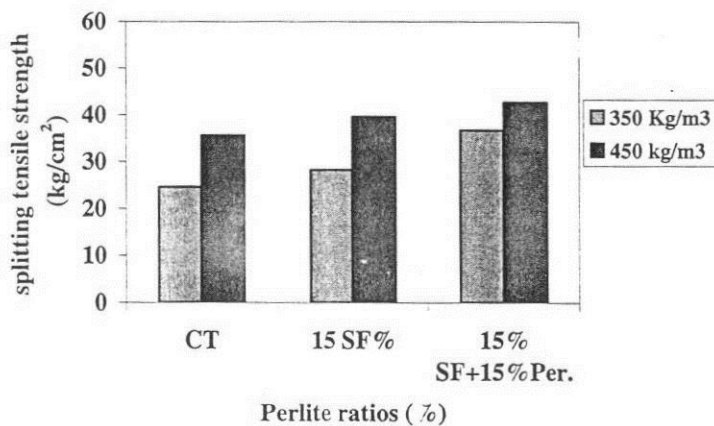


Fig (8) Effect of silica fume and perlite ratios on the splitting strength at cement content 350 Kg/m³ and 450 Kg/m³

3. CONCLUSIONS

- 1- It was observed that as the cement content increase the loss in the compressive strength decreased compared to conventional concrete as using expanded perlite aggregates as fine aggregate replacement.
- 2- The compressive strength of concretes containing expanded perlite aggregates lose more than 50% of its strength when using it as cement replacement at different cement contents.
- 3- The compressive strength of concretes containing 30% expanded perlite aggregates were decreased by (20 and 10%) at cement contents (350 and 450 Kg/m³) respectively compared to the conventional concretes which indicates that at higher dosages of perlite, there are an adequate loss of the mechanical properties of the concrete with improving the lightweight property.
- 4- It was observed that there was a positively effect of the combined addition of silica fume and EPA on the mechanical properties of concrete` due to the high reactivity of silica fume and its famous micro filler effect.
- 5- It was observed that as the cement content increased the permeability increased with the increase of EPA replacement ratios this was attributed to the very high absorption effect of the EPA.
- 6- According to results, the optimum strengths for lightweight concrete were obtained between 15% and 30% ratios at the dosage of 350 Kg/m³ and 450 Kg/m³ furthermore, results have shown that higher replacement of expanded perlite aggregate at 50% negatively affects both compressive and splitting strengths of concrete specimens, but positively affects the lightweight properties

REFERENCES

1. Mladenovic, A., Suput, J.S., Ducman, V., Skapin, A.S., 2004. Alkali-silica reactivity of some frequently used lightweight aggregates. *Cement Concrete Res.* 34 (10), 1809–1816.
2. Demirboğ̃ a, R., Gu̇ l, R., 2003. The effects of expanded perlite aggregate, silica fume and fly ash on the thermal conductivity of lightweight concrete. *Cement Concrete Res.* 33 (5), 723–727.
3. Demirboğ̃ a, R., Ȯ ru̇ ng, I., Gu̇ l, R., 2001. Effects of expanded perlite aggregate and mineral admixtures on the compressive strength of low-density concretes. *Cement Concrete Res.* 31 (11), 1627–1632.

4. Yu, L.H., Ou, H., Lee, L.L., 2003. Investigation on pozzolanic effect of perlite powder in concrete. *Cement Concrete Res.* 33 (1), 73-76.
5. T.R. Naik, S. Singh, B. Ramme, Mechanical properties and durability of concrete made with blended fly ash, *ACI Mater. J.* 95 (4) (1998).
6. T.R. Naik, S. Singh, B. Ramme, Mechanical properties and durability of concrete made with blended fly ash, *ACI Mater. J.* 95 (4) (1998).

Optimization of the Drilling Cycle on Conventional and CNC Machine Tools

Part I- Formulation of the Optimization Model for the Drilling Cycle

**Prof. Dr. / Mohamed A. El Hakim, Dr. / Wael S. Moughith & Engineer /
Ahmed S. Abd-Allah***

*Faculty of engineering – Ain shams university, Egyptian Armed Forces & Egyptian
Armed Forces*

*Corresponding author. Tel: 002-012-5713484, E-mail address: asabdallah75@yahoo.com

Abstract

The paper presents an investigation into the drilling process, which takes the technical, technological and economical factors of the drilling process into consideration and outlines the optimization strategies for drilling operations on conventional and CNC machine tools. The optimization method used is a logic algorithm based on the minimum machining cost as an objective function and incorporates various technical and technological constraints of importance in drilling which have not been considered by any of the previous investigators such as chatter, burr formation, drill breakage in deep hole drilling.....etc. The study highlights the increased benefits of using optimization in process planning in computer aided manufacturing.

Keywords: Drilling; Optimization strategies; Process planning; Deep hole drilling

1-Introduction

Although drilling seems to be relatively a simple machining process, It is in fact a severe process in which the cutting action takes place inside the workpiece; the only exit for the chips is the hole that is filled by the drill. The chip disposal and cutting fluid delivery to the drill lips present difficulties. Also friction between the drill and the hole walls results in heat that is additional to that due to chip formation. The selection of economic cutting conditions in drilling is becoming increasingly important in modern computer based manufacturing.

Compared with the optimization studies in turning, relatively little work has been published on the economics of drilling operations although drilling is also a major material removal process. Based on the optimization analyses for turning operations, Field et al. [1] attempted to study the optimization conditions in drilling operations. Using Taylor's tool life equation, they have given special objective functions for drilling to calculate the desired minimum production cost per component and maximum production rate. However, in those studies, the cutting speed was the only cutting variable to be determined and no constraints were considered.

Grieve and Griffiths [1] studied the economics of deep hole drilling processes using minimum production time and cost criterion as well as chip form and power constraints. They pointed out that over the practical feed and speed ranges, an increase in production rate was obtained by increasing feed and speed. When the minimum cost per component was considered, they suggested that the lowest speed and highest feed produced minimum cost for the allowable feed and speed ranges. However, when both criteria were considered, they noted that the production rate at minimum cost was not the maximum production rate, therefore implying that only one of the two strategies could be adopted either to maximize the production rate or to minimize cost, and both benefits would not be achieved simultaneously.

Wang [2] developed an optimization strategy for selecting the economic cutting conditions in drilling operations based on the criteria typified by the maximum production rate or minimum cost per hole and incorporating constraints of relevance to drilling on CNC machines. The analysis using the generic deterministic optimization approach with graphical assistance on the feed-cutting speed diagram results in clearly defined optimization strategies that ensure the global optimum solution but the analysis is complex and needs high computation capabilities.

Kee and Ibrahim [1] presented an optimization strategy and computer flow charts for rough drilling operations on CNC machine tools. The analysis is based on the maximum production rate criterion and incorporates various practical constraints of importance in rough drilling such as machine tool maximum and minimum feed and speed limits, maximum axial force, limiting torque and the

machine tool maximum power. The optimization strategy depends on representing the above constraints as feed and speed limits in the feed-speed diagram, which when combined with the objective function equation can provide the necessary information for the selection of the optimal feed and speed. The optimization strategies for this operation have been found to be complex. The complexity of these strategies lies in selecting the optimum parameters using the feed-speed diagrams while plotting many constraints.

Comparing the different methods of optimization dealt with in previous work, it can be seen that while the graphical solution is the simplest, it is quite impractical in case of repetition with different input data or if the depth of cut has to be varied e.g. when the occurrence of chatter is the predominant constraint governing the choice of the economic values of cut. Other techniques such as genetic algorithm are complex and need high computation capabilities. On the other hand, from the foregoing study the application of special logic algorithms provides a considerably easier and less expensive method.

Generally, there is still no reliable method for predicting and preventing drill breakage, so that it should be accounted for in the process planning stage by assigning safe machining variables under all expected conditions.

The aim of the present work is to establish an optimization model for the drilling process and to develop the possible optimization technique which enables the determination of the optimum values of the machining variables taking into consideration the decisive constraints which have not been previously accounted for such as chatter in hole enlarging, critical hole depth in deep hole drilling using standard drills, burr formation, hole positioning accuracy, surface roughness....etc.

It is aimed to select machining variables that are believed to:

- Control size of burr at the production stage to save the deburring costs as many of deburring techniques are expensive and add to the total cost of the components.
 - Create preferred burr types through the best choice of the drilling feed which is observed to be the most significant parameter which governs the size of burr.
 - Maintain chatter free machining by checking the stability limit against chatter.
 - Keep the drilling temperatures below the tool material softening temperature.
 - Prevent conventional twist drill breakage even when used for deep hole drilling considering the axial force and the drilling torque increase along hole depth due to other sources than chisel edge and cutting lips.
-

2-Development of an optimization model for the drilling process

In spite of the recent developments of metal cutting machine tools and cutting tool materials, considerably low production rates and consequently relatively high machining costs are still remarkable features in most machining shops.

This is mainly due to the inconvenient choice of the machining variables (the cutting speed and the feed) which is usually based on mere experience that varies widely from one person to another and from one factory to another due to the varying nature of the machining process or empirical rules or selection from engineering tables. Both methods for selection of machining variables either from handbook recommendations or according to experience do not take process constraints, machine capacity and machining economy into account and merely depend on the personal experience of the technologist and hence lead to values of cut which are too low in order to avoid overloading of the production equipment and tool failure. These values are too far from the economic values.

The reduction of the machining costs can be attained by reducing both the idle time and the machining time. Considerable reductions of the idle time have been achieved by increasing the degree of automation of machine tools especially in case of CNC machine tools. The handling time and the tool replacement time have been optimized using work study techniques, ingenious loading and unloading devices and jigs and fixture designs. The idle time could therefore be reduced to less than the half of the machining time. Likewise, the labour cost rate and the tool cost per failure have been minimized through good management and purchasing policy.

In spite of such improvement a significant reduction in the machining time and hence the machining cost can still be attained by increasing the rate of metal removal. This is however limited by some technical and technological constraints encountered in machining from the side of machine tool, cutting tools and workpiece.

The assignment of the machining variables should therefore be based on technical and technological bases, which mean that it is required to determine those economic values for the machining variables which lead to minimum manufacturing cost and at the same time satisfy the encountered constraints.

The problem has to be handled as an optimization problem to determine the best values of the machining variables.

(2-1)Machining variables to be optimized

In drilling operations, the drill diameter is pre-selected according to the process need while the available machine tool capacity, the hole depth and the tool-workpiece material combination are known. The machining process independent variables which should be selected to give the minimum manufacturing cost and the required machining performance are merely the

cutting speed (v) and the feed (s). These variables are independently set on any machine tool.

For a given drill diameter (D) the rate of metal removal is given by ($v \cdot s \cdot D/2$). It may appear that the increase of the cutting speed and the feed together will increase the production rate. This is however not true due to the tool life limitation.

It follows that the increase of feed with sub-sequent reduction of the cutting speed to retain a certain tool life increases the rate of metal removal while the increase of cutting speed with sub-sequent reduction of feed reduces it.

The machining variables have different effects on the machining performance. The feed and the drill diameter affect the cutting force and the drilling torque whereas the drill diameter has more effect; the cutting speed has the greatest influence on the cutting temperature and the tool life.

(2-2) Machining Process Constraints

The different technical and technological constraints encountered in machining are obtained empirically as functions of the machining variables.

The technical constraints are those imposed by the MFTW system such as permissible forces, torque, stresses and deflections. The technological constraints on the other hand are those imposed by the cutting process such as tool life, cutting temperature, chatter, critical depth and hole quality represented by surface roughness and burr.

The cutting force and the drilling torque are almost independent of the cutting speed so that the machine tool and drill bit strength constraints will in fact result in feed limit, for a selected diameter and drill-workpiece material combination.

(2-2-1) Constraints due to the machine tool capacity

The thrust force and the drilling torque generated in drilling act on the feed mechanism and the main drive of the machine tool and have to be constrained to the machine tool maximum permissible limits. The different constraints encountered in the drilling process due to the machine tool capacity are:-

(2-2-1-1) Column deflection

The machine column is subjected to torsional and bending moments during drilling which results in a displacement of the tool axis from the hole axis.

(2-2-1-1-1) Column deflection due to torsion

The permissible error due to torsional deflection of a column must be less than or equal to the center distance tolerance of the drilled hole [3].

$$X_t \leq \frac{Tol(\mu m)}{1000} \quad (2-1)$$

Where : X_t ...Error due to column deflection under torsion (mm) , Tol...Center distance tolerance in microns (μm).

For rectangular machine column the positional error due to such deflection is given by [3]:

$$X_i = \left(\frac{2M_d}{B_c} \right) \left(\frac{\beta}{E_m \cdot h_{cw} \cdot \alpha (1+\alpha)} \right) \left(4\beta^2 \alpha^2 + 3\alpha^2 + 2\alpha + \frac{1}{2} \right) (H_{sc} + CG) \tag{2-2}$$

Where : M_d ..Total drilling torque (N.mm), B_c .. Column side width (mm) , E_m ..Young's modulus of the material of the machine structure (N/mm²) , h_{cw} ...Column wall thickness ($h_{cw} = 0.05 H_c$) (mm) , α ...Ratio between column length and column width , β ... Ratio between overhanging column height and column side length , H_{sc} ...Distance between spindle and machine column (mm) , CG ...The co-ordinate of the center of gravity of the machine column cross section (mm).

From previous work [4] it was found out that the column deflection is responsible for 15% of the total deviation from the original position in the X-axis direction due to torsional moment, so that:

$$\therefore M_d \leq \left(\frac{E_m \cdot h_{cw} \cdot \alpha (1+\alpha) B_c^2 \cdot Tol(\mu m)(0.15)}{(2000)\beta (4\beta^2 \alpha^2 + 3\alpha^2 + 2\alpha + \frac{1}{2}) (H_{sc} + CG)} \right) \tag{2-3}$$

Substituting for the drilling torque (M_d) [3]:

$$M_d = K_{sm} \cdot K_{corr2} \left(D_2^{1.8} - D_1^{1.8} \right) S^{mf} \tag{2-4}$$

$$K_{corr2} = K_{dt} \left(\frac{L}{D} \right)^{y_4}$$

Where : K_{sm} ...Specific cutting resistance in radial direction (N/mm²) , K_{corr2} ...Correction factor accounting for drilling torque increase along hole depth , D ...Drill diameter (mm) , mf ...exponent for feed effect on axial force and drilling torque , S ...feed (mm/rev) , K_{dt} ...Material correction factor for drilling torque-hole depth equation.

The corresponding feed is given by:

$$\therefore S_1 \leq \left(\frac{E_m \cdot h_{cw} \cdot \alpha (1+\alpha) B_c^2 \cdot Tol(\mu m)(0.15)}{(2000)\beta (4\beta^2 \alpha^2 + 3\alpha^2 + 2\alpha + \frac{1}{2}) (H_{sc} + CG) K_{sm} \cdot K_{corr2} \cdot K_{f1} (D_2^{1.8} - D_1^{1.8})} \right)^{\frac{1}{mf}} \tag{2-5}$$

Where : K_{f1} ... Cutting fluid correction factor for axial force and drilling torque.

For circular machine column the positional error due to such deflection is given by [3]:

$$\therefore X_i = \frac{M_d \cdot l_{ov}}{G_m \cdot I_t} (H_{sc} + CG) \leq \left(\frac{Tol(\mu m)}{1000} \right) (0.15) \tag{2-6}$$

$$\therefore M_d \leq \left(\frac{G_m \cdot I_t \cdot Tol(\mu m)(0.15)}{l_{ov} (H_{sc} + CG)(1000)} \right)^{\frac{1}{y}}$$

Substituting for the drilling torque (M_d), the corresponding feed is given by:

$$\therefore S_1 \leq \left(\frac{G_m \cdot I_t \cdot Tol(\mu m)(0.15)}{l_{ov} (H_{sc} + CG)(1000) K_{sm} \cdot K_{corr2} \cdot K_{f1} (D_2^{1.8} - D_1^{1.8})} \right)^{\frac{1}{y}} \tag{2-7}$$

Where : l_{ov} ...Overhanging height (mm) , G_m ...Modulus of rigidity of machine structure material (N /mm²) , I_t ...Torsional moment of inertia of drill column (mm⁴).

(2-2-1-1-2) Column deflection due to bending

The permissible error due to column bending under the effect of axial load must be less than or equal to the center distance tolerance of the drilled hole. The error due to such a deflection is given by [3]:

$$X_b = \left(\frac{F_a(H_{sc} + CG)l_{ov}}{E_m \cdot I} \right) \left(\frac{l_{ov}}{2} - l_{tool} \right) \leq \left(\frac{Tol(\mu m)}{1000} \right) \tag{2-8}$$

Where : X_b ...Error due to column deflection under bending moment (mm) , F_a ...Axial thrust force (N) , I ...Bending moment of inertia of machine column (mm⁴) , l_{tool} ...Twist drill overhanging height (mm).

From previous work [4] it was found out that the column deflection is responsible for 14% of the total deviation from the original position in the Y-axis direction due to bending moment.

$$\therefore F_a \leq \left(\frac{Tol(\mu m) \cdot E_m \cdot I^{(0.14)}}{(1000)(H_{sc} + CG)l_{ov} \left(\frac{l_{ov}}{2} - l_{tool} \right)} \right) \tag{2-9}$$

The bending moment of inertia for drill column with circular cross-section:

$$I = \frac{\pi}{64} (D_{c1}^4 - D_{c2}^4) \tag{2-10}$$

The bending moment of inertia for drill column with rectangular cross-section:

$$I = I_1 + I_2 \tag{2-11}$$

For rectangular cross-section column:

$$I_1 = \left(\frac{B \cdot H_c^3}{12} \right) - \left(\frac{1}{12} (B_c - 2t)(H_c - 2t)^3 \right) \tag{2-12}$$

For slide way:

$$I_2 = (B_c \cdot h_{sw})(CG_1 + CG_2)^2 \tag{2-13}$$

Where : D_{c1} , D_{c2} ...Machine column outer and inner diameters respectively (mm) , h_{sw} ...Slide way thickness (mm) , H_c ...Column side length (mm) , t ...column wall thickness (mm).

The co-ordinate of the center of gravity of the machine column in case of rectangular cross-section:

$$CG = \frac{H_c}{2} \tag{2-14}$$

The co-ordinate of the center of gravity of the machine column in case of circular cross-section:

$$CG = \frac{D_{c1}}{2} \tag{2-15}$$

Substituting for the axial force (F_a) [5]:

$$F_a = K_{sa} \cdot K_{corr1} (D_2 - D_1) s^{mf} \tag{2-16}$$

$$K_{corr1} = k_{af} \left(\frac{L}{D} \right)^{x_4} \quad (2-17)$$

Where : K_{sa} ...Specific cutting resistance in axial direction (N/mm^2), K_{corr1} ...Correction factor accounting for axial force increase along hole depth, K_{af} ...Material correction factor for axial force-hole depth equation

The corresponding feed is given by:

$$\therefore S_z \leq \left(\frac{Tol(\mu m) \cdot E_m \cdot I(0.14)}{(1000)^{H_{sc}+CG} \cdot v_{av} \left(\frac{L_{ov}}{2} - L_{tool} \right) K_{sa} \cdot K_{corr1} \cdot K_{f1}(D_2 - D_1)} \right)^{\frac{1}{x_4}} \quad (2-18)$$

(2-2-1-2) Maximum permissible axial force (F_a)_p

The axial thrust force must be less than or equal to the maximum permissible axial force dictated by the feed drive [$F_a \leq (F_a)_p$], then the feed is given by:

$$\therefore S_z \leq \left(\frac{(F_a)_p}{K_{sa} \cdot K_{corr1} \cdot K_{f1}(D_2 - D_1)} \right)^{\frac{1}{x_4}} \quad (2-19)$$

Where : $(F_a)_p$...Maximum permissible axial thrust dictated by the feed drive (N).

(2-2-1-3) Maximum permissible drilling torque (M_d)_p

The drilling torque must be less than or equal to the maximum permissible torque transmitted by the main drive in order to avoid failure of the main spindle [$M_d \leq (M_d)_p$], then the feed is given by:

$$\therefore S_z \leq \left(\frac{(M_d)_p}{K_{sm} \cdot K_{corr2} \cdot K_{f1}(D_2^{1.8} - D_1^{1.8})} \right)^{\frac{1}{x_4}} \quad (2-20)$$

Where : $(M_d)_p$...Maximum permissible drilling torque transmitted by the main drive (N.mm).

(2-2-2) Constraints due to the twist drill

The different constraints encountered in the drilling process due to the twist drill strength are:

(2-2-2-1) Buckling of twist drill

Buckling may occur if the axial force is greater than the critical buckling force (P_{cr}) which can be calculated from Euler's equation or Johnson's equation. The buckling load is given by Euler's equation for slenderness ratio ($\lambda \geq \lambda^*$) as follows:

$$P_{cr} = \frac{C_E \cdot \pi^2 E_I \cdot I_{min}}{l_b^2} = P_{cr} = \frac{C_E \cdot \pi^2 E_I \cdot A}{\lambda^2} \quad (2-21)$$

Where $I_{min} = I_{xx} = 0.0558 \pi r^4$ [3] (2-22)

Whereas, for slenderness ratio ($\lambda < \lambda^*$), Johnson's formula is used as given by:

$$P_{cr} = [a_j - b_j (\lambda)^2] A \quad (2-23)$$

Where $a_j = \delta_y$, $b_j = \left(\frac{\delta_y}{2\pi}\right)^2 \frac{1}{C_E E_t}$ (2-24)

The slenderness ratio (λ) and the critical slenderness ratio (λ^*) for twist drill are given by:

$$\lambda = \frac{l_f}{i} \quad , \quad \lambda^* = \sqrt{\frac{2\pi^2 \cdot C_E \cdot E_t}{\delta_y}} \quad (2-25)$$

Where $i = \sqrt{\frac{I_{xy}}{A}}$, $A = 0.305d^2$ [5] (2-26)

Then the maximum axial force must be less than (P_{cr}):

$$F_a \leq \frac{P_{cr}}{Safety\ factor}$$

$$S_s \leq \left(\frac{P_{cr}}{K_{sa} \cdot K_{corr} \cdot i \cdot K_{f1}(D_2 - D_1)} \right)^{\frac{1}{2}} \quad (2-27)$$

Where : P_{cr} ...Critical load (N) , C_E ...End condition factor of buckling , E_t ...Young's modulus of twist drill material (N/mm²) , I_{min} ...Bending moment of inertia of the twist drill section about the axis of least moment of inertia (mm⁴) , l_b ...Buckling length (mm) , A ...Twist drill cross sectional area (mm²) , I_{min} ...Bending moment of inertia of the twist drill section about the axis of least moment of inertia (mm⁴) , r ...Drill radius (mm) , σ_y ...Yield stress on drill material (N/mm²) , a_j , b_j ...Constants in Johnson's formula for buckling load , l_f ...Drill flute length (mm) , i ...Radius of gyration of twist drill cross section (mm) , λ ...Slenderness ratio ($\lambda = l_f / i$) , λ^* ...Critical value for the slenderness ratio.

(2-2-2-2) Combined stress for twist drill

The normal stress can be expressed as follows: $\sigma_n = \frac{2\tau M_d}{D^3}$ [3] (2-28)

The torsional stress can be expressed as follows: $\tau = \frac{28M_d}{D^3}$ [3] (2-29)

The maximum combined stress (σ_c) resulting from both the normal and torsional shear stresses can be calculated for the hardened high speed steel drills using the maximum normal stress theory as follows [3]:

$$\sigma_c = 0.35\sigma_n + 0.65\sqrt{\sigma_n^2 + 4\tau^2} \leq \sigma_p \quad (2-30)$$

Which gives: $(\sigma_c)_{max} = \frac{36.6M_d}{D^3} \leq \sigma_p = \frac{\sigma_u}{Safety\ factor}$ (2-31)

The corresponding feed is given by:-

$$S_s \leq \left(\frac{\sigma_p \cdot D^3}{(36.6)K_{sm} \cdot K_{corr} \cdot 2 \cdot K_{f1}(D_2^{1.8} - D_1^{1.8})} \right)^{\frac{1}{2}} \quad (2-32)$$

Where : σ_c ...Combined stress resulting from both the normal and shear stresses (N/mm²) , $[\sigma_n , \sigma_p , \sigma_u]$...Normal, Permissible and Ultimate stresses on drill material respectively (N/mm²) . τ ...Torsional shear stress on drill cross section (N/mm²).

(2-2-2-3)Clamping torque on twist drill shank (M_c)

(2-2-2-3-1)In case of holding straight shank drills using a 3-jaw chuck

The clamping force per jaw of the 3 jaw chuck can be expressed as [5]:

$$P_{clamp} = 450 D_s \quad (N) \quad (2-33)$$

The clamping torque (M_c) is calculated as follows:-

$$M_c = 3 (450 D_s) \cdot \mu_c \cdot \frac{D_s}{2} = (675) \mu_c \cdot D_s^2 \quad (N.mm) \quad (2-34)$$

The drilling torque must be less than the clamping torque; therefore the corresponding feed is given by:

$$\therefore S_f \leq \left(\frac{(675)\mu_c \cdot D_s^2}{K_{sm} \cdot K_{corr2} \cdot k_{f1} (D_2^{1.8} - D_1^{1.8})} \right)^{\frac{1}{n}} \quad (2-35)$$

Where : P_{clamp} ...Clamping force per jaw of the 3 jaw chuck (N) , D_s ...Shank diameter of twist drill (mm) , M_c ...Clamping torque on the twist drill shank (N.mm), μ_c ...Coefficient of friction between twist drill shank and the chuck jaws.

(2-2-2-3-2)In case of holding straight shank drills using a collet chuck

The clamping force on the workpiece can be expressed as [3]:

$$W = \frac{2 F_h \cdot L_w}{d_m \tan (\alpha_1 + \lambda_1) [\tan (\alpha_2 + \lambda_2) + \tan \lambda_3]} - i_j \times 0.375 E_c y_c (d_1/l_1)^3 h_j (\phi' + \sin \phi' \cos \phi' - \frac{2 \sin^2 \phi'}{\phi'}) \quad (2-36)$$

The thread angle (α_1) is given by:

$$\alpha_1 = \tan^{-1} \frac{P_{h2}}{\pi d_m} \quad (2-37)$$

The clamping torque (M_c) is calculated as follows:

$$M_c = W \cdot \mu_4 \cdot \frac{D_s}{2} \quad (2-38)$$

The drilling torque must be less than the clamping torque; therefore the corresponding feed is given by:

$$\therefore S_f \leq \left(\frac{W \cdot \mu_4 \cdot D_s}{2 K_{sm} \cdot K_{corr2} \cdot K_{f2} (D_2^{1.8} - D_1^{1.8})} \right)^{\frac{1}{n}} \quad (2-39)$$

Where : W ...Clamping force on work piece in case of holding straight shank drills using a collet chuck (N) , F_h ...Hand clamping force(N) , L_w ...Wrench arm (mm) , d_m ... Mean diameter of collet clamping thread (mm) , α_1 ...Thread lead angle of collet clamping nut (degree) , α_2 ...Wedge angle of collet jaws (degree) , λ_1 ...Friction angle between threads (degree) , λ_2 ...Friction angle at collet jaw surface (degree) , λ_3 ...Friction angle between nut and collet (degree) , i_j ...Number of collet jaws , E_c ...Young's modulus for chuck material (N/mm²) , y_c ...Clamping distance (mm) , d_1 ...Minimum collet diameter (mm) , l_1 ...Collet overhanging length (mm) , h_j ...Collet jaw thickness (mm) , ϕ' ...Sector angle

of collet chuck (radian) , p_{th2} ...Clamping nut thread pitch (mm) , μ_4 ...Coefficient of friction between twist drill shank and collet chuck jaws.

(2-2-3) Drill breakage along the hole depth

In case of deep hole drilling, when the drill is fed into the hole continuously without withdrawal, the feed must be constrained with the following value to avoid drill breakage due to gripping inside the drilled hole [6]:

$$\therefore S_3 \leq \left(\frac{L_{hole}}{k_v \times 1. D^{z-1} \cdot K_{f4}} \right)^{\frac{1}{n}} \tag{2-40}$$

Where : v ...Cutting speed (m/min) , K ...Coefficient for work piece material effect on critical hole depth , K_{f4} ...Cutting fluid correction factor for critical hole depth.

(2-2-4) Surface roughness

Although the drilling operation is a roughing operation which is usually followed by semi-finishing and finishing operations and inspite of the fact that surface roughness is a criterion for finishing rather than for roughing from which it may seem that it has no significance in drilling, it does in fact affect the finish machining allowance left in rough machining to avoid excessive number of finishing passes.

The roughness height affects the grade of accuracy of the machined part. It is assumed that the roughness must not exceed half the radial tolerance [7].

The standard tolerance grade (diametral tolerance) is given by:

$$ITZ = (i_t) (IT_z) \tag{2-41}$$

The tolerance factor (i_t) is given by [10]:

$$i_t = (0.45)\sqrt[3]{D} + (0.001)D \tag{2-42}$$

According to the ISO 286-1/1988 for limits and fits, the values of (IT_z) are found to follow a geometric progression with a progression ratio $\sqrt[5]{10} = 1.585$, which is expressed as a function of the grade of accuracy (z) as follows:

$$IT_z = (1.586)^{z-1} \quad \text{for } 6 \leq z \leq 18 \tag{2-43}$$

As roughness height must be smaller than or equal to half radial tolerance [10]:

$$R_z \leq \frac{1}{2} (\text{Radial tolerance}) \tag{2-44}$$

The roughness height in drilling is therefore given by:

$$R_z = \frac{f/2}{\cot \phi + \cot \omega} \tag{2-45}$$

It follows that:

$$\therefore S_9 = 2 \left[(\cot \phi + \cot \omega) \left(\frac{R_z (LDN)}{1000} \right) \right] \tag{2-46}$$

Where : ITZ...Standard tolerance grade (μm) , IT_z...Number of tolerance units , i_t...Standard tolerance factor(μm) , z...Accuracy grade(z=1,2,.....,16) , R_z...Average peak to valley roughness height (μm) , ϕ ...Half point angle of twist drill (degree) . ω ... Flute helix angle (degree)

If the maximum allowable feed due to drilling process constraints will lead to a roughness height greater than the permissible value, the feed should be reduced to fulfill the surface roughness requirement since the feed is known to have a higher effect on surface roughness than the cutting speed.

(2-2-5) Permissible burr height

Burr height and consequently burr type can be predicted and controlled by controlling the cutting conditions. Assuming a permissible burr height, the corresponding feed is given by [e]:

$$\therefore s_{10} \leq \left(\frac{(Br)_p}{K_{Br} \cdot D^{x_2}} \right)^{\frac{1}{z_2}} \tag{2-47}$$

The maximum permissible value for burr height is taken (1 mm) which is the threshold value of uniform burr which is easy to be removed.

Where : [Br , (Br)_p]... Burr height and permissible burr height respectively (mm) , K_{Br}... Coefficient for work piece material in burr height formula.

(2-3) Objective function of the machining process

The cutting conditions for minimum cost are obtained by minimizing the cost equation, given by [3]:

$$K_v = \frac{C_1}{C_v} T^m \cdot s^{y_{ve}-1} \cdot a^{x_{ve}} + \frac{C_2}{C_v} T^{m-1} \cdot s^{y_{ve}-1} \cdot a^{x_{ve}} \tag{2-48}$$

Where C₁ and C₂ are the cost functions, where:

C₁ = $\left(\frac{\pi \cdot D \cdot L}{1000} \right) (K_l + K_{m/c})$ machine & labour cost function in L.E /minute.

C₂ = $\left(\frac{\pi \cdot D \cdot L}{1000} \right) (K_{TP} + K_{TR} + K_{TC})$ tool cost function in L.E /edge.

The condition for minimum machining cost is [5]:

$$T_{opt} = \left(\frac{1-m}{m} \right) \frac{C_2}{C_1} \tag{2-49}$$

Where : K_v...Variable machining cost per piece (L.E) , C₁...Machine and labour cost rate (L.E/min) , C₂...Tooling cost rate (L.E /edge) , [T , T_{opt}]... Tool life, Optimum tool life respectively (min) , m...Tool life exponent in the cutting speed-tool life relationship , C_v...Coefficient for work piece material in cutting speed tool-life relationship , a...Depth of cut in case of hole enlarging (mm) , K_l...Labour cost rate (L.E / min) , K_{m/c}...Machine cost rate (L.E / min) , K_{TC}...Tool changing cost per cutting edge (L.E /edge) , K_{TP}...Capital tool cost per cutting edge (L.E /edge) , K_{TR}...Tool regrinding cost per cutting edge (L.E /edge)

In the present work the minimum machining cost will be considered the objective function of the optimization problem while retaining certain surface quality.

(2-4) Optimization Strategy

In view of the machining process constraints, it can be realized that it is impossible to increase all of the machining variables (v, s) simultaneously to shorten the machining time and hence to reduce the manufacturing cost without exceeding one or more of the process constraints.

The optimum values of the machining variables should therefore be determined by following a careful strategy based on complete knowledge of the degree of influence of each individual variable on the different constraints encountered in machining.

Keeping a constant tool life, the rate of metal removal is found to increase with the increase of feed and decrease of the cutting speed.

Accordingly, for minimum manufacturing cost the maximum drill diameter is selected. Using this value the maximum possible feed has to be determined in view of the machining process constraints which are dependent on the feed and the drill diameter. The optimum cutting speed is to be calculated from tool life relationship.

Logic checks are to be carried out for the fulfillment of the rest of constraints which are dependent on the cutting speed beside the feed and introducing the necessary modifications at each step if any of the constraints is exceeded.

The strategy also aims not only to minimize the machining cost per hole but also to improve the hole quality as far as possible by reducing burr to minimum height and controlling surface roughness. Also, the optimum parameters must avoid the gripping of the drill inside the hole which leads to drill breakage especially in case of deep hole drilling by determining the critical hole depth which is also useful in the proper selection of deep hole and peck drilling cycle parameters on CNC machine tools. For a given set of inputs there will be a unique pair of optimum feed and speed for minimum machining cost per hole. The development of the optimization strategy for economic drilling conditions is shown in the flow chart figure (1).

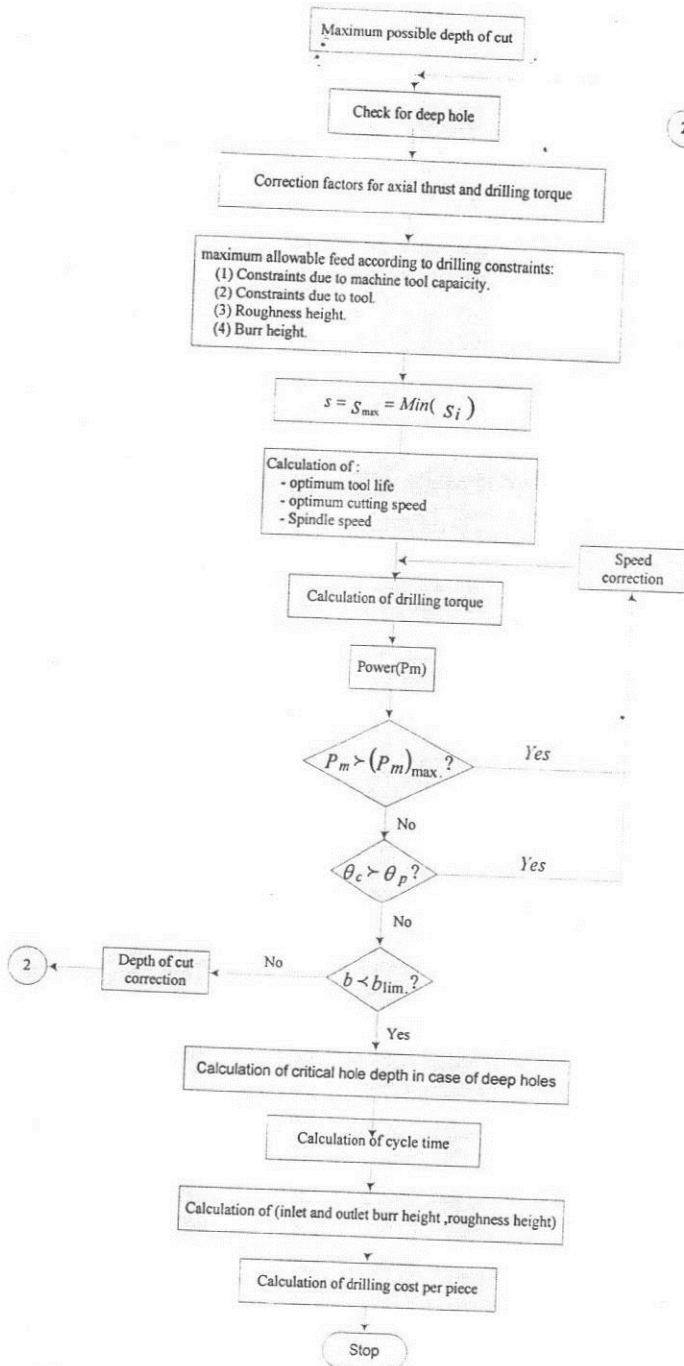


Fig. (1) Optimization strategy of the drilling process

(2-4-1) Determination of the initial values of the machining variables

(2-4-1-1)Depth of cut (a) : The initial value will be the largest possible depth of cut determined from the machining allowance.

In case of drilling in solid:
$$a_{max} = \frac{D}{2} \tag{2-50}$$

In case of enlarging a hole:
$$a_{max} = \frac{D_2 - D_1}{2} \tag{2-51}$$

(2-4-1-2)Feed (s) : The initial value of the feed will be the largest permissible value obtained from the different technical and technological constraints.

(2-4-1-3)Optimum tool life : The initial value of tool life will be the optimum value calculated according to the machining process which is the minimum machining cost.

$$T_{opt} = \frac{C_2}{C_1} \left(\frac{1-m}{m} \right) \tag{2-52}$$

(2-4-1-4)Optimum cutting speed (v) : Using Taylor's tool life relationship the optimum cutting speed (v_{opt}) is given by:-

$$v_{opt} = \frac{K_{tv} \cdot K_t \cdot K_{f2} \cdot C_{vs} \cdot D^{2vs}}{T^m \cdot s^{ys}} \quad \text{.....in case of drilling in solid} \tag{2-53}$$

Or
$$v_{opt} = \frac{K_{tv} \cdot k_t \cdot K_{f2} \cdot C_{ve} \cdot D^{2ve}}{T^m \cdot s^{ys} \cdot a^{2ve}} \quad \text{.....in case of enlarging holes} \tag{2-54}$$

Where : v_{opt} ...optimum cutting speed (m/min) , K_t ...Correction factor for drill material effect on cutting speed , K_{tv} ...Correction factor for cutting speed due to hole depth , K_{f2} ...Cutting fluid correction factor for cutting speed-tool life relationship , [C_{vs} , C_{ve}]...Coefficient for work piece material in cutting speed tool-life relationship in case of drilling in solid and hole enlarging respectively.

(2-4-2) Logic checks of the process constraints

The initial values (v,s,a) obtained are used for the calculation of the basic machining quantities which are power consumption (P_m), cutting temperature (θ_c) and the limiting width of cut (b_{lim}) at which chatter begins. Each of these quantities is compared with the corresponding permissible value. In case any of these values is exceeded the most proper machining variable is modified to attain safe limits.

(2-4-2-1) Power consumption : The power consumption in cutting is given by:

$$P_m = \frac{M_s \cdot 2\pi n}{(60000)\eta_m} \quad (kW) \tag{2-55}$$

The calculated motor power must be less than or equal to the maximum available motor power. If the calculated motor power is greater than the permissible value, it will be necessary to modify the cutting speed which has the most significant

effect on the power constraint in order to avoid an excessive reduction in the production rate.

$$v_{mod} = \left(\frac{(P_m)_{max}}{(P_m)} \right) v_{opt} \quad (2-56)$$

Where : P_m ...Motor power (at motor shaft) (kW) , n ...Spindle speed (r.p.m) , η_m ...Overall mechanical efficiency.

(2-4-2-2) Cutting temperature : The cutting temperature (θ_c) is given by the following relationship [8]:

$$\theta_c = C_\theta v^{x_3} s^{y_3} K_{f3} \quad (2-57)$$

If $\theta_c > \theta_p$ then
$$v_{mod} = \left(\frac{\theta_c}{\theta_p} \right)^{\frac{1}{x_3}} v_{opt} \quad (2-58)$$

Where : θ_c ...Cutting temperature in drilling ($^{\circ}C$) , θ_p ...Permissible cutting temperature ($^{\circ}C$) , C_θ ...Work piece and tool materials coefficient in cutting temperature relationship . K_{f3} ...Cutting fluid correction factor for drilling temperature.

(2-4-2-3) Dynamic stability against chatter : In order to guarantee chatter-free machining the width of cut should be sufficiently less than the limiting width of cut (b_{lim}) which is calculated for the used MFTW system under the given cutting conditions as follows[9]:

$$\therefore b_{lim} = \frac{2 K_d}{R} \quad \text{with} \quad R = r_h \cdot \left[\sqrt{4 + \left(\frac{r_v}{r_h} \right)^2} \right] \quad (2-59)$$

According to equation (2-54) the limiting width of cut can be determined for the assigned cutting conditions given that the system dynamic stiffness (K_d) has been determined. Invariably (K_d) can be deduced if (b_{lim}) has been experimentally determined. Similarly, the dynamic cutting coefficient (R) can be determined on a machine with known dynamic stiffness and limiting width of cut.

where
$$r_h^* = K_{rh} \cdot v^{x_5} \cdot s^{y_5} \quad , \quad r_v^* = K_{rv} \cdot v^{x_6} \cdot s^{y_6} \quad (2-60)$$

Accordingly, the specific dynamic cutting coefficient (R) can be determined as a function of work piece material and cutting parameters as follows:

$$R = K_r \cdot v^{x_7} \cdot s^{y_7} \quad (2-61)$$

The width of cut for a specified hole enlarging operation is given by:

$$b = \frac{D_2 - D_1}{2 \sin \varphi} = \frac{a}{\sin \varphi} \quad (2-62)$$

If $b > b_{lim}$ it will be necessary to reduce the depth of cut in order to avoid occurrence of chatter, the modified value of the depth of cut is given by:

$$a = b_{lim} \sin \varphi \quad (2-63)$$

Where : K_d ...System dynamic stiffness (N/mm) , R ...Specific dynamic cutting coefficient (N/mm²) , r_h^* ... Specific cutting stiffness (N/mm²) , r_v^* ... Specific negative damping coefficient (N/mm²) , K_{rh} ...Work piece and tool material coefficient in the specific cutting stiffness relationship , K_{rv} ...Work piece and tool material coefficient in the specific negative damping coefficient relationship , K_r ...Work piece and tool material coefficient in the dynamic cutting coefficient relationship.

(2-4-2-4) Feed limits: In practice, the machine tool maximum and minimum feed boundaries act as constraints. Also, the discrete feed steps on the conventional machines are considered as an additional constraint.

Moreover, in a drilling operation the undeformed chip thickness (h) and hence the feed per tooth (s_z) should not be smaller than a certain value, in order to avoid slipping and rubbing of the cutting edge without cutting, the smallest feed per tooth is given by [3]:

$$(S_z)_{\min} = 0.025 \text{ mm/tooth} \quad (2-64)$$

If the calculated feed for a given drill diameter is found to be smaller than this value or smaller than the available feed limit on the machine, the decision to be followed will depend on the type of constraint yielding this value of feed.

Where : s_z ...Feed per tooth ($s / 2$) (mm/tooth).

(2-4-2-4-1)Drilling machine capacity: In this case the selection of a smaller drill diameter to start with, followed by successive enlarging steps will help in selecting reasonably larger feed fulfilling such constraints.

(2-4-2-4-2)Drill strength constraints: In case the drill strength is the most decisive constraint in determining feed then manual instead of automatic feed must be carried out in case of conventional machines and the feed value will depend on the sensitivity of the labour while in case of CNC machines manual feed is not available so that non conventional machining method is recommended.

Any trial to reduce the drill diameter in this case will never lead to the increase of the feed due to the expected drastic reduction of the properties of the drill cross-section and hence the drill strength with the reduction of the drill diameter but will lead to failure of the twist drill under combined torsional shear and compressive stresses.

On the other hand if the calculated feed is greater than the maximum feed dictated by the machine then the maximum feed is to be selected. Also the feed is corrected, if necessary to suit the kinematic data of the machine where the nearest smaller feed is selected or the nearest higher feed if it does not exceed the calculated feed by 5 %.

(2-4-2-5) Spindle speed limits : The selected spindle speed should be within the machine available limits so that the machine tool maximum and minimum spindle speed boundaries act as constraints on the drilling process. Also, the discrete

spindle speed steps on the conventional machines are considered as an additional constraint.

If the selected spindle speed is greater than the maximum speed available on the machine tool, the highest speed can be selected, while when the selected spindle speed is lower than the minimum speed available on the machine, the intended drilling operation cannot be conducted on the selected machine tool so that an alternative machine tool with lower speeds should be used.

This spindle speed is corrected according to the available range of the machine where the nearest lower speed is selected or the nearest higher speed if it does not exceed the calculated speed by 5 %.

3-Conclusion

A logic algorithm has been established for the optimization of the machining variables in drilling. The algorithm is based on the minimum machining cost criterion. Decisive constraints which have not been previously accounted for are taken into consideration. The developed procedure overcomes the difficulties due to the non linear nature of the machining process and provides direct and simple means for the determination of the optimum machining variables.

4-References

- [1] Kee P.K. and Ibrahim R.N. , "Computer aided optimization of machining conditions in rough drilling operations", 4thIndustrial engineering research conference proceedings, Norcross, GA, USA., PP.1090-1100, 1995.
- [2] Jun Wang , "Development of drilling optimization strategies for CAM applications", Journal of materials processing technology, Vol.84, PP.181-188, 1998.
- [3] A.S.Abd Allah , "Optimization of the Drilling Cycle on Conventional and CNC Machine Tools", M.Sc Thesis ,Military Technical College ,Cairo , 2006.
- [4] El-Hakim M. and El-Mously M. , "Investigation of the static performance of a vertical drilling machine using a reduced scale model", Proceeding of first conference of mechanical power engineering, Ain-Shams university, Vol. III, 1977.
- [5] Abd El-Salam M. , "Computer aided selection of the optimum cutting conditions in drilling", Journal of engineering and applied science, Vol.6, No.6, faculty of engineering, Cairo university, December 1993.
- [6] EL-Hakim M.A. and Abd El-Salam M. , "In-process torque monitoring to avoid drill breakage in deep hole drilling using standard twist drills", Scientific bulletin, faculty of engineering, Ain-Shams university, Vol. 38 , PP.635-662, 2003.
- [7] Code of practice for surface roughness, Society of mechanical engineers, P.19, Egypt, Feb.1983.

- [8] **El-Hakim M.A.** , "The planning of machining processes by the aid of digital computers", Proc. Int. computer technology conference ASME, PP.158-172, 1988.
- [9] **Abd El-Salam M.** , "Effect of chisel edge and flank damping on chatter in drilling", Scientific bulletin, faculty of engineering, Ain shams university, Vol.33, No.1, PP.369-392, 1998.



Optimization of the Drilling Cycle on Conventional and CNC Machine Tools

Part II - Experimental Verification of the Optimization Model

Prof. Dr. / Mohamed A. El Hakim, Dr. / Wael S. Moughith & Engineer /
Ahmed S. Abd-Allah*

*Faculty of engineering – Ain shams university, Egyptian Armed Forces & Egyptian
Armed Forces*

*Corresponding author. Tel: 002-012-5713484, E-mail address: asabdallah75@yahoo.com

Abstract

The paper presents an experimental verification for the optimization model of the drilling cycle. A brief comparison of handbook recommended and optimal solutions has shown considerable machining cost advantage of the later and investigates the economic superiority of using optimum machining variables over the "feasible" handbook recommendations and highlights the increased benefits of using optimization in process planning in computer aided manufacturing.

Keywords: Experimental verification; Recommended machining variables; Optimum machining variables.

1- Introduction

Many machining handbooks provide only initial recommendations for the values of cut in drilling which are the feed and the cutting speed leaving most of the problem to the process planner to solve [1].

As stated both methods for selection of the values of cut either handbook recommendations or personnel experience do not take the process constraints into account and hence lead to values of cut which are too low in order to avoid overloading of the machine and tool failure. Moreover even if the recommended values of cut are feasible they are too far from the economic values [2].

A comparison between the recommended and optimized solutions is carried out to assess the developed optimization strategies [3]. Numerical simulation studies have been carried out to investigate both the optimal solutions and the handbook recommendations.

Each numerical study incorporates a quantitative comparison between the optimized and the handbook recommended values of cut for a certain hole, considering a given machine-fixture-tool-workpiece system.

2- Case studies for the application of the optimization algorithm

(2-1) Case study (1): Drilling a blind hole on each of a conventional and CNC machining center

The comparison is carried out for drilling a hole $\phi 10\text{mm} \times 20\text{mm}$ in St50 workpiece with HSS twist drill using a conventional drilling machine "2150" with maximum drilling capacity of $\phi 50\text{ mm}$ then using a CNC machining center "Fadal VMC15" applying dry cutting.

The case study represents drilling a shallow hole in solid in one step on each of a conventional and CNC machines. This case study aims to investigate the effect of the machine type on the selected machining variables and to demonstrate the effect of the optimum machining variables on the machining time and the machining cost. The specifications of the MFTW system are given in appendix (A).

(2-1-1) Drilling on conventional column drilling machine "2150"

(2-1-1-1) Optimum machining variables

Applying the optimization model [4], the machining variables leading to minimum machining cost are shown in table (1). The required diameter will be drilled in a single pass.

(2-1-1-2) Recommended machining variables

Twist drill handbook [5] provides recommended operating parameters for producing holes in a variety of materials with twist drills. According to the handbook, the recommended cutting speed and feed for drilling steel "St50" to the prescribed diameter is 16 m/min and 0.13 mm/rev. For machine 2150,

according to the kinematic data of the machine, the recommended spindle speed is 500 r.p.m and the recommended feed is 0.14 mm/rev.

Applying each of the recommended and the optimum values of the machining variables separately under the same drilling conditions to drill two holes of 10 mm diameter x 20 mm depth, the following was obtained:

- The optimum machining variables reduce the machining time by about 30% but reduce the machining cost by about 5% only due to the high idle time cost compared with the recommended machining variables.

Table (1) Optimum and recommended machining variables for drilling $\phi 10\text{mm}$ hole in St50

Machining variables	Recommended values	Optimum values
Cutting speed(m/min)	16	15.61
spindle speed (r.p.m)	500	500
feed (mm/rev)	0.14	0.2
machining time (min)	0.33	0.23
cycle time (min)	2.67	2.57
machining cost (L.E)	0.79	0.76

(2-1-2) Drilling on CNC machine "Fadal VMC15"

(2-1-2-1) Optimum machining variables

The machining variables leading to minimum cost are shown in table (2).

(2-1-2-2) Recommended machining variables

According to the handbook [5], the recommended cutting speed and feed for drilling a hole $\phi 10\text{mm}$ in St50 is 16 m/min and 0.13 mm/rev respectively.

Applying these machining variables separately in the same drilling conditions, the following was observed:

The optimum machining variables reduce the machining time by about 45% and consequently reduce the machining cost by about 13% compared with the recommended machining variable (which is important due to the high machine and labor cost rates).

Table (2) Optimum and recommended machining variables for drilling $\phi 10\text{mm}$ hole in steel "St50"

Machining variables	Recommended values	Optimum values
spindle speed (r.p.m)	509	472
feed (mm/rev)	0.13	0.26
machining time (min)	0.35	0.19
cycle time (min)	1.19	1.02
machining cost (L.E)	2.55	2.21

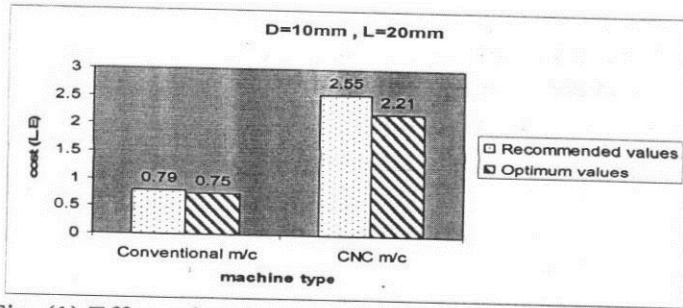


Fig. (1) Effect of optimum variables on the machining cost

(2-2) Case study (2) : Deep hole drilling in different materials

The comparison in this case is carried out for drilling a deep hole of diameter 8 mm for a depth 40 mm using St50 then steel grade CK50 as workpiece materials and HSS twist drill on conventional machine "2150" applying dry cutting.

This case study aims to:

- Investigate the problems of deep hole drilling using standard twist drills.
- Demonstrate the effect of the workpiece material on the value of the critical hole depth in case of deep holes.

(2-2-1) Drilling Structural steel "St50"

In this case study the data about the same hole $\phi 8\text{mm} \times 40\text{mm}$ is introduced, first selecting continuous feed then applying drill withdrawal as a feed type.

(2-2-1-1) Optimum machining variables

First continuous drilling is applied although the hole is a deep hole. Then applying drilling withdrawal in case of deep holes at the critical depth is selected as feed type.

In case of applying continuous drilling, the calculated value for the feed so as to avoid drill breakage along the hole depth will lead to small values of feed which are smaller than the smallest feed on the machine feed gear box which oblige the user either to use manual feed or to stop feeding and withdraw the drill before breakage.

So, in case of applying continuous drilling the algorithm confirms that continuous drilling will lead to drill breakage and applying drill withdrawal will lead to better results. The optimum machining variables are shown in table (3).

(2-2-1-2) Recommended machining variables

The recommended cutting speed and feed are 16 m/min and 0.1 mm/rev respectively. The cutting speed is decreased by a factor " K_v " and the feed is decreased by a factor " K_s " according to the hole depth to diameter ratio [5].

In our case study the ratio L/D is 5 denoting a value 0.7 for " K_v " and 0.45 for " K_s ". These correction coefficients are taken into consideration for proper,

comparison between the optimum and the recommended machining variables. So, the recommended cutting speed and feed are 11.2 m/min and 0.045 mm/rev respectively.

For machine "2150", the recommended spindle speed is 350 r.p.m and the recommended feed is smaller than the smallest feed on the machine gear box, leading to manual feed.

Applying the previous machining variables to drill two deep holes of diameter 8 mm to a depth of 40 mm in the same drilling conditions on the machine "2150", the following is obtained:

- Applying the optimum machining variables prevents drill breakage, as the user stops the feed and withdraw the drill when the hole depth approaches the estimated critical hole depth (23mm) then the drilling operation is resumed till the required depth is attained without breakage of the used twist drills. Also, the optimum machining variables reduce the cycle time by about 32% and consequently reduce the machining cost by about 31% compared with the recommended machining variables.
- For applying the recommended machining variables, manual feed is used, which depends on the sensitivity of the worker, without recommendation of the maximum permissible depth of the hole before tool gripping occurs, the unnecessary stops will increase the idle time while exceeding the critical depth will lead to drill breakage.

Table (3) Optimum and recommended machining variables for drilling deep hole $\phi 8\text{mm} \times 40\text{mm}$ in steel "St50"

Machining variables	Recommended values "continuous drilling"	Optimum values "withdrawing at 23.5 mm"
spindle speed (r.p.m)	355	500
feed (mm/rev)	manual feed	0.14
machining time (min)	2.1	0.61
cycle time (min)	4.6	3.13
machining cost (L.E)	1.34	0.92

(2-3-2) Drilling carbon Steel "CK50"

The data about the same hole $\phi 8\text{mm} \times 40\text{mm}$ is introduced, first selecting continuous feed then applying drill withdrawal as a feed type.

(2-3-2-1) Optimum machining variables

First continuous drilling is applied although the hole is a deep hole. Then applying drilling withdrawal in case of deep holes at the critical depth is selected as feed type.

In case of applying drill withdrawal at critical hole depth, the calculated value for the critical depth for material "CK50" at the maximum permissible feed and

the actual cutting speed is greater than the required hole depth which means that the drilling operation will continue till the assigned depth without drill breakage.

The interpretation of the difference between the two steel materials (St50,CK50) when calculating the critical hole depth at similar machining variables is due to the difference in ductility, as steel CK50 is less ductile than steel St50 which leads to less friction forces during drilling. So, the rate of increase of drilling torque and axial force with increasing hole depth is smaller in case of CK50 leading to greater values of critical depths in CK50 than St50. Then the optimum machining variables are shown in table (4).

(2-3-2-2) Recommended machining variables

The recommended cutting speed and feed are 14 m/min and 0.08 mm/rev respectively. As the hole is a deep hole the correction coefficients for cutting speed and feed are taken into consideration. In our case study the ratio L/D is 5 denoting a value 0.7 for "K_v" and 0.45 for "K_s". So, the recommended cutting speed and feed are 9.8 m/min and 0.036 mm/rev respectively.

For machine "2150", the recommended spindle speed is 350 r.p.m and the recommended feed is smaller than the smallest feed on the machine gear box, leading to manual feed.

Applying these machining variables separately in the same drilling conditions to drill two holes of 8 mm diameter to 40 mm depth in steel rod grade "CK50", the following was obtained:

- Applying the optimum machining variables, the drilling operation is continued till the required depth without drill breakage as the critical depth is not exceeded and no need for drill withdrawal. Also, the optimum machining variables reduce the cycle time by about 22% and consequently reduce the machining cost by about 23% compared with the recommended machining variables.
- For applying the recommended machining variables, manual feed is used, which increase the cycle time due the unnecessary stops.

Table (4) Optimum and recommended machining variables for drilling deep hole 8mm×40mm in steel "CK50"

Machining variables	Recommended values	Optimum values
spindle speed (r.p.m)	355	500
feed (mm/rev)	manual feed	0.1
machining time (min)	2.03	0.89
cycle time (min)	4.1	3.21
machining cost (L.E)	1.21	0.94

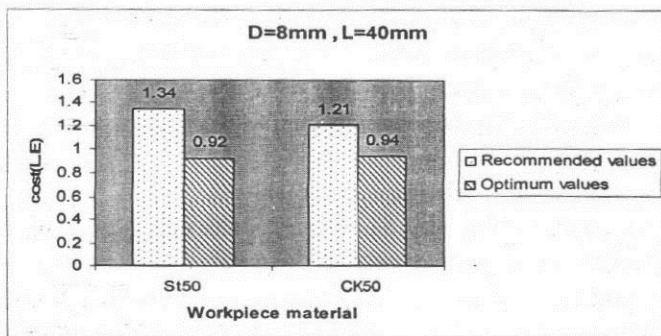


Fig. (2) Effect of optimum variables on the machining cost

(2-3) Case study (3) : Drilling deep holes on machining centers using fixed cycles G81* and G83*

The comparison is carried out for drilling a deep hole of diameter 10 mm for a depth 50 mm using structural steel "St50" as workpiece material and HSS twist drill on CNC machine "Fadal VMC15" applying dry cutting.

This case study aims to:

- Compare between continuous drilling and applying drill withdrawal and its effect on the cycle time and consequently the machining cost.
- Assignment of the parameters of the deep hole drilling cycles on CNC machine tools.

(2-3-1) Using continuous drilling

The drilling operation is performed applying continuous drilling although the hole is a deep hole. The optimum machining variables are shown in table (7). As shown the feed is limited to avoid drill breakage along the hole depth, which increase the machining time but reduce the idle time as drill withdrawal is not applied.

(2-3-2) Applying drill withdrawal

The data about the required hole is the same as in (2-3-1) except the feed type, where drill withdrawal in case of deep holes is selected. In case of drill withdrawal the optimum machining variables are shown in table (5).

The calculated value for the critical hole depth is 24.35 mm indicating that there will be two drill withdrawals for chip removal and drill cooling to avoid drill breakage.

- G81: Drilling cycle used for drilling shallow holes ($L/D < 2.5$) and for center drilling [4].
- G83: Deep hole drilling cycle used for materials producing long chips ($L/D \geq 2.5$) also called withdrawal drilling cycle. It is used mainly when the drill withdrawal for chip removal and drill cooling is essential [4].

As shown from the previous data, applying drill withdrawal at critical depth leads to an increase in feed by about 73% thus reducing the machining time by about 67.5% while the idle time is increased with about 1% (the increase in idle time is due to the withdrawal time which is very small due to the high rapid traverse speed in CNC machines).

(2-3-3) Recommended machining variables

The recommended cutting speed and feed for drilling the required hole are 16 m/min and 0.128 mm/rev respectively. As the correction coefficients for cutting speed and feed are taken into consideration. In our case study the ratio L/D is 5 denoting a value 0.7 for " K_v " and 0.45 for " K_s ". So, the recommended cutting speed and feed are 11.2 m/min and 0.06 mm/rev respectively.

For machine "Fadal VMC15", the recommended spindle speed is 357 r.p.m and the recommended feed is 0.06 mm/rev.

Applying these machining variables separately in the same drilling conditions, the following was observed:

- Applying the optimum machining variables in case of drill withdrawal, using the fixed cycle G83, it is observed that the feed is stopped and the drill is retracted above the part to R-level automatically each time the hole depth approaches the estimated critical hole depth. The drilling operation is then resumed until the assigned full depth is attained without breakage of the used twist drill.
- Applying the optimum machining variables in case of continuous drilling, using fixed cycle G81, and the drilling operation is continued till required depth without breakage.
- The optimum machining variables in case of drill withdrawal reduce the cycle time by about 44% than the cycle time in case of continuous drilling and consequently reduce the machining cost by about 43.6%.
- Applying the recommended machining variables, using fixed cycle G81, the drilling operation is continued till the required depth but the machining time is 2.57 minute and the cost is about 7.3 L.E which if compared with the machining time and cost in case of optimum machining variables while applying continuous feed, the optimum variables are found to reduce machining time by about 36.5% and reduce machining cost by about 27.5%, which shows that the recommended machining variables if they are feasible they are too far from the economic values.
- From previous numerical data and experimental observations it is clear that drill withdrawal is recommended for cases of severe cutting conditions inspite of the increased non productive times.

Table (5) Optimum and recommended machining variables for drilling deep hole $\phi 10\text{mm} \times 50\text{mm}$

Machining variables	Recommended values	Optimum values "continuous drilling"	Optimum values "Applying drill withdrawal"
spindle speed (r.p.m)	357	510	399
feed (mm/rev)	0.06	0.07	0.26
machining time (min)	2.57	1.63	0.53
cycle time (min)	3.4	2.46	1.38
machining cost (L.E)	7.29	5.29	2.98

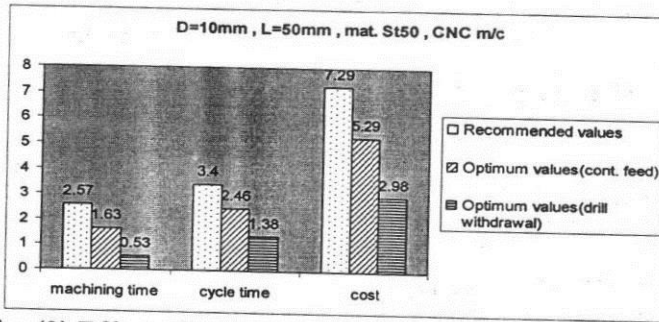


Fig. (3) Effect of optimum variables on the machining cost

3- Conclusion

The case studies have been experimentally implemented and reveal that:

- The optimum machining variables satisfy the constraints on the drilling process either due to the machine tool capacity or due to the twist drill itself.
- The use of the optimum machining variables leads to a considerable decrease of the machining time and hence the machining cost compared with the recommended machining variables especially on CNC machines.
- The reduction in the machining time and the machining cost when using the optimum machining variables is more obvious in case of CNC machines than conventional machine tools. This is referred to the high idle time cost in case of conventional machines and the discrete feed and speed steps on the feed and speed gear boxes in case of conventional machines. As a result this may lead to the reduction of the selected feed or spindle speed than optimum values according to the kinematics of the used machine compared with the stepples motors used in case of CNC machines.

- The value for the critical hole depth given by the optimization algorithm which is fed to the drilling cycle (G83) on CNC machines prevents drill breakage.
- Drill breakage caused by jammed chips in deep holes has not been encountered.

The optimization strategy demonstrated the effect of each of the elements of the MFTW system on selecting the optimum machining variables. The study indicates the importance of using optimization in process planning in modern computer based manufacturing.

4- Appendices

Appendix (A) Specifications of the MFTW system

- **Machine tools used:**

	2150	VS32	Fadal-15
<u>General specifications</u>			
Machine tool	2150	VS32	Fadal-15
Maximum drilling diameter(D_{max})....(mm)	50	32	76.2
Minimum drilling diameter(D_{min})....(mm)	1	2	1
Maximum spindle speed(n_{upper})....(r.p.m)	1400	2240	3750
Minimum spindle speed(n_{lower})....(r.p.m)	31.5	56	75
Maximum feed(S_{upper})....(mm/rev)	1.6	0.45	---
Minimum feed(S_{lower})....(mm/rev)	0.1	0.11	---
Maximum feed(U_{upper})....(mm/min)	---	---	6350
Minimum feed(U_{lower})....(mm/min)	---	---	0.254
Maximum permissible axial force(F_{ap})....(N)	16000	8000	6590
Maximum permissible torque(M_{tp})....(N.mm)	400000	80000	81818.2
Motor power(P_m)....Kw	5.625	2.25	5.625
Motor electrical efficiency(η_e)	0.85	0.85	0.85
Number of spindle speeds(Q_n)	12	9	---
Number of feeds(Q_s)	9	4	---
Rapid traverse speed(in z direction)....(mm/min)	---	---	10160
System dynamic stiffness(K_d)....(N/mm)	10000	6500	4000

• **Cutting tools used:**

Tool material : HSS
Helix angle(ω) : 20 degree
Tool end condition constant (C) : 2
Grinding machine cost rate ($G_{m/c}$) : 0.14 (L.E/min)
Tool life exponent (m) : 0.2
Coefficient of friction between drilling shank and 3 jaw chuck (μ_c) : 0.2
Coefficient of friction between drilling shank and collet chuck (μ_4): 0.2
Tool material correction factor for cutting speed calculation (K_t) : 1
Point angle(2ϕ) : 118 degree
Permissible cutting temperature(θ_p) : 500 (°C)
Tensile strength (σ_u) : 3000 (N/mm ²)
Grinding labor cost rate (G_{rl}): 0.18 (L.E/min)
Young's modulus for tool material(E_t) : 200000 (N/mm ²)

• **Tool fixation (in case of conventional machines):**

Nominal size : 3 jaw size 1	Chuck clamping factor (K_{jc}): 675
Chuck protruding height (L_{ch}) : 125 mm	

• **Tool fixation (in case of CNC machines):**

Nominal size : collet 10mm
Hand force (H): 200N
Wrench arm (L_w): 200mm
Mean diameter of clamping thread (d_m) : 24mm
Thread pitch (p_{th2}) : 1.5mm
Friction angle between threads (λ_1) : 6.56degree
Wedge angle (α_2) : 15degree
Friction angle at collet jaw surface (λ_2) :6.56degree
Friction angle between nut and collet (λ_3) :6.56degree
Collet jaw thickness (h) : 2mm
Young's modulus for chuck material (E_c): 200000

Sector angle (ϕ'): 45 degree
Minimum collet diameter (d_1): 10mm
Collet overhanging length (l_1): 25mm
Chuck protruding height (L_{ch}): 95mm
Number of jaws (i_c): 8
Clamping distance (y): 0.25mm

5- References

- [1] Jun Wang , "Development of drilling optimization strategies for CAM applications", Journal of materials processing technology, Vol.84, PP.181-188, 1998.
- [2] Kee P.K. and Ibrahim R.N. , "Computer aided optimization of machining conditions in rough drilling operations", 4thIndustrial engineering research conference proceedings, Norcross, GA, USA., PP.1090-1100, 1995.
- [3] EL-Hakim M.A. , Moughith W.S. and Abd-Allah A. S. , "Optimization of the Drilling Cycle on Conventional and CNC Machine Tools", "Part I- Formulation of the Optimization Model for the Drilling Cycle", Engineering Research Journal , Helwan university, vol.122 (June 2009), M26-M44 (under publication).
- [4] A.S.Abd Allah , "Optimization of the Drilling Cycle on Conventional and CNC Machine Tools" , M.Sc Thesis ,Military technical College, Cairo, 2006.
- [5] Twist drill handbook, Ghuring company, Germany.

Static and Dynamic testing of Simple Structures Produced by Rapid Prototyping Technique

Prof. Dr. / Mohamed A. El Hakim, Dr. / Atef A. Afifi & Engineer/ Hany F. Mokbel*

Faculty of engineering – Ain shams university, Faculty of engineering & material science – German university in Cairo & Egyptian Armed Forces.

*Corresponding author Tel: 002-012-4026684, E-mail address: hmokbel07@yahoo.com

Abstract

Rapid prototyping (RP) has been termed by many manufacturing scientists and engineers to be the ultimate solution to manufacturing whereby complex, convoluted and near-impossible shapes can be modeled and developed within a very short period. It has been implemented in all industries needed to reduce the time for the development of new products.

In the present work a novel application of rapid prototyping is presented, that is the use of RP in the fabrication of geometrically similar scale physical models (reduced, equal and enlarged) of an original simple structure (steel beam of rectangular cross-section). The used RP system is the 3D System's sinterstation-2500^{plus} which works with the Selective Laser Sintering technology and the raw material is the Duraform polyamide. These models were used in simulating the static and dynamic performance of the original simple structure. The most important physical and mechanical properties of the RP material have been determined in a previous work (tensile strength, modulus of elasticity, hardness, and density). The models have been tested statically to determine their load-deflection behavior and elastic lines, and have been tested dynamically to determine their natural frequencies and damping ratios. All the results have been transformed by the laws of similarity and compared with the results of the original steel beam.

Keywords: Rapid Prototyping, Similitude, CAD/CAM.

1- Introduction

Scale models may be used as a convenient way of obtaining various kinds of experimental data on the performance of structures, including for example deflections, strength and vibration characteristics. The use of scale models, which are geometrically similar to the full size structure, offers a much easier and less expensive qualitative and quantitative method for the investigation of machine tool performance [1]. They are easy to handle due to their light weight and smaller size. Modifications can be carried out in a much easier and cheaper way than in the case of the full-size structure. Models provide valuable information about the adequacy of the mathematical analysis describing the behavior of original structure. By use of models, it is possible to predict the characteristics of the actual structure in both the design and development stages. Models have been found to be faithful to the actual structures [2]. Models can be used as aids to the consideration of the ergonomic features and aesthetic qualities of a machine, as media for the communication of ideas between those responsible for different aspects of a product (design, manufacture, operation, and marketing), as aids to teaching, or to assess the design of structures for convenience of manufacture and assembly, and to evaluate both quantitative and qualitative aspects of their technical performance.

To reduce the lead-time and costs for the development of new industrial products, rapid prototyping has been recognized as a unique, layered manufacturing technique for making prototypes.

2- Rapid prototyping

Rapid prototyping RP is a new forming process and principle which is one of the important break-throughs of recent technological progress in the manufacturing industry [3]. It provides prototypes of very complex geometry directly from three-dimensional computer aided design (CAD) software. These processes build prototypes in a wide variety of materials such as polymer, wax, and paper without the benefit of specially designed tooling or fixturing [4].

Over the past few years, a variety of new RP technologies with wide ranging capabilities have been developed. These technologies are capable of directly generating physical objects from CAD databases [5]. They have a common important feature; the prototype is produced by adding material rather than removing it by machining. The model to be manufactured is mathematically sectioned (sliced) into a series of parallel cross-sections (planes) called layers. This simplifies the 3D part producing process to 2D layer adding process such that the part can be produced directly from its computer model [6, 7].

RP technology has the potential to ensure that quality-assured prototypes or parts are developed quickly for two major reasons; there are almost no restrictions on geometrical shapes, and the layered manufacturing allows a direct

and simple interface with CAD to CAM [8], which almost completely eliminates the need for process planning or the complex procedure for CNC machining.

The parts are directly shaped fully automatically according to CAD data, using the STL format (Standard Transform Language) [9]. The STL file, which is a defacto standard, is the most common interface between CAD and RP systems. 3D Systems developed and published the STL format in 1987 for converting 3D CAD models for use in Stereolithography apparatus [10].

Although the possible applications of RP are virtually limitless, nearly all fall into one of the following categories: Prototyping, Rapid tooling (*RT*) and Rapid Manufacturing (*RM*). Various different types of RP methods have been developed, these technologies include Stereolithography Apparatus (*SLA*), Selective Laser Sintering (*SLS*), Fused Deposition Manufacturing (*FDM*), Laminated Object Manufacturing (*LOM*), Three Dimensional Printing (*3D Printing*), Inkjets, and Laser Engineering Net Shaping (*LENS*).

3- Production of simple structure scale models by RP

For the sake of verification of the convenience of RP to produce geometrically similar models of mechanical structures, polyamide beams have been produced by rapid prototyping. These beams are geometrically similar to a steel beam of uniform rectangular cross-section (*St37*, Length $L=180\text{ mm}$, Width $b=30\text{ mm}$, Height $h=9\text{ mm}$). The polyamide beams have been produced on the sinter-station 2500^{plus}, which works with the Selective Laser Sintering (*SLS*) technology and contains a 100-watt CO₂ continuous-wave laser that operates at a 10.6-micron wavelength. The raw material (duraform) is a mixture of a fine polyamide powder and a binding material.

The material properties have been obtained experimentally as follows: Tensile strength $46.8 \pm 1.9\text{ Mpa}$, Modulus of elasticity $2000 \pm 78\text{ Mpa}$, Hardness $43 \pm 2.2\text{ Shore-Scleroscope}$, Density $0.95 \pm 0.008\text{ gm/cm}^3$ [11].

These beams were produced with different scales of; 1:1, 1:2, and 2:1 with respect to the steel beam. Both of the steel and RP beams are statically and dynamically tested as cantilever beams clamped from one side in a vice while the other side is free.

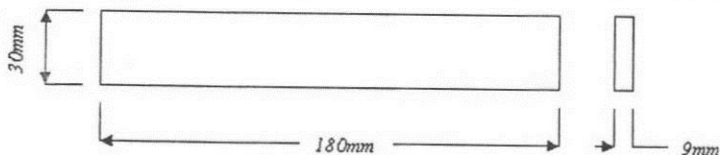


Fig. (1) The steel beam (St 37).

Static testing of the steel and RP beams is carried out to determine the force-deflection curves for the steel beam and the different scale RP beams. As well as the elastic-lines of the steel beam and the 1:1 scale RP beam. Dynamic tests have been carried out to determine the natural frequencies and the damping

ratios of the beams. All measurements of the RP beams are transformed to the steel beam as a reference, using the laws of similarity for the sake of comparison.

4- Static testing of the beams

A 0.01 mm increment, 10 mm range dial indicator is used for the deflection measurement of the beams. Loading is done by a 2kN-loading device, having a resolution of 6 N and uncertainty of ± 8.5 N for 95% confidence level [12].

For the steel and the 1:1 scale RP beam, the clamping is done on the first 30 mm while the free length of the beam is 150 mm. For determining the load-deflection curves of these beams, the loading device and the dial indicator are mounted at the same section at 145, 125, and 100mm from the fixed end.

For determining the elastic behavior of the beams, the loading device is fixed ahead of the free end of the beam at 150mm from the fixed end, and the dial indicator is mounted at positions $X=145$ mm, $X=125$ mm, and $X=100$ mm and $X=75$ mm from the fixed end.

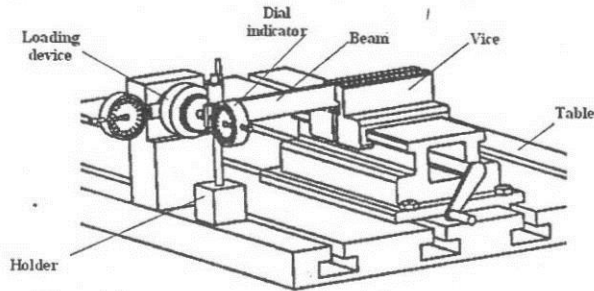


Fig. (2) Static testing of the steel and RP beams.

The deflections at these positions are calculated theoretically by the equation:

$$Y = \frac{F}{2EI} \left[LX^2 - \frac{X^3}{3} \right]$$

For the steel beam: $I=1890.2\text{mm}^4$, $b=30.1\text{mm}$, $h=9.1\text{mm}$, $E=210$ GPa, $F=0$, 180, 420, and 720 N and $L=145$, 125, and 100 mm.

For the 1:1 scale RP Polyamide cantilever beam: $I=1734.2\text{mm}^4$, $b=29.8\text{mm}$, $h=8.87\text{mm}$, $E=2000$ MPa, $F=0$, 12, and 18 N and $L=145$, and 125 mm.

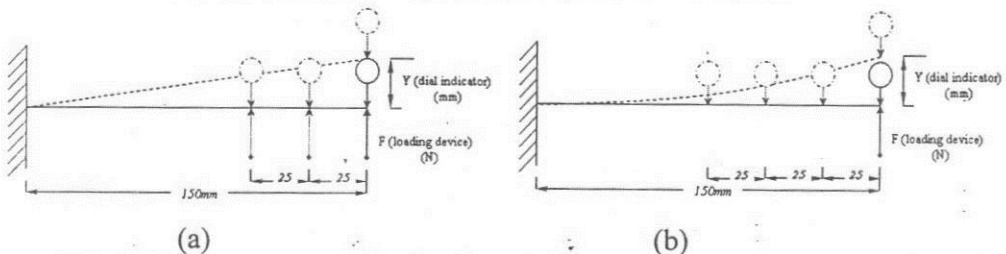


Fig. (3) Measurement of the Load-Deflection behavior (a) and Elastic line (b)

Table (1) Dimensions of the steel and RP beams

Condition	Steel beam	Rapid Prototyping beams		
		Scale 1:1	Scale 1:2	Scale 2:1
Length (L) (mm)	180	180	90	360
Width (b) (mm)	30	30	15	60
Height (h) (mm)	9	9	4.5	18
Fixation length (mm)	30	30	15	60
Free length (mm)	150	150	75	300

Table (2) Load-Deflection data of the steel and the 1:1 scale RP cantilever beams

Distance		Steel beam			RP beam scale 1:1		
		Load (F) (N)	Deflection (Y) (mm)		Load (F) (N)	Deflection (Y) (mm)	
			Theoretical	Experimental		Theoretical	Experimental
Distance of the loading device and dial indicator from the fixed end (X)	X=145 mm	0	0	0	0	0	0
		180	0.46	0.45	12	3.5	3.6
		420	1.08	1.07	18	5.27	5.49
		720	1.84	1.81	—	—	—
	X=125 mm	0	0	0	0	0	0
		180	0.3	0.30	12	2.3	2.4
		420	0.7	0.69	18	3.38	3.52
		720	1.18	1.17	—	—	—
	X=100 mm	0	0	0	—	—	—
		180	0.17	0.17	—	—	—
		420	0.37	0.38	—	—	—
		720	0.61	0.63	—	—	—

Table (3) Load-Deflection data of the 2:1 and the 1:2 scale RP cantilever beams

Distance		RP beam scale 2:1			RP beam scale 1:2			
		Load (F) (N)	Deflection (Y) (mm)		Distance	Load (F) (N)	Deflection (Y) (mm)	
			Theoretical	Experimental			Theoretical	Experimental
Distance of the loading device and dial indicator from the fixed end (X)	X=295 mm	0	0	0	X=70 mm	0	0	0
		60	9.2	9.3		9	4.6	4.7
		90	13.89	13.99		15	7.63	7.74
	X=250 mm	0	0	0	X=62.5 mm	0	0	0
		60	5.7	5.8		9	3.3	3.6
		90	8.45	8.63		15	5.43	5.99
	X=200 mm	0	0	0	X=50 mm	0	0	0
		60	2.9	2.7		9	1.7	1.6
		90	4.33	3.82		15	2.78	2.57

Table (4) Elastic lines data of the 1:1 scale RP cantilever beam.

Distance along the beam (X) from the fixed end (mm)	Deflection (Y) (mm)					
	Load	Theoretical	Experimental	Load	Theoretical	Experimental
75		1.75	—		1.17	—
100		2.98	—		1.93	—
125		4.19	4.22		2.79	2.96
145		5.27	5.49		3.52	3.75

It is clear that applying a load $F=720N$ to the steel beam results in the maximum deviation between theoretical and experimental results of 4.13% at minimum free length ($X=100mm$). This may be attributed to the opening of the vice jaws. A minimum deviation is -1.35% at $X=125mm$. The Stiffness of the cantilever steel beam was also calculated theoretically and experimentally at free lengths $L=145mm$, $L=125mm$, and $L=100mm$ by the equations: $k = \frac{3EI}{L^3}$, and $k = \frac{F}{Y}$ respectively.

Table (5) Stiffness of the steel and the 1:1 scale RP cantilever beams.

Distance along the beam (X) from the fixed end (mm)	Stiffness (k)(N/mm)			
	Steel		RP	
	Theoretical	Experimental	Theoretical	Experimental
145	390.63	398.340	3.41	3.28
125	609.7	617.76	5.33	5.11
100	1190.83	1142.86	—	—

Also, the maximum deviation of the measured stiffness is -4.03% at distance of $X=100mm$ from the fixed end, while the minimum deviation is 1.3% at distance of $X=125mm$ from the fixed end.

For the 1:1 scale polyamide cantilever beam, the load-deflection curve at the applied load of $F=18N$, has a maximum deviation of 4.17% at $X=145mm$, and the minimum deviation is 4.14% at $X=125mm$, which gives a good indication for the stability of the mechanical properties and behavior of the polyamide structures. At a distance $X=145mm$ from the fixed end, the deviation in the elastic behavior is 6.5% at the applied load of $F=12N$. The increase of the deviation at lower loads may be explained by the fact that the uncertainty of load measurement increases as the load approaches the min. measurable value (6N).

The deviation in the measurement of the stiffness between the theoretical and experimental results is -3.93 % at a distance $X=145mm$ from the fixed end, and -4.05% at distance $X=125mm$.

5- Transformation of the static results to the steel beam

The Load-Deflection curves of the Steel and different RP Polyamide cantilever beams are governed by the equation $\frac{Y_1}{Y_2} = \frac{F_1}{F_2} \cdot \frac{L_1^3}{L_2^3} \cdot \frac{E_2}{E_1} \cdot \frac{I_2}{I_1}$. So that, for the results of the 1:1 scale Polyamide beam at $F_2=18N$, $I_2=1734.2mm^4$ and $L_1=L_2$, the resulting deflection in the steel beam will be:

$$\therefore Y_1 = Y_2 \cdot \frac{F_1}{F_2} \cdot \frac{E_2}{E_1} \cdot \frac{I_2}{I_1} = Y_2 \cdot \frac{F_1}{210} \cdot \frac{2}{1890.2} \cdot \frac{1734.2}{18}$$

$$Y_2=5.274\text{mm (theoretically)} \Rightarrow Y_1=1.843\text{mm at } F_1=720\text{N.}$$

$$Y_2=5.49\text{mm (Experimentally)} \Rightarrow Y_1=1.918\text{mm at } F_1=720\text{N.}$$

The results of the 2:1 scale Polyamide beam at $F_2=90\text{N}$ and $I_2=27726.165\text{mm}^4$ are

$$Y_2=13.89\text{mm (theoretically at } L_2=295\text{mm)} \Rightarrow Y_1=1.84\text{mm at } F_1=720\text{N.}$$

$$Y_2=13.99\text{mm (Experimentally at } L_2=295\text{mm)} \Rightarrow Y_1=1.86\text{mm at } F_1=720\text{N.}$$

At $L_1=145\text{mm}$

The results of the 1:2 scale Polyamide beam at $F_2=15\text{N}$ and $I_2=112.3875\text{mm}^4$ are

$$Y_2=7.63\text{mm (theoretically at } L_2=70\text{mm)} \Rightarrow Y_1=1.84\text{mm at } F_1=720\text{N.}$$

$$Y_2=7.74\text{mm (Experimentally at } L_2=70\text{mm)} \Rightarrow Y_1=1.87\text{mm at } F_1=720\text{N.}$$

At $L_1=145\text{mm}$

From the results of the Load-Deflection values of the steel and the transformed different RP Polyamide cantilever beams, at the applied load of $F=720\text{N}$, the deviation for the 1:1 scale polyamide beam is 6.08% at distance $X=145\text{mm}$ from the fixed end, and 5.58% at $X=125\text{mm}$. For the 2:1 scale polyamide beam, at the same applied force, the deviation is 2.71% at $X=145\text{mm}$, and 3.45% at $X=125\text{mm}$. For the 1:2 scale polyamide beam, at the same applied force, the deviation is 3.49% at $X=145\text{mm}$, and 11.75% at $X=125\text{mm}$.

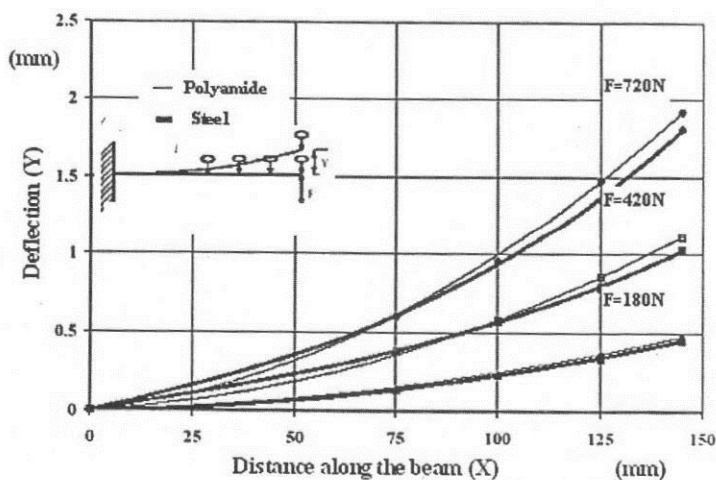


Fig. (4) Experimental elastic lines of the 1:1 scale steel and RP cantilever beams (RP to steel transformation).

From the transformation of the elastic lines of the 1:1 scale polyamide cantilever beam to the steel beam results, at distance $X=145\text{mm}$ from the fixed

end and load $F=720N$ the deviation in the experimental results between the both beams reaches 6.08%, this is the accumulated deviation from both the deviation in the measurements of the steel and the polyamide cantilever beams. This deviation is decreased to 4.07% when comparing the experimental results of the polyamide beam with the theoretical one of the steel. Of course, the deviation reaches 0% when comparing both the theoretical results, so that for the same distance at $X=145mm$, but with different loads, the deviation in the experimental results is 8.75% at $F=420N$, and 5.727% at $F=180N$, where it is decreased to be 4.09% at $F=420N$, and 4.12% at $F=180N$ when comparing the transformed experimental results of the polyamide beam with the theoretical results of the steel.

Table (6) Experimental Load-Deflection data of the steel and different scales RP cantilever beams (RP to steel transformation).

Distance of the loading device and dial indicator from the fixed end (X)	Load (F) (N)	Deflection (Y) (mm)				Steel
		(polyamide to steel transformation)				
		Scale 1:1	Scale 2:1	Scale 1:2		
X=145mm	0	0	0	0	0	
	720	1.92	1.86	1.87	1.81	
X=125mm	0	0	0	0	0	
	720	1.23	1.21	1.30	1.17	

Table (7) Experimental and theoretical elastic lines data of the 1:1 scale steel and RP cantilever beams (RP to steel transformation).

Load (F) (N)	Distance along the beam (X) from the fixed end (mm)	Deflection (Y) (mm)			
		Polyamide to steel transformation		Steel	
		Theoretical	Experimental	Theoretical	Experimental
F=720	0	0	0	0	0
	75	0.61	—	0.61	0.60
	100	1.04	—	1.01	0.96
	125	1.46	1.48	1.46	1.35
	145	1.84	1.92	1.84	1.81
F=420	0	0	0	0	0
	75	0.36	—	0.36	0.38
	100	0.61	—	0.59	0.58
	125	0.85	0.86	0.85	0.79
	145	1.08	1.12	1.08	1.03
F=180	0	0	0	0	0
	75	0.15	—	0.15	0.14
	100	0.26	—	0.25	0.24
	125	0.37	0.37	0.37	0.34
	145	0.46	0.48	0.46	0.45

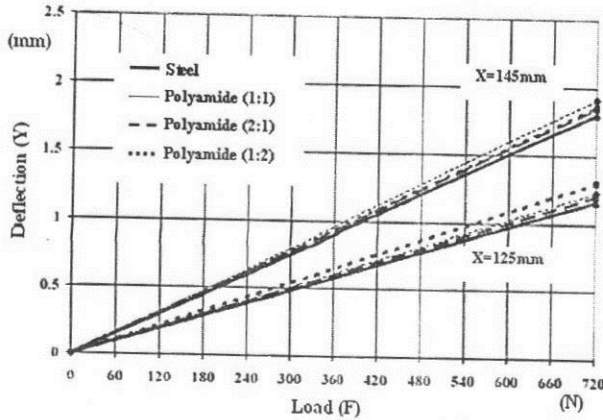


Fig. (5) Experimental Load-Deflection curves of the steel and different RP cantilever beams (RP to steel transformation).

The figure below shows a comparison between the deflection of the steel cantilever beam due to applied force $F_1=720N$ at positions $L_1=145mm$ and $125mm$ and the deflection of the different scales RP Polyamide cantilever beams transformed to the steel. It is clear that the total max. deviation in the transformed deflections is the steel-Polyamide scale 1:2 transformation is 6.7%. The min. deviation is the Steel-Polyamide scale 2:1 transformation that reaches a deviation of 2.9%. The Steel-Polyamide scale 1:1 deflection transformation reaches a deviation of 5.9%. The increase of the deviation in the case of the 1:2 scale polyamide cantilever beam is due to the low applied force, due to the small dimensions of the beam, and the low deflection values. While, at the enlarged scale polyamide beam (scale 2:1), the values of the load increases with the beam dimensions resulting in decreasing the deviation caused by the low sensitivity and the uncertainty of the loading device.

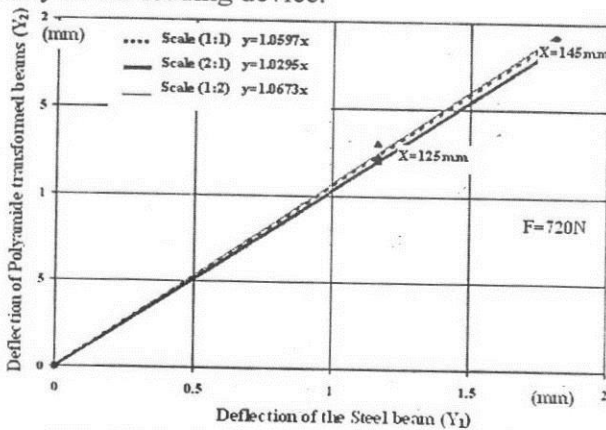


Fig. (6) Deflection of the steel and RP cantilever beams (RP to steel transformation).

The results of the stiffness of the different simple beams transformed to the steel cantilever beam at free lengths $L_1=145mm$ and $125mm$ are shown

Table (8) Stiffness of the steel and different scales RP beams (RP to steel transformation).

Free length of the beam (L) (mm)	Stiffness (k) N/mm			
	Scale 1:1	Scale 2:1	Scale 1:2	Steel
L=145	375.32	387.68	384.89	398.34
L=125	585.04	597.33	552.4	617.76

It is clear that, at the free length $L=145mm$, the deviation of the stiffness for the 1:1 polyamide beam is -5.78% and -2.68% for the 2:1 scale polyamide beam, and -3.38% for the 1:2 scale polyamide beam. While at the free length $L=125mm$, the deviation is -5.3% for the 1:1 scale polyamide beam, -3.31% for the 2:1 scale polyamide beam, and -10.58% for the 1:2 scale polyamide beam for the afore mentioned reasons.

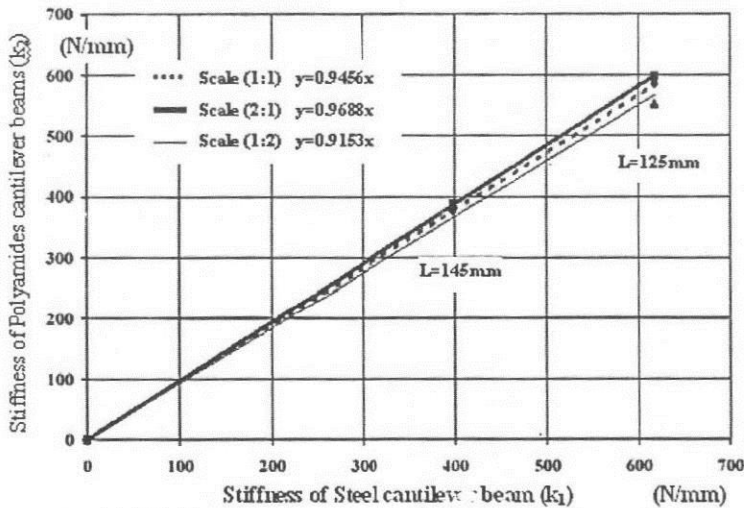


Fig. (7) Stiffness of the steel versus RP cantilever beams (RP to steel transformation).

It is clear that the total maximum deviation in the transformed stiffness is that of the steel-Polyamide scale 1:2 transformation that reaches a deviation of 8.5% . The minimum deviation is that of the Steel-Polyamide scale 2:1 transformation that reaches a deviation of 3.1% . The Steel-Polyamide scale 1:1 stiffness transformation reaches a deviation of 5.4% .

6- Dynamic testing of the beams

Each beam is tested separately to determine its natural frequency. The beam is fixed in a vice from one end, while the other end is left free as a cantilever beam (the same fixation as in the static tests).

The test is carried out for two different overhanging lengths. The beam is subjected to a slight impact from a rubber hammer. A piezoelectric accelerometer type *KD12*, is mounted at the end of the beam free length. The accelerometer is connected to a charge amplifier type *SDM132*, which is connected to a PC-Scope type *PCS64i* (an interface for vibration analysis) that delivers the results to the computer. The dynamic response is shown in the time domain and in the frequency domain, from which the natural frequency and the damping ratio are determined for each case.

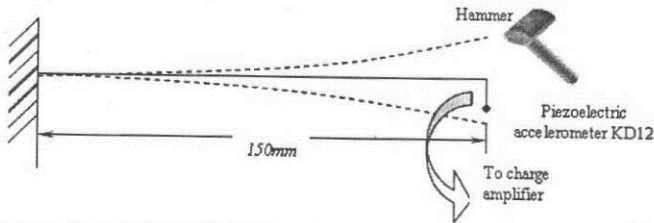


Fig. (8) Dynamic testing of the steel and the 1:1 scale RP cantilever beams

The natural frequency of a cantilever beam with negligible mass having an attached mass m at a distance X from the fixed end is given by the equation:

$$f = \frac{1}{2\pi} \sqrt{\left(\frac{3EI}{mX^3}\right)} \quad (\text{Hz})$$

The natural frequency of a cantilever beam of mass M is the same as that of a mass-less beam having an attached mass $=M/4.23$ at the beam end, which is:

$$f = \frac{1}{2\pi} \sqrt{\left(\frac{3EI}{0.24ML^3}\right)} \quad (\text{Hz})$$

When an additional mass m is mounted at a distance X from the fixed end, the natural frequency is:

$$f = \frac{1}{2\pi} \sqrt{\left(\frac{3EI}{L^3(0.24M + m(X/L)^3)}\right)} \quad (\text{Hz})$$

This is the case of a cantilever beam on which an accelerometer of mass m is mounted at a distance X to determine the natural frequency by an impulse. The measured frequency will be lower than the actual beam frequency. A correction factor k_{corr} is therefore needed to obtain the actual natural frequency from the measured value.

$$k_{corr} = \sqrt{\left(\frac{0.24M + m(X/L)^3}{0.24M}\right)} = \sqrt{\left(1 + 4.23 \cdot \frac{m}{M} \cdot \left(\frac{X}{L}\right)^3\right)}$$

So that, the correction factor (k_{corr}) with $m=0.021kg$, and the theoretical results of the natural frequency of the different cantilever beams will be as follows:

Table (9) Natural frequencies of the different cantilever beams.

	Free length	Natural frequency (f) (Hz)			
		Measured	k_{corr}	Corrected	Theoretical
Steel	150 mm	279	1.107	308.85	340.88
	100 mm	565	1.142	654.23	766.99
Polyamide scale 1:1	150 mm	81	1.0028	81.23	92.92
	100 mm	184	1.014	186.58	209.06
Polyamide scale 2:1	300 mm	40	1.00068	40.03	46.35
	200 mm	90	1.0034	90.31	104.29

For the steel cantilever the deviation of the measured and corrected values of the natural frequency with respect to the calculated theoretical one is -9.4% at the free length $L=150mm$, while the deviation is -14.7% at the free length $100mm$. These deviations seem to be high when compared with the deviations in the static performance of the same beam, but we have to take into consideration that the dynamic performance is affected strongly by the fixation conditions, the impulse force value, duration, and position as well as by the resolution of the PC-scope that tends to reach a value of 8 Hz. In addition there is the effect of the interference of the different response modes of the beam and the vise.

For the dynamic response of the 1:1 scale RP Polyamide cantilever, the deviation of the measured and corrected values of the natural frequency with respect to the calculated theoretical one is -12.58% at the free length of $L=150mm$, while the deviation is -10.75% at the free length of $L=100mm$.

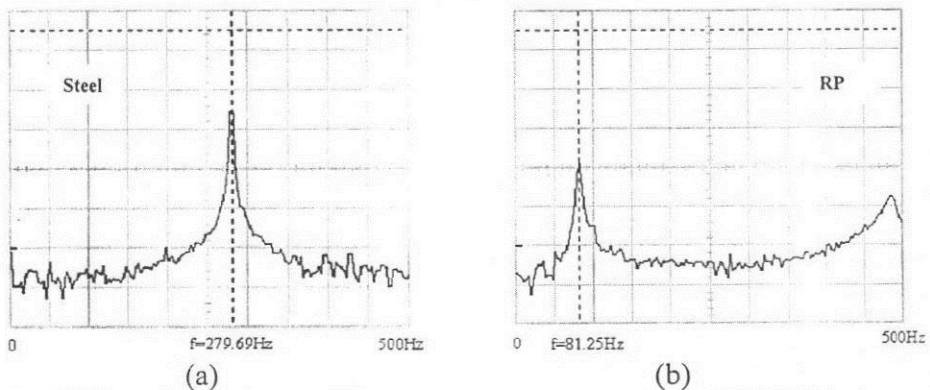


Fig. (9) Dynamic response of the steel (a) & the 1:1 scale RP cantilever beam (b) due to an impulse input at free length $L=150mm$ (frequency domain).

7- Transformation of the dynamic response results to the steel beam

For the 1:1 scale RP Polyamide cantilever beam:

$$\frac{f_1}{f_2} = \tau^{-1} = \sqrt{\left(\frac{1}{K^2} \cdot \frac{E_1}{E_2} \cdot \frac{\rho_2}{\rho_1}\right)} \quad \tau^{-1} = 3.576 = \frac{f_1}{f_2}$$

The results of the measured values of the natural frequencies of the steel cantilever beam, the 1:1 scale polyamide cantilever beam, and the 2:1 scale polyamide cantilever beam, as well as the corrected values of these natural frequencies transformed to the steel beam are shown. In addition the calculated theoretical natural frequencies of these cantilever beams transformed to the steel beam are also shown.

The deviation of the measured natural frequencies of the 1:1scale polyamide cantilever beam (corrected and transformed to the steel beam) compared with the theoretical values of the steel cantilever beam reaches a value of -14.79% at free Length of $L=150mm$, and -13.01% at free length of $L=100 mm$.

The deviation of the measured values of the natural frequency of the 2:1 scale polyamide cantilever beam (corrected and transformed to the steel beam) compared with the theoretical values of the steel cantilever beam reaches a value of -16.02% at a free Length of $L=300mm$, and -15.79% at a free length of $L=200mm$.

Table (10) Natural frequencies of the different cantilever beams (RP to steel transformation).

Beam	Free length	Natural frequency (f) (Hz)		
		Measured	Corrected (transformed)	Theoretical (transformed)
Steel	150 mm	279	308.85	340.88
	100 mm	565	654.23	766.99
Polyamide scale 1:1	150 mm	81	290.47	332.27
	100 mm	184	667.21	747.581
Polyamide scale 2:1	300 mm	40	286.27	331.51
	200 mm	90	645.87	745.9

8- Conclusion

Rapid Prototyping (RP) is a new technology that can be used to produce geometrically similar models of mechanical structures with a reasonable accuracy whatever are the details or complexity of the real structure.

During this work it has been clearly shown that duraform RP polyamide parts have shown good similitude of the static and dynamic behavior of the geometrically similar models for the original steel beam structure (When transformed to steel the reduced, equal, and enlarged scales RP beams have a deviation in the deflections of 6.7%, 5.9% & 2.9% respectively, and 8.5%, 5.4%

& 3.1% respectively in the stiffness. While the deviation in the dynamic behavior ranges between -13.01% and -16.02%.

References

- [1] F.M. Stansfield, "Models", Engineering Design Guides 16, published for the design council, the British Standards Institution, and the Council of Engineering Institutions by Oxford University press (1976).
- [2] M.A. EL Hakim, H. EL Mously, "Investigation of the static performance of a vertical drilling machine using a reduced-scale model", Proceedings of 1st conference of Mechanical Power Engineering, Cairo, Feb 1977, vol. 3.
- [3] Detlef Kochan, Chua Chee Kai, Du Zhaohui, "Rapid Prototyping issues in the 21st century", Computers in industry 39 (1999), pp. 3-10.
- [4] D. King, T. Tansey, "Alternative materials for rapid tooling", Journal of Materials Processing Technology 121 (2002), pp. 313-317.
- [5] K. Murali, A.N. Chatterjee, P. Saha, R. Palai, S. Kumar, S.K. Roy, P.K. Mshra, A. Roy Choudhury, "Direct selective laser sintering of iron-graphite powder mixture", Journal of Materials Processing Technology 136 (2003), pp. 179-185.
- [6] Xue Yan and P Gu "A review of rapid prototyping technologies and systems", Computer-Aided Design, vol.28, No.4, 1996, pp. 307-318.
- [7] S.H. Masood, A. Soo, "A rule based expert system for RP system selection", Robotics and Computer Integrated Manufacturing 18 (2002), pp. 267-274.
- [8] S. -M. Hur, K. -H. Choi, S. -H. Lee, P.-K. Chang, "Determination of fabricating orientation and packing in SLS process", Journal of Materials Processing Technology 112 (2001), pp. 236-243.
- [9] Frank Kreith; "The CRC Hand book of Mechanical Engineering", (1998).
- [10] Gan G.K. Jacob, Chua Chee Kai, Tong Mei "Development of a new rapid prototyping interface", Computers in industry 39 (1999), pp. 61-70.
- [11] Hany Fathalla Mokbel, "Computer Aided Manufacturing of Reduced Scale Models for Machine Tool Structures Using Rapid Prototyping", Msc. thesis, Military Technical College, Cairo 2005.
- [12] M.A.EL Hakim, "The influence of some design features on the static performance of a milling machine frame", Ph.D. thesis, faculty of engineering Ain Shams University, 1969.



1- Introduction

Previous manufacturing and design processes depend on the experience of engineers, which has been acquired along their life. Due to the great advance of the computer capabilities, in both software and hardware, engineers tend to develop different and efficient means to help in the design and manufacturing by the aid of computers. This effort has led to the development of Computer Aided Design (CAD), which depends on creating and modifying different geometric shapes from primitives, and Computer Aided Manufacturing (CAM), which can be defined as the use of computer systems to plan, manage, and control the operations of the manufacturing plant. (CAD/CAM) have significantly improved the traditional production, design and manufacturing. However, the gap between CAD and CAM has remained unfilled in the creation of physical models and prototypes necessary for testing the performance of the designed products.

A large part of the product developing cycle is consumed in fabricating a model or prototype in the workshop, which takes weeks or even months after releasing the design. Several tests are performed to make sure that its performance conforms to the design and the consumers' requirements. Alterations and modifications are needed in most cases, which increase the time-to-market for a new product [1].

Although, the use of reduced scale models has shown good results in solving some modeling problems, but the manufacturing of prototypes is still a time and money consuming. On the other hand mathematical models are not able to formulate the working conditions of the original design, the types of joints, end conditions, type of fit, and frictional conditions of the mating surfaces. Oversimplifications are usually assumed which lead to considerable deviations from actual systems.

In order to substantially shorten the time for developing models and prototypes, Rapid Prototyping (RP) has emerged, which allows the computer-aided production of a prototype within few hours, and which makes alternatives and modifications easier [2].

The aim of the present work is to produce a reduced scale model of a horizontal milling machine structure, with the rapid prototyping technique, using polyamide as a suitable material. The model is tested statically and dynamically and has been compared with the full scale original machine in order to check the convenience of the RP technique in the production of reduced scale models for testing machine tool structures. The original machine and the reduced scale model thereof will be geometrically similar, while the applied loads will satisfy the loading similarity conditions (same nature and distribution of the loads and same end conditions). Moreover, the testing results will be compared with those

of a 1:4 scale welded steel model used in a previous work [5] to find out which model gives better results.

2- Rapid prototyping

Rapid prototyping has been recognized as a unique, layered manufacturing technique for making prototypes. A variety of new rapid prototyping (RP) technologies with wide ranging capabilities have been developed. These technologies are capable of directly generating physical objects from CAD databases. The model to be manufactured is mathematically sectioned (sliced) into a series of parallel cross-sections (planes) called layers. This simplifies the 3D part producing process to 2D layer adding process such that the part can be produced directly from its computer model [2, 3].

In the Rapid Prototyping technique shapes of machine parts are created by building up layers of material, unlike the material removal technique that shapes by gradual machining using a cutting tool. In this sense, rapid prototyping resembles the joining technique of small particles or thin layers. Various different types of rapid prototyping methods have been born over the last few years, the technologies developed include Stereolithography Apparatus (SLA), Selective Laser Sintering (SLS), Fused Deposition Manufacturing (FDM), Laminated Object Manufacturing (LOM), Three Dimensional Printing (3D Printing), Inkjets, and Laser Engineering Net Shaping (LENS). The parts are directly shaped fully automatically according to CAD data, using the STL (Standard Transform Language) format [4], which is the most common interface between CAD and RP systems. The STL format was developed and published in 1987 by 3D Systems for converting 3D CAD models to be used in Stereolithography apparatus [5]. Other names of the Rapid Prototyping technique are Layered Manufacturing (LM), Layered Forming, Free Form Fabrication (FFF), and Solid Freeform Fabrication (SFF).

3- Models

The fabrication of models and prototypes usually requires long time and high expenses especially if special tooling and fixtures are required. On the other hand it has been reported that manufacturing of prototypes on CNC machine tools is extremely difficult [6]. Generally the models are produced more rapidly and at a much lower cost than the original machine. Moreover, the testing of models is easier, considerably faster, and less expensive than the original structure. The effects of different factors affecting the performance can be investigated so that significant factors can be separated from insignificant factors. Reduced scale model techniques find application in aircraft design, aerospace field, hydraulic machines, machine tools, etc. Figure 2.1 shows the sequence of the modeling technique (Theory of Models), it is clear that the

relationship between the model and the original structure is governed by the laws of similarity.

Many studies [7, 8] have shown that a good resemblance with respect to static and dynamic performance can be obtained between steel models and cast iron full size machines. Reduced scale models should strictly follow the geometric- as well as the load similarity to obtain reliable results.

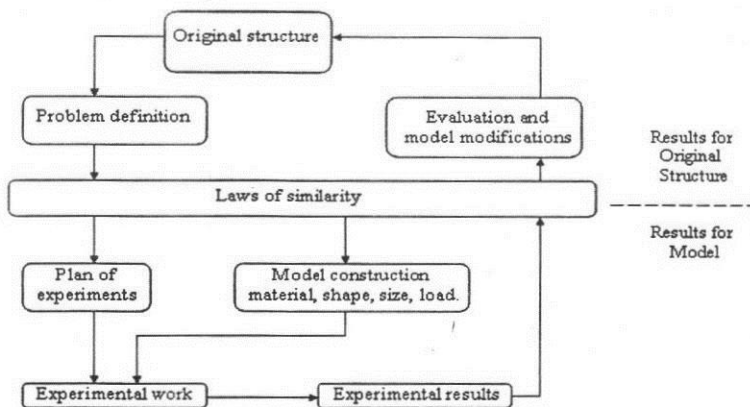


Fig. (1) Block diagram of the modeling technique

4- Similitude

Similitude refers to the formulation of a description of a physical behavior that is general and independent of the individual dimensions, physical properties, forces, etc. [4]. In the present work the treatment of similitude is restricted to the dimensional analysis method which is based on the principle that all additive or equated terms of a complete relationship between the variables must have the same net dimensions [4, 9].

Rules of similitude:

1. Physically similar systems have basic quantities of the same nature [L (length), F (force), M (mass), A (area), θ (angular displacement), etc.],
2. All quantities of the same nature have the same scale.
3. Physical systems will have similar behavior under the effect of the same physical factor (when they are geometrically similar; enlarged or reduced scale models).
4. The differential equations describing both the original system and its geometrically similar model including end conditions and initial conditions are necessarily the same. The dimensionless ratios of any two physical quantities (L, F, M, A, θ , V, etc....) of the same type, having the

same dimensions (L, M, T) are equal for the model and the original structures: $\frac{\Delta L1}{L1} = \frac{\Delta L2}{L2}$

In the present work, according to geometric similarity, the full size machine (1) dimensions are related to the model (2) dimensions by the following relationships:

$$K = \frac{L_1}{L_2} \quad P = \frac{F_1}{F_2} \quad \tau = \frac{t_1}{t_2} \quad \frac{A_1}{A_2} = \frac{b_1 h_1}{b_2 h_2} = K^2 \quad Y = \frac{FL^3}{3EI}$$

$$\frac{I_1}{I_2} = \frac{b_1 h_1^3 / 12}{b_2 h_2^3 / 12} = K^4 \quad \frac{M_{b1}}{M_{b2}} = \frac{F_1 L_1}{F_2 L_2} = PK \quad \frac{T_1}{T_2} = \frac{F_1 \cdot r_1}{F_2 \cdot r_2} = PK$$

$$\frac{k_1}{k_2} = \frac{dF_1 / dY_1}{dF_2 / dY_2} = \frac{P}{K} \quad \frac{m_1}{m_2} = \frac{\rho_1 V_1}{\rho_2 V_2} = \frac{\rho_1}{\rho_2} \cdot K^3$$

$$\frac{f_1}{f_2} = \tau^{-1} = \sqrt{\left(\frac{1}{K^2} \cdot \frac{E_1}{E_2} \cdot \frac{\rho_2}{\rho_1} \right)}$$

$$\frac{Y_1}{Y_2} = \frac{F_1}{F_2} \cdot \frac{L_1^3}{L_2^3} \cdot \frac{E_2}{E_1} \cdot \frac{I_2}{I_1} \quad \frac{Y_1}{Y_2} = \frac{P}{K} \cdot \frac{E_1}{E_2} = K \quad P = K^2 \cdot \frac{E_1}{E_2} = \frac{F_1}{F_2}$$

Note: K & P are required for static similarity, while K, P, & τ for dynamic similarity.

5- Production of the RP model

Since machine tool structures are made of beam like structures incorporating members of hollow box rectangular sections interconnected by bolted sliding joints, the selective Laser Sintering (SLS) technique has been found to be the most suitable method for producing the required reduced scale models. The RP models have been fabricated by means of 3DSYSTEMS (Sinterstation 2500^{plus}) which contains a 100-watt CO₂ continuous-wave laser that operates at a 10.6-micron wavelength. The laser itself is a class IV laser.

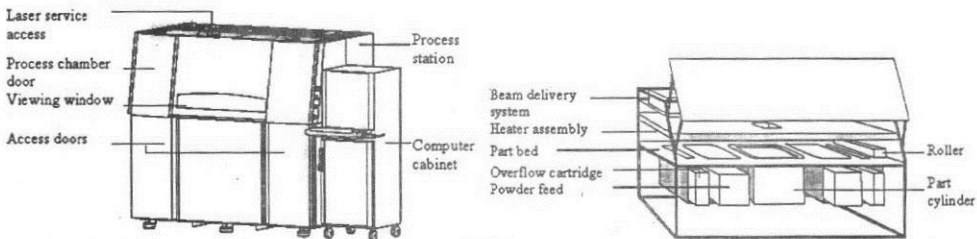


Fig. (2) The Sinterstation 2500^{plus} system & the process chamber [10].

The raw material (duraform) is a mixture of a fine polyamide powder and a binding material. The powder is placed into the right and left feed pistons, which are moved sequentially upwards a specified distance (0.254mm). After each

movement of the feed pistons, the roller moves from one side to another to deliver the powdered material in a very thin layer ($0.1mm$) across the flat platform (part bed). The laser beam traces across this layer, fusing the powder in specific areas to create a cross-section of the current part. The part bed lowers slightly by the layer thickness ($0.1mm$), the other feed piston moves up another step ($0.254mm$), the roller delivers another thin layer of powder to the part bed, and the laser sinters the next cross-section which bonds to the previous one. This process is repeated till finishing of the whole part.

In the present case, the part height is $325.08mm$. Adding $1.25mm$ for the standard base below the part and $0.75mm$ between the part and the standard base, the total build height is $327.08mm$. A layer thickness of $0.1mm$ results in the total number of layers for the whole build of 3271, total number of facets of 21050 and takes about 37 hours for build completion.

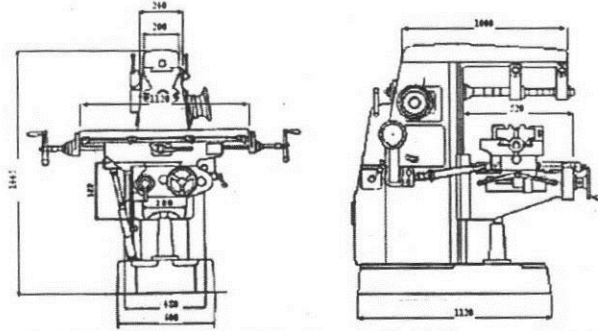


Fig. (3) The original horizontal milling machine.

A geometrically similar $1:4$ scale welded steel model of the selected milling machine has been developed in a previous machine tool research [11], which has proved to show a good static and dynamic resemblance to the full size machine [7, 8].

The reduced scale rapid prototyping model of the horizontal milling machine will be geometrically similar to both the full size machine and the reduced scale steel model but with a different scale. The new scale was chosen depending on two main factors; firstly the size of the available loading device that limits reducing the scale of the RP model, and secondly the size of the process chamber of the RP system that limits enlarging the scale of the RP model. The new RP model will be $0.9:1$ scale of the steel model, or $1:4.44$ scale of the original machine. The CAD/CAM software used for drawing and preparation of the CAD models is Pro/Engineer. The dimensions of the machine were taken from the original drawings from its manual. The model dimensions were taken practically on the steel model with the aid of its original drawings [5].

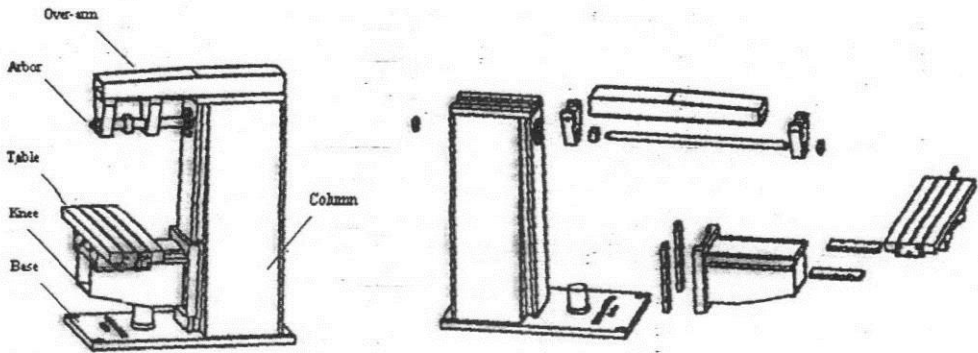


Fig. (4) Three-dimensional drawing of the RP model of the milling machine.

The 3D RP milling machine model is completely similar to the steel model in the type of joints and end conditions of the model parts. The model overarm is connected to the column through a dovetail and the arbor is free to rotate in its bearings, the model column is completely fixed to the base, the table is connected to the knee through a dovetail, and the knee is clamped using two straps on the column flat slide guide way by means of eight screws (Fig. 4).

6- Testing of the steel and RP models

Static and dynamic tests have been carried out on the steel and the RP models. All the results are transformed to the original machine by the laws of similarity for the sake of comparison. All the tests have been carried out exactly under the same conditions; the method of fixation of the model base onto the table, the nature and position of the applied load, the loading device, the measuring instruments, and the positions of measurement, are all the same for the steel and the RP models. The data of the static testing is used to determine the load-deflection and elastic behavior of the model structural components; over-arm, column, and knee, while the dynamic tests is used to determine the natural frequencies and damping ratios of the overall structure.

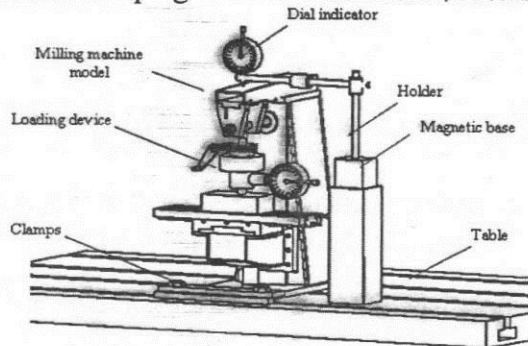


Fig. (5) Measuring the static performance of the reduced scale models.

For determining the load-deflection behavior of the over-arm of the milling machine models, the over-arm has been measured in 11 positions with equal spacing. At each position the applied load has been changed from 0 to 1800N for the steel model and from 0 to 180N for the RP model, and the deflection has been measured at different steps of the load. For measuring the elastic lines of the over-arm at a specified value of the load, the deflection has been measured along the over-arm at that constant load. The same procedures are repeated to the other applied loads within the load range.

The load-deflection behavior of the models' knee has been measured over 5 different positions. The elastic lines of the knee have been measured at 6 different values of the load ranging from 250 to 1800N for the steel model and from 0 to 180N for the RP model.

For the models' columns, the load-deflection behavior has been measured over 5 different positions. The elastic lines of the columns have been measured at 5 different values of the load ranging from 250 to 1800N for the steel model and from 0 to 180N for the RP model.

Each model was tested to determine its dynamic response to an impulsive force. The model is subjected to a slight impulse from a rubber hammer at the free end of the over-arm, a piezoelectric accelerometer type KD12, is mounted at 10 mm from the free end of the over-arm. The accelerometer is connected to a charge amplifier type SDM132, which is connected to a PC-Scope type PCS64i with FFT analysis interface connected to the computer.

For the sake of comparison between the steel model (1) ($E=210 \text{ Gpa}$, $\rho=7.8 \text{ gm/cm}^3$), the polyamide model (2) ($E=2 \text{ Gpa}$, $\rho=0.95 \text{ gm/cm}^3$) [12] and the Cast iron original machine (o) ($E=105 \text{ Gpa}$, $\rho=7.4 \text{ gm/cm}^3$), the results of the RP model are transformed to the steel model using the equations of similarity. For the steel model the deflection is Y_1 , and for the RP Polyamide model the deflection is Y_2 and the RP model is 0.9:1 scale of the steel model, so that:

$$K = \frac{L_1}{L_2} = \frac{1}{0.9} = 1.111$$

$$Y_1 = Y_2 \cdot \frac{L_1^3}{L_2^3} \cdot \frac{F_1}{F_2} \cdot \frac{E_2}{E_1} \cdot \frac{I_2}{I_1} = Y_2 \cdot K^3 \cdot \frac{F_1}{F_2} \cdot \frac{2}{210} \cdot \frac{1}{K^4} \quad \therefore Y_1 = \frac{Y_2 \cdot F_1}{(116.655) F_2}$$

$$\frac{f_1}{f_2} = \sqrt{\left(\frac{1}{(1.111)^2} \cdot \frac{210}{2} \cdot \frac{0.95}{7.8} \right)} = 3.2188 \quad \frac{f_o}{f_1} = \sqrt{\left(\frac{1}{(4)^2} \cdot \frac{105}{210} \cdot \frac{7.8}{7.4} \right)} = 0.1815$$

The results of the original machine are taken from a previous work [7]. The results of the static testing of the RP polyamide model and the steel model will be transformed and compared with the results of the original machine. For the purpose of comparison the results of the reduced scale RP model have been transformed to the steel model and then transformed to the cast iron original horizontal milling machine.

Table (1) Loading data of the over-arms of the steel model, the polyamide model and the original machine (all to original machine transformation).

Load (F) (N)	Deflection (Y) (mm)											
	Distance of the dial indicator from the start point of the over-arm (X) (mm)											
	Pos.1	Pos.2	Pos.3	Pos.4	Pos.5	Pos.6	Pos.7	Pos.8	Pos.9	Pos.10	Pos.11	
	Orig	0	100	200	300	400	500	600	700	800	900	1000
	St.	0	25	50	70	100	125	150	175	200	225	250
	Pol.	0	22.5	45	67.5	90	112.5	135	157.5	180	202.5	225
0	Orig	0	0	0	0	0	0	0	0	0	0	0
	St.	0	0	0	0	0	0	0	0	0	0	0
	Pol.	0	0	0	0	0	0	0	0	0	0	0
2000	Orig	0	0	0	0	0.01	0.03	0.04	0.06	0.08	0.1	0.12
	St.	0	0	0	0	0.01	0.03	0.04	0.06	0.081	0.1	0.12
	Pol.	0	0	0	0	0.01	0.02	0.04	0.06	0.08	0.11	0.12
4000	Orig	0	0	0	0	0.02	0.05	0.08	0.12	0.16	0.20	0.24
	St.	0	0	0	0	0.02	0.06	0.09	0.12	0.162	0.20	0.24
	Pol.	0	0	0	0	0.02	0.04	0.08	0.12	0.15	0.22	0.24
6000	Orig	0	0	0	0	0.04	0.07	0.12	0.17	0.235	0.29	0.36
	St.	0	0	0	0	0.04	0.09	0.13	0.18	0.237	0.29	0.35
	Pol.	0	0	0	0	0.04	0.06	0.13	0.175	0.23	0.32	0.36
8000	Orig	0	0	0	0	0.04	0.09	0.16	0.23	0.315	0.39	0.48
	St.	0	0	0	0	0.05	0.12	0.18	0.24	0.32	0.39	0.46
	Pol.	0	0	0	0	0.04	0.09	0.17	0.23	0.3	0.42	0.48
10000	Orig	0	0	0	0	0.05	0.12	0.20	0.28	0.39	0.49	0.59
	St.	0	0	0	0	0.06	0.14	0.22	0.31	0.4	0.49	0.57
	Pol.	0	0	0	0	0.05	0.11	0.20	0.29	0.37	0.52	0.60

Table (2) Loading data of the knees of the steel model, the RP model and the original machine (all to original machine transformation).

Load (F) (N)	Deflection (Y) (mm)					
	Distance of the dial indicator from the fixed end of the knee (X) (mm)					
	X=0 mm	Position 1 X=120 mm	Position 2 X=220 mm	Position 3 X=320 mm	Position 4 X=420 mm	Position 5 X=520 mm
0	Orig	0	0	0	0	0
	St.	0	0	0	0	0
	Pol.	0	0	0	0	0
2000	Orig	0	-0.01	-0.01	-0.02	-0.02
	St.	0	-0.01	-0.02	-0.02	-0.02
	Pol.	0	-0.01	-0.01	-0.02	-0.02
4000	Orig	0	-0.02	-0.02	-0.03	-0.04
	St.	0	-0.02	-0.03	-0.04	-0.04
	Pol.	0	-0.02	-0.03	-0.03	-0.04
6000	Orig	0	-0.02	-0.04	-0.05	-0.06
	St.	0	-0.03	-0.05	-0.05	-0.06
	Pol.	0	-0.03	-0.04	-0.05	-0.06
8000	Orig	0	-0.03	-0.05	-0.06	-0.07
	St.	0	-0.03	-0.05	-0.07	-0.08
	Pol.	0	-0.05	-0.07	-0.08	-0.09
10000	Orig	0	-0.04	-0.06	-0.08	-0.10
	St.	0	-0.05	-0.07	-0.09	-0.10
	Pol.	0	-0.05	-0.06	-0.08	-0.10

Table (3) Loading data of the columns of the steel model, the RP model and the original machine (all to original machine transformation).

Load (F) (N)		Deflection (Y) (mm)				
		Distance of the dial indicator from the start point of the column (X) (mm)				
		Position 1 X=0 mm	Position 2 X=200 mm	Position 3 X=400 mm	Position 4 X=600 mm	Position 5 X=800 mm
0	Orig	0	0	0	0	0
	St.	0	0	0	0	0
	Pol.	0	0	0	0	0
2000	Orig	0.004	0.003	0.002	0.0004	0
	St.	0.004	0.003	0.002	0.001	0
	Pol.	0.004	0.0022	0.0012	0.0006	0
4000	Orig	0.008	0.006	0.003	0.001	0
	St.	0.007	0.006	0.004	0.002	0
	Pol.	0.008	0.0044	0.0026	0.0012	0
6000	Orig	0.012	0.009	0.005	0.002	0
	St.	0.011	0.008	0.006	0.003	0
	Pol.	0.0124	0.0064	0.004	0.0016	0
8000	Orig	0.016	0.012	0.007	0.002	0
	St.	0.014	0.011	0.008	0.004	0
	Pol.	0.0160	0.0088	0.0052	0.0022	0
10000	Orig	0.020	0.015	0.008	0.003	0
	St.	0.018	0.014	0.010	0.004	0
	Pol.	0.0196	0.0108	0.0064	0.0028	0

Table (4) Natural frequencies of the original machine and the different models.

	Natural frequency (f) (Hz)			Damping ratio
	Measured	Transformed to steel	Transformed to original machine	
Original machine	107	—	107	0.065
Steel model	455	455	82.56	0.011
Polyamide model	160	515	93.5	0.07

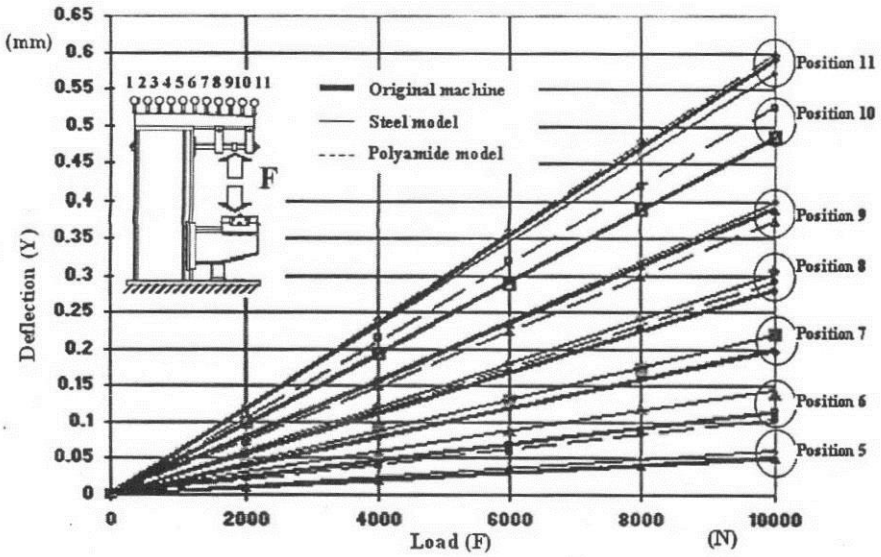


Fig. (6) Load-Deflection curves of the over-arms transformed to original machine

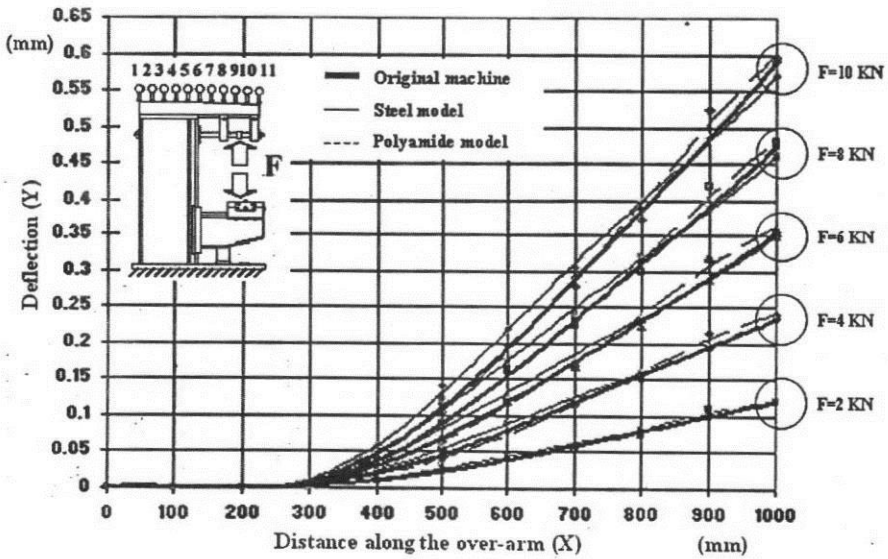


Fig. (7) Elastic lines of the over-arms transformed to original machine

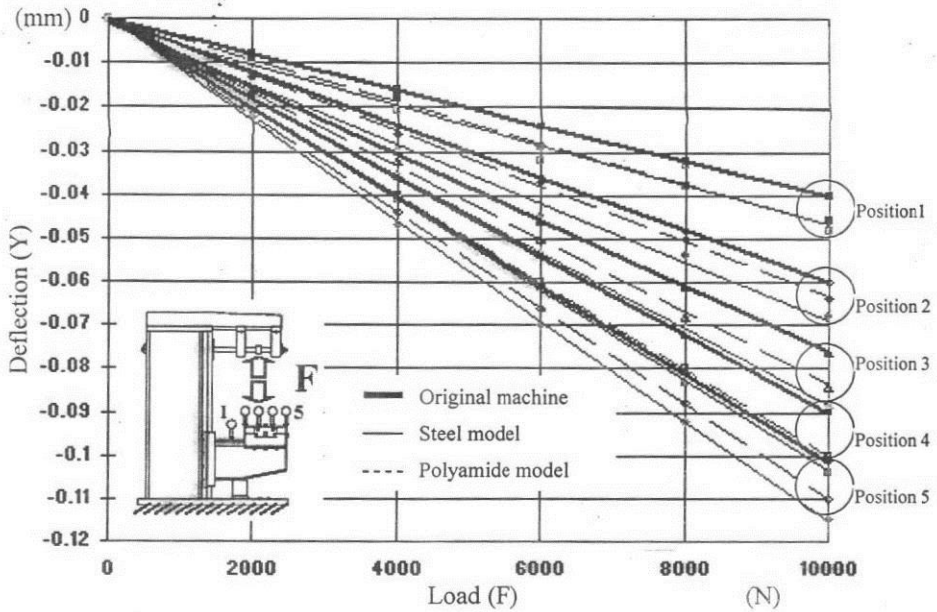


Fig. (8) Load-Deflection curves of the knees transformed to original machine

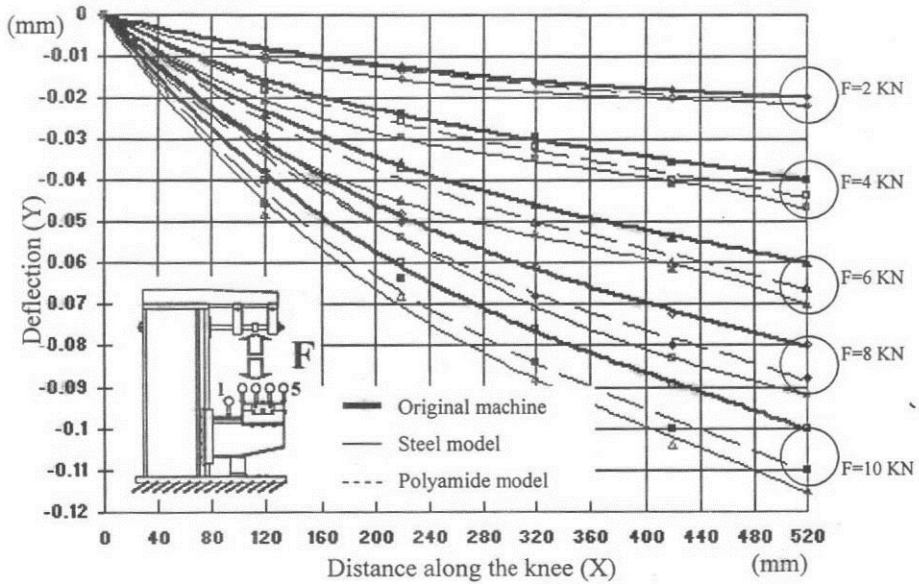


Fig. (9) Elastic lines of the knees transformed to original machine

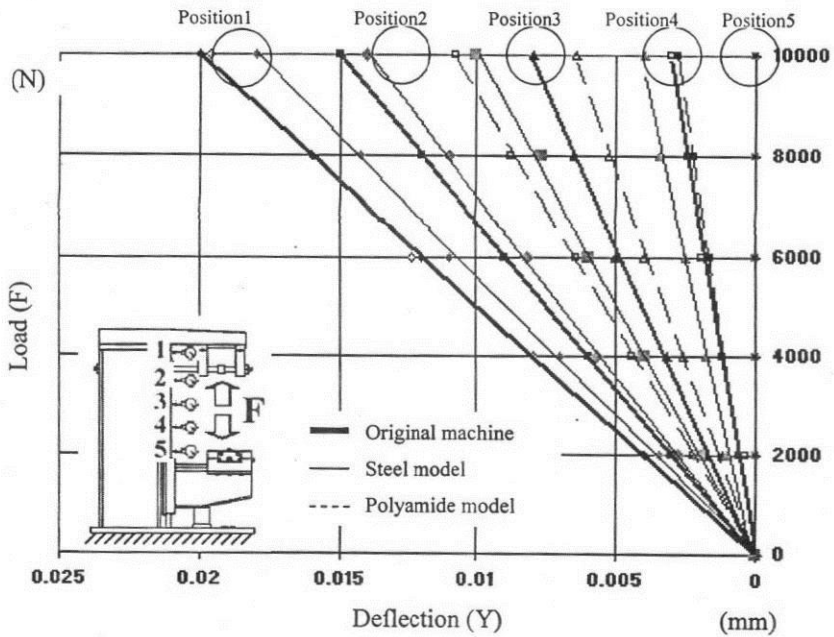


Fig. (10) Load-Deflection curves of the columns transformed to original machine

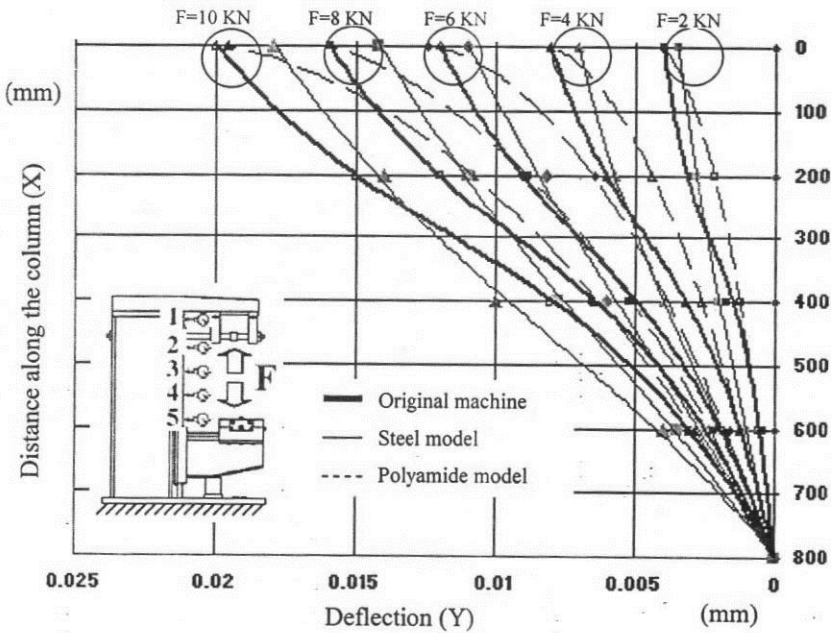


Fig. (11) Elastic lines of the columns transformed to original machine

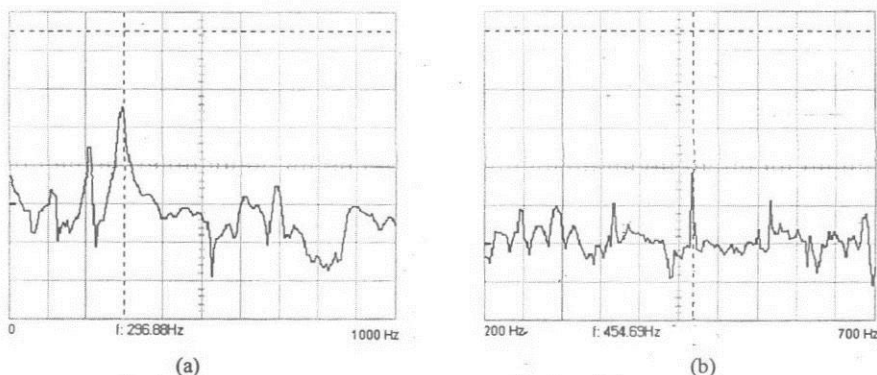


Fig. (12) Frequency response of the Steel (a) & RP (b) models.

From the comparison of the load-deflection behavior of the over-arms of both the steel, the RP model and the original horizontal milling machine (both models to original machine transformation), at the max applied load of $F=10000N$, it is clear that for the steel model the deflection ranges from 0 at position 1 to 0.57 mm at position 11, the max deviation is 0.025 mm at positions 6 and 8. However, the max deviation is 21.74% (position 6), and the min is 0% (position 10) and the average deviation is 8.79%. For the RP model the deflection ranges from 0 at position 1 to 0.595 mm at position 11, the max deviation of the model from the original machine is 0.039 mm at position 10. The max relative deviation is -8.7% (position 6), and the min is 0.51% (position 7).

The comparison of the load-deflection behavior of the knee of the RP model and the original machine knees at the max applied load of $F=10000N$, have a max deviation of 15% at position 1 and min deviation of 6.67% at position 2. While, the results of the load-deflection behavior of the knee of the steel model at the same load gives a max deviation of 20% at position 1 and min deviation of 13.33% at position 2. It is clear that the test results of the polyamide model knee are closer to the original machine than the steel model.

The results of the comparison of the steel model and the original machine columns deflections range between 0 to 0.018 mm at the max applied load ($F=10000N$). The deviation ranges from -0.002 mm to 0.001mm and from 33.33% to -10%, with average deviation of 10.42%. While the deviation of the RP model when transformed to the original machine ranges from -28% to -2%.

The transformed value of the natural frequency for the steel milling machine model is 22.84% lower than that of the original machine due to the lower rigidity of the welded structure. On the other hand, the natural frequency of the RP Polyamide model is only 12.62% higher than the original machine. Moreover, the RP model exhibits a damping ratio of 0.07, which approaches that of the original machine (0.065).

7- Conclusion

It is clear that the polyamide RP model gives closer results to the original cast iron machine structure for the load-deflection behavior and elastic-lines (max. deviation of -8.7%, 15% & -28%, and min. of 0.51%, 6.67% & -2% for the Over-arm, Knee and Column respectively) than the geometrically similar steel model (max. deviation of 21.74%, 20% & 33.33%, and min. of 0%, 13.33% & -10% for the Over-arm, Knee and Column respectively). Also the natural frequency has a deviation of 12.6% for the RP model and -22.84% for the steel model. Which can be due to the defects of the welded joints of the steel model structure, e.g. imperfections, cracks, etc. So Polyamide RP models can be successfully used to predict the static and dynamic performance of the cast iron machine tool structures in design, research and development phases.

References

- [1] Chris McMahan, J. Brown, Addison Wesley, "CAD/CAM from principles to practice", (1993).
- [2] Frank Kreith; "The CRC Hand book of Mechanical Engineering", (1998).
- [3] Frank M. White, "Fluid Mechanics" fourth edition (1999).
- [4] Gan G.K. Jacob, Chua Chee Kai, Tong Mei "Development of a new rapid prototyping interface", Computers in industry 39 (1999), pp. 61-70.
- [5] M.A.EL Hakim, "The influence of some design features on the static performance of a milling machine frame", Ph.D. thesis, faculty of engineering Ain Shams University, 1969.
- [6] M.A.EL Hakim, M.Y.Affifi, M.I.Khattab, "An optimized tunable damper for horizontal milling machines", Proceedings of 1st conference of Mechanical Power Engineering, Cairo, vol. 3 Feb 1977.
- [7] M.I.Khattab, "An optimized vibration damper for horizontal milling machines", M.Sc.Thesis, faculty of engineering Ain Shams University, 1977.
- [8] Sherif D. EL Wakil, "Processes and Design for Manufacturing", (2000).
- [9] S.H. Masood, A. Soo, "A rule based expert system for RP system selection", Robotics and Computer Integrated Manufacturing 18 (2002), pp. 267-274.
- [10] Xue Yan and P Gu "A review of rapid prototyping technologies and systems", Computer-Aided Design, vol.28, No.4, 1996, pp. 307-318.
- [11] "Sinterstation system user's guide", 3D systems co. December 2001.
- [12] Hany Fathalla, Mokbel, "Computer Aided Manufacturing of Reduced Scale Models for Machine Tool Structures Using Rapid Prototyping", Msc. thesis, Military Technical College, Cairo 2005.

AN EXPERIMENTAL INVESTIGATION OF THE EFFECT OF MAGNETIC FUEL TREATMENT ON SI ENGINE PERFORMANCE

Ahmed A. Abdel-Rehim*, Ramadan Abdel-Aziz*, Khairy H. El-Nagar*
Hamdy H. Maarouf**

* *Shoubra Faculty of Engineering, Benha University, Cairo, Egypt*

** *PetroJet, Cairo, Egypt*

ABSTRACT

The pressure imposed on science and scientists to attack all possible (and may be impossible) methods to achieve higher fuel and engine efficiency is well known. Not only driven by the extremely dangerous environmental situation (global warming and pollution), but also by other factors like fluctuating oil prices and depletion of fossil fuel resources. Due to these factors, research is going everywhere at a tremendous level to better use of available resources.

In the present study, a series of experimental work is introduced to explore the impact of fuel magnetic treatment on engine performance. Two main types of magnetic treatments were tested; the first type is depending on a permanent magnet, while the second type is depending on an electromagnetic magnet.

Two different designs for the electromagnetic device were examined to explore the effect of number of coils, material, source of electricity and some other parameters on engine performance.

Two fuels were examined, gasoline as a liquid fuel and Natural gas as a gaseous fuel. Some attractive results showed that we can increase engine power by 20 % and reduce fuel consumption by the same percentage depending on engine operating conditions. Promising results were obtained for the reduction in engine main pollutants (CO, HC, and NO_x).

I. INTRODUCTION

There are many ideas for fuel conditioning have been tried based on different techniques such as filters, catalysts, additives, etc.

Many inventors propose fuel saving products depending on the idea that combustion can be improved by treating the fuel with a magnetic field. Many of these magnetic products or devices have been patented and produced in order to reduce fuel consumption and engine emissions [1-18].

Technologies have ranged from simple clamp-on magnets to a variety of electric and electronic devices. Many of these products have met with limited success because there are a number of factors to take into account and variables to accommodate. For example, a device that applies a constant magnetic field of a constant strength will have a limited effect because different fuels can be fed at different rates through pipes of different materials, thicknesses and bores. Therefore, a somewhat more sophisticated approach is required.

For these reasons, the US Environmental Protection Agency (EPA) has published their reports, after testing some of these devices, to conclude that vehicles equipped with these devices (permanent magnets) did not show any improvement in fuel economy or in emissions reduction [19-23].

There are many different magnetic treatment methods used to treat engine fuels. A permanent magnet is a device which consists of multi-magnetic strips organized in an enclosure and produces a high frequency magnetic field on the fuel which passes through the device. Electromagnetic coils depend on generating the magnetic field from electricity using different circuit designs. In this case full control on the magnetic field strength is applicable depending on the operating conditions.

In the present study, a series of experimental work is introduced to explore the impact of fuel magnetic treatment on engine performance. Two main types of magnetic treatments were tested; the first type is depending on a permanent magnet, while the second type is depending on an electromagnetic magnet.

Two different designs for the electromagnetic device were examined to explore the effect of number of coils, material, source of electricity and some other parameters on engine performance.

Two fuels were examined, gasoline (92 Octane Number) as a liquid fuel and Natural gas (NG) as a gaseous fuel. Results were compared at the same conditions using the following indications:

- 1- When the engine is running without any modifications e.g. without applying any magnetic field the following expression is used (WITHOUT MAG).
- 2- When a permanent magnet is used, the following indication is used (PERMANENT MAG).
- 3- When the iron coil is used alone, it is indicated by (IRON COIL).
- 4- When the fiber coil is used alone, it is indicated by (FIBER COIL).

5- When the two coils are used together, the iron and the fiber ones, it is indicated by (DOUBLE COIL).

According to the source of the electricity, an alternative current is indicated by (AC), while a direct current is indicated by (DC).

II. EXPERIMENTAL SETUP

The experiments were conducted on a single-cylinder Honda model (GX390K1) 13 HP engine with a cylinder bore of 88 mm and a stroke of 64 mm. The compression ratio of the engine is 8.

Three different magnetic coils were used. The first coil is a permanent magnetic device which is used commercially in the market. The other two electromagnetic coils were custom made with the specifications shown in table (1). Appendix (A) shows a schematic diagram of the experimental setup

	Iron Coil	Fiber Coil
Core Material	Iron	Fiber
Wire length (L)	55 m	
Number of wire turns (N)	500	
Magnetic flux intensity (B)	5.56xI mTesla Where I is the current	
Current (I)	0.18 – 6.66 Amp.	

Table (1) Electromagnetic coils specifications

III. EFFECT OF MAGNETIC FLUX INTENSITY AND COIL MATERIAL

One important part to explore is the effectiveness of controlling magnetic flux intensity on engine performance and comparing the results with the permanent device.

Three different values for the magnetic flux intensity have been chosen to indicate the low, medium and high values as shown in table (2). These values were chosen as an average depending on the specifications indicated in table (1), the circuit design and temperature limitations.

No.	Description	Magnetic Flux Intensity (mT)
1	Low Flux	6.97
2	Medium Flux	13.95
3	High Flux	26.16

Table (2) Magnetic flux intensity used in the experiments.

Limited effect is shown in figure (1) for the iron and fiber coils when low flux was used compared to the permanent device. Not only limited effect from the low flux, but also the permanent magnetic flux seems to be more effective in this case. This can be explained by two effective properties for the permanent coil:

- 1- Design factor which results in magnetic flux migration between the different sets of north poles and south poles where the fuel passes in this case through a swirling magnetic movement between the north and south poles.
- 2- The length of the permanent magnetic coil, which reflects the whole fuel traveling distance, is relatively longer than the other two coils. This means that there is a longer contact path in the case of permanent magnet.

When a high flux was tested as shown in figures (2, 3 and 4) the magnetic effect started to be observed where table (3) summarizes the results.

Device type	Average increase in the output power (%)
Fiber coil –AC	7.5
Fiber coil –DC	7.9
Iron coil –AC	12
Iron coil –DC	13
Double coil –AC	12.3
Double coil –DC	14.4
Permanent coil	3.63

Table (3): Average increase in the output power (%) at the same engine speed for different types of magnetic coils.

As clearly seen in table (3), the following points can be stated:

- 1- The average increase in the engine power is 3.63% for the permanent coil over the range of speed and power in the present investigation.
- 2- Using high flux over the fiber coil doubled this effect.
- 3- Using iron coil at the same conditions increases the engine power compared to the fiber coil and this can be explained by the ability of iron to collect and concentrate the electromagnetic waves which means that the coil material is one important factor affecting the results.
- 4- In spite of this improvement in the coil effect on engine power when the iron coil was used, there is a side effect to increase the magnetic flux which is increasing the coil temperature. Increasing the coil temperature can burn the coil out. Accordingly we have limitations in using iron coil with variable or controllable flux.
- 5- Using the two coils in series (double coil) produced the maximum effect as shown in table (3). The reason behind this is the properties of the magnetic waves produced where the double coil has two properties: The first one is the nature of magnetic flux which is affected by the two coil specifications. The second is the total length of the two coils together.

IV. EFFECT OF CURRENT SOURCE AC OR DC.

Another important parameter to explore is the effect of the origin of the current used. AC current from the outlet lab source was used accompanied by a suitable circuit, while the engine battery was used to generate the DC current using another suitable circuit.

When fiber coil was tested with AC and DC, figure (2), no difference between the two sources was observed except the last point at high power and high speed.

The experiment was repeated for the iron coil, and double coils where the same trend is clearly seen in figure (3) and figure (4) respectively.

Accordingly from these observations, there is no difference between AC and DC current on the engine power, except the stability in the behavior of the data recorded by the DC current, which can be explained by the nature of the AC current which behaves as a sine wave compared to constant behavior of the DC current. Regardless of the initial observation of no difference between AC and DC, both types will be under investigation in most of the study.

V. IMPACT OF MAGNETIC TREATMENT ON LIQUID FUEL (GASOLINE)

V.1 Fuel Consumption

Figures (5.a) and (5.b) represent a relationship between engine power and the corresponding fuel consumption for AC & DC current sources. The engine speed was maintained constant for the same compared power value while the throttling position was adjusted to obtain the same speed and power.

The figures show reductions in fuel consumption by using magnetic fuel treatment.

As clearly seen, using double coil with high flux results in better effect on the fuel consumption where a reduction of 20% can be achieved compared to 9 % for the permanent coil.

A direct comparison between AC current and DC current is illustrated in figure (5.c). The previous observations still applied on this figure.

Figure (6.a) shows the effect of magnetic field when allowing engine speed to be varied and maintaining the same throttling position for the engine power.

The same trend was obtained as discussed earlier where the double coil is still producing the best effect over the other coils with an average reduction of 20 %.

The whole experiment was repeated using DC current as shown in figure (6.b) and both current sources were compared in figure (6.c) where no effective variation between both currents is recorded.

V.2 Effect of Magnetic Treatment on Brake Specific Fuel Consumption (BSFC)

The effect of magnetic treatment on engine BSFC is shown in figure (7.a) for the coils under investigation. In this experiment AC current was used.

As clearly seen in the figure the three coils (iron, fiber and double coil) are very close in their effect.

But at the same time, the figure shows a noticeable reduction in BSFC when the magnetic effect is considered even for permanent magnet.

The same treatment is obtained when the experiment is repeated using DC source as shown in figure (7.b).

Figure (7.c) shows a comparison between the two current sources where no significant change is observed.

Figures (8.a) and (8.b) show the effect of magnetic treatment when maintaining the same throttle position at the same power value. In this case, as mentioned earlier, it was allowed to the engine speed to change according to the output power. In this case the maximum reduction in engine BSFC of 26 % was obtained for the double coil using AC current, while the maximum reduction of 28.5 % in engine BSFC was obtained for the double coil using DC current.

Figure (8.c) shows a direct comparison between AC and DC current. In this figure limited enhancement is observed and the difference between the two sources varied from 1 % to 6.2 %.

V.3 Effect of Magnetic field Treatment on Engine Exhaust Emissions

In this section, the impact of using magnetic field on engine emissions was investigated. In this case, measurements of unburned hydrocarbons (HC), carbon monoxide (CO), nitrogen oxides (NO_x) were plotted for the three coils using DC current source. Three different output powers, 1500W, 3000W, 4500W were chosen to illustrate this effect.

Figures (9, 10, and 11) represent the effect of magnetic flux intensity generated from DC current source on CO, HC, and NO_x emissions for the three coils at three different output powers. The following points can be observed from the figures:

- a) A fairly linear relationship between the magnetic flux intensity and engine emissions for the three coils.
- b) The double coil represents the best choice due to its effect on CO, HC, and NO_x emissions which recorded to reach 61.5, 53, and 50 % respectively at the maximum flux compared to the initial point (where no magnetic effect).
- c) Variable magnetic fluxes produce better effect on engine CO emissions compared to the permanent coil.
- d) There is no significant reduction in NO_x emissions with increasing flux intensity compared to CO and HC. This can be explained by the dependence of

NO_x formation on operating temperatures which are affected by the engine power.

VI. EFFECT OF MAGNETIC TREATMENT ON GASEOUS FUEL (NATURAL GAS)

It was reported in the previous sections that magnetic fuel treatment has an impact on the engine performance; especially the rate of fuel consumption and it was discussed that double coil has the best effect compared to the other two coils. Also, it was reported that DC current produces more stable output data compared to AC current.

In the present section, the effect of magnetic field on gaseous fuels (specifically NG) is presented. Most parameters related to engine performance are discussed again for natural gas but in this case the investigation is limited to the double coil which proved to treat the fuel better than the others.

VI.1 Effect of Magnetic Treatment on Fuel Consumption, Brake Power and BSFC for NG

Figure (12) shows a comparison between the rate of fuel consumption without magnetic treatment and with magnetic treatment using double coil and AC source. The results show an increase in the range of 2.5-7% in engine's power at the same fuel flow rate or a reduction of about 4-10% in fuel consumption at the same power. At the same conditions, a reduction of 6.5-13.8% in BSFC can be obtained using magnetic treatment as shown in figure (13).

VI.2 Effect of Magnetic Treatment on Exhaust Emission for NG

The effect of magnetic treatment on HC, CO and NO_x emissions using NG as a fuel is indicated in figure (14). The maximum reductions in CO, HC, and NO_x emissions for the three tested loads are summarized in table (4).

Figure (15) represents a comparison between the effect of magnetic treatment on gasoline and NG for CO, HC, and NO_x emissions at 1500 watt. Table (5) summarizes this comparison. The comparison shows that the magnetic treatment is more effective on gasoline fuel than NG fuel which can be explained by the tendency of liquid fuel molecules to change their random organization to a more simple structure which simplifies the combustion reactions. On the other hand, it is not easy to force the gaseous molecules to keep their new positions for a long period of time. Accordingly, losing the magnetic effect on gaseous fuels is faster than liquid fuels due to the effect of their density. Another important reason that natural gas does not contains additives which increase the fuel tendency to the magnetic field effect.

Pollutant	Maximum reduction		
	1500W	1900W	2500W
CO	15.5%	19%	20%
HC	19.1%	13.5%	9.7%
NO _x	55.5%,	25%,	26.4%

Table (4) Maximum reductions in engine emissions when NG was used

Pollutant	Maximum reduction	
	Gasoline	NG
CO	32.7%	19.1%
HC	52%	15.5%
NO _x	46.4%,	55.7%,

Table (5) Maximum reductions in engine emissions when NG was used

From the previous discussion, it can be concluded that using magnetic fuel treatment enhances the combustion characteristics of natural gas which results in better combustion and reduction in engine exhaust emissions. This reduction can reach 50% or more for some of these emissions.

VII. CONCLUSIONS

In the present study, two sets of experiments were carried out; the first set was focused on exploring the impact of magnetic fuel treatment on engine performance using gasoline as a liquid fuel, while the second set was concerned with natural gas as a gaseous fuel.

Three different coils having different features were compared at different operating conditions. The main results are summarized as follows:

1. Magnetic coil design has a considerable effect on the engines measured parameters. Total wire length, coil length, magnetic flux intensity, current source are some examples of these design parameters. The difference between AC and DC current on the engine performance parameters is limited to the stability in the behavior of the data recorded by the DC current compared to AC current.
2. Magnetic fuel treatment has an acceptable effect on engine performance. Fuel consumption was reduced by more than 20 % at some operating conditions, and BSFC was reduced by more than 27 % for some other conditions.
3. A reduction in the engine pollutants was clearly observed when magnetic field was applied to reach reductions of 50 % or more depending on the operating conditions and design of the coil used.
4. Higher influence of magnetic fuel treatment was recorded for liquid fuels compared to gaseous fuels.

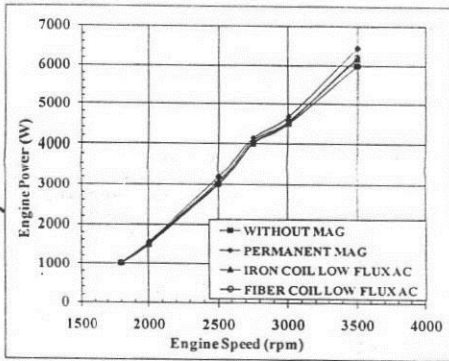


Figure (1) Effect of low flux intensity on engine power using AC current.

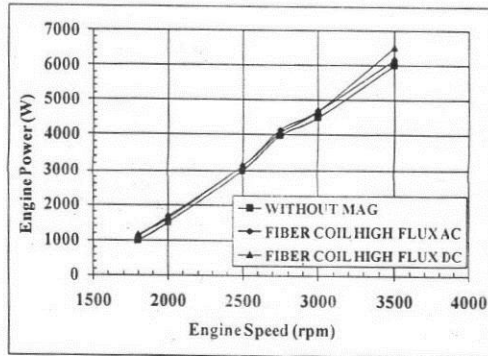


Figure (2) Effect of current source (current type) on the engine output power using fiber coil at high flux.

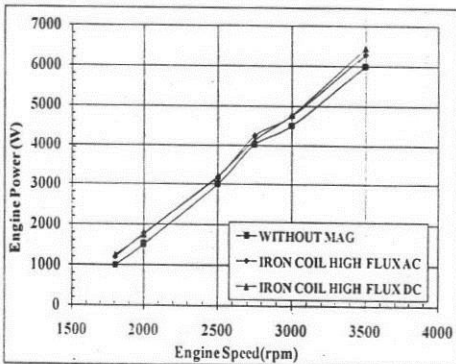


Figure (3) Effect of current source (current type) on the engine output power using iron coil at high flux.

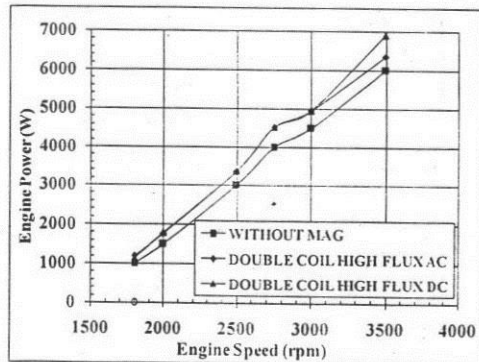


Figure (4) Effect of current source (current type) on engine output power using double coil at high flux.

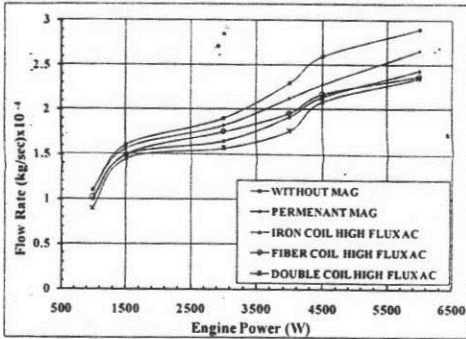


Figure (5.a) Effect of magnetic treatment on fuel flow rate using AC.

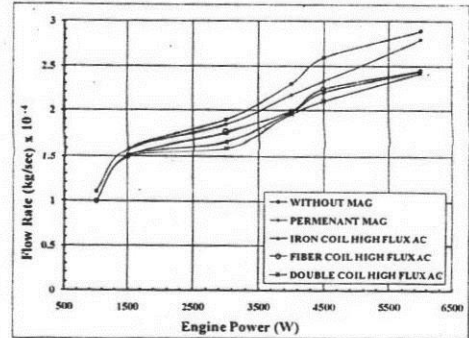


Figure (6.a) Effect of magnetic treatment on fuel flow rate using AC.

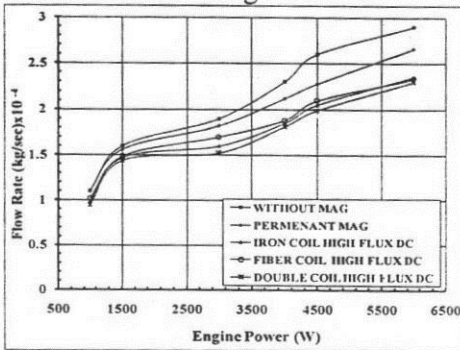


Figure (5.b) Effect of magnetic treatment on fuel flow rate using DC.

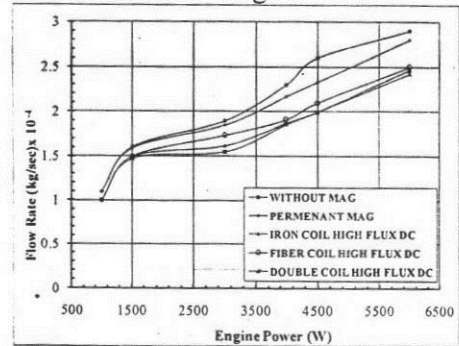


Figure (6.b) Effect of magnetic treatment on fuel flow rate using DC.

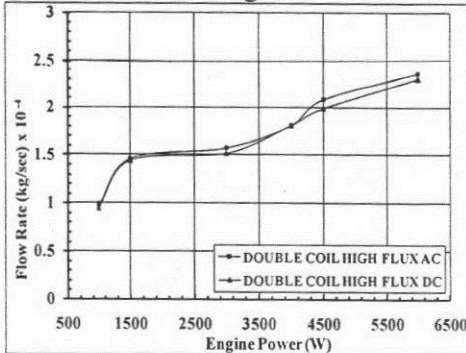


Figure (5.c) Comparison between AC and DC.

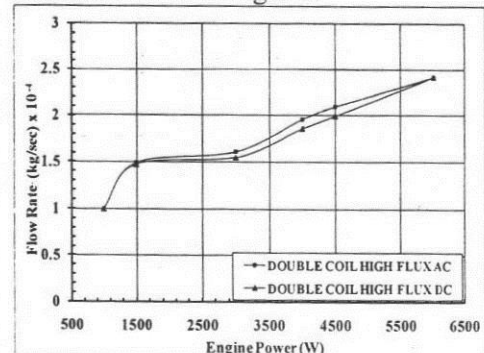


Figure (6.c) Comparison between AC and DC.

Figure (5) Effect of magnetic treatment on fuel flow rate using AC and DC current sources and maintaining the engine speed constant at the same power.

Figure (6) Effect of magnetic treatment on fuel flow rate using AC and DC current sources and maintaining the same throttling position at the same power.

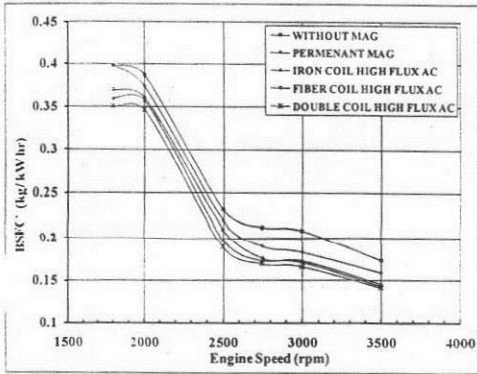


Figure (7.a) Effect of magnetic treatment on BSFC using AC.

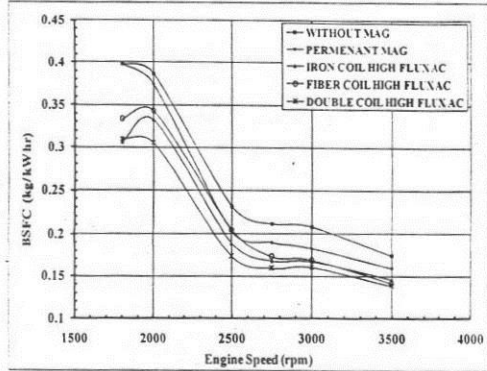


Figure (8.a) Effect of magnetic treatment on BSFC using AC.

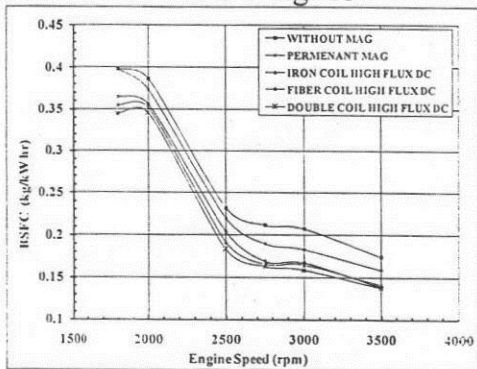


Figure (7.b) Effect of magnetic treatment on BSFC using DC.

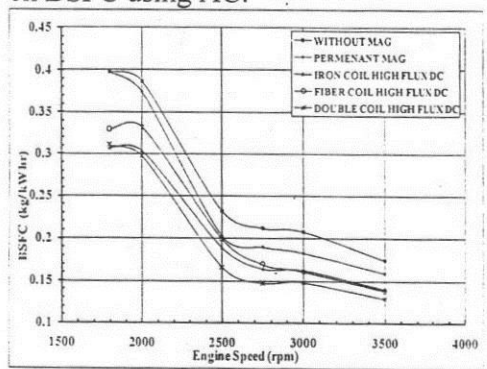


Figure (8.b) Effect of magnetic treatment on BSFC using DC.

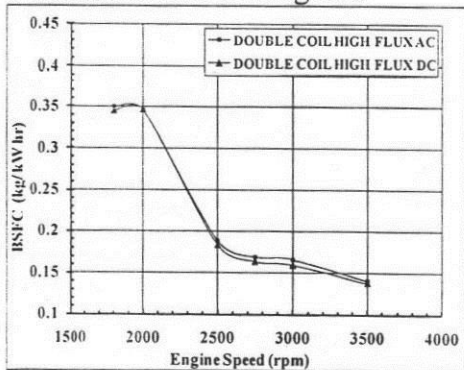


Figure (7.c) Comparison between AC and DC sources.

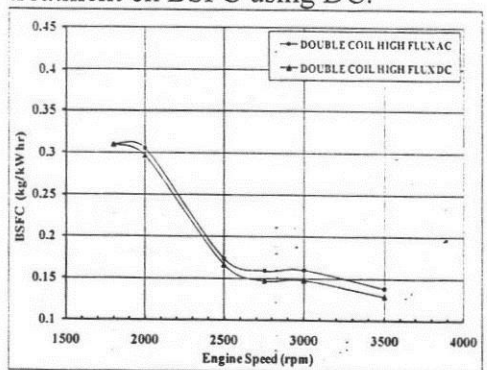


Figure (8.c) Comparison between AC and DC sources.

Figure (7) Effect of magnetic treatment on BSFC using DC and AC sources while maintaining engine speed at the same compared power.

Figure (8) Effect of magnetic treatment on BSFC using AC and DC sources and maintaining the same throttling position at the same power.

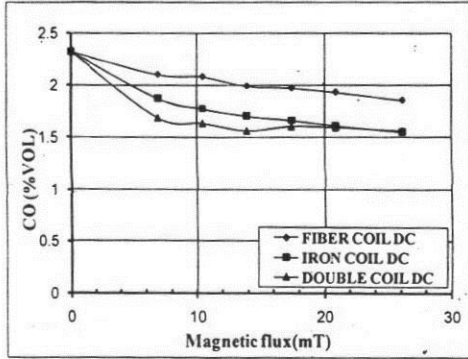


Figure (9-a) 1500 W, 2000 rpm.

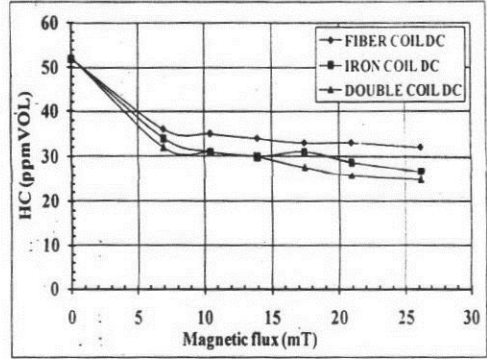


Figure (10-a) 1500W, 2000 rpm.

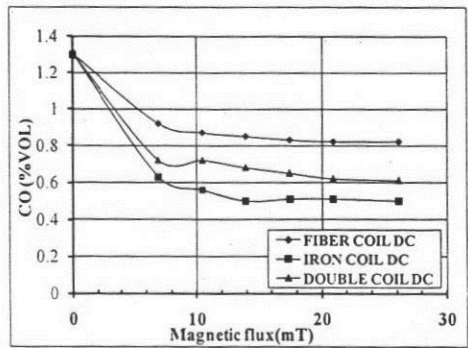


Figure (9-b) 3000 W, 2500 rpm.

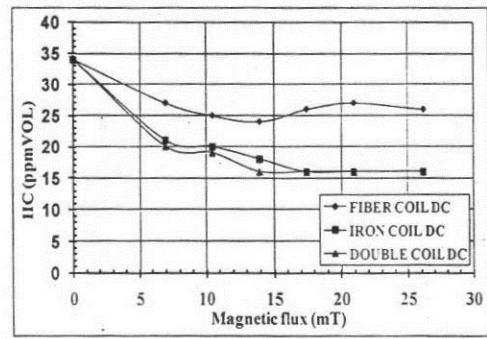


Figure (10-b) 3000W, 2500rpm.

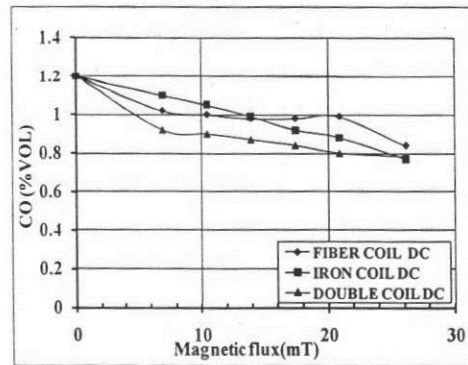


Figure (9-c) 4500 W, 3000 rpm.

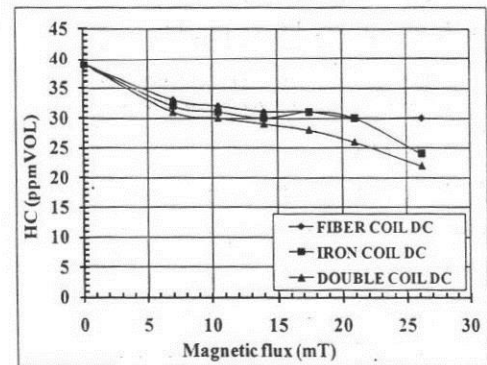


Figure (10-c) 4500W, 3000rpm.

Figure (9) Effect of magnetic treatment on CO emission using DC for different output powers and speeds.

Figure (10) Effect of magnetic treatment on HC emission using DC for different output powers and speeds

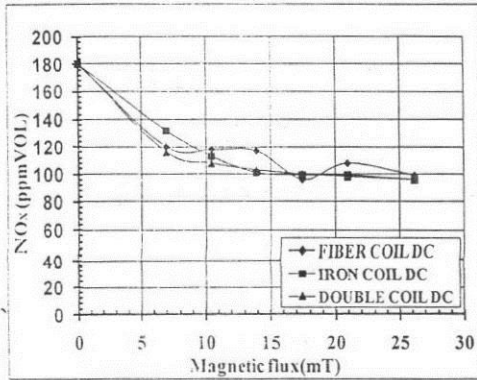


Figure (11-a) 1500 W, 2000 rpm.

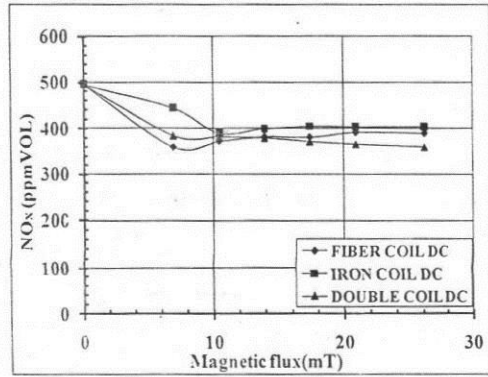


Figure (11-b) 3000 W, 2500 rpm.

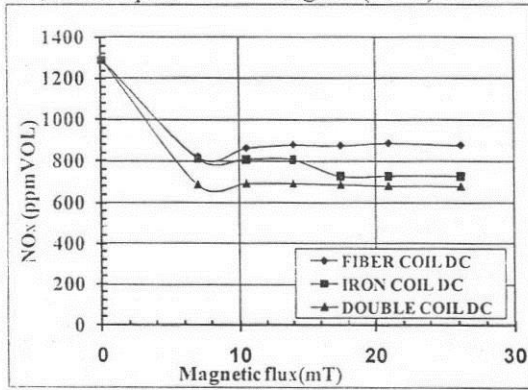


Figure (11-c) 4500 W, 3000 rpm.

Figure (11) Effect of magnetic treatment on NOx emission using DC at different output powers and speeds.

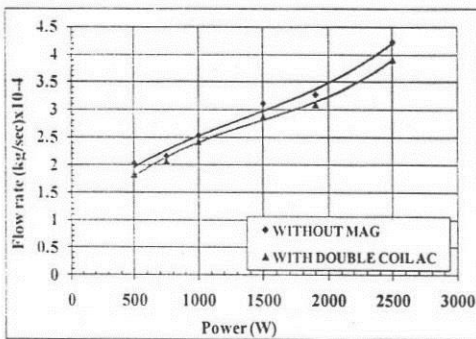


Figure (12): Effect of magnetic treatment on fuel flow rate for NG.

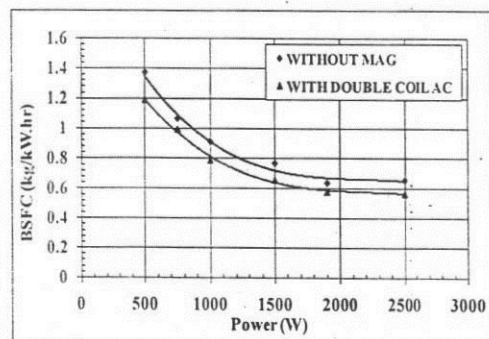


Figure (13): Effect of magnetic treatment on BSFC for NG.

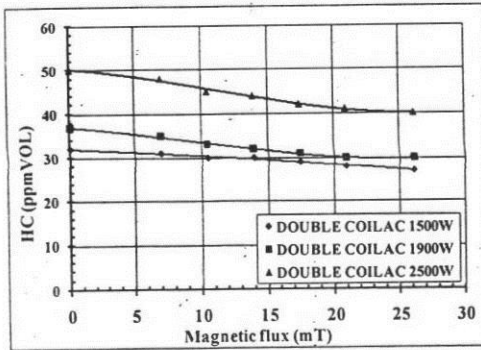


Figure (14.à) HC

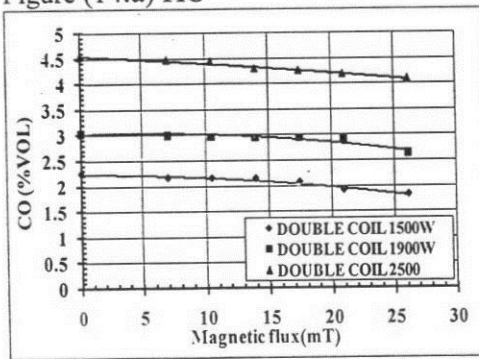


Figure (14.b) CO

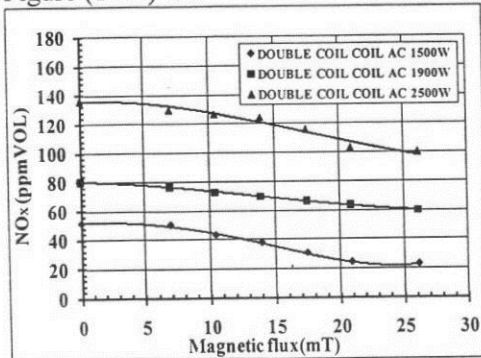


Figure (14.c) NOx

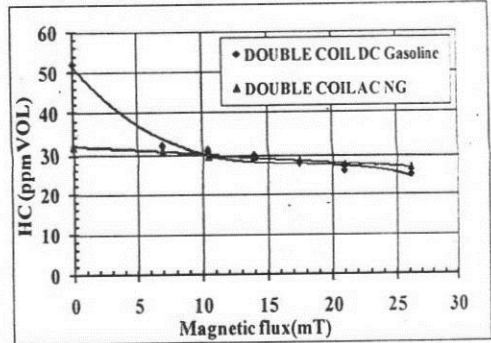


Figure (15.a) HC comparison.

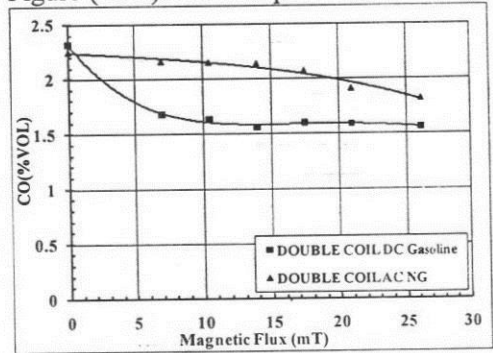


Figure (15.b) CO comparison

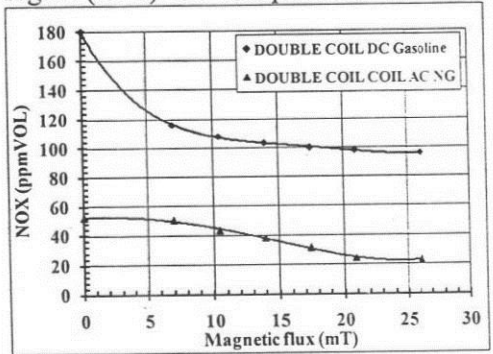


Figure (15.c) NO_x comparison

Figure (14) Effect of magnetic treatment on CO, HC, and NO_x for NG at 1500, 1900, 2500 Watts and variable speeds.

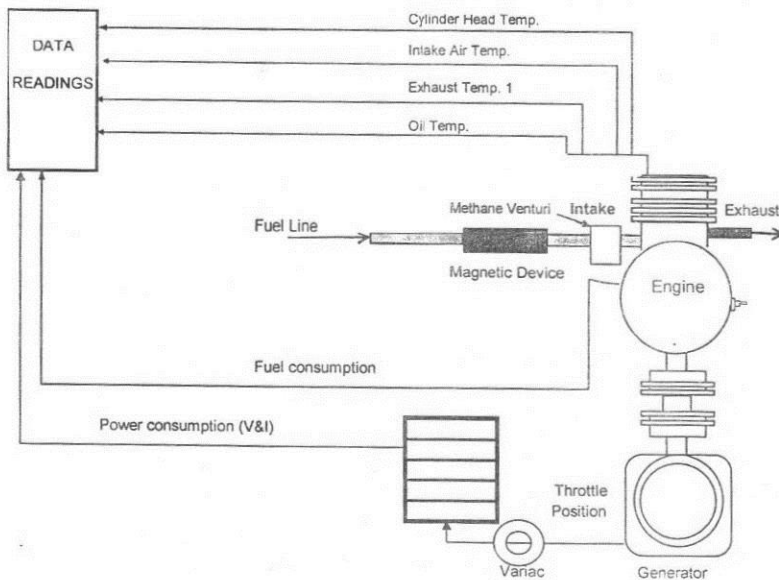
Figure (15) A comparison between the effect of magnetic treatment on gasoline and NG for engine emissions at the same conditions of $\lambda = 0.95$, 1500W and maintaining engine speed at the same compared points.

I. REFERENCES

1. Michael J. Kwartz; "Device for internal combustion engines", United States Patent Office no.3, 116,726, patented Jan.7, 1964.
2. Doyle H. Miller; "Process and apparatus for effecting efficient combustion", United States Patent Office no.3, 830,621, patented Aug.20, 1974.
3. Charles H. Sanderson; "Device for the magnetic treatment of water and liquid and gaseous fuels", United States Patent Office no.4, 357,237, patented Nov.2, 1982.
4. Karl Heckel; "Electromagnetic fuel saving device", United States Patent Office no.4, 381,754, patented May.3, 1983.
5. Bill H. Brown; "Fuel treating device and method", United States Patent Office no.4, 429,665, patented Feb.7, 1984.
6. Edward Chow; "Fuel treating device ", United States Patent Office no.4, 461,262, patented Jul.24, 1984.
7. Carl Wolf; "Liquid Fuel treatment apparatus ", United States Patent Office no.4, 469,076, patented Sep. 4, 1984.
8. Koichi Wakuta; "Method of combustion fuel in an internal combustion engine and its apparatus ", United States Patent Office no.4, 538,582, patented Sep.3, 1985.
9. John Mitchell; "Magnetic fuel line device ", United States Patent Office no.4, 572,145, patented Feb.25, 1986.
10. Claud W. Walker; "Pollution control through fuel treatment ", United States Patent Office no.4, 715,325, patented Dec.29, 1987.
11. Ben C. Song; "Device for magnetically treating hydrocarbon fuels "; United States Patent Office no.4, 933,151, patented Jun.12, 1990.
12. Wallace R. Jone; "Fuel treating device "; United States Patent Office no.4, 930,483, patented Jun.5, 1990.
13. Clark L. Daywalt; "Fuel treating device "; United States Patent Office no.5, 048,499, patented Sep.17, 1991.
14. Andrew Janczak & Edward Krensel; "Permanent magnetic power cell system for treating fuel lines for more efficient combustion and less pollution "; United States Patent Office no.5, 124,045, patented Jun.23, 1992.
15. Charlie W. Richard; "Fuel treating methods, compositions and device "; United States Patent Office no.5, 069,190, patented Dec. 3, 1991.
16. Romulo V. Dalupin; "Magnetic apparatus for treating fuel"; United States Patent Office no.5, 127,385, patented Jul.7, 1992.
17. Brain Pascall; "Fuel conditioning device "; United States Patent Office no.5, 533,490, patented Jul. 9, 1996.
18. David J. Butt; "Hydrocarbon fuel modification device and a method for improving the combustion characteristics of fuels "; United States Patent Office no.6, 024,073; patented Jul. 9, 2000.

19. Barth E. A., "EPA Evaluation of the PETRO-MIZER Device under Section 511 of the Motor Vehicle Information and Cost Savings Act", EPA report, EPA-AA-TEB-511-83-2, December 1982.
20. Barth E. A., "EPA Evaluation of the POLARION-X Device under Section 511 of the Motor Vehicle Information and Cost Savings Act", EPA report, EPA-AA-TEB-511-82-9, August 1982.
21. Barth E. A., "Second EPA Evaluation of the POLARION-X Device under Section 511 of the Motor Vehicle Information and Cost Savings Act", EPA report, EPA-AATEB-511-85-2, April 1985.
22. Hashby H. A., "EPA Evaluation of the Super-Mag Fuel Extender under Section 511 of the Motor Vehicle Information and Cost Savings Act", EPA report, EPA-AATEB-511-82-3, January 1982.
23. Shelton J. C., "EPA Evaluation of the Wickliff Polarizer under Section 511 of the Motor Vehicle Information and Cost Savings Act", EPA report, EPA-AA-TEB-511-81-17, June 1981.

Appendix (A): A schematic diagram of the experimental setup



MATHEMATICAL MODELS SIMULATE SCOUR DEPTH UNDER EFFECT OF GATE OPERATING SYSTEMS [A COMPARISON STUDY]

Abdelmoez. M. Hesham* and Mohamed A. Nassar**

*Professor, Physics and Eng. Mathematics Dept., Mataria Faculty of Engineering, Helwan University, Cairo, Egypt, Email: hahdelmoez@yahoo.com,

**Assistant Professor, Water & Water Structures Engineering Dept., Faculty of Engineering, Zagazig University, Zagazig 44519, Egypt, Email: nasserzagazig@yahoo.com

ABSTRACT:

This paper describes how the data analysis function contained within the Microsoft Excel® 2007 spreadsheet package can be used to simulate scour depth. The data analysis function is readily employed to create a simple functional solution to the problem of not only single but also generalized regression curve fitting. The method is illustrated with four worked practical examples. They are four mathematical models for simulating the effect of sudden and ordinary opening of the gates on scour characteristics DS of multi vent regulators. The approach suggested is simple to understand and apply, and only requires that any proposed model can be described using the standard mathematical and statistical functions contained within Excel. The method is thus capable of fitting a wide range of different models and, because of the simplicity of the solution approach, can be readily applied to evaluate the 'comparative goodness of fit' of several different models.

KEYWORDS:

Mathematical modeling, statistical analysis, gate operation, scour.

1- INTRODUCTION

Fitting an appropriate curve or model to a series of data points and then extrapolating the model is a fundamental requirement in the disciplines of civil Engineering. One of the most popular fields of study in the branch of open channel hydraulics together with irrigation structures is the effect of gate operating systems on scour depth downstream (DS) of regulators [3]. These systems are namely sudden and ordinary gate operating systems. The sudden case simulates the gate opening after the winter closure or at the beginning of operation after the construction stage, in which the DS reach was completely dry while the water level in the US reach was at the maximum stage corresponding to the passing discharge. In contrast, the ordinary case simulates the opening while the tail water level at the normal stage [4].

A broader understanding of how to fit a particular mathematical model and why that model should be selected are frequently overlooked. This paper suggests how the available standard curve fitting functions, contained in Microsoft Excel [6, 8] spreadsheet package can be enhanced by employing the built in regression functions to create a simple functional solution to the two mathematical models problems.

2- OVERVIEW

Frequently in engineering, data is collected and plotted as a graphical representation of the variables involved. The next reaction is to create an association between the variables by connecting the points with a line [2]. Once drawn, the line is examined and a mathematical model which best fits these data points, assumed. This is then fitted and used to replace the existing set of data points as 'the appropriate mathematical model'. Having thus mathematically modeled the data, this model is used to predict future values of one variable, given changes in the other extrapolation.

The foregoing statement covertly mentions several features of the problems that often inhibit achievement and limit confidence in any subsequent extrapolation from the mathematical model. These are:

- The validity of the assumption, that the data points are, or can be, connected.
- That the mathematical model selected, is the most appropriate one for the collected data.
- That a curve fitting method is available, useable, and understandable.
- That the mathematical model parameters can be obtained.
- That present facts are reflective of future behavior.

Most head- and cross-regulators constructed along the main and branch canals of the irrigation network have few vents. In the last few decades, the characteristics of local scour DS of the regulators have been investigated using single-vent models. In addition, a few studies investigated the effect of gate operation on flow and scour characteristics such as: design of the sudden expansion and radial stilling basins DS of multi-vent regulators [5], and the effect of different operating systems of multi-vent regulators on scour characteristics [1]. The literature survey reveals that there is no study available for investigating the effect of gates management and operation on scour characteristics DS of multi-vent regulators [10].

3- DIMENSIONAL ANALYSIS

The local scour DS regulators with radial stilling basins is very complicated phenomenon. The dimensional analysis was employed to drive an expression relating the different variables affecting the phenomena, see Fig. (1). The main function expressing the scour phenomenon characteristics can be presented as:

$$d_s/y_1 = f(F_1, e, \text{ and } y_2/y_1) \tag{1}$$

in which: d_s/y_1 is the relative scour depth, F_1 is the initial Froude number, e is the expansion ratio, and y_2/y_1 is the relative jump depth.

4- EXPERIMENTAL WORK

The experimental work was carried out in the Hydraulics Laboratory of the Faculty of Engineering, Zagazig University. The experiments were carried out in a re-circulating laboratory flume 30cm wide, 46.8cm deep with an overall length of 15.6m. The discharge was measured using a pre-calibrated orifice-meter installed on a feeding pipeline. The middle part of the model consisted of three-adjacent vents, each one of 7cm wide, 35.5cm deep and 23cm length. The width of the pier is 1.2cm and the wing wall width is 3cm. The different operating scenarios of the three-vent regulator model were tested under the same flow conditions, as defined in Table (1).

Table (1): Features of Different Scenarios for Operating 3-Vents Regulator

Flow Condition	Symmetric Case			Asymmetric Case		
	e = 1.41	e = 2.12	e = 4.22	e = 1.41	e = 2.12	e = 4.22
Expansion Ratio	3-Gates	2-Gates	1-Gate	3-Gates	2-Gates	1-Gate
Operating System	(A+B+C)	(A+C)	(B)	(C)+(1+2)	(A)+(3)	(A)
Gate Symbol	(A+C)+(2)	(1+3)	(2)	(A)+(3)	(1+2)	(1)
	(B)+(1+3)	(A)+(3)		(A)+(2)		
	(1+2+3)					

The rest of the flume (7.5m) is covered by two types of sediment, consisting of 10 cm sand layer. The first type is a coarse type according to the soil classification, which was proposed by the subcommittee on the sediment terminology of the American Geophysical Union. It has been used for the sudden opening cases, D_{50} of 0.6 mm. The second type is a medium type; it has been used for the ordinary opening cases, D_{50} of 0.275 mm. The sieve analysis of each type of sand is presented as shown in Figs. (2A, 2B), respectively.

5- DIFFICULTIES WITH MATHEMATICAL MODEL SELECTION

A brief examination of most standard texts on data and its analysis will show that commonly only a limited number of standard models are normally described. Those frequently mentioned are the simple linear model ($y = ax + b$) or those that can

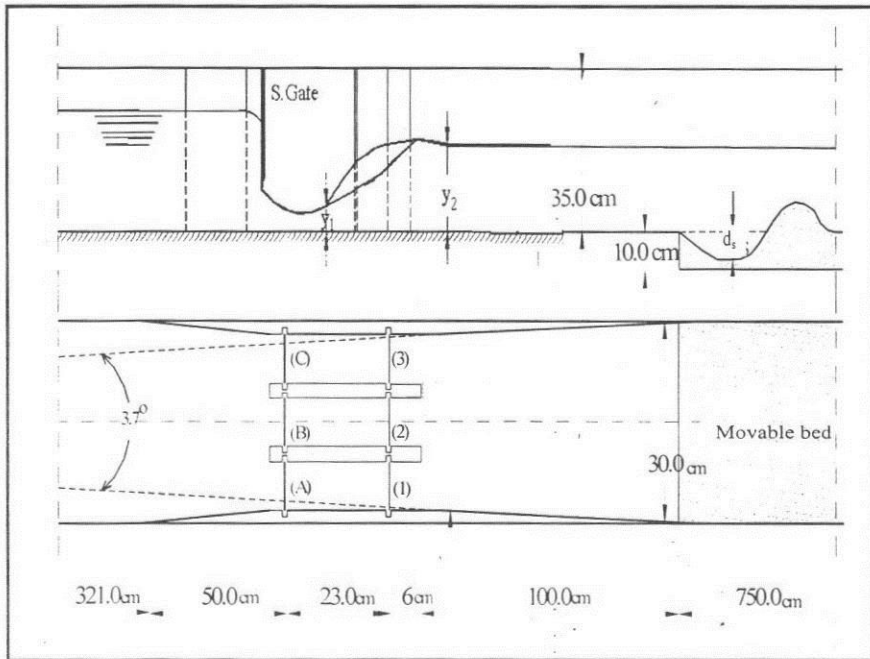


Figure 1 A definition sketch for the experimental model.

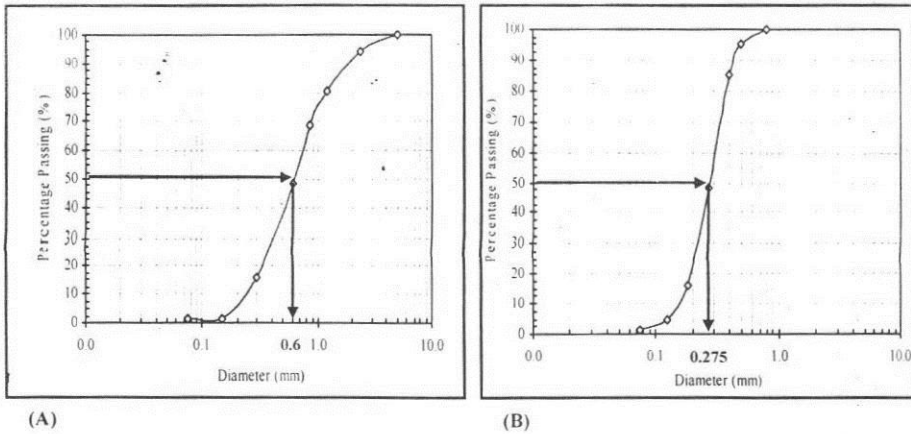


Figure 2 The sieve analysis of the sand specimens (A) coarse type (B) medium type

easily be transformed into a simple linear form ($y = ae^x$) [7]. Invariably, the text will offer a discourse on the theory of curve fitting, followed by a derivation of the normal equations and conclude with advice on how simple curves can be either mathematically transformed or linearised with the aid of specialist graph paper. The usual advice given will be to prepare a simple plot of the data, either on linear or logarithmic graph paper, confirm that the data exhibits a linear tendency, undertake the necessary transformation and then apply the least squares criteria to obtain the *line of best fit*. Typically little or no advice will be offered on the selection, fitting or choice of model for a given data set, nor how more unusual curves can be fitted.

As an example of a more unusual model, consider the curve fitting problems associated with causality [which expresses the relationships between cause and effect in a system]. Data collected from a causality situation is frequently modeled as a hyperbolic tangent (tanh) function. Although best fits for such models can be obtained, using mathematical transformations, or linearised using the less common graph papers, very few analysis will be capable of recognizing these models and even fewer will have the expertise to undertake the necessary curve fitting.

The problem of selecting the most appropriate model has been, and continues to be, one of the most difficult aspects of data modeling. Experience in data modeling is vital if good data fits are to be obtained. Experience comes from practice, coupled with a good understanding of function plots and the parameters that affect them. The best advice that can be offered to any would-be model builder is to employ a spreadsheet system to create a whole range of simple function plots, experiment with changing the parameters and examine the resulting plot forms. By this means it is possible to experiment with a wide range of models in a short time period. The problem of selecting the most

appropriate model can be readily resolved by employing the method detailed in this paper on a number of models and comparing both the coefficient of determination (R^2) and the sum of the squared errors or standard error (E) values for each model.

Since the advent of popular computing in the early 1970's, there have been a number of major developments in the availability of applications packages to undertake curve fitting. In the formative years it was common for machine manufacturer, specialist computing groups or programming language providers to provide the necessary software. These were invariably subroutines which could be called from within a program. They were not user-friendly and often machine or software specific.

In time, as personal computing developed and the software platforms and operating environments established, portable third-party software packages flourished such as SPSS, MATHCAD, MAPLE, and etc.... However they were and still are specialist application packages for those who have the time and knowledge to use them. However, once the more universal computing era began (integrated word processor, spreadsheet and database applications package), the need for simple curve fitting models and standard statistical data analysis tools, became evident. Consequently, spreadsheet providers have since incorporated both powerful data analysis tools and curve fitting add-ins into such packages. In the context of the curve fitting add-ins these were inevitably tailored to the limited demands of the typical user. Consequently those users who wished to consider and fit more complex models have had to undertake the task themselves or resort to specialist applications packages, such as those previously mentioned. Regrettably such packages are often mounted outside a normal work environment and can be problematic in effecting the import/export of data between applications.

Experienced users of Excel [9] will be familiar with the standard curve fitting functions and how they are evoked. Typically the user will enter the data into a range of cells, create a chart, point with the mouse to the data plotted on the chart to highlight the data series and then click on the toolbar to activate the *Trendline* function via the right click popup menu. The available models are:

- Linear ($y = ax + b$);
- Logarithmic ($y = a \ln x + b$);
- Polynomial ($y = b + a_1x + a_2x^2 + a_3x^3 + \dots$);
- Power ($y = ax^b$); and
- Exponential ($y = ae^{bx}$).

The *Trendline* function permits the user to obtain a least squares fit to a given data series using any of the above models. Once undertaken, the fitted equation can be displayed on the chart.

Excel versions 2007 and above, have an add-in facility included in the Data menu, called *Data Analysis*. It is an optimization procedure which can be used to generate solutions to a wide spectrum of linear non-linear and integer

problems. It uses regression to find the optimum values for a given y-cells and the changed values of x-cells according to assumed mathematical model. Thus to solve a problem we need knowledge of:

Destination y-cells.

Target changed x-cells.

Once these have been defined, and the search conditions and solution parameters specified, a solution to a particular problem can be then obtained. Once a solution has been generated, *Data Analysis* permits the user to keep, or reject, the solution found. Additionally, it can create reports which summaries important statistical properties for the solution obtained such as the *Determination Coefficient* (R^2) and the standard error (E).

6- ANALYSIS OF EXPERIMENTAL DATA

The effects of the different hydraulic operating systems have been discussed in the following sub-sections. Three main categories were performed to express the phenomena. These relationships are translated into graph figures concluding (x-y) relationships.

Now we want to design the mathematical model to fit a general equation which passes throughout most of graph point illustrated in those graph Figures. First of all we try to use the linear regression to have a starting basis. To decide which model we will start with, the trend line function of excel is used to get higher correlated function. The right conclusion of this process was to use the polynomial function $y = f(x)$. Assuming that: $y = d_i/y_1$, $x_1 = F_1$, $x_2 = y_2/y_1$, $x_3 = e$, and x_4 is a function of x_1 , x_2 , and x_3 , then the linear mathematical model required for linear regression can be presented as following:

$$y = a_0 + a_1x_1 + a_2x_2 + a_3x_3 \quad (2)$$

After giving the input data to Excel and recall for regression statistical function, the output information were as follows: $a_0 = 0.7622$, $a_1 = 0.5107$, $a_2 = -0.2475$, $a_3 = -0.1919$, determination coefficient $R^2 = 0.4340$, standard error $E = 0.3452$ and the correlation coefficient is $R = 0.6588$. Fig (3) shows the relationship between the predicted function $y = f(x)$ and the measured one plotted on a Pearson graph. Fig (4) shows the relationship between the predicted function $y = f(x)$ and the residuals. Both graphs indicate that the linear correlation between data and corresponding information in this case have *weak-to-good* (0.5 ~ 0.8) positive correlation since the estimated correlation coefficient is only 0.66.

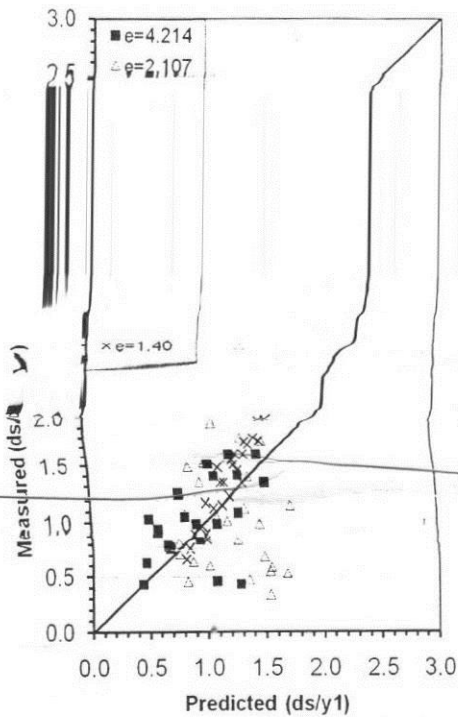


Figure 4 Relation between the predicted y and the residuals for linear regression case in eq. no. (2).

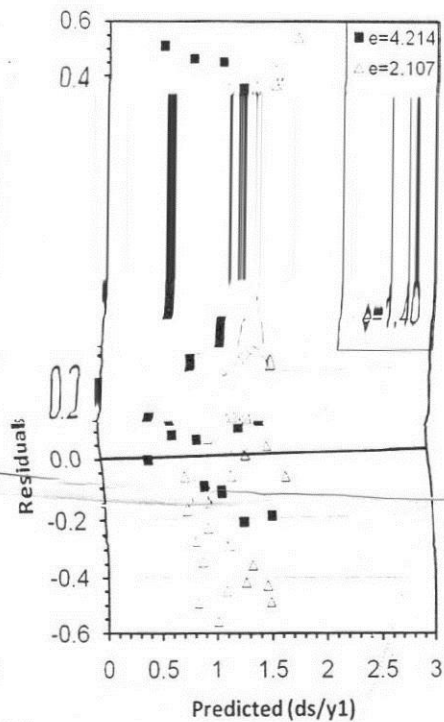


Figure 3 Pearson graph for predicted and measured y for linear regression case in eq. no. (2).

The band width of the scattered points between them lies in a wide range as well. This needs to be improved throughout the promotion to nonlinear regression.

To start carrying out such nonlinear regression procedure, we have to develop the linear polynomial mathematical model in eq. no. (1) into nonlinear one using the method of trial and error. So that many proposed trial models were probed. Among these, we present the different proposed mathematical models as shown in table (2). Figs(5,6) include the main statistical properties of a few representative sample models of these trials. The tried mathematical models are arranged so that gradual determination coefficient (R^2) and standard error (E) are computed for comparing purposes. In addition to this, the polynomial function y may not only contain algebraic functions, but also transcendental functions as well.

From above table and figures we notice that the linear regression case has weak results and these are improved using nonlinear regression analysis. Actually, we added another term to the polynomial y. Of course this will raise its degree of complication, but the more the polynomial complication, the less the standard error. Moreover the model number (10) is divided into three phases for each expansion ratio (e). The results are improved accordingly as it is seen from figs (5, 6). If we take all the three phases in one cumulative process the resulting statistical properties will be as follows:

Table (2): Proposed mathematical models

MN.	Mathematical model's equation
0	$y = 0.7622 + 0.5107x_1 - 0.2475x_2 - 0.1919x_3^3$
1	$y = -0.5848 + 1.4737\ln x_1^{1.5} - 2.1388\ln(\ln x_2) - 0.5932\ln(\ln x_3)$
2	$y = -0.8824 + 3.7790\ln x_1^{0.7} - 1.9382\ln(\ln x_2) - 0.6472\ln(\ln x_3)$
3	$y = 0.1550 + 3.8642\ln x_1^{0.7} - 3.0588\ln(\ln x_2)^{0.7} - 0.6562\ln(\ln x_3)$
4	$y = 1.5732 + 3.8831\ln x_1^{0.7} - 4.4970\ln x_2^{0.5} - 0.6558\ln(\ln x_3)$
5	$y = 4.8437 + 3.8695\ln x_1^{0.7} - 7.7573\ln x_2^{0.3} - 0.6502\ln(\ln x_3)$
6	$y = 44.7483 + 3.8077\ln x_1^{0.7} - 47.6071\ln x_2^{0.65} - 0.6361\ln(\ln x_3)$
7	$y = 20.8652 + 3.8239\ln x_1^{0.7} - 23.7386\ln x_2^{0.1} - 0.6395\ln(\ln x_3)$
8	$y = 1.0343 + 2.8059x_1^{0.5}x_2 - 2.5742\ln x_1$
9	$y = 0.4620 + 3.2983\ln x_1 - 2.5750\ln x_2 - 0.0413x_4^2$
10	$y = 0.0803 + 2.1517\ln x_1 - 0.7241\ln x_2 + 0.0082x_3^{1.5} - 0.0861x_4^2$

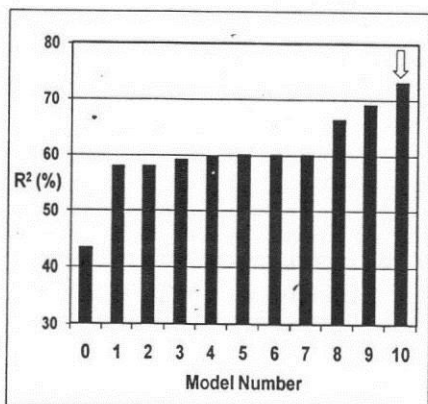


Figure 6 Error values for proposed mathematical models

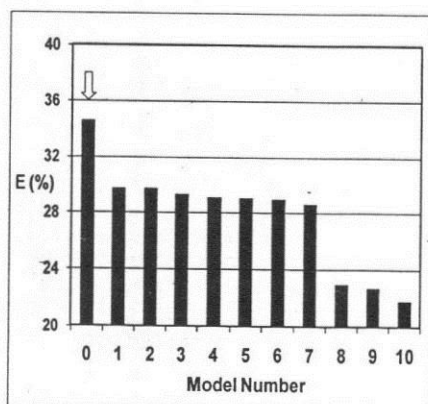


Figure 5 Coefficients for determinations for proposed mathematical models

$R^2 = 0.3909$, $R = 0.6252$, $E = 0.3607$, that still need to be improved. This is why we decide to separate this case into three phases, each phase has its own expansion ratio (ϵ). According to gate operating system whether it is ordinary or sudden opening the chosen model will be decided. This means that for ordinary gate operating system, the mathematical model will be separated into three

phases depending on expansion ratio (e) while in case of sudden gate operating system the model will be generalized for the three expansion ratios (e).

6-1 Ordinary Gate Opening

In this case of study the mathematical model no (10) in table (2) is improved as follows:

$$y = a_0 + a_1 \ln x_1 + a_2 \ln x_2 + a_3(x_1)^{1.5} + a_4(x_2)^{1.5} \quad (3)$$

Fig (7) shows the relationship between the predicted function $y = f(x)$ and the measured one for mathematical model of eq. (3) plotted on a Pearson graph. Fig (6) shows the relationship between the predicted function $y = f(x)$ and the residuals. From eq. no. (3) and figs (7, 8) we can easily notice that both the correlation and the

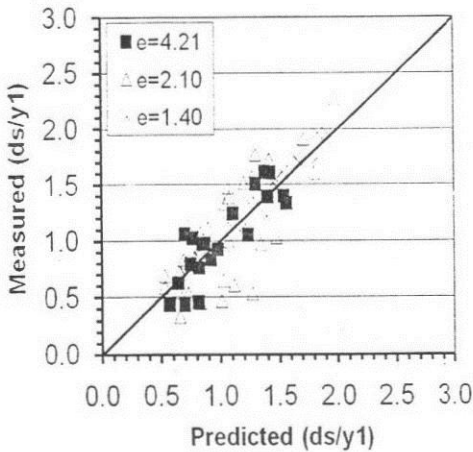


Figure 7 Pearson graph for predicted and measured y for nonlinear regression case (MN 10).

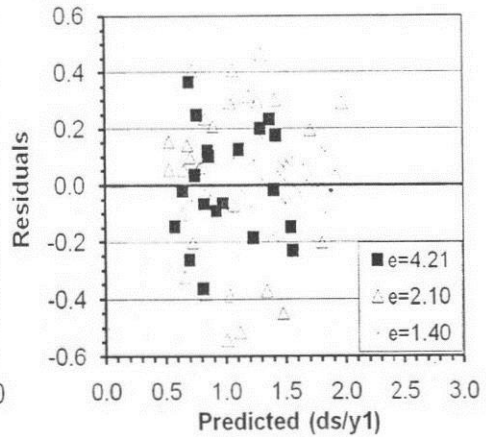


Figure 8 Relation between the predicted y and the residuals for nonlinear regression case (MN 10).

band width of the scattered point data are recognizably improved more than linear model in eq. no. (2). This is in addition to the uniform distribution of this band around the horizontal axis for the three expansion ratio phases (e). This is because of the increase in positive correlation coefficient from *weak-to-good* into *good*. It is known that the good correlation exceeds the value of (0.8).

6-1-1 Modeling of d_s/y_1 In Case Of Three-Operating Gates, ($e = 1.41$)

Figure (9) present relationships between the initial Froude number F_1 versus the relative scour depth d_s/y_1 , for different operating systems. The considered gate opening scenarios in this stage, include three operating gates, (i.e. $e = 1.41$). These operating systems may be summarized as follows:

- *Three main gates*, in which a part of the created free hydraulic jump has been formed within the prismatic channel between the piers, while the other part is formed on the stilling basin,
- *Three emergency gates*, in which the free hydraulic jump was formed DS all gates within the stilling basin, and
- *The combination between the main and the emergency gates*. In this case, the free hydraulic jump was formed DS the main gates only, while the emergency gates were subjected to a submerged hydraulic jump.

It is clear that, case of operating the three-emergency gates gave the maximum relative scour depth d_s/y_1 see Fig. (9). As mentioned before, the hydraulic jump in this case was formed DS the gates close to the movable bed. It meant that, a large percent of the turbulences and eddies resulted from the hydraulic jump, reached the movable bed. As a result, the drag force exerted on the soil particles was increased, and hence both of the scour hole depth and protection length were increased as well.

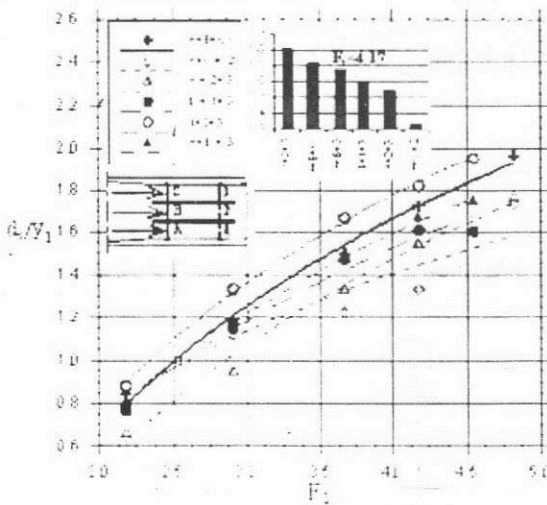


Figure 9 Relationship between d_s/y_1 and F_1 for different operating systems $e=1.41$.

The resulting statistical information for this mathematical model in this case ($e = 1.41$) will be as follows: $R^2 = 0.9377$, $R = 0.9684$, $E = 0.1021$, that can be represented by the following equation:

$$y = -0.0356 + 0.9376 \ln x_1 + 0.0815 \ln x_2 + 0.1534(x_1)^{1.5} - 0.0977(x_2)^{1.5} \quad (4)$$

It can be said that the mathematical model in eq. no. (4) is considered the most representative mathematical model for this case of expansion ratio ($e = 1.41$). Fig (10) shows the relationship between the predicted function and the measured one plotted on a Pearson graph. Fig (11) shows the relationship between the predicted function and the residuals.

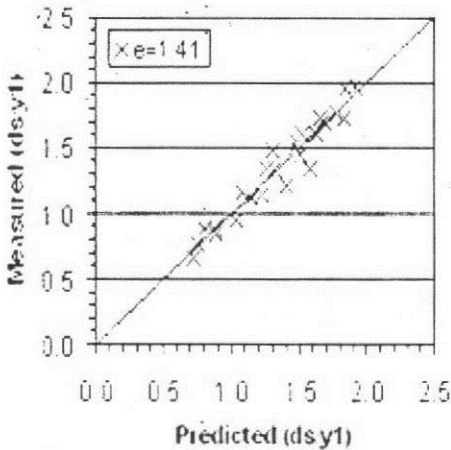


Figure 10 Pearson graph for predicted and measured y for nonlinear regression of Eq. no. (4)

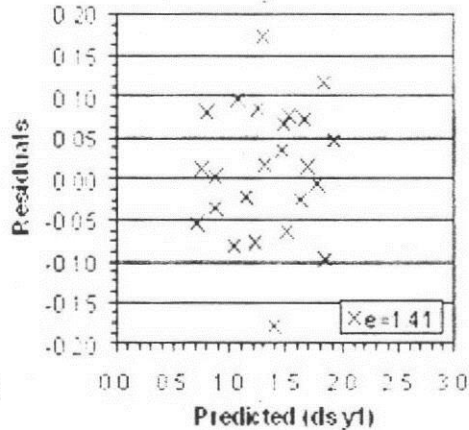


Figure 11 Relation between the predicted y and the residuals for nonlinear regression of Eq. no. (4)

It can be easily noticed that both the correlation and the band width of the scattered point data are recognizably improved more than linear model in eq. no. (2). This is in addition to the uniform distribution of this band around the horizontal axis for the expansion ratio ($e = 1.41$). This means that the designed mathematical model in eq. no. (4) is the best fit of the present experimental data.

6-1-2 Modeling of d_s/y_1 In Case Of Two-Operating Gates ($e = 2.1$)

The gate operating systems considered in this stage include the following scenarios: Symmetric\ asymmetric two-main gates, Symmetric\ asymmetric two-emergency gates and Symmetric\ asymmetric mixing of main and emergency gates. In these cases, the emergency gate was subjected to a submerged hydraulic jump, while the main gate was exposed to a free one.

Figure (12) shows the relationships between d_s/y_1 versus the initial Froude number F_1 , for different operating systems of the same expansion ratio, $e = 2.1$. It is clear that, the case of operating the two-side emergency gates (asymmetrical operating system) gave the maximum relative scour depth d_s/y_1 . In contrast, operating the two-separated main gates (symmetrical operating system) gave the minimum values of the scour parameters.

Finally, it can be said that, the increasing of the relative scour depth was resorted to the length of the turbulence zone. It is obvious that the case of operating the two side emergency gates was the only case in which the turbulence reached the movable bed. As a result, it gave the maximum scour parameters. Moreover, the operating system efficiency of flow distributing played an important role to decrease the scour parameters. It is obvious that, the case of operating the two separated main gates gave the best flow distribution, consequently it gave the minimum scour parameters. It can be said that, the emergency operating systems gave the maximum scour parameters compared to the main operating systems or the mixing cases at the same flow condition. Also, the symmetric operating systems gave small relative scour depth compared to the asymmetric operating systems at the same flow conditions.

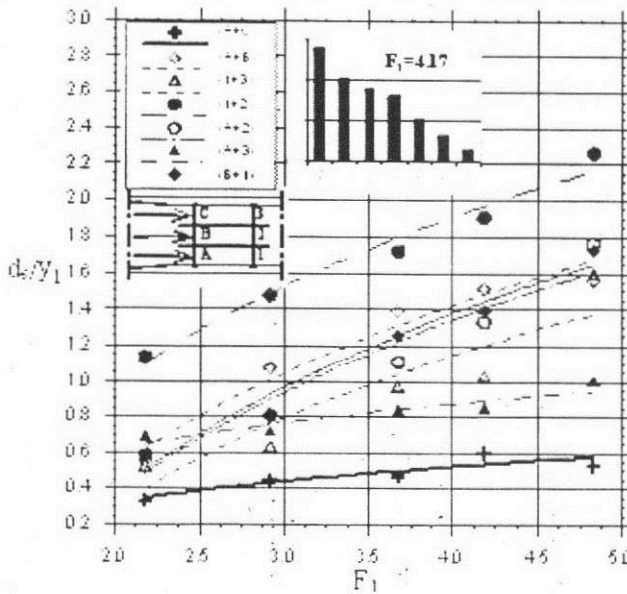


Figure 12 Relationship between d_s/y_1 and F_1 for different operating systems, $e=2.1$.

The resulting statistical information for this mathematical model in this case ($e = 2.1$) will be as follows: $R^2 = 0.5594$, $R = 0.7479$, $E = 0.3593$, that can be represented by the following equation:

$$\hat{y} = 0.09 - 0.1630 \ln x_1 + 0.02581 \ln x_2 + 0.3561(x_1)^{1.5} - 0.1024(x_2)^{1.5} \quad (5)$$

This information are considered accepted results because the correlation is still positive and between (0.5~0.8), i.e. weak to good. This means that the mathematical model in eq. no. (5) is considered a satisfactory representative mathematical model for this case of expansion ratio. Fig (13) shows the relationship between the predicted function and the measured one for mathematical model plotted on a Pearson graph. Fig (13) shows the relationship between the predicted function and the residuals. It can be easily noticed that both the correlation and the band width of the scattered point data are recognizably improved more than linear model in eq. no.

(2). This is in addition to the uniform distribution of this band around the horizontal axis for the expansion ratio ($e = 2.1$). This means that the designed mathematical model in eq. no. (5) is the best fit found of the present experimental data.

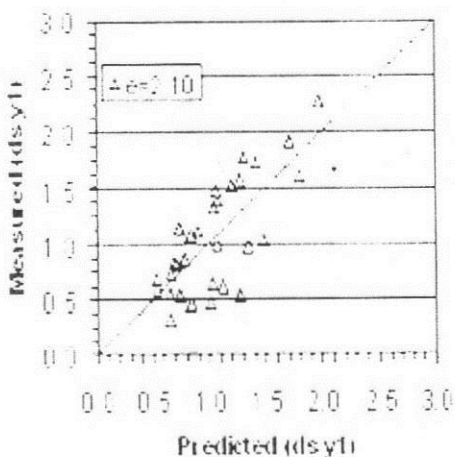


Figure 13 Pearson graph for predicted and measured y for nonlinear regression of Eq. no. (5).

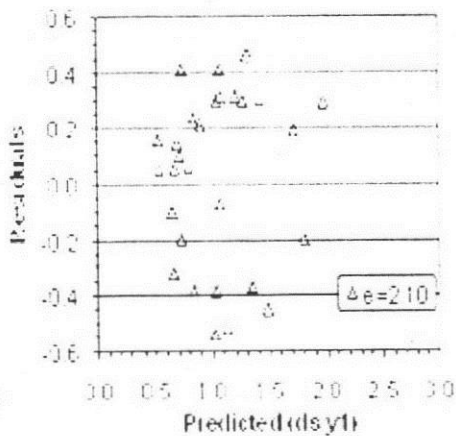


Figure 14 Relation between the predicted y and the residuals for nonlinear regression of Eq. no. (5).

6-1-3 Modeling of d_s/y_1 In Case Of One-Operating Gate ($e = 4.21$)

The gate operating systems considered in this stage include the following scenarios: Main\ emergency symmetrical operating gate, and Main\ emergency asymmetrical operating gate. Figure (15) presents the relationship between the initial Froude number F_1 and d_s/y_1 for the different operating systems. It can be noticed that, case of operating the middle main gate (symmetric operating

system) gives the minimum relative scour depth; d_s/y_1 . In contrast, case of operating the one side emergency gate (asymmetric operating system) gives the maximum scour parameters.

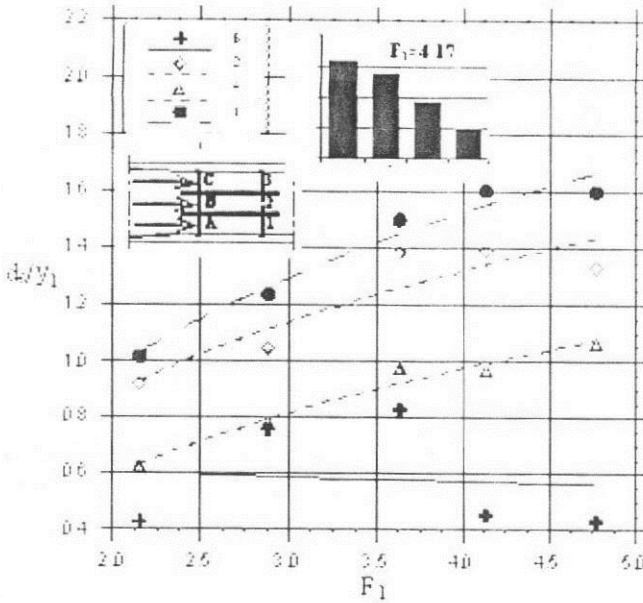


Figure 15 Relationship between d_s/y_1 and F_1 for different operating systems, $e=4.21$.

It is obvious that, operating the emergency gates give larger values of d_s/y_1 compared to the cases of main gate operations. Moreover, the asymmetrical operating systems give higher scour parameter compared to the symmetrical operating systems. The resulting statistical information for this mathematical model in this case ($e = 4.21$) will be as follows: $R^2 = 0.7324$, $R = 0.8558$, $E = 0.2182$, that can be represented by the following equation:

$$y = 0.0803 + 2.1517 \ln x_1 - 0.7241 \ln x_2 + 0.0082(x_1)^{1.5} - 0.0861(x_2)^{1.5} \quad (6)$$

This equation is considered accepted because the correlation is still positive and exceeds (0.8), i.e. good correlation. This means that the mathematical model in eq. no. (6) is considered a representative mathematical model for this case.

Fig (16) shows the relationship between the predicted function and the measured one for the proposed mathematical model plotted on a Pearson graph.

It can be easily noticed that both the correlation and the band width of the scattered point data are recognizably improved more than linear model in eq. no. (2). Fig (17) shows the relationship between the predicted function and the residuals. This is in addition to the uniform distribution of this band around the horizontal axis for the expansion ratio ($e = 4.21$). This means that the designed

mathematical model in eq. no. (6) is the best fit found of the present experimental data.

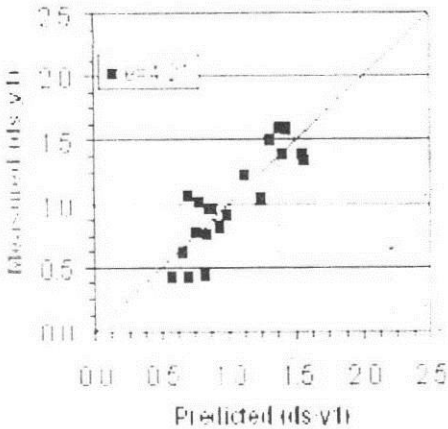


Figure 16 Pearson graph for predicted and measured y for nonlinear regression of Eq. no. (6)

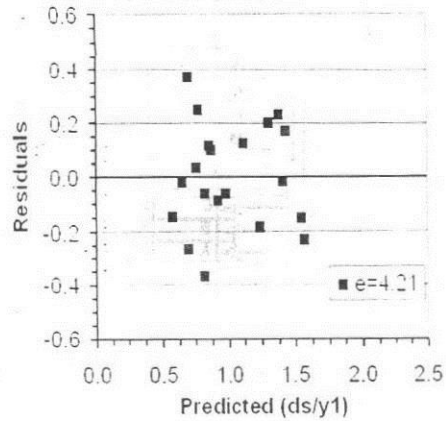


Figure 17 Relation between the predicted y and the residuals for nonlinear regression of Eq. no. (6)

6-2 Sudden Gate Opening

As assumed before the gates may be opened suddenly or ordinarily. For the case of sudden opening, the relationship between d_s/y_1 and F_1 for the different operating systems has been presented as shown in Fig. (18). It can be noticed that, the relative scour depth for the sudden opening case are larger compared to the ordinary case. In some cases, the sudden opening increases the relative scour parameters more than 3 times than ordinary gate operation.

6-2-1 Effect of Opening Systems on Scour Parameters

In case of the sudden opening, the flow leaves the operating gates as a supercritical flow with a high velocity, i.e. sheet flow. It reaches the dried movable bed in the same state. This case persists for a period of time, till the tail water depth grows to a level sufficient to form the free hydraulic jump. No doubt, this time period mainly depends on the quantity of the passing discharge, in addition to the length of the DS reach. In this time period the passing sheet flow magnifies the flow velocity and increases the drag force exerted on the soil particles. As a result, the mobile reach exposed to an extensive scour process with a high depth and length. On the other hand, in case of the ordinary opening,

the movable soil was subjected to a sub-critical flow overall time and so the soil particles were exposed to a weak flow velocities and minified drag forces compared to the case of sudden opening.

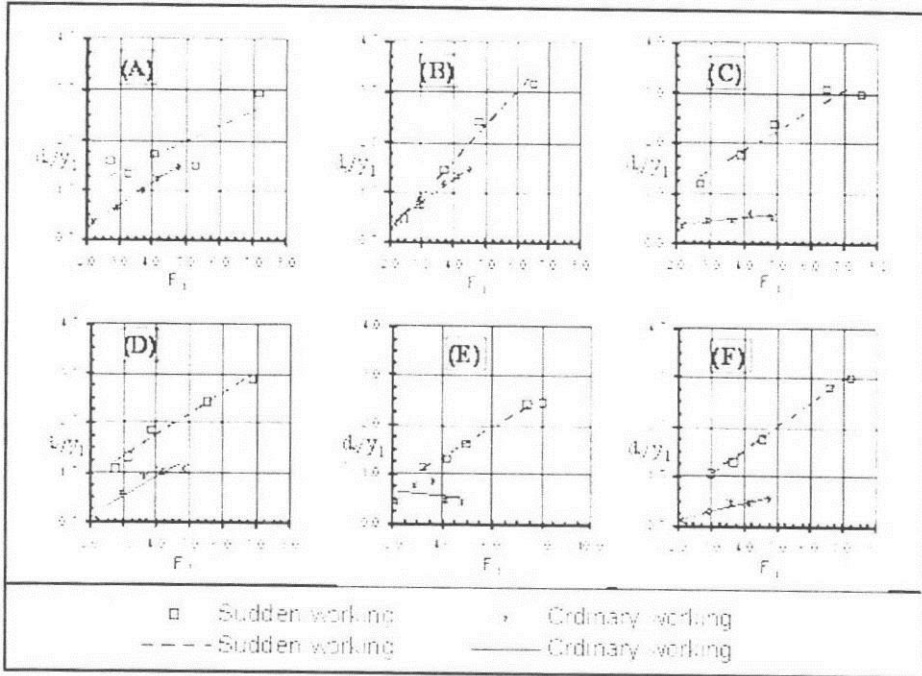


Figure 18 Relationship between d_s/y_1 and F_1 for different operating systems. (A) three main vents, $e=1.41$, (B) three emergency vents, $e=1.41$, (C) two separated service vents, $e=2.1$, (D) two side service vents, $e=2.1$, (E) middle service vent, $e=4.22$ and (F) side service vent, $e=4.21$.

Finally, the sudden opening should be averted. On the other hand, the operating system, which gives the maximum symmetrical expansion ratio, should be used, (i.e., case of operating the middle main gate, $e = 4.21$). This case is advised as a tool to fill the channel cross section DS the regulator at the beginning of the operating. In the contrary, it should not be adopted for the continuous operating system, as mentioned before.

For the sudden gate opening operating system, we proposed a generalized mathematical model that satisfies all the three expansion ratio cases since its results are considered satisfactory. The resulting statistical information for this mathematical model for all expansion ratio cases are as follows: $R^2 = 0.7618$, $R = 0.8728$, $E = 0.4324$, that can be represented by the following equation:

$$y = -0.838 + 2.4998 \ln x_1 - 0.7241 \ln x_2 - 0.1446 \ln x_3 - 0.0341 \ln x_3 - 0.0043 x_1^{1.5} - 0.0241 x_2^{1.5} - 0.0898 x_3^{1.5} \quad (7)$$

This equation is considered a good result since the correlation is still positive and exceeds (0.8), i.e. good correlation. This means that the mathematical model in eq. no. (7) is considered a good representative mathematical model for the purpose of this research work suited for all three cases of expansion ratio (e).

Fig (19) shows the relationship between the predicted function and the measured one for mathematical model of eq. (7) plotted on a Pearson graph. Fig (20) shows the relationship between the predicted function $y = f(x)$ and the residuals.

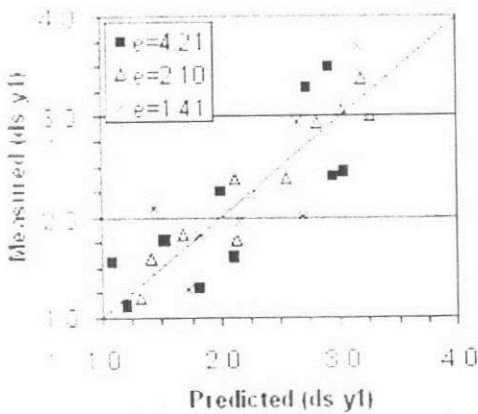


Figure 19 Pearson graph for predicted and measured y for nonlinear regression of Eq. no. (8)

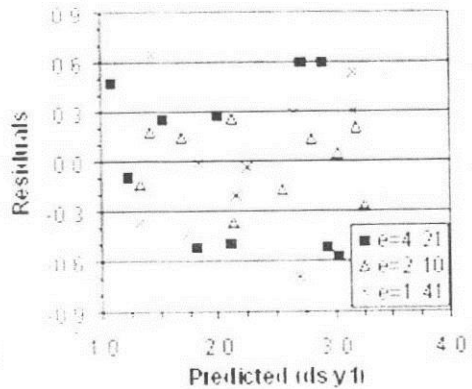


Figure 20 Relation between the predicted y and the residuals for nonlinear regression of Eq. no. (8)

It can be easily noticed that both the correlation and the band width of the scattered point data are recognizably improved more than linear model in eq. no. (2). This is in addition to the uniform distribution of this band around the horizontal axis for all expansion ratios cases (e). This means that the designed mathematical model in eq. no. (7) is the best found fit of the present experimental data.

7- CONCLUSION

The present experimental paper investigates the local scour under the effect of different operating systems. Also, the paper uses how the data analysis function contained within the Microsoft Excel® 2007 spreadsheet package can be used to simulate scour depth. The data analysis function is readily employed to create a simple functional solution to the problem of not only single but also generalized regression curve fitting. The method is illustrated with four worked practical examples. It was found that, the different relative scour parameters give an increasing trend as the initial Froude number F_1 increases and vice versa. In Case of three-Operating Gates: The case of operating the three-emergency gates gives the maximum scour depth, in case of two-Operating Gates, in case of operating the two-separated main gates gives the minimum scour parameters. In Case of one-Operating Gate; Case of operating the middle main gate gives the minimum scour depth for the different flow conditions.

Four mathematical models for simulating the effect of sudden and ordinary opening of the gate operating system on scour characteristics DS of multi vent regulators are built. The approach suggested is simple to understand and apply, and only requires that any proposed model can be described using the standard mathematical and statistical functions contained within Excel. The method is thus capable of fitting a wide range of different models and, because of the simplicity of the solution approach, can be readily applied to evaluate the '*comparative goodness of fit*' of several different models.

8- NOTATIONS

d_s	maximum scour depth	[L]
e	expansion ratio	[-]
F_1	initial Froude number	[-]
y_1	initial depth of hydraulic jump	[L]
y_2	sequent depth of hydraulic jump	[L]

REFERENCES

- 1- Abdel-Aal, G.M., Elfiky, M.M., Negm, A.M. and Nasser, M.A., "Effect of Management and Operation on Scour Characteristics Ds of Multi Vent Regulators", Sc. Bull., Fac. of Eng., Ain Shams Univ., Vol. 39, No. 4, pp. 385-400, Dec., 2004.
- 2- Dickey, D.A. and Arnold, J.T. "Teaching Statistics with Data of Historic Significance: Galileo's Gravity and Motion Experiments", Journal of Statistics Education, v.3, n.1, 1995.
- 3- Elfiky, M.M. "Effect of End Sill on Free Hydraulic Jump Characteristics D.S. Multi Vent Regulators", Sc. Bull., Fac. of Eng., Ain Shams Univ., Cairo, Egypt, Vol. 39, No. 4, pp. 331-343, Dec., 2004.
- 4- Dey, S. and Westrich, B., "Hydraulics of Submerged Jet Subject to Change in Cohesive Bed Geometry", J. Hyd. Eng., Vol. 129, No. 1, pp. 44-53, Jan. 2003.
- 5- Fahmy, M.R., "Design of Stilling Basins DS of Multi-Vent Regulators", Unpub. Ph.D, Fac. Of Eng., Zagazig Univ., 2001.
- 6- Langer S. F. J. "Efficient exponential regression with exact fiducial limits to fit cardiac pressure data". Computer methods and programs in biomedicine, Ingenta, vol. 53, no. 1, pp. 57, 1997.
- 7- Lin Y.; Liu S. "Law of Exponentiality and Exponential Curve Fitting Systems Analysis Modelling Simulation", Ingenta, vol. 38, no. 4, pp. 621-636, 2000.
- 8- Lin Yi; DeNu Roman; Patel Narendra, "True distance fit of exponential curves and tests of applications". Int. J. Appl. Math. 9, no. 1, 49-68, 2002.
- 9- Microsoft Excel 2007 Users Guide, Microsoft Corporation, 2007.
- 10- Saleh, O.K., Negm, A.M., Wahedeldin, O.S. and Ahmad, N.G., "Effect of end sill on scour characteristics downstream of sudden expanding stilling basins". Proc. of 6th Int. Conf. On River Eng., Ahvaz, Iran, 28-30 Jan, 2003.

MATERIALITY IN ARCHITECTURE A STUDY ON THE TRANSFORMATION IN THE MEANINGS OF MATERIALS

Gabr, M. *, Amin, A. **, EL-Fiki, S. *** & Kattaria, T. ****

**Professor of Architecture, Arab Academy for Science, Technology & Maritime Transport, Alexandria, Egypt.*

***Associate Professor of Architecture, Cairo University, Cairo, Egypt.*

****Assistant Professor of Architecture, Arab Academy for Science, Technology & Maritime Transport, Cairo, Egypt.*

***** Teaching Assistant, Arab Academy for Science, Technology & Maritime Transport, Cairo, Egypt.*

ABSTRACT

The integration between material selection and architectural design has, in many incidents, been realized in late stages of projects development, where the prime function of materials becomes "dressing the building in the most economic way". Conversely, materials involvement in the initial design phases can convey valuable meanings and generate innovative design messages.

Materiality is a branch of science that synthesizes material quality with design intension. In terms of materiality, materials have several meanings to conduct, which can significantly influence architectural design.

The theoretical framework of the present study first identifies the role of materials in architectural design, in terms of the Vitruvian goals of architectural design. It also discusses the term *Materiality* with its two principal poles '*design intention*' and '*material quality*'. Since the meanings of materials are constantly evolving and transforming over time, the study is meant to trace the transformation in these meanings since the Ancient Egyptian dynasty, until the

present contemporary architecture. This is applied to four building materials, namely bricks, stones, glass and metals, being particularly selected due to their persistent use throughout long consecutive ages, which should allow for an extended study to their various historic transformations. Finally, the main findings are illustrated towards setting a conclusion that identifies the transformation in the meaning of building materials and its impact upon architectural design, in order to respond to designers' inspirations and to fulfill their aspirations.

Keywords:

Materiality, Material Quality, Design Intention, Meaning, Transformation

INTRODUCTION

It is quite rare for an architectural review or discussion not to address "Materials". This is due to their significant architectural role in expressing identity, structure, form and overall qualities of buildings, with their textures, colors, strengths and characteristic attributes. Therefore, 'materials' may be considered as design generators. Additionally, it is quite often that they are the aspect that first draws people's attention to a building, and promote their appreciation to its qualities.

While materials are often chosen at the end of design process, or even during the generation of the construction documents, this study suggests an insight to the relationship between materials and architectural design, where selection of materials is taken into consideration at earlier stages, just as recommended by the so-known contemporary theme of '*materiality*'. According to the doctrine of '*materiality*', a material is not only a finishing surface or a building envelope, but rather an expression of meanings and a design generator that plays a significant role in improving the quality of architectural design. This is not only the case in present-day architecture, but also in the architecture of many ancient civilizations, though not tagged yet under *materiality* term. Therefore, the present research aims at outlining the transformation in these meanings throughout different historic ages, towards better understanding of their role in promoting architectural design qualities.

In order for the research to deal with the above propounded problem, it is important to recognize some goals. These goals include highlighting the role of materials' selection in architectural design, identifying several meanings of building materials, examining these meanings throughout different historic

periods, and synthesizing the transformation in these meanings over time towards recognizing more profound architecture.

In brief, this study sets a theoretical framework for understanding the role of material in architectural design. This framework also discusses the term *Materiality* with its two principal poles '*design intention*' and '*material quality*'. Since the meanings of materials are constantly evolving and transforming over time, the study is meant to trace the transformation in these meanings since the ancient Egyptian dynasties, until the present contemporary architecture. This is applied to four building materials, namely bricks, stones, glass and metals, being particularly selected due to their persistent use throughout long consecutive ages, which should allow for an extended study to their various historic transformations. Finally, the main findings are illustrated towards setting a conclusion that identifies the transformation in the meaning of building materials and its impact upon architectural design, in order to respond to designers' inspirations and to fulfill their aspirations.

1. THE ROLE OF MATERIALS IN ARCHITECTURAL DESIGN

In architectural terms, materials may reshape the contemporary themes of architecture and act as a design solution for sophisticated architectural problems, which demand distinguished inspiration, innovation and new technologies to respond to architect's aspirations (Weston, 2007). In the pursuit of this goal, this research employs the goals of architectural design, as recorded by Vitruvius in his written work of 27 BC "*ten books on architecture*", to realize the impact of materials upon architecture. The main Vitruvian goals of architecture were meant to strike the balance between "*firmness, utility and delight*" (Tisdell, 1992).

On another hand, "*going green*" is becoming a major architectural concern nowadays. In response to this theme, '*environmental architectural design*' was introduced, encompassing environmentally friendly, environmentally conscious, energy conscious, sustainable, greener design, and many regards dealing with new functions for building-design, and achieving optimal cost-efficiency through the integration of building operations and material-use into one green production system (DA, 2009). Notwithstanding, Vitruvius dealt with contemporary "green" concepts in terms of "*utility*" as "resource efficiency, human thermal comfort and recognition of regional environmental factors" (Tisdell, 1992).

1.1 THE IMPACT OF MATERIALS UPON UTILITY

The choice of materials to suit and accommodate a specific use in a particular space should conform to design utility. For example, while durability of corridors and stairs finishing-materials is a paramount to resist friction, soundproof materials may be more dramatically important in other spaces (Weston, 2003). This may draw attention towards articulating materials by function through 'material's texture', which plays a dual role in sensorial and functional quality (Leatherbarrow & Mostafavi, 2005). Likewise, it may be through 'material changes' which convey important visual information, announcing a change in level or direction during movement and circulation for safety purposed (Motloch, 2001).

Many architects reveal nothing about what goes inside the buildings, but others do in a way of "symbolic utility" to symbolize the buildings function such as Mies van der Rohe and his selection of the glass that played a major role in detecting the buildings function (Roth, 1998). Other architects like Louis Kahn merged between the human's psychology and architecture, who declared that the study of architecture was the study of human beings, their highest aspirations and most profound truths. He searched for forms and materials to express the subtlety and grandeur of life. In his designs, the realization of this vision appears in the luminous surfaces that evoke a fundamental awe, silent courtyards that speak of the expansiveness and the sanctity of the spirit, monumental columns and graceful arches that embody dignity and strength, especially those using specific materials like 'bricks' to accentuate such "psychological utility" of the building (Kahn & Lobell, 2008).

In 'green' terms, materials' impact upon "environmental utility" may be assessed by a number of measuring tools for measuring the impact materials might have upon the environment. One common method is the "Life Cycle Analysis" (LCA), which measures the environmental impact that is brought about by the use of particular materials, as well as the embodied energy and energy consumption at different stages of building life (Hagen, 2001). Manufacturing and transportation of materials are two influential parameters in affecting LCA of a building / material. In fact, environmental building design aims to lessen impacts upon environment through energy control and other applications. Therefore natural and local materials can be an ideal solution for an environmental design towards a green environment.

1.2 THE IMPACT OF MATERIALS UPON FIRMNESS

Firmness mainly refers to material's durable qualities in handling structural loads, which obviously influences the form of "physical structure" (ibid). The following discussion sheds light upon the structural behavior of stones, bricks, wood, cast iron, wrought iron, steel, reinforced concrete, light fabrics and tensile cables, and how their properties have influenced building forms.

Stones and bricks are known to be strong in compression, but weak in bending and tension. Therefore, they are ideal when a designer is required to transmit the loads by compression. This may be an explanation why they generate forms that are characterized by closely-spaced columns and compressive arches. Likewise, cast iron shares properties with stone. It is brittle in tension and bending loads, hence shaped in an arch-like form to transmit loads by compression. Nevertheless, its cast possibility in refined shapes introduced new forms which are characterized by lightness, yet at the same efficiency as stones.

Wrought iron and steel represent the development of cast iron, overcoming the brittleness problem, and creating a slender membrane that can carry tension forces and stimulating further development of structural concepts. Similarly, wood is strong in tension, compression and bending. Therefore, it is suitable for frames, trusses and cantilevered structures.

On another hand, reinforced concrete combines tensile properties as well as compressive strength, which allows for easily-shaped fluid and shell-like structures. Light fabrics and high tensile cables are very good in bearing tensile loads but buckle when subject to bending or compression, so they lead to another set of forms.

In brief, designers shape materials into elements which are capable of handling particular patterns of loading. These elements are integrated into forms which are designed to collectively transmit loads in a manner that is most compatible with the nature of materials (Ashby & Johnson, 2006). Therefore, the above discussion may propose transforming the prominent quote:

"Form follows function" into "Form follows materials".

Humans also grow up with a good sense of gravity and are aware of its effect on the objects all around. In accordance with the above discussion, this is draws attention to "perceptual structure", presuming that what man sees is not necessarily the true structure. In 'Lever House' for example, the actual structure

was covered by a suspended skin of green glass which was perceived by viewers as a cheated gravity (Roth, 1998).

1.3 THE IMPACT OF MATERIALS UPON "DELIGHT"

Architecture is often defined as "*the art that envelope us*". Frank Lloyd Wright believed that the essence of architecture was in space; this idea was expressed also by Kakuzo, O. in his 'Book of Tea'. Therefore, the present research addresses the impact of materials upon the delight of architectural spaces. For example, 'perceptual space delight' [which is a detection of space from a space], was embodied in large sheets of glass allowing vision out into the perceptual spaces. In the 'Lloyd Lewis House', a glass screen in the living space allows view outwards to the countryside, into a large perceptual space (ibid.).

On the other hand, 'duality of space delight' is defined as the delight through connecting spaces, glass as a transparent material can play a major role in this regard. They may create what has been described as fluid or flowing spaces. For example, in the 'Edger Kaufmann Residence', space is molded in a fluid way through the glass sheets connected with outer wooden elements (Roth, 1998).

2. MATERIALS BETWEEN VERNACULAR AND PROFESSIONAL ARCHITECTURE

After exploring materials role and impact upon the architectural design goals, this raised the question of, *what is beyond and before materials' impacts and applications in architectural design*. According to professional architecture, materials represent various intentions, providing technical functions, aesthetic associations and conceptual thoughts. This was particularly evident after the Renaissance and Baroque ages, when the intention of architectural design was characterized by its individuality through the use of different materials. Being an architect's concern to select, apply and think of materials as an elementary design tool, it is crucial to explore not only how professional designers thought of materials, but also to address their traditional vernacular thinking and applications.

2.1 PROFESSIONAL THINKING OF MATERIALS

Architects are particularly inspired by looking at real materials, as well as the act of making real things (Olotuah & Arum, 2006). Viollet le-Duc was considered to be the first theorist of modern architecture, his theory was mainly based on finding the ideal forms for "*specific materials*" and to use these forms

to realize his buildings. He believed that the appearance of a building should reflect its rational structure, specifically in terms of the building's facades (Weston, 2003).

The professional materials' thinking flow begins by considering the abilities of the material and ends by selecting a specific material. Architects depend on the vast variety in building materials to fulfill their design aspirations. Therefore, many contemporary architects look for innovation in the so-called "smart materials", which have changeable properties in response to changes in the surrounding environment. Sometimes, such transformation takes place within the material physical properties, in other incidents, materials act as a vehicle to transform other things. In the second case, transformation takes place either as property-changing materials, or energy exchanging material.

More recently, 'intelligent' materials have been created through the use of 'nanotechnology' – i.e. it is the study of the fabrication of the small molecular structures that measure between one nanometer and 100 nanometers in at least one dimension. Nanotechnology has actually produced a variety of materials that hold novel properties offering new approaches to the fabrication of architecture in the future. One of the earliest architects to identify the emergence of nanotechnologies in architecture is John M. Johansen who published two books about nano-application in architecture, like nano-engineered materials, self-cleaning coatings, anti-fogging, anti-graffiti and antibacterial products, as well as other thermally-enhanced and fire resistant products (Yeadon, 2008).

2.2 TRADITIONAL 'VERNACULAR' THINKING OF MATERIALS

Vernacular architecture is linked to the traditional uses of building materials, where these traditions have been developed and refined empirically over years. According to Brunskill the ultimate accomplishment in vernacular architecture would be designed by an amateur without any training in design; the function of a building would be the dominant factor with minimal aesthetic considerations; while materials are most necessarily local (Brunskill, 2000).

A lot of beautiful buildings that are built all over the world are considered as "*buildings without architects*" at all, those people who built their buildings, actually grew up simply without any architectural/constructional academic education, but gained their knowledge from traditional experience with the best means of using their locally-available materials (Morris, 1978).

In vernacular architecture, dwellers usually use their available surrounding materials. Even if these materials were weak, dwellers developed techniques

and skills in using them effectively to construct their homes, just as in the example of Ma'dan Marsh Arabs villages in Southern Iraq, where the available materials were reeds and grass (Oliver, 2003).

On another hand, professionals perceived local materials and vernacular architecture variably from the mere picturesque to the profound awareness of the 'primitive' artistic value, like William Morris and John Ruskin who believed in the 'truth of materials'. Contrarily to modern architects, it was not only an artistic conceptual value, but more importantly an appropriate response to economic dynamics.

Hassan Fathy explained his architectural philosophy in a book titled '*Architecture for the Poor*'. It explains how the use of mud bricks combined the aesthetic, social and physical functionality. Many theorists interpreted this as a contemporary expression of "green architecture". It is evident that many contemporary designers were inspired by the local traditions of 'vernacular architecture' and its materials. A distinguished example is the 'Jean-Marie Tjibaou Cultural Centre' in New Caledonia, which was designed by Renzo Piano, being primarily constructed with local bamboo (Ferdine, K. 2008).

3. MATERIALITY AS AN INSTRUMENTAL METHODOLOGY

A contemporary theme that combined an *architect's design intention with the qualities of the material, is a synthesis called "materiality"*. This can be phrased as

$$\text{(Materials Qualities + Design Intention = Materiality)}$$

In order to integrate these two components together, design/build programs were developed in many countries – e.g. the Rural Studio at Auburn University the United States. This program has demonstrated the effectiveness of learning the combination of design and materials' construction methods (Bell, V. & P. Rand, 2006). Since materiality is a major element for this research, it is necessary to address its two main poles "Design intention and Material quality" in the following section.

3.1 DESIGN INTENTION

Although each design has an intention, or a main goal which is significantly important, yet it remains just one feature of what it takes to achieve a successful project. A truly successful project is one where project intention is identified at the beginning, and where the interdependencies of all building systems are

coordinated along with the planning and programming phase. Some of the significant building design intentions are utility, aesthetics, cost effectiveness, functionality/operation, historic preservation, productivity, security/safety, and sustainability, etc. The interrelationships of those design intentions must be understood, evaluated, and appropriately applied (NIBS, 2009).

3.2 MATERIAL QUALITIES

The real importance of material qualities might be seen as their relative appropriateness to design intentions. Moreover, the qualities of materials carry much of the design content in which architecture engages the immediacy of humans' sensory perceptions (Malnar & Vodvarka, 2004).

'Material quality' depends on the physical properties and natural characteristics of materials, which differ from one material to another. When 'materials qualities' are not taken into consideration or are not fully understood during the selection of material for a specific application, problems are more likely to occur (SCT, 1998). Material qualities are generally classified as durability, economic, sensorial, and associational qualities. First, durability is based on the materials' physical properties, characteristics and the environmental conditions to which it will be or is subjected too (ibid). On the other hand, economical qualities refer to the economics of quarrying, manufacturing, transportation and installation of materials (Malnar & Vodvarka, 2004). Sensorial quality relates to human senses which perceive them; they are classified into (color, texture, temperature, sound and taste). At last, associational qualities of material refer to its physical and natural properties, as well as their association with designer's memory, culture, education, thoughts and believes, which collectively play a major role in the selection of materials (ibid).

3.3 MATERIALITY AND THE MEANING OF MATERIALS

Materiality provides meanings through which people communicate identities; without material meaning, communication relationships between architecture and human have little substance in reality. Materiality always seeks to consider the relationship between people and objects, not only in terms of the ways that people come to know a work through an affective experience, but through the ways that objects have effects in the world at large producing meanings (Sofaer, 2007).

"Material meaning" has been tagged by contemporary architecture in the term "*materiality*". Whenever a person interacts with an object, considerable change occurs. A relationship between the person and the object is established; a

transaction takes place. This transaction has the ability to determine the human's mode, and so can a person shape meanings for life. Actually, objects themselves could be perceived as signs, or as objectified forms of psychological energy. Also, meanings are the outcome of perception. In conclusion, 'meaning' may be defined as a core component within the perceptual process, which acts as a necessary element in all paradigms attempting to explain behavior (Halton, 1981). Meaning is a determination of a formal type of expression and emotions by consumers. Those meanings exist in the brain by a formation of a pattern of neural activity that embodies its immediate goal; this operation depends on and requires information from the environment (Walter, 2004).

3.4 APPROACHES TO MATERIALITY

Designers used *materiality* to support their ideals. Auguste Perret began the use of reinforced concrete in France in the early 1900s. Perret believed that he used reinforced concrete "As a representation of a new architectural style", not just as a replacement of stone. This was applied to a Paris-based Renault garage in 1905, as well as the 'Theatre des Champs-Elysees' in Paris 1913. Moreover, Le Corbusier used concrete to achieve the monolithic and sculptural qualities at a time when concrete was not a common material. On the other hand, Mies van der Rohe used glass and steel to reach a level of purity in construction and a minimalist quality in space (Bell, V. & P. Rand, 2006). Other prominent examples are Pierre Chareau's use of glass at the Maison de verre (1932), Alvar Alto's love of wood and Eero Saarineris' obsession with concrete.

On another hand, early post-modernists believed that "architecture's approach to materiality had spun 180 degrees since that of the early modernists". The 1980s post-modernists chose to deny materiality as a part of architecture. This was a result of the lack in distinction between what is real and what is false, which became even harder due to the use of veneers.

Today, the trend of materiality is considered a major driving force to generate new materials (e.g. smart materials) in addition to new uses for existing materials. The industries served materiality in producing these new materials that are more effective, efficient, sustainable and more environmentally sensitive. As a matter of fact, the technology of materials in contemporary architecture allowed materials to fit the unique needs of a building. An example for this is Frank Gehry's signature metals panels, introduced by sophisticated technology as a new expression in the glory of materials and their qualities (ibid).

3.5 MATERIALITY AND TRANSFORMATION

As discussed previously, materiality conveyed meanings for materials which served the design intention. This synthesis between materials and design is not surprising, on the basis that materials have been used to express meanings for ages. Since this research is about exploring the transformations in materials' meanings, it is necessary to set an understanding to the term "*transformation*". Linguistically, *transform* comes from the Latin word *transformare*, which means to change the nature, function or condition. This concept of transformation may be applied on various entities.

One type of transformation which is more planned, and its results are positively and normally sought, is "organizational transformation". It is defined as the core concept of the Theory of Evolution. The "time" Darwin referred to in his study of natural forms, was not simply chronological time; it was the irreversible time of transformation. In the Theory of Evolution, transformation is the means by which time and variety are brought into an inextricable relationship (Hacker & Roberts, 2003).

Since Materiality transforms through periods, it is necessary to explore the transformation in design intention. The history of European architecture is a fine example of transformation. Its design intention; its theories as well as its styles are well documented from antiquity until present. The dominant goal of the design theory is that small and large transformations have long been frequent, and each of them has caused a visible change in the prevailing style of design (Routio, 2007).

Human societies change continually, the utility value of any design intention and theory varies in time, so normal transformations happened in society, changes in design intentions and designers go through changing the trends of design intention (ibid). For example, when Modernism was refined, materiality supported the design intention of those willing to look at materials in novel ways. Contrarily, post-modernisms chose to deny it as a part of their architecture, where the use of faux veneers and imitation materials expressed an intention that showed little regard for an ethic of truth to materials. The following table is developed by the authors to briefly introduce the main transformations in design intentions throughout major historic dynasties.

Design Intention	Historic Period
Religious Believes	Ancient Egyptian
Utility, firmness and beauty	Greek and Roman
Religious salvation	Gothic
The Vitruvius's goals were revived	Renaissance
	Baroque
	Rococo
	Neo-classical
Individualism	Art-Nouveau and other individuals
Utility	Modernism
Economy of the building	Postmodernism
Environmental	Contemporary

Table (1) Transformation in the design intention through Architectural Periods (Authors)

4. APPLICATION: TRANSFORMATION OF MATERIAL MEANINGS OVER HISTORY

Following the above introduction to materiality, its approaches, meanings and transformation, the significance of materials meanings in the design process is revealed. Next is an application of the previous findings to a selection of four building materials, namely bricks, stones, glass and metals. This application traces the transformation in the meanings of these materials throughout consecutive ages from ancient Egyptians to contemporary architecture, towards examining the applicability of materiality concepts as design generators.

4.1 BRICKS

Bricks played a major role in serving many cultures to fulfill their innovative thoughts. For ancient Egyptians, bricks held the meanings of impermanent, short life, structural innovation and magical powers. Where, in Greek and Roman architecture, bricks merely represented an economical and decorative solution. Likewise, in Gothic architecture it was an economical and stylish element, especially in the German '*Backsteingotik*' style (Rael' 2008; Rapp, 2002).

However, in Gothic-revival, it revitalized its economical meanings in line with the Industrial Revolution. It then expressed natural and structural concepts as in the works of William Morris, Violet-le-Duc and Butterfeild. Afterwards, it returned as an economical expression in modernism, and eventually as a messenger of green ideologies and structural innovation in contemporary architecture (Weston, 2003).

4.2 STONES

In Ancient Egyptian thoughts, stones held spiritual and structural innovation meanings, where it represented a decorative and structural 'tectonic' expression in Greek and Roman civilizations. In Gothic architecture, it also represented the spiritual, lightness and the decorative structural 'tectonic' expressions.

On the contrary, it was mainly contextual in Islamic architecture. It then returned to its decorative meaning during the Renaissance, especially in Florence's 'lineament', and Baroque's 'plasticity'. In more recent experiences, stones have been declared by pioneer designers as to serve several specific meanings, e.g. natural material by William Morris, structural solution by Viollet-le-Duc, decorative / symbolic meanings by Art Nouveau followers, and economical meanings by modernist architects.

Last but not least, it is seen as a technical innovation and a green introduction by many contemporary architects (Sallis, 1994; Wildung, 2004).

4.3 GLASS

Glass was not used as a building material until the Roman Empire, who pioneered its use in the meanings of lightning and warmth. In Gothic and Islamic architecture, it was more spiritual than functional. Conversely, during the Renaissance, Baroque and Rococo – it was used in secular buildings to convey the meaning of day lightning. In Gothic-revivalism, glass and iron combination acted as *icons* of the Industrial Revolution expressively representing the meanings of modulation, day lighting, and freedom.

Glass had an innovative environmental meaning to Le Corbusier "*Mur neutralizing*", while it had a functional meanings to Frank Lloyd Wright. Louis Sullivan put hands on the meaning of transparency. At present, it represents a technical innovation in terms of green meanings (Toman, 2004; Hassan, 2008).

4.4 METALS

Amongst all metals, gold and silver were particularly used to cover Ancient Egyptian '*benbens*' to express their spiritual meanings. Other metals were used for auxiliary and decorative purposes by Greeks and Romans. Again, in Gothic architecture, metals expressed the meanings of insulation, lightness and decorative features. In addition to decorative meanings, safety was a common expression of metals in Islamic architecture. Metals, particularly lead and copper, then revived the meaning of insulation during the Renaissance, Baroque and Rococo.

Iron was the icon for the Industrial Revolution; it was described as the generator of that age. Cast iron was characterized by its structural meanings of formal flexibility and bearing compression, which consequently, gave rise to the meanings of innovative aesthetical value, changeable scale, and Viollet-le-Duc's meanings of honesty. It was later developed into wrought iron, which was characterized by its structural meanings of tensile and fibrous features, as well as the decorative and symbolic meaning in the Art Nouveau, as embodied in the works of Antonio Gaudi and Victor Horta.

After the famous Chicago burn-up, steel was used to represent verticality, safety and innovative aesthetics. Metals in general, and steel in particular, have been declared by modernist pioneers to serve various meanings. The mere common meaning to them all was *Architectonic*. Metals are being widely used nowadays in environmental and technical innovation industries, to promote more sustainable and green architecture (Baer, 1983; Trebilcock & Lawson, 2004; Schultz et al, 2000).

CONCLUSION

The research has outlined the significance of materials involvement in the initial design phases, to convey valuable meanings and generate innovative design messages. In this context, the role of materials in architectural design was discussed in the light of the Vitruvian goals of architectural design, i.e. firmness, utility and delight.

Materiality was also studied with its two principal poles: 'design intention' and 'material quality', together with the concepts of 'meaning' and 'transformation' in materiality. A discussion of the backgrounds of materiality in vernacular and professional architecture clarified the roots of the studied area.

An application of the idea of transformation in materiality was examined by an application to four building materials, namely bricks, stones, glass and metals. This application came in the form of a historic trace to the transformation in the meanings of these four materials, since the early Ancient Egyptian dynasties, until the present contemporary architecture, with its environmental orientations.

In conclusion, it is now significantly evident that materials have meanings which are in a constant state of evolution and transformation, as suggested by materiality. Therefore, it is extremely crucial for a designer to understand these meanings, and grasp their evolution, to be capable of developing appropriate designs, that respond to community aspirations in a fashion that is in harmony with the environment.

REFERENCES:

- Ashby, M. & Johnson, K. (2006) Materials and Design, Italy: Elsevier.
- Baer, E. (1983) Metalwork in medieval Islamic art, Albany: Suny Press
- Brunkill, W. (2000) Vernacular Architecture, USA: Yale University Press.
- Bell, V. & P. Rand (2006) Materials for Architectural Design, China: Princeton Architectural Press.
- Cook, J. (1999) A Green Vitruvius, London: James & James press.
- Doerr Architecture (2009) Definition of Sustainability and the Impacts of Buildings/Green architecture, sustainable or ecological boulder Colorado architecture, <http://www.doerr.org/services/sustainability.html> (accessed 17/9/2009)
- Ferdine, K. (2008) which Material should be used in Green design/Quazen, <http://quazen.com/arts/architecture/which-materials-should-be-used-in-green-design/> (accessed 4/7/2009)
- Goldhagen S. & Kahn, L. (2001) Louis Kahn's situated modernism, USA: Yale University Press
- Hacker, S & Roberts, T. (2003) Transformational leadership, Milwaukee, WI: ASQ Quality Press
- Hagen, S. (2001) Taking Shape, Oxford: Architectural Press
- Halton, E. (1981) The Meaning of Things: Domestic Symbols and the Self, England: Cambridge University Press
- Hassan, M. (2008) Transparency in twentieth century architecture: Between theory and Practice, (unpublished thesis), Egypt: Ain Shams University
- Kahn, L. & Lobell, J. (2008) Between Silence and Light: Spirit in the Architecture of Louis I. Kahn, China: Shambhala
- Leatherbarrow, D. & Mostafavi, M. (2005) Surface Architecture, England: MIT Press
- Malnar, J. & Vodvarka, F. (2004) Sensory Design, Minneapolis: University of Minnesota Press
- Motloch, J., (2001) Introduction to Landscape Design, United States: Wiley
- Morris, W. (1978) Architecture Industry and Wealth Collected Papers, New York: Garland Publisher
- National Institute of Building Sciences, (2009) Design Objectives/Whole Building Design Guide, <http://www.wbdg.org/design/designobjectives.php> (accessed 18/9/2009)
- Oliver, P. (2003) Dwellings, China: Phaidon Press.
- Olutuah O. & Arum C. (2006) The Nexus of Intention and Knowledge of Structure in Architecture, Department of Architecture, Federal University of Technology, Akure 34001, Nigeria, Department of Civil Engineering, Federal University of Technology, Akure 34001, Nigeria, 2006
- Rael, R. (2008) Earth Architecture, N.Y: Princeton Architectural Press
- Rapp, G. (2002) Archaeo-mineralogy, N.Y: Springer-Verlag
- Roth, L. (1998) understanding architecture, Great Britain: Herbert Press.
- Routio, P. (2007) Evolution of Normative Theory, <http://www2.uiah.fi/projects/metodi/126.htm> (accessed 20/8/2009)

- Sállis, J. (1994)** Stone. Bloomington: Indiana University Press.
Stone Care Techniques, (1998) Durability,
<http://www.stonecaretechniques.com/7.htm> (accessed 16/10/2009)
- Schulitz, H., W. Sobek & K. Habermann (2000)** Steel construction, Germany: Birkhäuser
- Sofaer, J. (2007)** Material Identities, United Kingdom: Blackwell.
16/10/2009)
- Tisdell, C. (1992)** "The nature of sustainability and of sustainable development" In: Moving towards global sustainability, policies and implications for Australia 5 pp. 7-12
- Toman, R. (2004)** the Art of Gothic, EU: KÖnemann
- Tsien, B., (2003)** Young architects 4: material process, China: Princeton Architectural Press
- Trebilcock, P. & Lawson, M. (2004)** Architectural Design in Steel, Great Britain: Spon Press
- Walter, J. (2004)** "How and why brains create MEANING-T from sensory information" In: international Journal of Bifurcation and Chaos 14 (2) pp. 515-530
- Weston, R. (2003)** Materials, Form and Architecture, Singapore: Laurence King.
- Wildung, D. (2004)** Egypt from Prehistory to the Romans: Taschen
- Wright, F. (1928)** "In the Cause of Architecture" In: New York: Architectural Record p. 175. In: F. Gutheim (ed.) 1975, in the cause of architecture, Frank Lloyd Wright: essays, New York: Architectural Record Books
- Wright, L., Devane, A. & Gutheim, F. (1975)** in the cause of architecture, Frank Lloyd Wright: essays, New York: Architectural Record Books
- Yeadon, P. (2008)** "Smarticles: Nanotechnology Materializes", in: ab - architectureboston 11 (4) pp. 25-29.

Exploring Green Architecture Through Eras

Dr Zeinab El Razaz

Associate Professor, Architectural Department, Helwan University, Cairo, Egypt.

ABSTRACT:

The natural ecology of the planet should be the macro model for architects to use as a model for a green building. Architecture can model itself on the planetary system to copy the natural 'green' environment, making a new building, or adapting an existing building, both environmentally friendly, in terms of materials used and the space it occupies, and energy efficient, including solar technology. (1)

Through the years a particular view of 'green architecture' has developed in the public mind. Today, as a holistic approach to Green Architecture energy is a critical component, green design also considers other environmental impacts as they relate to sustainability. The Green Building Movement has its roots in the energy crisis of the 1970s and the creative approaches for saving energy that came with it, including the use of active and passive solar design and tighter building envelopes. But are these strategies new? Did the movement towards respecting environment is new?

The efforts done in this piece of work is devoted for tracing the origins of green architecture in the course of historical eras starting from ancient architecture till the modern architecture, to explore its innovative practices and enhances to help architects now in their challenge to design and construct green buildings.

1. INTRODUCTION:

With the world facing serious environmental concerns, it is necessary for the building industry to take all steps to reduce the environmental impact of the industry. Green building techniques will go a long way to mitigate the adverse environmental effects. The building solutions should incorporate mandatory provisions for green buildings. The engineers, architects and builders should take up the challenge and play their role in delaying, if not preventing, this world fast slipping towards environmental catastrophe.

With the rising costs of energy and the rapid depletion in the supply of natural resources, incorporating green building strategies into architectural design is essential. Successful green building does not depend on the building form. It is both the design and the construction which can make a building truly sustainable and green, and the architect should pay careful attention to both aspects of the entire process. (1)

Green architecture is a sustainable method of green building design: it is design and construction with the environment in mind. Green architects generally work with the key concepts of creating an energy efficient, environmentally friendly building. (1)

2. RESEARCH OBJECTIVES:

Green architecture can be wonderful examples of the possibility of humans living harmoniously within the environment. The opportunities exist to design beautiful, energy efficient and environmentally friendly residences and workplaces that demonstrate our human ability to adapt to and peacefully live within the ecology of the natural world. (2)

Green building practices aim to reduce the environmental impact of buildings. Green building brings together a vast array of practices and techniques to reduce and ultimately eliminate the impacts of buildings on the environment and human health.

So, the main objectives of this paper are to:

- Discover the early beginning of green architecture.
- Discuss the evolution of green architecture throughout history.
- Realize the relationship between the green architecture and the technology used at the same age.
- Analyze the aspects which make building green.

3. WHAT IS GREEN ARCHITECTURE?

Green architecture is an approach to building which has become more prevalent in the last 35 to 40 years. Also recently known as sustainable design, green architecture is simply a method of design that minimizes the impact of building on the environment. Once thought of as unconventional and nonstandard, green architecture is quickly becoming accepted by both regulatory agencies and the public alike as a socially responsible and logical means of construction.

The beginnings of today's green revolution can be traced back to the social awareness of the 1960s and European designs. From these origins, new construction techniques have led to the development of innovative materials and design concepts. Indeed, successfully designed green projects can involve an extensive array of factors, ranging from the resourceful use of materials, to careful consideration of function, climate, and location. Also, using local resources, local craftsmanship and utilizing what the geographical location has to offer is important in green design.

4. WHAT MAKES BUILDING GREEN?

The concepts about green architecture can generally be organized into several areas of application. The most important include materials, energy efficiency, land use, and waste reduction: (3)

4.1 Materials

Green buildings are not only designed for a present use, but consideration is also being given to future uses as well. An adaptable structure can be "recycled" many times over the course of its useful life. If specific technical issues prevent use of the building for a new function, then the materials used in its construction are designed to facilitate ease of recycling and reprocessing of materials.

Buildings consume a variety of materials in their construction. Green design reduces the dependence on resource intensive products and materials. Today, there are an increasing number of products available made from efficient, earth-friendly, or recycled materials. In a green building, consideration is also given to the construction process itself. Materials that minimize waste or can be recycled help contribute to an efficient and environmentally sensitive construction process.

4.2 Energy Efficiency

Another important aspect of green design is the integration of energy efficient mechanical systems and conservation methods. Green buildings are designed to reduce or eliminate the dependence on fossil fuels.

Additionally, green designs further help to minimize waste through the use of gray water recycling and other sustainable energy strategies.

4.3 Land Use




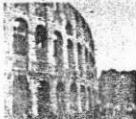
Site selection and building orientation also play a critical role in green design. A green building is located to take advantage of its climate and surroundings. These conditions not only affect the efficiency of a building, but of the community and society as a whole. Planning for responsible land use addresses these issues through the consideration of climate, transportation, and the natural environment.

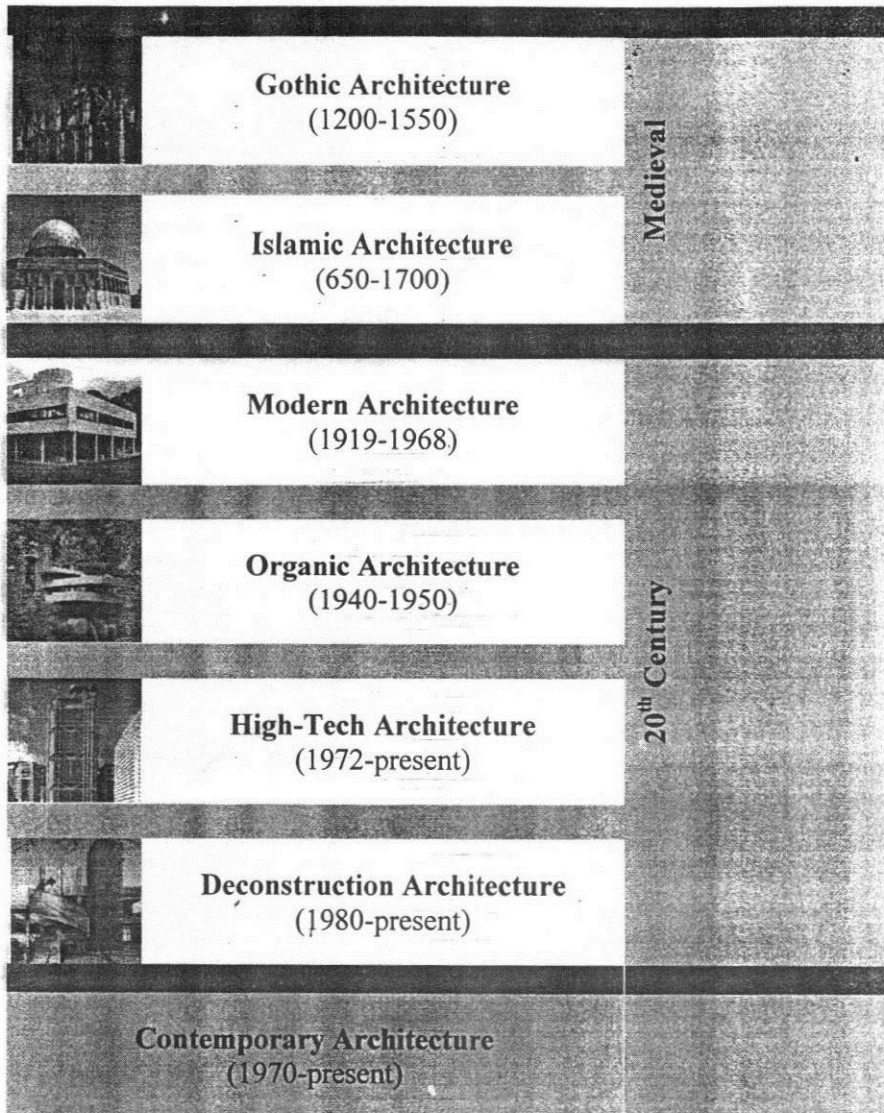
4.4 Waste Reduction

An amazing amount of waste is generated by the construction of a typical building. Green buildings are designed to eliminate waste by using modular systems of construction, recycled products, and efficient use of materials. The ideal green building would create no waste either during construction or use, so the impact on the environment and resources is minimized.

5. HIGHLIGHT OF GREEN ARCHITECTURE THROUGH ERAS:

In this section the researcher navigate through selected eras trying to discover and pick some ideas offering green principles in order to introduce more and more criteria during both design and construction process of buildings.

	Neolithic Architecture (6000-3000BC)	Prehistoric
	Sumerian Architecture (4500-2000BC)	
	Egyptian Architecture (3000BC-400AD)	
	Roman Architecture (800BC-600AD)	



5.1 PREHISTORIC AGES:

1. Neolithic Architecture:

Neolithic architecture is the architecture of the Neolithic period. In Southwest Asia, Neolithic cultures appear soon after 10000 BC, initially in the Levant and from there spread eastwards and westwards.

Neolithic peoples in the Levant, Anatolia, Syria, northern Mesopotamia and Central



Fig. 1, Excavated dwellings at Skara Brae. Europe's most complete Neolithic village.

Asia were great builders, utilizing mud-brick to construct houses and villages. (Fig.1) At Çatalhöyük, houses were plastered and painted with elaborate scenes of humans and animals. In Europe, long houses built from wattle and daub were constructed. Elaborate tombs for the dead were also built. These tombs are particularly numerous in Ireland, where there are many thousand still in existence. Neolithic people in the British Isles built long barrows and chamber tombs for their dead and causewayed camps, henges flint mines and cursus monuments. Perhaps the most famous megalithic structure is Stonehenge in England (Fig.2), although many others are known throughout the world.



Fig.2, Stonehenge is the most famous Neolithic structure in England

Skara Brae, the Orkney Islands, Scotland. (3100-2500)

o *Overview:*

Skara Brae is a large stone-built Neolithic settlement. (Fig. 3) It is Europe's most complete Neolithic village and the level of preservation is such that it has gained UNESCO World Heritage Site status. Skara Brae's inhabitants were apparently makers and users of grooved ware. On average, the houses measure 40 square meters in size with a large square room containing a large hearth which would have been used for heating and cooking. The dwellings contain a number of stone-built pieces of furniture. Fig.4 A sophisticated drainage system was even incorporated into the village's design.



Fig. 3, Outline of Skara Brae settlement

Green Aspects:

o *Land Use*

The houses used earth sheltering but, being sunk into the ground, they were built into mounds of pre-existing domestic waste. (Fig.5) Although it provided the houses with a small degree of stability, its most important purpose was to act as a layer of insulation against Orkney's harsh winter climate.

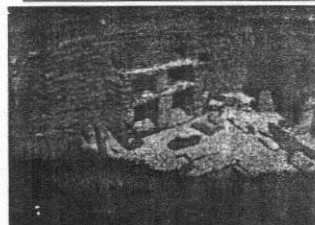


Fig. 4, Evidence of home furnishings. Neolithic village.

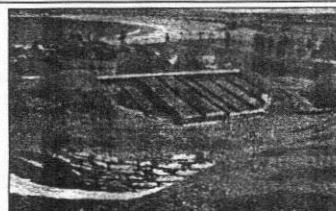


Fig. 5, View over the settlement.

o *Materials*

As few trees grow on the island, the people of Skara Brae used driftwood and whalebone, with turf thatch, to roof their dwellings.

o *Sustainability*

One of these buildings was used as a workshop to make simple tools such as bone needles or flint axes.

2. Sumerian Architecture:

Sumerians were a people who lived in Mesopotamia from the 4th millennium BC to the 3rd millennium BC. The most famous Sumerian buildings are the ziggurats (Fig.6); large mud-brick terraced platforms with temples on top. Such ziggurats may have been the inspiration for the Biblical Tower of Babel. Sumerian temples and palaces made use of more advanced materials and techniques, such as buttresses, recesses, half columns, and clay nails.

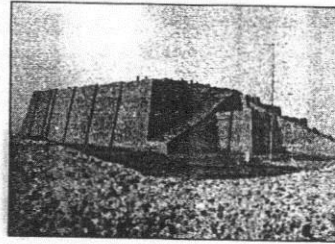


Fig. 6, The Great Ziggurat of Ur. Southern Iraq.

Chogha Zanbil, Khuzestan, Iran (1250 BC)

o *Overview*

Chogha Zanbil is an ancient Elamite complex in the Khuzestan province of Iran. It is one of the few extant ziggurats outside of Mesopotamia. (Fig.7)



Fig.7, Chogha Zanbil.

It was built about 1250 BC by the king Untash-Napirisha, mainly to honour the great god Inshushinak. The complex is protected by three concentric walls which define the main areas of the town. The inner area is wholly taken up with a great ziggurat dedicated to the main god, which was built over an earlier square temple with storage rooms also built by Untash-Napirisha.

Green Aspects:

o *Land Use*

One practical function of the ziggurats was a high place on which the priests could escape rising water that annually inundated lowlands and occasionally flooded for hundreds of miles.

The water of the river Karkheh was not among the healthiest, so it was necessary to clean it before it could be used at the shrine. (Fig.8)

o **Waste Reduction**

The height of the ziggurat allowed the smoke to blow away without polluting city buildings.

o **Materials**

The Tigris-Euphrates plain lacked minerals and trees. Sumerian structures comprised plano-convex mud brick, fixed without mortar or cement. As plano-convex bricks (being rounded) are somewhat unstable in behavior, Sumerian bricklayers would lay a row of bricks perpendicular to the rest every few rows. They would fill the gaps with bitumen, straw, marsh reeds, and weeds.

o **Sustainability**

Mud-brick buildings eventually deteriorate, so they were periodically destroyed, leveled, and rebuilt on the same spot. This constant rebuilding gradually raised the level of cities (Fig.9), so that they came to be elevated above the surrounding plain. The resulting hills are known as tells, and are found throughout the ancient Near East.



Fig. 8, There were small channels for water.

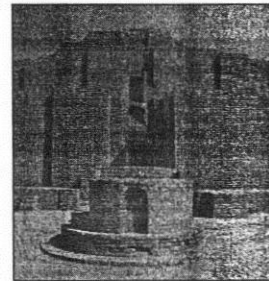


Fig. 9, The installation in which the water was refined.

3. Egyptian Architecture:

The architecture of Egypt took place from the 3rd millennium B.C. to the Roman period. Religious beliefs of eternal life, resulted in an impressive sepulchral architecture, tomb building started as soon as a Pharaoh was named, and continued throughout his life until his death. Massive, static, and serene architecture emerged from the need to obtain stability in stone walls.

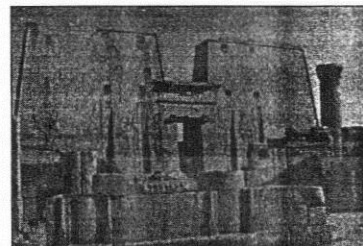


Fig. 10, The temple of Horus at Edfu is an exemplar of Egyptian architecture.

Statues of Pharaohs and sanctuaries of gods in temples, and sarcophagus in tombs dominated the whole architectural layout. Walls are immensely thick and sloping as a structural requirement for balancing. (Fig.10) Stone Columns closely spaced as large spans were not possible. Stone Lintels are massive with

short spans; stone is a material that has a weak tensile strength. Flat roofs were used because domes and vaults were unknown in ancient Egypt. Their buildings have small openings; large doors and windows are not possible in stone construction, this also secured privacy to the religious structures inaccessible to the public. Temples were single storey.

Granite, limestone and sandstone were used in monumental buildings. Wood rarely used as a building material, since there are no natural resources of wood in Egypt. Sun dried bricks were used extensively in dwellings and small buildings, few examples have therefore survived time.

The basic construction method was post and lintel. Buildings were erected without mortar, so the stones had to fit and cut precisely together.

Great Pyramid, Giza, Egypt (2570 BC)

○ Overview

Great Pyramid of Giza, also called the Pyramid of Khufu, is the oldest and largest of the three pyramids in the Giza Necropolis bordering what is now Cairo, Egypt in Africa, and is the only remaining member of the Seven Wonders of the Ancient World. (Fig.11)

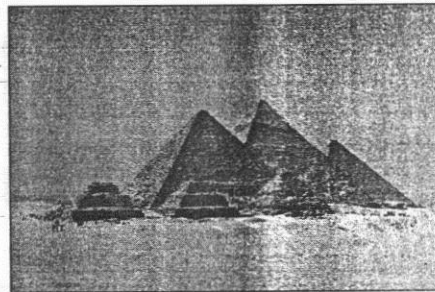


Fig. 11, A view of the pyramids at Giza from the plateau to the south of the complex.

It is believed the pyramid was built as a tomb for Fourth dynasty Egyptian pharaoh Khufu and constructed over a 20 year period concluding around 2560 BC. The Great Pyramid was the tallest man-made structure in the world for over 3,800 years. Many of the casing stones that once covered the structure can still be seen around the base of the Great Pyramid. There have been varying scientific and alternative theories regarding the Great Pyramid's construction techniques. Most accepted construction theories are based on the idea that it was built by moving huge stones from a quarry and dragging and lifting them into place. (Fig. 12)

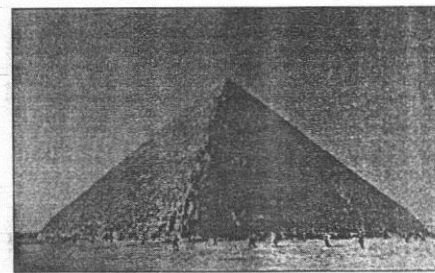


Fig. 12, A view of the Great pyramid.

There are three known chambers inside the Great Pyramid. The lowest chamber is cut into the bedrock upon which the pyramid was built and

was unfinished. A passage from the Grand Gallery leads to the Queen's Chamber, while an antechamber leads from the Grand Gallery to the King's Chamber.

Green Aspects:

o *Sustainability*

Casing stones and other building material from the complex were reused for new building projects in the area of Cairo. This process was not exclusive to Khufu's pyramid and in fact, the reuse of material from older structures was not even uncommon during the age of the pharaohs. However, even this did not happen to the Great Pyramids until, in the Middle Ages, a series of earthquakes loosened the casing stones and allowed them to be harvested for other projects.

o *Land Use*

The Giza Plateau has a fairly level granite bedrock base, in essence, a flat topped mountain. Other regions near the Great Pyramid could not have supported the immense weight of the structure.

The Great Pyramid is the most accurately aligned structure in existence and faces true north.

(Fig. 13)

With the original surrounding courtyards and temples in place, the pyramid was used as a sundial. (Fig. 14)

The polished surfaces of the original mantle reflected heat, sunlight, and moonlight and was probably used as to aid Nile river navigation at night.

o *Waste Reduction*

The Great Pyramid is at the northern edge of the Giza plateau and close to the cliff there. (Fig. 15) Much of the rubble and debris from construction was dumped over the cliff and actually acts to strengthen the cliff from crumbling due to the tremendous weight and closeness of the Great Pyramid.

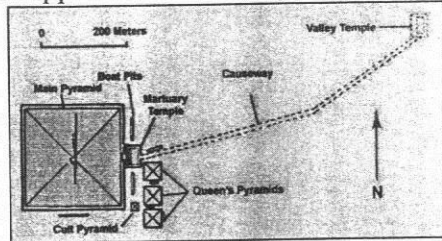


Fig. 13, The Great Pyramid is the most accurately aligned structure in existence and faces true north

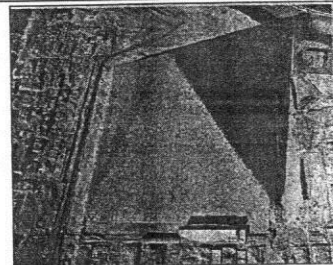


Fig. 14, The pyramid with its surrounding was used as a sundial

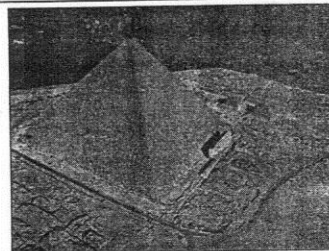


Fig.15, The Great Pyramid close to the cliff of the Giza

o **Energy Efficiency**

There is so much stone mass in the pyramid that the interior temperature is constant and equals the average temperature of the earth, 20 degrees Celsius.

Only the Great Pyramid has "air shafts". (Fig. 16)

The King's Chamber has 2, about 5 inches in diameter which connect to the exterior. The Queen's Chamber has 2 which stopped just short of the walls of the chamber and which do not penetrate completely to the exterior.

The cross sections of these shafts are sometimes oval, sometimes domed, and sometimes rectangular. (Fig. 17)

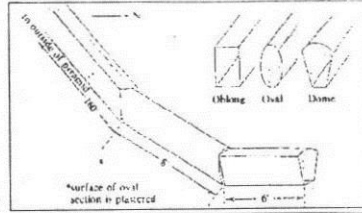


Fig. 16, sections of air shafts connecting the chambers to the exterior.

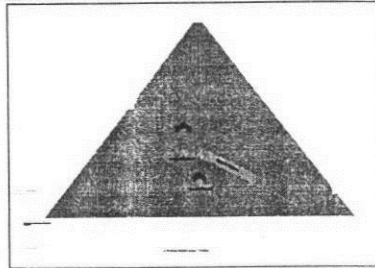


Fig.17, Section through the great pyramid showing its three chambers.

4. Roman Architecture:

Romans were famous for their advancement in architecture and engineering. Before the Romans, the most commonly used building style was the post and lintel. This way of building was of course limited in the weight it could carry and therefore the span between the supports.

The Roman Architecture changed all this and advanced this by introducing new methods of architecture; The Columns and The Arches. (Fig.18) With these methods the Romans were able to construct bigger temples and buildings than ever before.



Fig.18, The colosseum

Green Aspects:

o **Materials**

Innovation started in the first century BC, with the invention of concrete, a strong and readily available substitute for stone. Tile-covered concrete quickly supplanted marble as the primary building material and more daring buildings soon followed, with great pillars supporting broad arches and domes rather



Fig.19, Dome of St. Peter's Basilica in Rome

than dense lines of columns suspending flat architraves. (Fig.19) The freedom of concrete also inspired the colonnade screen, a row of purely decorative columns in front of a load-bearing wall. In smaller-scale architecture, concrete's strength freed the floor plan from rectangular cells to a more free-flowing environment.

The PANTHEON

o *Overview*

The Pantheon is a building in Rome which was originally built as a temple to all the gods of Ancient Rome.

The building is circular with a portico of three ranks of huge granite Corinthian columns under a pediment opening into the rotunda, under a coffered, concrete dome, with a central opening (oculus), the Great Eye, open to the sky. A rectangular structure links the portico with the rotunda. The height to the oculus and the diameter of the interior circle are the same, 43.3 meters. (Fig.20)

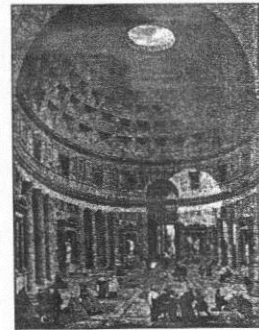


Fig.20, the Pantheon in Rome, Italy. The Great Eye is the source of all light.

Green Aspects:

o *Energy Efficiency*

The Great Eye at the dome's apex is the source of all light. The oculus also serves as a cooling and ventilation method. (Fig.21) During storms, a drainage system below the floor handles the rain that falls through the oculus.

o *Materials*

The coffers for the concrete dome were poured in molds, probably on the temporary scaffolding. This coffering was not only decorative, but also reduced the weight of the roof, as did the elimination of the apex by means of the Great Eye. (Fig.22) The top of the rotunda wall features brick-relieving arches, visible on the outside and built into the mass of the brickwork.

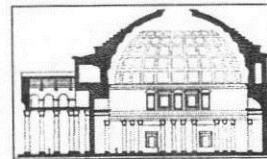


Fig.21, Pantheon Cross Section

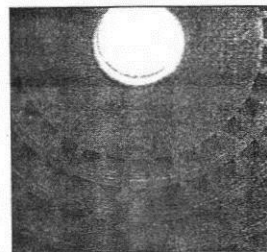


Fig.22, The skylight oculus of 8.9m in diameter

Roman Town house

o *Overview*

The Roman town house, or domus, was a single family house. The most popular design for this structure was based around the atrium, which had its roots in early Etruscan homes. (Fig.23)

These houses had a single main room with many small rooms opposite the entrance, or, in some cases, a set of small rooms around a courtyard, from which the atrium developed.

Houses were generally built with wattle or daub infill set on foundations of low stone. Mud brick was also commonly used.

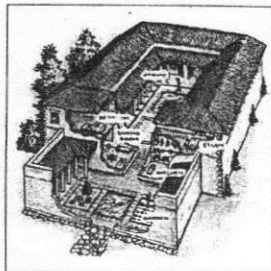


Fig.23, Typical Roman Town house

Green Aspects:

o *Energy Efficiency*

The need of the natural light derived the idea of a court at the back of the tablinum, open to the sky, surrounded by various rooms, and planted with flowers, trees, shrubs, and often a fountain in the middle.

The atrium also received its light from a central opening in roofs, the compluvium, a sloped hole in the room through which to filter in light and air. (Fig.24)

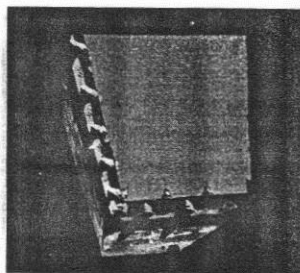


Fig.24, The compluvium, a sloped hole in the room

o *Water Conservation*

In the center of the atrium, directly beneath the compluvium was a shallow pool (Fig.25), impluvium, which was not only decorative but also it caught the rainwater coming through the open roof and channeled it into underground water storage tanks.

(Fig.26, 27)

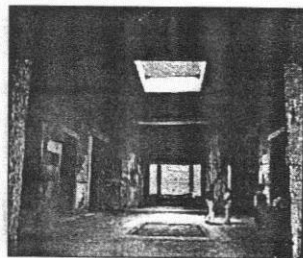


Fig.25, A shallow pool directly beneath the compluvium

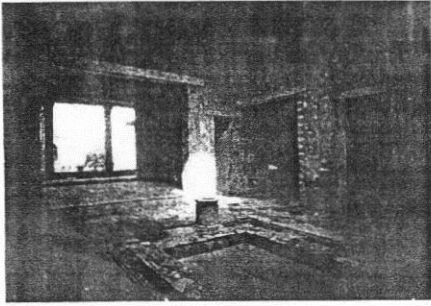


Fig.26, Impluvium catches the rainwater into underground water storage tanks

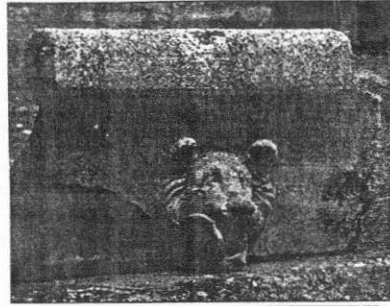


Fig.27, Special tiles with animal-head waterspouts caught the rainwater and channeled it into the pool

5.2 MEDIVAL AGES:

1. Gothic Architecture:

Gothic architecture is a style of architecture which flourished during the high and late medieval period. It evolved from Romanesque architecture and was succeeded by Renaissance architecture.

Originating in 12th-century France and lasting into the 16th century. Its characteristic features include the pointed arch, the ribbed vault and the flying buttress. Gothic architecture is most familiar as the architecture of many of the great cathedrals, abbeys and parish churches of Europe. (Fig.28) It is also the architecture of many castles, palaces, town halls, guild halls, universities, and to a less prominent extent, private dwellings.

It is in the great churches and cathedrals and in a number of civic buildings that the Gothic style was expressed most powerfully, its characteristics lending themselves to appeal to the emotions. A great number of ecclesiastical buildings remain from this period, of which even the smallest are often structures of architectural distinction while many of the larger churches are considered priceless works of art. ;

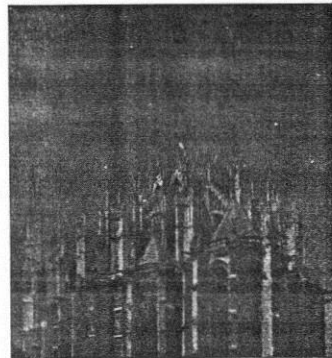


Fig.28, Amiens Cathedral of Notre-Dame



Fig.29, The nave lit by its own source of light.

Green Aspects:

o *Energy Efficiency*

The basilica type of church is constructed with a nave and at least two side aisles, the nave and aisles being separated by arcades. The nave is higher than the aisles so that it can be lit by its own source of light. (Fig.29, 30, 31)

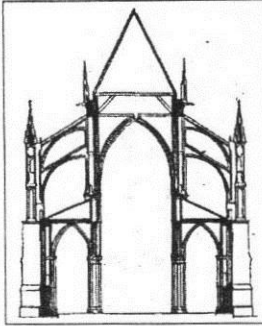
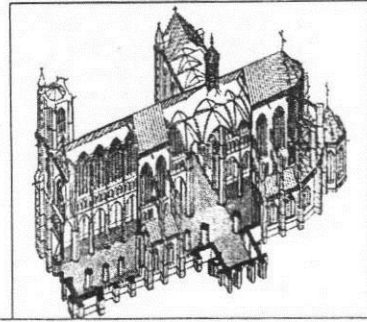


Fig.30, Cross section of basilica with buttressing



Nave
 Aisle
 Pier buttress
 Flying buttress

Fig.31, Cutaway of basilica showing buttressing making possible to obtain full height windows.

o *Materials*

A further regional influence was the availability of materials. In France, limestone was readily available in several grades, the very fine white limestone of Caen being favored for sculptural decoration.

The architectural innovations of the gothic style were employed to divert the weight of the massive roof away from the walls making the use of large windows possible. (Fig.32) One of the most distinctive features of the gothic cathedral is large stained glass windows. (Fig.33)

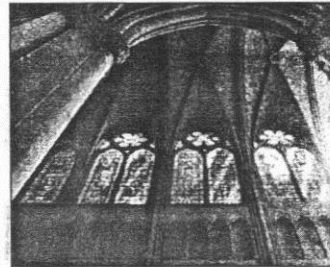


Fig.32, The nave is taller than the aisles, having windows which light the central space.

The availability of timber also influenced the style of architecture. It is thought that the magnificent hammer-beam roofs of England were devised as a direct response to the lack of long straight seasoned timber by the end of the Medieval period, when forests had been decimated not only for the construction of vast roofs but also for ship building. (Fig.34)

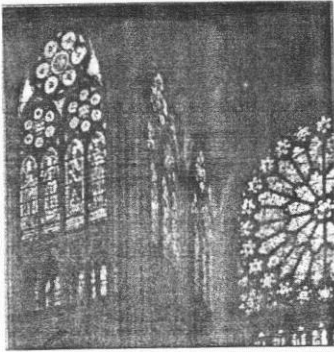


Fig.33 The significant effect of natural light streaming in through stained-glass windows .



Fig.34, Westminster Hall with hammer-beam roofs

○ **Land use**

Most Gothic cathedrals orientation is east-west with entrance on west façade. (Fig.35)

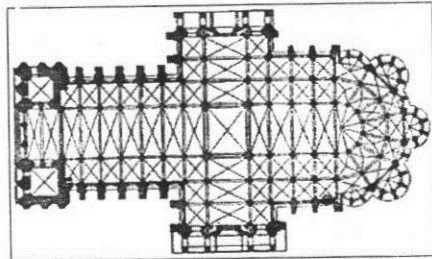


Fig.35, Gothic cathedrals orientation.

2. Islamic Architecture:

Islamic Architecture is highly diverse but unified by climate, culture, and a love of geometric and ornaments, as well as by the mobility of ideas, artisans, and architects throughout the region. The central public buildings are mosques, often with a dome and minaret; domestic houses face an inner courtyard and are grouped together, with vaulted streets linking the blocks. (Fig.36)



Fig.36 The Dome of the Rock, 691 AD

Green Aspects:

○ **Land Use**

In Islamic architecture Site has a great affect which is varied from place to another in Islamic world, this part comprises different elements of major influences on architecture shape creation,

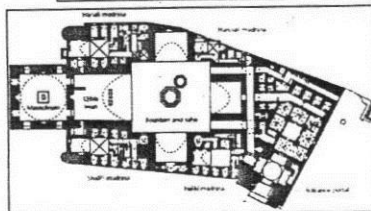


Fig.37, Plan of the Sultan Hasn in mosque showing the fountain and Sahn.

and the choice of construction techniques, from these elements we can mention, climate and environment effect, culture and local traditions, geography, topography and the underground resources. (Fig.37)

The dry weather and hot climate in the Islamic architecture lead the formation of high walls around the terrace, and the small openings looking outside which oriented diagonally to prevent and control dust and sun light and passing breeze as a mean of ventilation. (Fig.38)

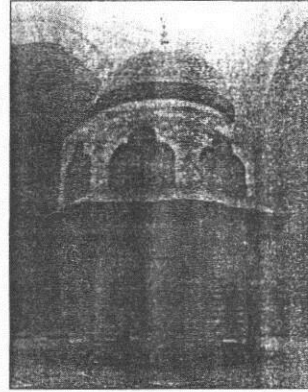


Fig. 38, The fountain and Sahn in Sultan Hasan mosque.

o *Water Conservation*

Desserts are a common feature of the Islamic world. Any desert settlement must make some provision for obtaining and storing water, usually from wells or seasonal rainfall, although occasionally sites are dependent on water brought from elsewhere.

The unpredictability of rain and the high evaporation rates in the desert mean that elaborate water catchment and storage facilities are developed. Sites dependent on seasonal and sometimes erratic rain usually employ a system of dams, cisterns and run-off channels to maximize the catchment area. If water needs to be transported some distance, underground channels (Qantas) are built to minimize evaporation. (Fig.39)

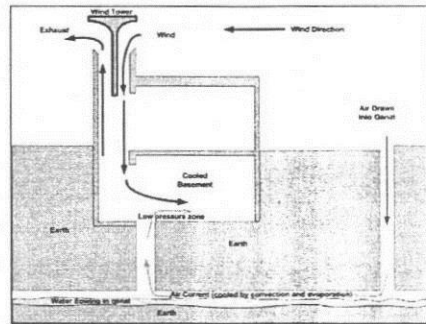


Fig.39, Wind-Tower-and-Qanat-Cooling

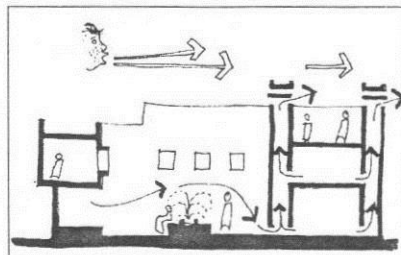


Fig.40, Traditional Islamic courtyard housing used shade and a water fountain to cool air within the courtyard, which was then exhausted via wind towers to assist cooling of the habitable rooms.

o *Energy Efficiency*

Social patterns and family values were not the only factors instrumental in determining the spatial configurations of Cairene houses.

The real ingenuity of their designs lies in the structural modifications introduced into traditional spaces (like the qa'a, maq'ad, takhtabush, etc.) to produce autonomous spatial units adapted to climatic conditions. (Fig.40) While the open courtyard functions as a temperature regulator, diffusing cool air which it retained from the night into the rooms of the house during the day, the spatial units that look onto it have varying temperatures during the day, depending on their orientation to the sun. (Fig.41,42) The takhtabush provides a cool sitting area in the morning; the maq'ad, which always faces north to catch the prevailing wind, is the favorite entertainment area in the evening. The qa'a is an indoor space which can be conveniently heated in the winter. The domed opening in the roof of the central part of the qa'a, which acts as an outlet for hot air, along with high ceilings, a water fountain below the domed opening, thick walls, marble surfaces, and the mashrabiyya screens keep the interior of the qa'a cool in the summer. (Fig.43) Finally, cold air is conducted to the inner parts of the house through a malqaf or wind catcher, (Fig.44) Climatic adaptations transcend typical utilitarian designations of the various units; activities are shifted from one unit to the other according to the hours of the day and the seasons. Islamic architecture used a natural ventilation system that depends on the difference of pressure between

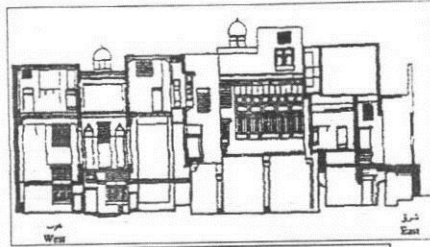


Fig.41, Longitudinal section through El-Suhaymi House

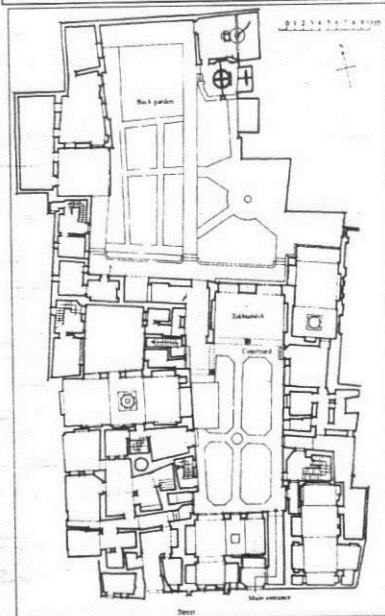


Fig.42, El-Suhaymi House Plan, illustrating the pleasant atmosphere that can be created within the courtyard and the arrangement of the surrounding



Fig.43, Courtyard balcony (maq'ad) and west courtyard

the inside and outside that is built on sucking air from high pressure zone outside to that of low pressure inside, and that what was discovered by Ventury in the twentieth century. (Fig.45)



Fig.44, Exterior view, malqaf

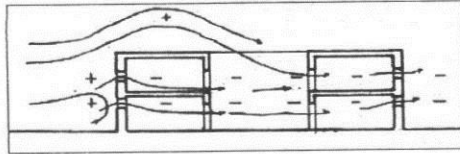


Fig.45, System of natural ventilation used in most Islamic

Qasr al-Harraneh

o Overview

This imposing structure is situated about 65 km east of Amman and 18 km west of Qusayr Amra. Harraneh is one of the best-preserved Umayyad monuments in the Jordanian steppe. It consists of 61 rooms arranged into 2 levels surrounded by a porticoes central courtyard. (Fig.46) These rooms are grouped as self-contained units (bayts), each consisting of a central hall flanked on 2 sides by a pair of rooms opening onto the central hall.

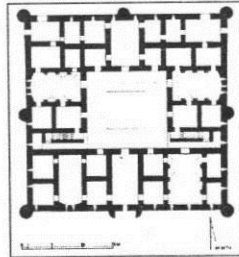


Fig.46, Upper floor plan

Green Aspects:

o Land Use

The identification and the characteristics of the site can be seen clearly in Qasr al-Harraneh.

o Energy Efficiency

The exterior walls are pierced by narrow openings for lighting and ventilation (Fig.47,48).

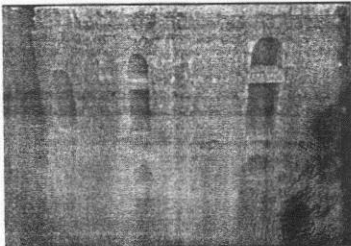


Fig.47, Wide windows open on the internal surrounded courtyard

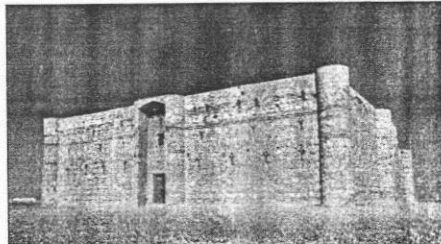


Fig. 48, Narrow windows is sucking air from outside due to pressure vary

o **Water Conservation**

A small water tank stood in the middle of the courtyard to collect rainwater from the rooftops. Additional water was obtained from seep-holes dug in the adjacent valley-bed (Fig.49).

o **Materials**

They used too new techniques and materials like wood lintel that gives flexibility for the building to resist earthquakes, and that can be shown clearly when compare between our Qasr and the others, Al-Harraneh still standing, others in the same era were completely destroyed.

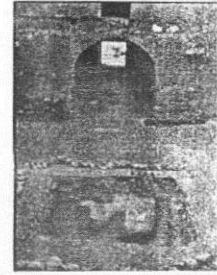


Fig.49, A shallow cistern in the courtyard

5.3 20th Century:

1. Modern Architecture:

Modern architecture is a term given to a number of building styles with similar characteristics, primarily the simplification of form and the elimination of ornament. (Fig.50) The style was conceived early in the 20th century. Modern architecture was adopted by many influential architects and architectural educators, however very few "Modern buildings" were built in the first half of the century. It gained popularity after the Second World War and became the dominant architectural style for institutional and corporate buildings for three decades.

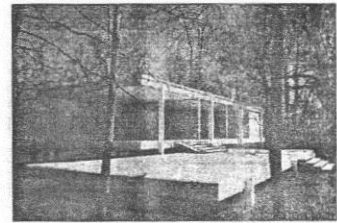


Fig.50, The landscape runs under the house.

Green Aspects:

o **Land Use**

The first and last point of Le Corbusier's Five Points of Architecture, the pilots elevating the mass off the ground and the roof garden, restoring, supposedly, the area of ground covered by the house, minimized the footprints of buildings on the natural environment. (Fig.51,52)

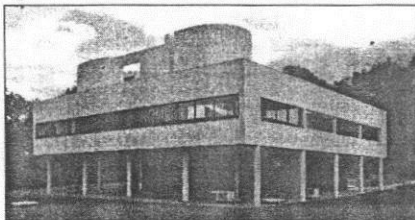


Fig.51, The house is up in the air, far from the ground.

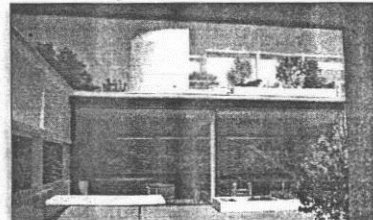


Fig.52. The roof gardens make full use of rainwater and reduced the heat on the roof.

o **Energy Efficiency**

Modern architecture was initially intended to create openness and to provide room for light and sun (Fig.53). Dark cellars should be broken open and vistas opened up. The aim was to create an interchange between interior and outside; private space should be brought into relationship with the public realm (Fig.54).

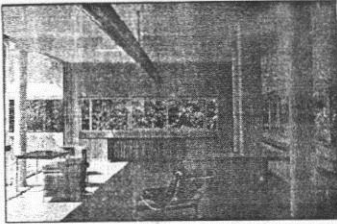


Fig.53. The horizontal windows provide natural light deep into interior.

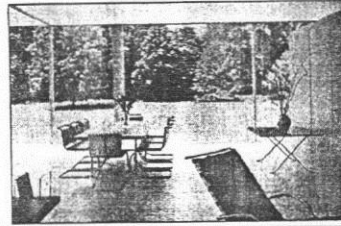


Fig.54. The principle of openness and providing room for light and sun.

o **Materials**

Modern Architects believed that the luxury material is well made, neat and clean, pure and healthy and its bareness reveals the quality of its manufacture. (Fig.55)

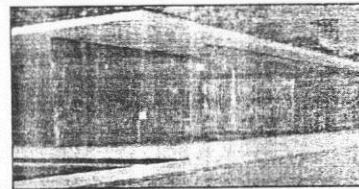


Fig.55. Using of materials in it natural state make the environment more healthy.

2. Organic Architecture:

Organicism was an integrative approach to architectural design that concerned itself with the limitations of function, landscape, and materials. Instead of designing a structure and then forcing all other considerations to conform to it, architects such as Louis Sullivan and Frank Lloyd Wright sought to integrate their designs seamlessly with their place and purpose. (Fig.56)

As an approach, Organicism was more than simply a look to nature as a guide for the design process -- it was a conscious resistance to the ever-increasing emphasis on science, technology, and development.

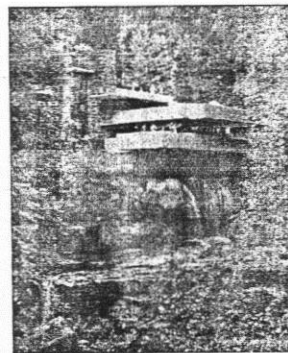


Fig.56. Water falling house showing the harmony and integration with the site

They resisted the domination of scientific materialism, which seemed to sacrifice all ideas of value for industrial progress. As an alternative, they sought inspiration in nature and in the diversity and harmony of its forms. They tried to create a philosophy that would approach life organically: integrating fields of knowledge while remaining aware of their place in the larger frameworks of society and environment.

Green Aspects:

o *Land Use*

Harmony with the environment is a broad principle in Organic Architecture that means to be sensitive to the forces of nature; the climate, wind, and sun. The design also pays respect to the particular features of the site; the topography and landform, rocks, water, and vegetation. (Fig.57)

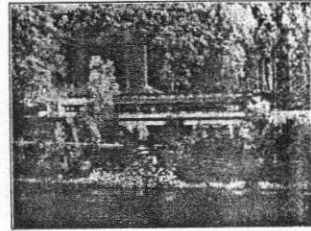


Fig.57, Spring Green Restaurant its form grows from its site, in sympathy with its surrounding.

o *Feedback*

Organic architects' designs for educational facilities recognize the importance that the environment has in edifying young people. Buildings subtly support learning in ways beyond functionality. They seek to impart certain qualities of life to the People through the character of the architecture itself.

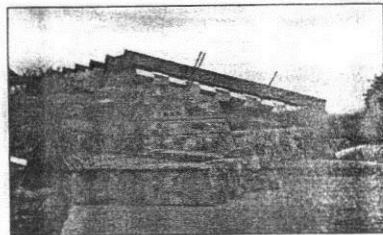


Fig.58, Building geometry achieves the optimum solar orientation in the desert.

o *Materials*

One of organic architecture principle is the nature of materials, that doesn't mean that the materials that you should use in a building are ones that can be found naturally on the site, but the word nature refers to the individual attributes, or special qualities, that

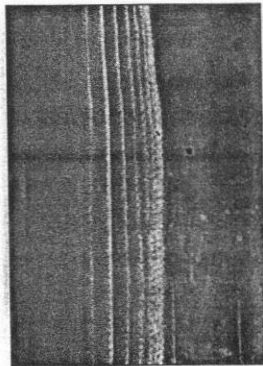


Fig.59, Giant Saguaro cactus.

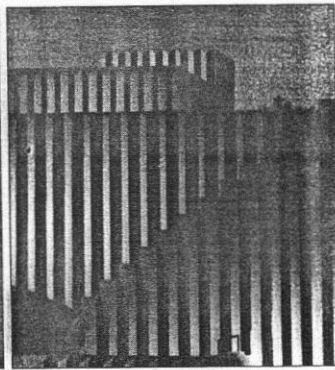


Fig.60, The Focus House blending with the textures of the desert.

characterize each material and give it distinction.

They expressed the natural aesthetics of materials by introducing unfinished surfaces. (Fig.58,59,60)

o *Energy Efficiency*

In Johnson Wax building the use of tubular lighting glass in horizontal bands, set in conjunction with a brick facing to admit light during the day and illumination at night, provides brilliant warmth to the interior. (Fig.61)

Sunlight is introduced to the interior of the organic building by clerestory windows or interior courtyards.



Fig.61, A natural well-lit, cheerful work room promotes efficiency

Using roof overhangs which create shade, keep the sun and rain off walls and glass surfaces, increasing comfort and save energy. (Fig.62,63,64)

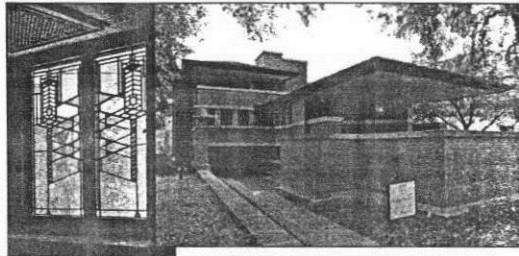


Fig.62, Roof overhangs and stained glass windows in Robie house.

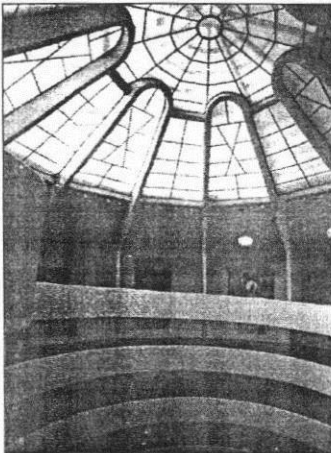


Fig.63, The skylight allowing copious light to cascade into the space from above.

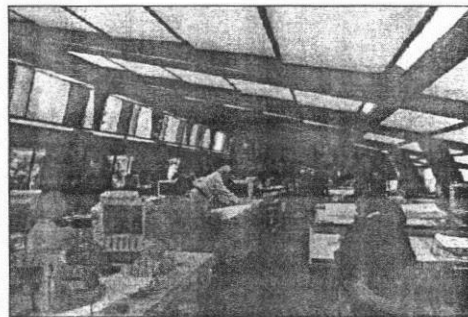


Fig.64, Canvas roof cut heat but allow light.

3. High-Tech Architecture:

Born as a revamped emissary of Modernist functionality, the High Tech design style is based on uncomplicated plans that rigorously combine the use of factory-produced materials and a tendency to expose a building's structural systems. Perhaps most importantly, High Tech architecture gives little consideration to the symbolic form of the building, relying instead on technological sophistication to ground its aesthetic.

Green Aspects:

o *Land Use*

The principle of High-Tech architecture relies on nothing more than a combination of machined parts that are maximally flexible and, ideally, interchangeable. The Pompidou Centre, while in fact being a museum, could easily have functioned as a warehouse, or an office building. (Fig.65)

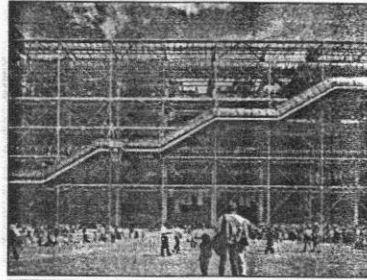


Fig.65, The Pompidou Centre, France, is one example of high-tech architecture.

Buildings usually be made of distinct components and will often appear to hover a few inches above the site as if, one day, they might be dismantled or moved. (Fig.66)

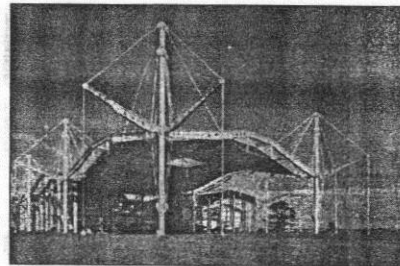


Fig.66, Renault headquarter, the building makes minimum impact on its site.

o *Materials*

Characteristics of high-tech architecture have varied somewhat, yet all have accentuated technical elements. They included the prominent display of the building's technical and functional components, and an orderly arrangement and use of pre-fabricated elements. (Fig.67) Glass walls and steel frames were also immensely popular. High-Tech building used maintenance-free stainless steel for all structure elements.

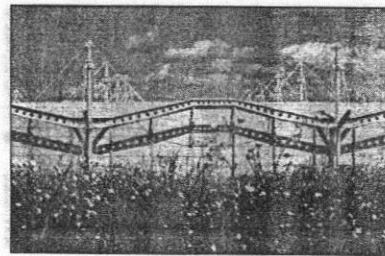


Fig.67, Respecting the relation between the building and its surroundings.

o Sustainability

Because the building is an assembly of tough, dry components, the elevation and the plan, become an abstract grid that can accommodate a number of different functions: an insulated panel, a door, an opening window, or a metal louver. (Fig.68) When the function of the space changes, the configuration of the external wall can respond accordingly, the change can be made in a matter of minutes with simple tools and no mess. (Fig.69)

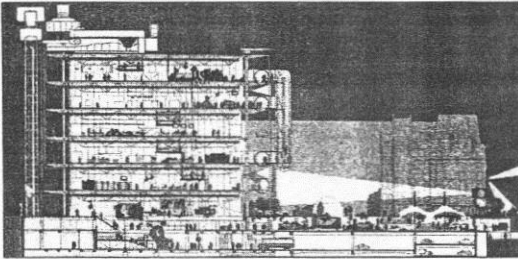


Fig.68, At the Centre Pompidou, sections of the upper floors are omitted to form open roof terraces

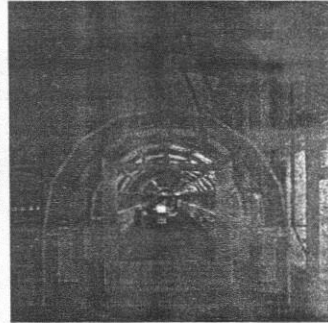


Fig.69, Paper Studio on top of the Pompidou Center, France

Energy Efficiency

High-Tech Architects' work has rigorously pursued a deep interest in environmental issues. (Fig.70) Their work addresses the continuing need to employ technology in the development of new architectural prototypes when faced with the increasingly limited resources of our burgeoning cities. (Fig.71,72)

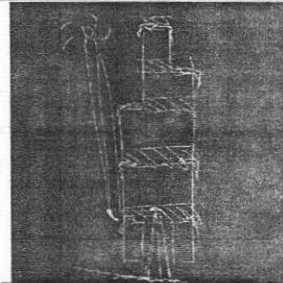


Fig.70, Natural light considerations take place in the early

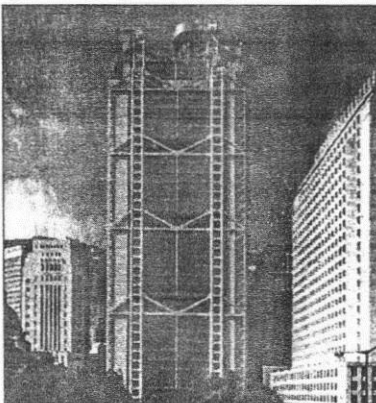


Fig.71 The high-tech buildings make persistent use of glass curtain walls and steel structure.

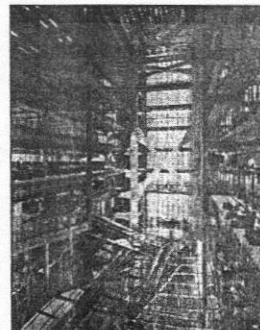


Fig.72, The whole building is submerged with natural

New computer techniques give unlimited choices by simulating ultimate computer-generated building which facilitates the architect to achieve the best orientation and shape. (Fig.73)

In High-tech Architecture the building's form and geometry is generated as a result of thorough scientific analysis, aiming to reduce solar gain and heat loss via the building's skin. (Fig.74, 75)

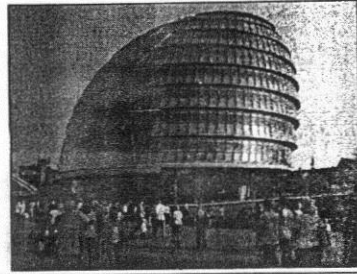


Fig.73, City Hall, London, The building has an unusual bulbous shape, intended to reduce its surface area and thus improve energy efficiency

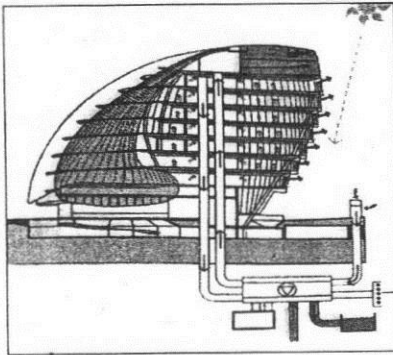


Fig.74, The water is extracted from the water table beneath London through two bore holes and used to cool the building and then used in toilets and for irrigation savings on mains water

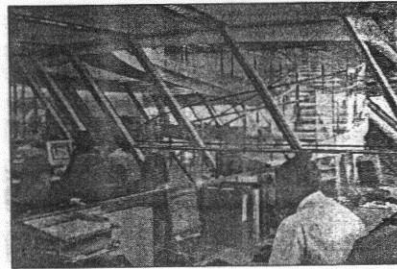


Fig.75, Heat generated by computers and lights is recycled. The deep-plan floors allow for the collection of heat at the building's core, which can then be redirected to its periphery.

High-tech architecture uses advanced materials and construction techniques to combine open space plan to let the sun penetrate deep into its interior. (Fig.76) High control mechanism facilitates the control of light and to make a mixture with artificial and natural sources of light. (Fig.77)



Fig.76, The impression of one vast open space is remarkable for its transparency and the interplay of natural and artificial light with it.

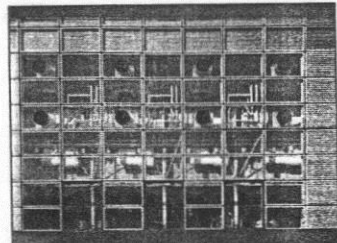


Fig.77, Aluminum louvers, linked to light sensors, provide a flexible system for the control of natural and artificial

Developing new ideas for its ecology and working patterns, Central to this concept is a reliance on natural systems of lighting and ventilation. (Fig. 78,79)

Every office in the tower is daylight and has openable windows, allowing occupants to control their own environment, and resulting in energy consumption levels equivalent to half those of conventional office towers. (Fig.80,81)

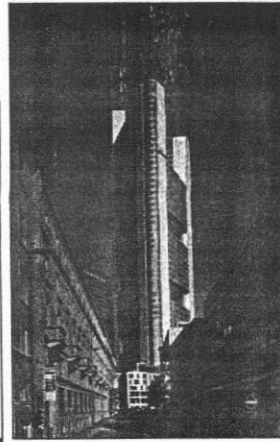
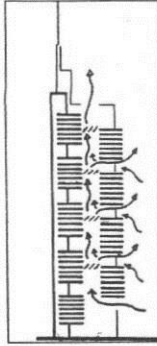


Fig.78, Commerzbank Headquarters, at fifty-three storeys, the Commerzbank tower is the world's first ecological office tower and the tallest building in Europe.

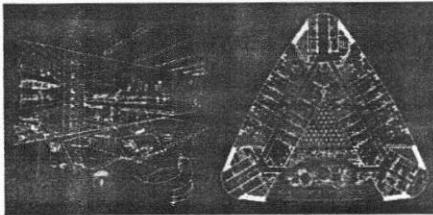


Fig.79, The project explores the nature of the office environment, developing new ideas for its ecology and working patterns.

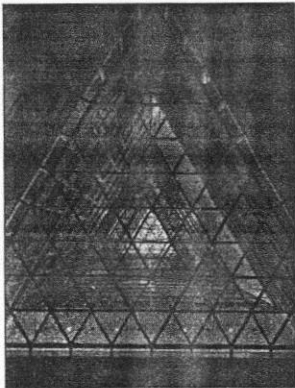


Fig.81, The central atrium

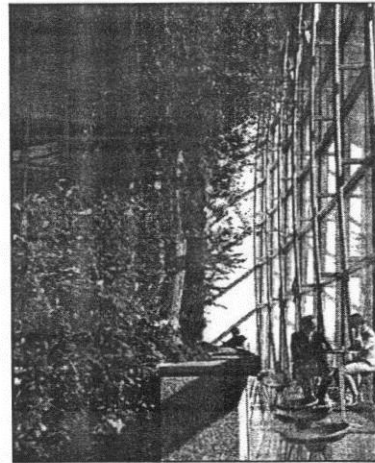


Fig.80, Sky gardens that spiral around the building bring daylight and fresh air into the central atrium and are the visual and social focus for village-like clusters of offices.

4. Deconstruction Architecture:

Deconstructivism in architecture has very little to do with any given philosophy of design, Emerging from the theoretical concerns of the past 25 years. As originally conceptualized by the French philosopher Jacques Derrida, Deconstruction is a method of inquiry, not a philosophy in and of itself. (Fig.82)

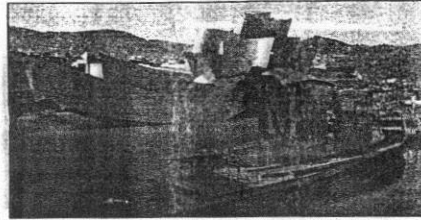


Fig.82, The Guggenheim Museum Bilbao by Frank Gehry, on the Nervión River in downtown Bilbao, Spain

Deconstructivism provided a neat method to critique the supposedly unifying, and thereby totalizing and idealistic, project of the Modern movement. Deconstructivism architects focused on a series of theoretical projects and sought to decenter the concept of classical order and space.

Green Aspects:

o *Land Use*

The replacement of the traditional, form follows function, relationship with the superimposition or juxtaposition of each make an optimum use of site with maximum flexibility.



Fig.83, The Parc de la Villette, Paris. The largest discontinuous building in the world.

o *Sustainability*

The adoption of fragmentation as an analytical device with grid system provides the buildings easy implement and maintenance. (Fig.83)

o *Materials*

Deconstruction has strong ties to environmental sustainability. In addition to giving materials a new life cycle, deconstructing buildings helps to lower the need for virgin resources. The building itself could be a source of materials after demolition using the Design for



Fig.84, Habitat 67, Montreal, Canada. A residential structure consisting of separate, functional apartments that could be put together in a variety of ways. As people moved in or out, the units could be reconfigured as desired.

Deconstruction (DfD) strategy. (Fig.84)

5. Contemporary Architecture: Green Architecture

Pre-20th Century, structures were designed and built by builder-architects who had an ability to understand the entire building from design through construction and lifetime operations. They incorporated enduring passive design and simple mechanical systems to heat, cool and light buildings.

Architects in the 21st Century will look back upon these ideas to relearn the basics of climatic design.

The EpiCenter, Artists for Humanity

o Overview

The EpiCenter is a simple, functional building that achieves the highest levels of sustainability on a tight budget. The building uses energy and water efficiently, incorporates recycled materials, makes full use of natural daylight, and promotes the health of its occupants. The EpiCenter also offers an opportunity to build public awareness of sustainable, economic, and environmental principles among the immediate community and beyond.

Green Aspects:

o Land Use

Important to urban teens without cars, the site is easily reachable by public transportation from most areas of Boston. Investigate property for possible contaminants (e.g., toxic or hazardous wastes, dumps). (Fig.85)

Provide showers and changing areas for bicycle and pedestrian Visitors.

o Energy Efficiency

- 1) Minimize number of east and west windows.
- 2) Use large exterior windows and high ceilings to increase day lighting.
- 3) Use operable windows.
- 4) Reduce internal heat gains by improving lighting and appliance efficiency.
- 5) Use a photovoltaic (PV) system to generate electricity on-site.
- 6) Site the building for southern exposure.

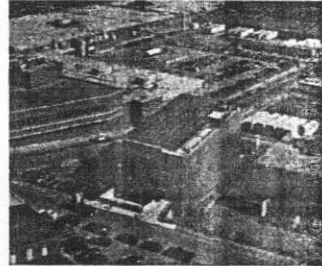


Fig.85, Aerial photography showing photovoltaic panels on roof and urban context.

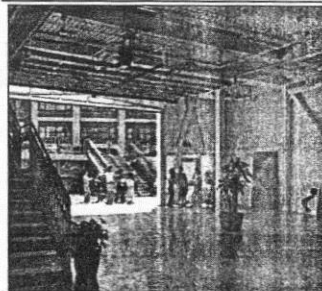


Fig.86, Low emitting paint, sealants, carpet, and composite wood throughout the building provide healthy indoor air quality

- 7) Use modulating photoelectric daylight sensors.
- 8) Use variable frequency drives for fans.

o **Water Conservation**

- 1) Use automatic faucet controls for lavatories.
- 2) Collect and store rainwater for landscape irrigation.

o **Materials**

- 1) Use materials with integral finish. (Fig.86)
- 2) Consider the use of structural materials that do not require application of finish layers.
- 3) Consider exposing structural materials as finished surfaces.
- 4) Use materials and systems with low maintenance requirements.
- 5) Handrail system made from salvaged automobile windshields. (Fig.87)

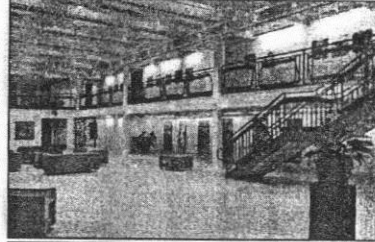


Fig.87, Handrail system made from salvaged automobile windshields

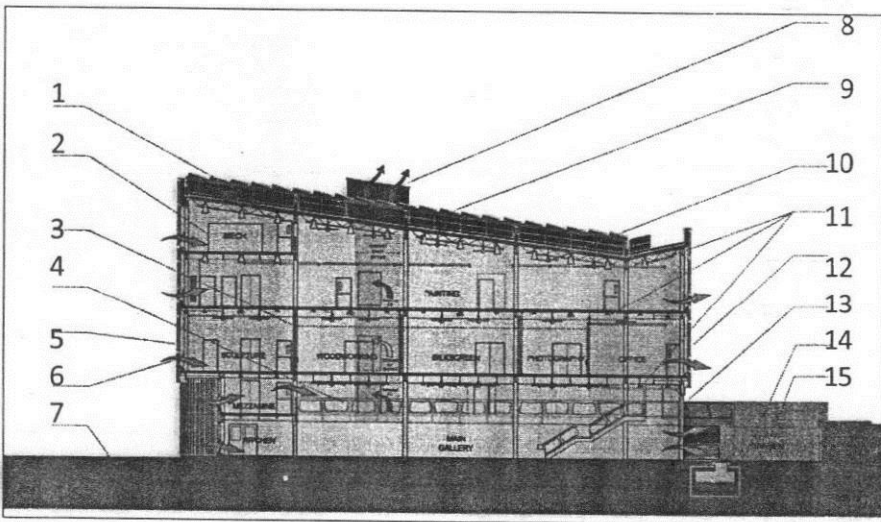


Fig.88, Longitudinal Section

- 1) Light colored roofing reduces heat island effect at roof.
- 2) Mechanical loft removes equipment from roof to allow more room for PV array.
- 3) Interior walls made of clear, corrugated acrylic provide daylight and views even in the interior rooms
- 4) Handrail system made from salvaged automobile windshields.

- 5) Large floor-to-floor height and floor-to-ceiling glazing on north and south facades allow daylight to penetrate deep into floor plan.
- 6) Operable windows on north and south facades allow flow through natural ventilation and occupant comfort control
- 7) Light colored paving and shaded site reduce heat island effect at ground.
- 8) Large fans on the roof with exhaust vents on each floor supplement the natural ventilation system and provide night-time cooling for building mass
- 9) Roof slope provides optimal orientation for PV array, 49 kW, grid connected, provides more electricity than needed on site.
- 10) Ceiling fans throughout the building improve occupant comfort in both heating and cooling seasons.
- 11) Energy efficient lighting with automatic controls and daylight dimming reduces energy demand.
- 12) Large floor-to-floor height and floor-to-ceiling glazing on north and south facades allow daylight to penetrate deep into floor plan.
- 13) Large, glazed overhead door allows gallery to open into garden courtyard.
- 14) Underground tank stores rainwater harvested from roof for use in landscape irrigation.
- 15) Recessed garden courtyard provides protected green space. Drought tolerant landscaping reduces water use.

The Blaustein International Studies

o Overview

The multi-use International Center complex is the main educational facility of the Blaustein Institute for Desert Research at Sede-Boqer. The building houses a cafeteria and lounge, classrooms, administration and eight housing units for students and visitors, totaling approximately 800m².

Green Aspects:

o Land Use

The campus is located in the arid Negev Highlands region of southern Israel. Local climate is characterized by sharp daily and seasonal thermal fluctuations, dry air and clear skies, and intense solar radiation. Prevailing winds are northwesterly and often laden with dust. The structure and courtyard are sunken

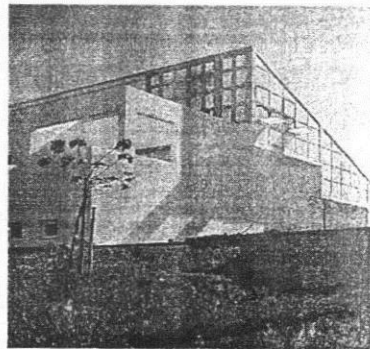


Fig.89, South view

below grade, with earth berms covering the ground floor level and part of the first apartment level. (Fig.89)

Earth sheltering increases the building's thermal insulation, as well as providing thermal mass to stabilize the extreme temperature swings characteristic of the desert climate.

o **Energy Efficiency**

A number of climatic response strategies were integrated in the building's design, which is organized around an enclosed central courtyard.

Desert solarium acts as a man-made oasis, moderating the harsh climate in various modes according to seasonal conditions, which acts as a seasonally-selective solar interface.

In summer: air within the courtyard is cooled by a large down-draft evaporative cool tower, which uses water sprayers to create a flow of cool air into the lower part of the courtyard, while warmer air is exhausted through operable upper windows. Excess water spills into a terraced pool which is the centerpiece of a network of water channels and landscaping that also promote evaporative cooling. (Fig. 90, 91)

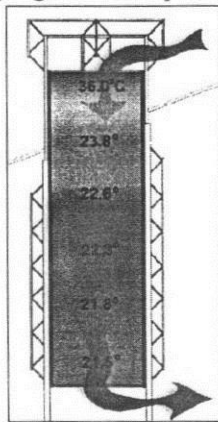


Fig.90, Hot air ducted to floors

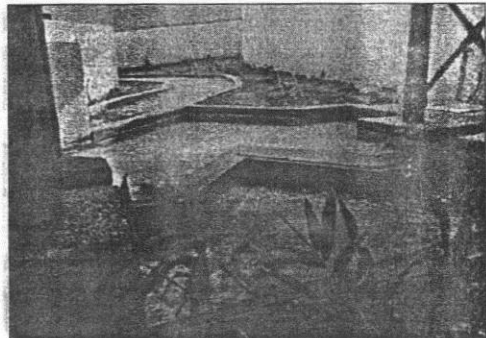


Fig.91, Water Sprayers

In winter, the courtyard functions as a solar greenhouse: heated air rising by convection is drawn from the warmest part of the atrium near the roof ridge, and ducted to the apartments on the two upper floors. (Fig.92)

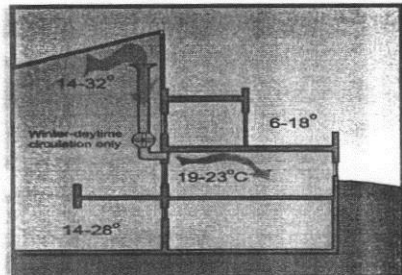


Fig.92, Hot air ducted to floors

Materials

All exposed walls are concrete masonry covered by an external 5cm layer of expanded polystyrene insulation.

A special glass having a definite angel of refraction had been used in the roof. (Fig.93)

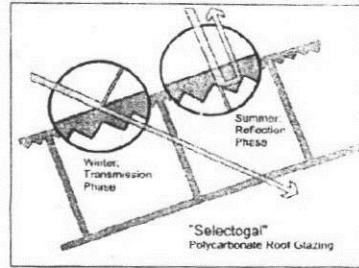


Fig.93, Roof covering

6. Conclusion

If it's true that "there is nothing new under the sun"; then the practice of looking back in time for fresh ideas makes complete sense; Specially, in the case of Green Architecture, it has been a fruitful search.

Green specifications initially developed as guidelines for best practice, but there is now a global movement to standardize these rules into a set of legal requirements.

The overall design of Green Architecture has been inspired by traditional architecture throughout eras. After the previous journey throughout eras to trace the innovative practices of Green Architecture, it can be concluded that:

- o The architecture history is full of evidences tracing the presence of green architecture strategies.
- o What's called a green architecture today is a natural evolution of design prototypes back to many thousands years ago.
- o Green design strategies and best practices evolve over time through documented performance and shared knowledge of lessons learned.
- o New technologies were a main reason of the regressive movement in architecture in which architects began to ignore climate issues and their effect on buildings and occupants, but in other hand, nowadays technologies assist architects in the green design process from the early concept till the execution of building on site and through its life cycle also.
- o Today, green design is becoming a natural part of an increasing number of buildings. As natural resources dwindle, green design will take a critical role in our built environment.

7. References:

1. Energy Efficient Homes, What Are Green Building Design Principles?
http://www.ehow.com/facts_5038834_green-building-design-principles.html
2. **Sustainable Build**, What is Green Architecture?
<http://www.sustainablebuild.co.uk/what-green-architecture.html>
3. **ATCA: Green Architecture, London, UK - 24th August 2009**,
<http://www.mi2g.com/>

Neolithic Architecture:

1. **Neolithic Architecture**, From Wikipedia, the free encyclopedia
http://en.wikipedia.org/wiki/Neolithic_architecture
2. **Skara Brae**, From Wikipedia, the free encyclopedia
http://en.wikipedia.org/wiki/Skara_Brae
3. **Neolithic Skara Brae Orkney**, Scotland
<http://www.scotshistoryonline.co.uk/scara.html>
4. **Skara Brae**, The buildings
<http://www.orkneyjar.com/history/skarabrae/skarabl.htm>

Sumerian Architecture:

1. **Chogha Zanbil**, Greatest Contribution in the Ancient World
http://www.iranataglance.com/historical-buildings/ziggurat_chogha_zanbil.php
2. **Chogha Zanbil**, From Wikipedia, the free encyclopedia
http://en.wikipedia.org/wiki/Chogha_Zanbil
3. **Ziggurat**, From Wikipedia, the free encyclopedia
<http://en.wikipedia.org/wiki/Ziggurat>

Egyptian Architecture:

1. **Al Dokkan**: Arts: Egyptian architecture
<http://www.aldokkan.com/art/architecture.htm>
2. **Britannica Concise Encyclopedia**: Egyptian architecture
<http://www.answers.com/topic/ancient-egyptian-architecture>
3. **Egypt Feature Story**, The Pyramid of Khufu at Giza in Egypt, an introduction by Alan Winston.
<http://www.touregypt.net/featurestories/greatpyramid1.htm>
4. **Symbolism And Coincidences Of The Great Pyramid**, Tim G. Hunkler.
http://www.hunkler.com/pyramids/pyramid_symbolism.html

Roman Architecture:

1. **Architecture of ancient Rome**, From Wikipedia, the free encyclopedia

http://en.wikipedia.org/wiki/Roman_architecture

2. **Compluvium**, Sources for the Roman House

<http://www.vroma.org/~bmcmanus/compluvium.html>

3. **History of Roman Architecture**,

<http://web.kyoto-inet.or.jp/org/orion/eng/hst/roma.html>

4. **Pantheon, Rome**, From Wikipedia, the free encyclopedia

http://en.wikipedia.org/wiki/Pantheon%2C_Rome

5. **SPQR ONLINE**, Daily Life, Roman Houses,

<http://library.thinkquest.org/26602/romanhouses.htm>

Gothic Architecture:

1. **The Art of Gothic**, Architecture, Sculpture, Art. Rolf Toman Konemann; English ed edition (February 1999)

2. **History of Western Civilization**, Gothic Cathedral, understanding the middle ages,

<http://mason.gmu.edu/~ddonald/imageassignment/cathedral>

3. **Gothic: Architecture**, Sculpture, Painting, by Rolf Toman

<http://www.librarything.com/work/99414>

4. **Gothic architecture**, From Wikipedia, the free encyclopedia

http://en.wikipedia.org/wiki/Gothic_architecture

5. **Medieval Architecture**, Medieval Gothic Cathedrals

<http://www.medieval-spell.com/Medieval-Gothic-Cathedrals.html>

Islamic Architecture:

1. **East of Amman: The Desert Castle Loop**

<http://www.kinghussein.gov.jo/tourism5.html>

2. **Qasr Kharana**, From Wikipedia, the free encyclopedia

http://en.wikipedia.org/wiki/Qasr_Kharana

3. **Qasr Kharaneh**, Jordan Desert Castles,

http://www.atlastours.net/jordan/qasr_kharaneh.html

4. **Qasr al-Kharrana**, Digital Library

http://archnet.org/library/sites/one-site.jsp?site_id=7356&order_by=dictionary_name

5. **Wind-Tower-and-Qanat-Cooling-1.jpg**, From Wikipedia, the free encyclopedia

<http://en.wikipedia.org/wiki/File:Wind-Tower-and-Qanat-Cooling-1.jpg>

Modern Architecture:

1. **Le Corbusier's Five Points of Architecture**
<http://www.geocities.com/rr17bb/LeCorbusier5.html>
2. **Modern Architecture**, From Wikipedia, the free encyclopedia.
http://en.wikipedia.org/wiki/Modern_architecture
3. **Villa Savoye, Poissy, France**, Le Corbusier and Pierre Jeanneret 1929, Galinsky
<http://www.galinsky.com/buildings/savoye/index.htm>

Organic Architecture:

1. **A Living Architecture**, Frank Lloyd Wright and Taliesin Architects, John Rattenbury,
<http://frank.lloydwright.info/architectural/taliesin-west.html>
2. **Fallingwater**, From Wikipedia, the free encyclopedia
<http://en.wikipedia.org/wiki/Fallingwater>
3. **Organic Architecture**,
<http://www.organic-architecture.com/>
4. **Organic architecture**, From Wikipedia, the free encyclopedia
http://en.wikipedia.org/wiki/Organic_architecture
5. **Wright, Frank Lloyd**, Sighted in Arizona
http://www.doney.net/aroundaz/celebrity/wright_franklloyd.htm

High Tech Architecture:

1. **Foster +Partners**
<http://www.fosterandpartners.com/>
2. **High Tech Architecture**, Colin Davies.
<http://www.crowstep.co.uk/hightecharchitec.html>
3. **High-tech architecture**, From Wikipedia, the free encyclopedia
http://en.wikipedia.org/wiki/High-tech_architecture

Deconstruction Architecture:

1. **Deconstructivism**, From Wikipedia, the free encyclopedia
<http://en.wikipedia.org/wiki/Deconstructivism>
2. **Featured in Architecture**, living green,
<http://www.artandculture.com/categories/2-architecture>
<http://www.artandculture.com/cgi-bin/WebObjects/ACLive.woa/wa/movement?id=132>

Contemporary Architecture:

1. **EpiCenter**, Artists For Humanity, the American Institute of Architects
http://www.ariatopen.org/hpb/grid2007.cfm?project_id=0§ion=11
2. **Greenbuilding**, The Blaustein International Studies
<http://www.greenbuilding.com/greenHistory.html>

المنطقة أكثر تدهوراً ، وكلما اقتربت القيمة من الصفر كانت المنطقة بها بعض التدهور، أما إذا كانت القيمة متوسطة ما بين ذلك، فهذا يعني أن المنطقة في طريقها إلى التدهور.

المراجع العربية والأجنبية:

- RehabiMed Training Course " Rehabilitation & Artisans", Cairo, Egypt. 2006
- UNDP & GOPP: "Improving living condition within informal settlements through adopting participatory planning", Ministry of Housing, Utilities and Urban Development, 2006-2007
- Hernardo De Soto: "The Other Path, The Invisible Revolution in the Third World", Harper & Row, Inc., New York, 1990
- Ivo Imparato & Jeef Ruster: " Slum Upgrading and Participation: Lessons from Latin America", The World Bank, Washington, 2003
- Azza Hussein: "The Rehabilitation of Deteriorated Residential Areas- A proposed Model", Unpublished PhD. In Architecture, Cairo University. Cairo, 1989
- David R. Anderson, Dennis J. Seweeney, and Thomas A. Williams: " An Introduction to management science, quantitative approaches to decision making", Eleventh Edition, South-Western publishers, pp727-735, 2005
- هناء الجوهري: " ثقافة التحايل- دراسة ميدانية لنماذج من التجمعات العشوائية بالقاهرة "، مركز البحوث والدراسات الاجتماعية، كلية الآداب- جامعة القاهرة ٢٠٠٤.
- مركز الدراسات التخطيطية والمعمارية بالاشتراك مع الهيئة العامة للتخطيط العمراني: "دلائل أعمال التخطيط العمراني - إعداد المخططات الإرشادية للمناطق المتخلفة بالمدن " ، القاهرة ١٩٨٨.
- رويده كامل: "الاسكان والتجديد العمراني- توفيق عمليات الارتقاء الحضري للمناطق السكنية"، رسالة دكتوراه غير منشورة، كلية الهندسة، جامعة القاهرة. القاهرة، ١٩٩٣
- حازم ابراهيم: "الارتقاء بالمناطق التاريخية"، ندوة الارتقاء بالبيئة العمرانية للمدن، القاهرة، ١٩٨٦

2.37	متوسط (مساوي للحد الأدنى للدخل)		العام	الاقتصادية
0.20	مرتفع (أكثر من الحد الأدنى للدخل)			
7.24	مرتفعة (أعلى من ٦٠% من قوة العمل)		نسبة البطالة	
2.88	متوسطة (من ٦٠% - ٢٥% من قوة العمل)			
0.27	منخفضة (أقل من ٢٥% من قوة العمل)			
3.87	مرتفعة (أعلى من ٦٠% من الأفراد)		نسبة كبار السن والأطفال	
1.36	متوسطة (من ٦٠% - ٢٥% من الأفراد)			
0.13	منخفضة (أقل من ٢٥% من الأفراد)			
4.18	لا يوجد		وجود حرف تقليدية	
1.40	يوجد وغير منتشرة			
0.00	يوجد ومنتشرة			

المرجع: بتصريف الباحثة عن حسابات استمارات الاستبيان

النتائج :

خلص البحث إلى تقديم مجموعة متكاملة من معايير قياس التدهور للمناطق السكنية، تغطي هذه المعايير البيئة العمرانية ككل، سواء الجوانب العمرانية (مباني، مرافق، خدمات، طرق) أو جوانب اقتصادية واجتماعية للسكان أو جوانب بيئية عامة للمنطقة. وقد تم تحديد الوزن النسبي المناسب لكل معيار بما يعبر عن مدى تأثيره في تدهور المنطقة. وتم وضع ذلك في استمارة مجمعة لقياس التدهور، وتتسم هذه الاستمارة بالمرونة حيث يمكن إضافة أي معايير مستقبلية يمكن أن تؤثر في تدهور المناطق السكنية، كما تتسم الاستمارة بسهولة وسرعة الاستخدام، وخاصة إذا ما تم وضعها كبرنامج للحاسب الآلي. وباستخدام هذه الاستمارة يمكن قياس مدى تدهور المنطقة السكنية، وبالتالي اختيار الأسلوب الأمثل للتدخل لتتميتها، وكلما اقتربت القيمة من النهاية العظمى للاستمارة (١٠٠%) كانت

0.11	غير كافية	رياضية		
0.00	كافية			
0.74	غير موجودة	خدمات أمنية وإدارية		
0.29	غير كافية			
0.00	كافية			
4.24	مرتفعة (أعلى من ١٥٠ فرد/فدان)		الكثافة السكانية	
1.55	متوسطة (١٥٠ فرد/فدان)			
0.17	منخفضة (أقل من ١٥٠ فرد/فدان)			
3.61	مرتفعة (أعلى من ٦٠% من الأفراد)		نسبة الأمية	
1.36	متوسطة (من ٦٠% - ٢٥% من الأفراد)			
0.16	منخفضة (أقل من ٢٥% من الأفراد)			
2.98	مرتفعة (أكثر من ٥ أفراد)		متوسط حجم الأسرة	
1.08	متوسطة (٤ - ٥ أفراد)			
0.12	منخفضة (أقل من ٤ أفراد)			
3.65	مرتفع (أكثر من ١.٥ فرد/غرفة)		معدل التراحم	الخواص الاجتماعية
1.65	متوسط (١.٥ فرد/غرفة)			
0.57	منخفض (أقل من ١.٥ فرد/غرفة)			
3.68	منتشرة (يعاني منها أكثر من ٦٥% من السكان)		الأمراض الاجتماعية	
1.22	غير منتشرة وموجودة			
0.00	غير موجودة			
3.87	المنطقة مصدر أوبئة		الأمراض العضوية	
1.59	المنطقة تتركز بها أمراض متوطنة / بيئية			
0.00	المنطقة نظيفة من الأمراض المتوطنة والأوبئة			
6.49	منخفض (أقل من الحد الأدنى للدخل)		متوسط الدخل	الخواص

0.69	إشغالات ثابتة / دائمة	إشغالات الطرق	
0.25	إشغالات متحركة / غير دائمة		
0.00	لا يوجد إشغالات		
0.76	رديئة	حالات الطرق	
0.24	متوسطة		
0.00	جيدة		
0.53	لا توجد إنارة	إنارة الطرق	
0.19	الإنارة غير كافية		
0.00	الإنارة كافية		
0.76	النقل العام لا يوجد	الوصول للمنطقة	
0.27	النقل العام غير كاف/ الاستعانة بالنقل خاص		
0.00	النقل العام كاف		
0.95	لا يمكن	وصول الطوارئ	
0.00	يمكن		
0.37	غير موجودة	خدمات دينية	
0.15	غير كافية		
0.00	كافية		
0.75	غير موجودة	خدمات تعليمية	
0.28	غير كافية		
0.00	كافية		
0.82	غير موجودة	خدمات صحية	
0.28	غير كافية		
0.00	كافية		
0.50	غير موجودة	خدمات تجارية	
0.17	غير كافية		
0.00	كافية		
0.33	غير موجودة	خدمات ترفيهية	

0.21	معظمها < ٦٥%			
0.87	لا يوجد	توصيل الكهرباء		
0.36	بعضها > ٦٥%	للوحدات السكنية		
0.10	معظمها < ٦٥%			
1.38	لا يوجد	توصيل الصرف		
0.67	بعضها > ٦٥%	الصحي للوحدات		
0.27	معظمها < ٦٥%	السكنية		
0.67	محقة في > ٢٥%	الإضاءة الطبيعية		
0.37	محقة في ٢٥% - ٦٠%	والتهوية		
0.16	محقة في < ٦٠%			
1.72	غير موجودة بالحي			
0.94	مؤقتة (فناطيل)	شبكة مياه نقية		
0.38	موضعية (صنابير عامة)			
0.00	دائمة (شبكة عامة)			
1.81	غير موجودة بالحي			
0.70	موضعي (خزانات/بيارات/شبكة خاصة)	شبكة الصرف الصحي		
0.00	دائم (شبكة عامة)			
1.20	غير موجودة بالحي		شبكات المرافق	
0.65	مؤقتة (سرقة التيار الكهربائي)			
0.25	موضعية (محطة كهرباء أو مولدات خاصة بالحي)	شبكة الكهرباء		
0.00	دائمة (شبكة شاملة)			
0.38	غير موجودة بالحي			
0.10	موجودة وغير كافية	شبكة الاتصالات		
0.00	موجودة وكافية			
0.80	غير صالحة للحركة الآلية	الصلاحية للحركة الآلية		
0.25	ممكن استخدامها للحركة الآلية		شبكات الطرق	
0.00	صالحة للحركة الآلية			

0.00	لا يوجد			
1.28	يوجد	مخلفات صلبة		
0.00	لا يوجد			
2.84	ردئية ٦٠% فأكثر من مباني المنطقة ردئية	حالات المباني		
1.14	متوسطة ٢٥% إلى ٦٠% من المباني ردئية			
0.23	جيدة ٢٥% فأقل من مباني المنطقة ردئية			
2.68	< ٦٥% من مباني المنطقة صفيح وعشش	نوع الإنشاء الغالب	المباني	العمراتية
1.56	< ٦٥% من مباني المنطقة طوب لين			
0.64	< ٦٥% من مباني المنطقة حوائط حاملة			
0.13	< ٦٥% من مباني المنطقة هيكلية			
1.27	لا يوجد	توافر الأراضي	استعمالات الأراضي	
0.00	يوجد	الفضاء		
1.81	يوجد	تواجد استعمالات		
0.00	لا يوجد	متعارضة - مقلقة - ملوثة		
0.74	لا تتوافر	توافر		
0.00	تتوافر	الاستعمالات المختلفة		
4.43	مرتفعة	الكثافة البنائية		
1.71	متوسطة			
0.35	منخفضة			
1.16	لا يوجد	توصيل المياه	الوحدات السكنية	
0.55	بعضها > ٦٥%	للوحدات السكنية		

وذلك كما هو مبين بعاليه. ويتم تكرار نفس هذا الأسلوب على باقي معايير القياس. وبناء على الشرح السابق، تكون استمارة التقييم المقترحة، وقيم معايير القياس لكل معيار منها موضحة في الجدول التالي:

جدول (٣): معايير قياس التدهور المقترحة وتقسيماتها المختلفة، ومعايير قياس كل منها

قيمة معايير القياس	معايير القياس	المعايير الثانوية	المعايير الفرعية	المعايير الرئيسية
4.89	رديء		مستوى النظافة العامة	بيئية
2.02	متوسط			
0.40	جيد			
6.23	يوجد مخاطر طبيعية		المخاطر الطبيعية	
0.00	لا يوجد مخاطر طبيعية			
4.46	لا يوجد وتلقى القمامة داخل المنطقة		أسلوب جمع القمامة	
1.27	يوجد أسلوب منتظم لجمع القمامة			
0.00	يوجد أسلوب منتظم وحديث لجمع القمامة			
0.72	يوجد	ضوضاء	تلوث بيئي ذاتي	
0.00	لا يوجد			
1.45	يوجد	غازات		
0.00	لا يوجد			
1.65	يوجد	سوائل		
0.00	لا يوجد			
1.77	يوجد	مخلفات صلبة		
0.00	لا يوجد			
0.53	يوجد	ضوضاء		تلوث بيئي خارجي
0.00	لا يوجد			
1.06	يوجد	غازات		
0.00	لا يوجد			
1.21	يوجد	سوائل		

الفرعي "مستوى النظافة العامة" معايير قياسه هي (رديء أو متوسط أو جيد)، وحيث أن الوزن النسبي لهذا المعيار الفرعي هو (4.8883505)، فيتم تقسيم هذا الوزن النسبي على معايير القياس الخاصة بالمعيار حسب قوة تأثير كل منها به، وقوة تأثير معايير القياس يمكن حسابها كنسبة مئوية من الاستبيان Questioner، وبالنسبة لهذا المثال فكانت نسب قوة التأثير لمعايير القياس كالتالي:

جدول (٢): حساب الأوزان النسبية لمعايير قياس معيار "مستوى النظافة العامة"

المعيار الفرعي	الوزن النسبي *	معايير القياس	قوة تأثير معايير القياس % *	الأوزان النسبية لمعايير القياس
مستوى النظافة العامة	4.8884	رديء	58.63636	2.8664
		متوسط	33.18182	1.6220
		جيد	8.181818	0.4000
			% 100	4.8884

* هذه البيانات تم حسابها من تحليل استمارات الاستبيان المرجع: الباحثة بناء على بيانات الاستبيان

وبعد حساب الأوزان النسبية لمعايير قياس كلاً من المعايير الفرعية والثانوية كما تم توضيحه في الجدول السابق، يتم عمل توزيع تراكمي Cumulative Distribution لهذه الأوزان النسبية لتعبر عن قيمة التدهور الصحيحة، وهذه الأرقام التراكمية هي ما سيتم إدراجه بإستمارة التدهور المقترحة، وعلى ذلك يكون:

$$\begin{aligned}
 \text{قيمة معيار القياس "جيد"} &= 0.4000 \\
 \text{قيمة معيار القياس "متوسط"} &= 0.4000 + 1.6220 = 2.0220 \\
 \text{قيمة معيار القياس "رديء"} &= 0.4000 + 1.6220 + 2.8664 = 4.8884
 \end{aligned}$$

حيث أنه في هذه الحالة (مستوى النظافة العامة) إذا كان مستوى النظافة العامة رديء (أي الأسوأ) فمن المنطقي أن يكون مقدار التأثير هو كل القيمة المخصصة لهذا المعيار (4.8884 أي 100% من القيمة)

٤/٤. تحديد الأوزان النسبية لمعايير التقييم المقترحة:

تم تحديد الأوزان النسبية للمعايير المقترحة الرئيسية والفرعية والثانوية كالتالي:
 أولاً: إيجاد المتوسطات الحسابية للأوزان المختلفة المفرغة من استمارات الاستبيان (ملحق ٢)، وطبقاً
 للمقياس الموضح فيها حيث (١) أقل تأثير على التدهور، (٥) أقصى تأثير على التدهور.
 ثانياً: استخدام طريقة Analytical Hierarchy Process (AHP) الإحصائية، والتي صممها
 العالم Thomas L. Saaty لحل multi-criteria decision problems، وتحتاج طريقة AHP
 من صانع القرار أن يعطى قيمة نسبية لكل معيار من المعايير التي تؤثر في تحديد موضوع معين،
 وهو ما تم استخدامه في هذا البحث لقياس مدى التدهور.
 وقد يتم استخدام طريقة Ratio System for Obtaining Weights للحصول على الأوزان النسبية
 لكل من العوامل الرئيسية المؤثرة في مدى التدهور، ويتم استخدام Scoring Model لتحديد الوزن
 النسبي لكل معيار باستخدام المعادلة الآتية:

$$S_j = \sum_i w_i r_{ij}$$

حيث:

$$r_{ij} = \text{القيمة لمعيار (i) وموقع (j)}$$

$$w_i = \text{الوزن النسبي لمعيار (i)}$$

$$S_j = \text{القيمة لموقع (j)}$$

وبعد تحديد الأوزان النسبية للمعايير الرئيسية، تم تحديد الوزن النسبي للأوزان الفرعية والثانوية عن
 طريق حساب المتوسطات الحسابية لكل معيار فرعي أو ثانوي، وتقسيم الوزن النسبي للمعيار
 الرئيسي عليهم حسب قيمة تأثيرهم في المعيار الرئيسي. وكانت الأوزان النسبية كما هي مبينة في
 جدول (٣).

٤/٥. الأوزان النسبية لمعايير قياس التدهور:

كل معيار من المعايير السابقة لها معايير تقاس بها، يمكن تسميتها بمعايير القياس، ويتم حساب
 الأوزان النسبية لمعايير القياس بناء على قيمة المعيار الفرعي أو الثانوي الذي يقاسه، فمثلاً المعيار

وقد قامت الباحثة بزيارة الهيئات الحكومية والخاصة المهتمة بالتعامل مع المناطق المتدهورة، مثل هيئة التخطيط العمراني، صندوق تطوير العشوائيات، المعونة الألمانية بالقاهرة GTZ، إدارة تطوير العشوائيات في محافظتي القاهرة والجيزة، حي بولاق الدكرور، حي منشأة ناصر، مكتب ARCHPLAN، مكتب ADAPT، كلية الهندسة جامعة القاهرة، كلية الهندسة جامعة عين شمس، المركز القومي لبحوث الإسكان والبناء، وبعض الجمعيات الأهلية NGOs، ومجموعة من المهندسين العاملين بمشاريع التطوير والارتقاء العمراني بالقاهرة والجيزة.

٢/٢/٤. أساليب تجميع البيانات:

وقد تم إجراء الاستبيان عن طريق المقابلات الشخصية أو المراسلات بالبريد الإلكتروني. ومن خلال اللقاء مع الخبراء في مجال التعامل مع المناطق المتدهورة تم:

- شرح سريع لفكرة البحث وترتيب المعايير وكيفية الإجابة عن الأسئلة.
- قراءة أسئلة الاستمارة والإجابة عن أي استفسار، وقد تم الحصول على الإجابات مباشرة في بعض اللقاءات، وفي البعض الآخر تم تحديد موعد تالي لاستلام الرد.

٣/٢/٤. تفرغ بيانات الاستبيان:

تم تفرغ بيانات الاستبيان على الحاسب الآلي باستخدام برنامج Excel، وتم حساب الأوزان النسبية لكل معيار من المعايير الرئيسية والفرعية والثانوية ثم التفصيلية.

٣/٤. معايير قياس التدهور المقترحة:

تتكون مجموعة المعايير الرئيسية من معايير فرعية وتقسم أكثر تفصيلاً إلى معايير ثانوية ثم معايير تفصيلية في المستوى الرابع للتقسيم، وذلك للمعايير التي تحتاج إلى مزيد من التفصيل. ومثل هذه الحالة التي يوجد بها معايير ومستويات متعددة تعرف بـ Multi-criteria decision problems، وذلك لضمان قياس كل جوانب التدهور في المنطقة محل الدراسة على قدر الإمكان، وأيضاً لتحويل المعايير النوعية إلى معايير كمية يمكن قياسها. ويمكن تعديل أو إضافة أي معايير جديدة مستقبلاً لهذه المجموعة من المعايير بشرط أن يدرج معها مقياس التدهور الخاص بها Scale، وأن يتم تحويلها إلى معايير كمية حتى يمكن قياسها.

وبدراسة هذه الاستمارة وجد أنها لا تغطي كل جوانب التدهور التي يمكن قياسها في البيئة العمرانية المبنية أو غير المبنية سواء كانت عمرانية أو اجتماعية أو اقتصادية. كما أنها تغفل الجوانب الأمنية والمتعلقة بسلامة المنطقة في المقام الأول، مثال على ذلك منطقة الدويقة والتي أدى انهيار صخرة كبيرة من المقطم عليها إلى كارثة كبرى والمئات من الضحايا.

٤. خطوات إعداد استمارة تقييم متكاملة للمناطق المتدهورة:

١/٤. تجميع معايير التدهور المقترحة

ولإكمال معايير التدهور السابقة والوصول إلى استمارة تقييم متكاملة، فقد قامت الباحثة بتجميع كافة المعايير المتوقع تأثيرها في تدهور البيئة العمرانية وغير العمرانية في المناطق السكنية، وقد تم الخروج بمجموعة من المعايير وتكوين استمارة جديدة متكاملة.

٢/٤. إجراء الاستبيان

ولإختبار هذه المجموعة من معايير التدهور تم عمل إستبيان للرأي Questionnaire لعينة من الخبراء والمتخصصين في مجال التعامل مع المناطق العمرانية المتدهورة وتميبتها في مصر. وقد تم إختيار استمارة الاستبيان مبدئياً بعدة زيارات للخبراء، ثم تم تعديلها وتطويرها حسب الملاحظات المعطاه لنصل إلى استمارة الاستبيان النهائية.

وقد حقق الاستبيان ومناقشة الخبراء هدفاً أساسيان:

الهدف الأول: إختيار معايير التدهور المقترحة، ومعرفة أوجه القصور بها وإكمالها، وكذلك إضافة أي معايير مقترحة من الخبراء، ثم تعديل الاستمارة مرة أخرى للوصول إلى مجموعة متكاملة من معايير التدهور.

الهدف الثاني: وضع أوزان نسبية مناسبة لكل معيار تدهور، حيث يعبر هذا الوزن النسبي عن أهمية تأثير كل معيار على تدهور البيئة العمرانية وغير العمرانية. ويتم وضع هذه الأوزان النسبية من قبل القائمين بعملية الاستبيان.

١/٢/٤. معايير إختيار عينة الدراسة:

تم وضع المعايير التالية لإختيار عينة الدراسة:

الخبرة - الاستعداد لإجراء التقييم - المقدرة على تحديد قيم المعايير

	٠	غير موجودة	خدمات تعليمية	
	١	غير كافية		
	٢	كافية		
	٠	غير موجودة		خدمات صحية
	١	غير كافية		
	٢	كافية		
	٠	غير موجودة	خدمات ترفيهية ورياضية	
	١	غير كافية		
	٢	كافية		
	٠	غير موجودة	خدمات أمنية وإدارية	
	١	غير كافية		
	٢	كافية		
	٠	مرتفعة (أعلى من ١٥٠ فرد/فدان)	الكثافة السكانية	
	١	متوسطة (١٥٠ فرد/فدان)		
	٢	منخفضة (أقل من ١٥٠ فرد/فدان)		
	٠	منخفض (أقل من الحد الأدنى للدخل)	متوسط الدخل العام	
	١	متوسط (مساوي الحد الأدنى للدخل)		
	٢	مرتفع (أكثر من الحد الأدنى للدخل)		
	٠	منتشرة	الأمراض الاجتماعية	
	١	غير منتشرة وموجودة		
	٢	غير موجودة		
	٠	المنطقة مصدر أوبئة	الأمراض العضوية	
	١	المنطقة تتركز بها أمراض متوطنة / بيئية		
	٢	المنطقة نظيفة من الأمراض المتوطنة والأوبئة		
	٦٣	إجمالي نقاط التقييم		

٨. صفات الاجتماعية

المرجع: مركز الدراسات التخطيطية والمعمارية بالاشتراك مع الهيئة العامة للتخطيط العمراني: "دلائل أعمال التخطيط العمراني - إعداد المخططات الإرشادية للمناطق المتخلفة بالمدن"، القاهرة ١٩٨٨.

٤. شبكات المرافق العامة	شبكة مياه نقية	غير موجودة بالحي	٠
		مؤقتة (فناطيس)	١
		موضعية (صنابير عامة)	٢
شبكة الصرف الصحي	دائم	غير موجودة بالحي	٠
		موضعي (خزانات/بيارات/شبكة خاصة)	٢
		(شبكة عامة)	٢
شبكة الكهرباء	دائمة (شبكة شاملة)	غير موجودة بالحي	٠
		مؤقتة (سرقة التيار الكهربائي)	١
		موضعية (محطة كهرباء أو مولدات خاصة بالحي)	٢
٥. شبكات الطرق	الصالحة للحركة الآلية	غير صالحة للحركة الآلية	٠
		يمكن استخدامها للحركة الآلية	١
		صالحة للحركة الآلية	٢
	إشغالات الطرق	إشغالات ثابتة / دائمة	٠
		إشغالات متحركة / غير دائمة	١
		لا يوجد إشغالات	٢
	حالات الطرق	رديئة	٠
		متوسطة	١
		جيدة	٢
	الإضاءة	لا يوجد إنارة	٠
الإضاءة غير كافية		١	
الإضاءة كافية		٢	
٦. النقل العام	النقل العام لا يوجد	٠	
	النقل العام غير كاف/ الاستعانة بالنقل خاص	١	
	النقل العام كاف	٢	
٧. الخدمات الدينية	غير موجودة	٠	
	غير كافية	١	
	كافية	٢	

	٠	أرض فضاء ملك الدولة- موضوع عليها اليد	أراضي فضاء	٢. البيئة العامة
	١	أرض فضاء ملك الدولة- حكر		
	٢	أرض فضاء ملك الدولة- ملكية عامة		
	٣	أرض فضاء ملك الأفراد- ملكية خاصة	مستوى النظافة العامة	
	٠	ردي		
	١	متوسط		
	٢	جيد	أسلوب جمع القمامة	
	٠	لا يوجد وتلقى القمامة داخل المنطقة		
	١	يوجد أسلوب منتظم لجمع القمامة		
	٢	يوجد أسلوب منتظم وحديث لجمع القمامة	تلوث بيئي ذاتي	
	٠	يوجد ضوضاء		
	٢	لا يوجد		
	٠	يوجد غازات		
	٢	لا يوجد		
	٠	يوجد سوائل		
	٢	لا يوجد		
	٠	يوجد مخلفات		
	٢	لا يوجد		
	٠	يوجد ضوضاء		
	١	لا يوجد		
	٠	يوجد غازات		
	١	لا يوجد		
	٠	يوجد سوائل		
	١	لا يوجد		
	٠	يوجد مخلفات		
	١	لا يوجد		
	٠	رديئة ٦٠% فأكثر من مباني المنطقة رديئة	٢. الحالة العامة للمباني	
	١	متوسطة ٢٥% إلى ٦٠% من المباني رديئة		
	٢	جيدة ٢٥% فأقل من مباني المنطقة رديئة		

ويتم استخدام هذه الاستمارة بهدف تحديد درجة تدهور هذه المنطقة، وبالتالي ترتيب أولويات التدخل مع المناطق المتدهورة على مستوى المدينة، وتحديد أسلوب التدخل (الأفضل) لكل منطقة حسب درجة تدهورها ونوعيتها.

ولتحديد مدى التدهور، يتم اختيار احد الخيارات المقابلة لكل معيار تدهور، كما هو مبين في الاستمارة، وفي النهاية يتم جمع القيم المقابلة لهذه الاختيارات، لتعطي قيمة من (٦٣ نقطة) وهي إجمالي النقاط للإستمارة ككل. وكلما اقترب القيمة من الصفر كانت المنطقة أكثر تدهوراً، وكلما اقتربت من القيمة العظمى (٦٣ نقطة) كانت المنطقة أقل تدهوراً أو غير متدهورة حسب القيمة. هذه الطريقة في حساب قيمة المعايير تعتبر غير صحيحة بدرجة كافية، حيث أن الاستمارة أغفلت الأوزان النسبية لكل معيار. فلا يمكن حساب قيمة معيار "مستوى النظافة العامة" أو "إنارة الشوارع" مثل معيار "الحالة العامة للمباني" من حيث مجموع النقاط، حيث أنه لكل معيار قيمته النسبية وتأثيره على تدهور المنطقة، وهناك معايير شديدة الخطورة ولا يمكن إغفالها مثل نقص الخدمات الأساسية كالتعليم والصحة والأمن، ولكننا يمكن أن نعتبر المنطقة أقل تدهوراً لو افتقدت معايير أخرى أقل خطورة على السكان والبيئة العامة مثل افتقار المنطقة للخدمات الترفيهية والرياضية مثلاً.

ونلاحظ في هذه الاستمارة أنها تعرض بعض عوامل التدهور للمناطق السكنية، والتي حددتها هيئة التخطيط العمراني بناء على قانون التخطيط العمراني، تقسم هذه العوامل إلى مجموعات كالتالي:

(ملكية الأراضي - البيئة العامة - الحالة العامة للمباني - شبكات المرافق العامة - شبكات الطرق - الوصول الى الحي - الخدمات - الصنفات الاجتماعية). وهذه ليست كل جوانب التدهور في البيئة العمرانية وغير العمرانية، فهي تغفل الجوانب التنظيمية والإدارية للمنطقة وكذلك لم تذكر الجوانب الاقتصادية للسكان، والتي تعتبر جانب مهم في عمليات التنمية.

جدول (١): استمارة تقييم عناصر الحي - هيئة التخطيط العمراني -

ملاحظات	نقاط التقييم	رقم	نوع
	أرض غير مملوكة للبياني - بناء غير قانوني	٠	أراضي مبنية ملكية
	أرض مملوكة للبياني - بناء غير قانوني	١	
	تقسيم مرخص - بناء غير قانوني	٢	
	تقسيم مرخص - بناء قانوني	٣	

٢/٢. معايير الحكم على النواحي الاجتماعية:

- الخصائص الاجتماعية للسكان:
- توزيع السكان من حيث العمر والنوع.
- حجم الأسرة، ونوعية تركيبها (نسبة الأسر بدون أولاد ونسبة الأسر نوى الأولاد).
- نسبة التعليم من حيث النوع والعمر (نسبة نوعية التعليم عام - فنى -عالى) ونسبة الأمية بين السكان.
- معدلات الجرائم الاجتماعية والمشاجرات.
- نسبة كبار السن وصغار السن (الفئة غير النشطة).
- نسبة السكان من حيث نوع العمل (حرفيين / مهنيين / موظفين).

٣/٢. معايير الحكم على النواحي الاقتصادية:

- معايير على مستوى المنطقة ككل:
- نوعية النشاط الاقتصادي السائد بالمنطقة.
- وجود حرف تقليدية أم لا.
- معايير على مستوى الأفراد:
- متوسط دخل الأسرة ومتوسط دخل الفرد ونسبة العائلات (بالنسبة لمستوى الدخل).
- نسبة معدل البطالة بين السكان.
- نسبة العاملين في نفس المنطقة وخارجها (بالنسبة للعمل).

٣. كيفية تحديد مدى التدهور:

يتم تحديد مدى تدهور المناطق العمرانية حالياً عن طريق "استمارة تقييم مدى التدهور" المعمول بها في هيئة التخطيط العمراني. ويوضحها جدول (١). وهي عبارة عن استمارة تضم معايير التدهور السابق ذكرها، ويتم إعطاء أوزان نسبية لكل المتغيرات في الاستمارة، بحيث يأخذ المتغير الذي يشير إلى تدهور أكثر درجات منخفضة، مع مراعاة تحويل كل المتغيرات النوعية إلى مؤشرات كمية للتدهور يمكن قياسها.

٢. معايير تقييم درجة تدهور منطقة عمرانية:

تستخدم هذه المعايير للحكم على منطقة سكنية بأنها متدهورة أم لا، أو الحكم على مدى تدهور منطقة ما. وتشمل هذه المعايير العديد من الجوانب. ويمكن إيجاز أهم المعايير فيما يلي:

١/٢. معايير للحكم على البيئة العمرانية:

أ- استعمالات الأراضي : وتشمل على معايير للحكم على:

- مدى توافق الاستعمالات المختلفة ومدى وجود استعمالات متعارضة ومقلقة للراحة وملوثة ونسبة الاستعمالات غير السكنية إلى السكنية.
- مدى كفاءة الخدمات الأساسية بالمنطقة من حيث الكم والتوزيع وتشمل (خدمات تعليمية- صحية- إدارية- تجارية- أمنية) ومدى كفايتها وتوائمها مع حجم السكان وإمكانية الوصول إليها.

- مدى كفاية المرافق الأساسية وصلاحيتها وجودها من عدمه وتشمل (نظام التغذية بالمياه النقية للشرب ونظام الصرف الصحي والكهرباء والشوارع والممرات والرصف)
- نسبة الاستعمالات الترفيهية والمناطق المفتوحة.

ب- المباني السكنية: وتشمل على معايير لكل من:

- إمكانية الوصول للمباني السكنية (وصول سيارات الإسعاف والحريق وغيرها)
- توصيل المرافق للمباني والوحدات السكنية.
- الإضاءة الطبيعية والتهوية للمباني والوحدات السكنية المختلفة.
- درجة التزامم بالوحدات السكنية (فرد / غرفة) وعدد الأفراد للوحدة السكنية (فرد/وحدة).
- نسبة الوحدات المؤجرة إلى التملك.
- قيمة الوحدات السكنية القائمة بالمنطقة (تقدير ثمن الوحدة السكنية).
- الكثافة البنائية والكثافة السكانية بنسبة الإشغال والحالة الإنشائية للمباني بالمنطقة.

ج- النقل والمرور:

مثل: درجة رصف الطرق وتمهيدها- توافر وسائل النقل للمنطقة- المرور العابر ونسبته.

د- البيئة العامة المحيطة:

- نسبة التلوث بالمنطقة (التلوث الهوائي والضوضاء والأدخنة).
- النظافة بالشوارع ونسبة تراكم القمامة بالطرق.

ومن خلال المخططات الإرشادية في المدن الصغيرة يتم التعامل مع أبرز المشاكل الملحة بها، ومناطق ضغط السكان، ومشاكل المناطق المتدهورة بها.

لذا فالمخطط الإرشادي لمدينة يحمل في طياته عناصر المخطط الإرشادي للمناطق المتدهورة (المتخلفة)، ويقوم بالرد على متطلباته. والمخطط الإرشادي للمدن يظهر بحالتين:

أ. مكتمل العناصر: فبالتالي ليس هناك ضرورة لإعداد مخطط إرشادي للمناطق المتدهورة. ويكتفي بإصدار قرار من المحافظ المختص ببيان الأحياء والمناطق المراد إزالتها أو تحسينها أو أي سياسة أخرى. مع تحديد أولويات إعداد المشروعات لهذه المناطق والأحياء وإيقاف إصدار التراخيص لها.

ب. غير مكتمل العناصر: وذلك لحدوث متغيرات بعد إعداد المخطط الإرشادي للمدينة، فيتم عمل دراسات عاجلة تغطي قصور البيانات في إطار تجديد بيانات المخطط الإرشادي. ثم يعد مخطط عاجل يبين مواقع المناطق المتدهورة ودرجة تدهورها والسياسات المختلفة للتعامل معها، وأولويات العمل بها. ثم يتم إصدار قرار من المحافظ المختص ببيان الأحياء والمناطق المتدهورة وأسلوب التعامل معها وأولوياتها وإيقاف إصدار تراخيص بها.

٣/١. حالة عدم وجود مخطط عام أو إرشادي للمدينة:

في حالة عدم وجود مخطط عام أو إرشادي للمدينة، يتم إعداد مخطط إرشادي للمناطق المتدهورة، لحل المشاكل العاجلة بهذه المناطق ومناطق ضغط السكان، وذلك على أساس أن يتم إعداد مخطط سريع وعاجل وليس بالأسلوب التقليدي، بغرض تقديم حلول للمشاكل العاجلة بالمناطق المتدهورة دون عمل دراسات مستفيضة تستغرق الكثير من الوقت والجهد والمال. والمخطط الإرشادي للمناطق المتدهورة هو مخطط نوعي، وليس بديلاً للمخطط العام أو الإرشادي للمدينة.

والغرض من إعداد المخطط الإرشادي للمناطق المتدهورة (المتخلفة) هو الإجابة على الأسئلة الآتية:

١. أين توجد الأحياء أو المناطق المتدهورة؟
٢. ما هي مظاهر تخلف كل حي أو منطقة؟
٣. ما هي أولويات العمل بين الأحياء أو المناطق؟
٤. ما هي أساليب التعامل مع كل حي أو منطقة؟

١ . كيفية تحديد المناطق المتدهورة:

حتى يتم تحديد مدى تدهور منطقة حضرية معينة، يجب أولاً تحديد هذه المناطق في المدينة، ويتم تحديد المناطق المتدهورة في المدينة عن طريق إعداد المخطط الإرشادي للأحياء والمناطق المتدهورة (المتخلفة) وحالات إعداده هي:

١/١ . حالة وجود مخطط عام للمدينة:

يمثل المخطط العام للمدينة سياسات بعيدة المدى تقوم على دراسات مستفيضة، ومن المفترض أن يحتوي المخطط العام في طياته على المخطط الإرشادي للمناطق المتدهورة (المتخلفة) بالمدينة. ويتم التعامل مع المناطق المتدهورة كمواقع عمل تفصيلية دون ظهور الحاجة لإعداد المخطط الإرشادي الخاص بالمناطق المتدهورة. والمفروض أن المخطط العام يقوم بأعمال تجديد مستمرة لبياناته كجزء من العملية التخطيطية. ويوجد هذا المخطط في حالتين:

أ. مكتمل العناصر: تكون أعمال المخطط الإرشادي للمناطق المتدهورة (المتخلفة) ضمناً من أعمال المخطط المعتمد ويكتفي بإصدار قرار من المحافظ المختص ببيان الأحياء والمناطق المراد إزالتها أو تحسينها أو أي سياسة أخرى لها. مع تحديد أولويات إعداد المشروعات لهذه المناطق والأحياء وإيقاف إصدار تراخيص لها.

ب. غير مكتمل العناصر: نتيجة لحدوث متغيرات بعد إعداد المخطط العام ولم يتم تجديدها في المخطط. فيتم عمل دراسات عاجلة تغطي هذا النقص، وبعد مخطط عاجل يبين مواقع المناطق المتدهورة ودرجة تخلفها وسياسات التعامل معها من إزالة، تحسين، إرتقاء .. وأولويات العمل بها. ثم يتم إصدار قرار من المحافظ المختص ببيان الأحياء المتدهورة وأسلوب التعامل معها أو دراستها مع إيقاف إصدار تراخيص لها.

٢/١ . حالة وجود مخطط إرشادي للمدينة:

يمثل المخطط الإرشادي للمدينة نوع من المخططات العاجلة، لنتمكن المحليات من توجيه أعمال التنمية العمرانية للمدن وحل مشاكلها العاجلة دون الانتظار لحين إعداد دراسات المخطط العام. وتعتبر إعداد المخطط الإرشادي للمدينة أكثر مناسبة لظروف بلادنا من إعداد مخطط عام لها. ويلائم المخطط الإرشادي المدن الصغيرة بالمحافظات أكثر من عواصم المحافظات والتي تعد لها مخططات عامة أو يوجد لها أصلاً.

نحو إعداد منظومة متكاملة لمعايير قياس التدهور في المناطق والأحياء السكنية

* هايدي أحمد شلبي

مدرس مساعد بقسم الهندسة المعمارية- كلية الهندسة- جامعة الزقازيق

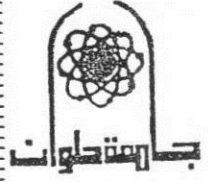
المقدمة:

تعتبر ظاهرة التدهور العمراني للبيئة السكنية القائمة هي إحدى سمات مشكلة الإسكان في الوضع الراهن، وبالرغم من اختلاف وتعدد صور ونماذج هذه المناطق السكنية المتدهورة إلا أنها جميعاً تشترك وتتشابه بدرجة كبيرة في مشكلاتها وملامحها وأسباب تدهورها، لذلك فإن استراتيجيات وسياسات التعامل مع هذه المناطق تتجاوز عن هذا الاختلاف وغالباً ما تطبق عليها نفس الأهداف، ويكون الغرض هو التحسين والارتقاء بالجوانب العمرانية (المبنى/ المسكن ومحيطه المباشر) وبالجوانب غير العمرانية (الاجتماعية والثقافية- الاقتصادية والتمويلية- الإدارية والتنظيمية). ويتناول هذا البحث كيفية تحديد المناطق المتدهورة في المدينة، ومعايير التدهور المعمول بها لتحديد مدى تدهور هذه المنطقة، وما إذا كانت متدهورة أم لا؟

المشكلة البحثية:

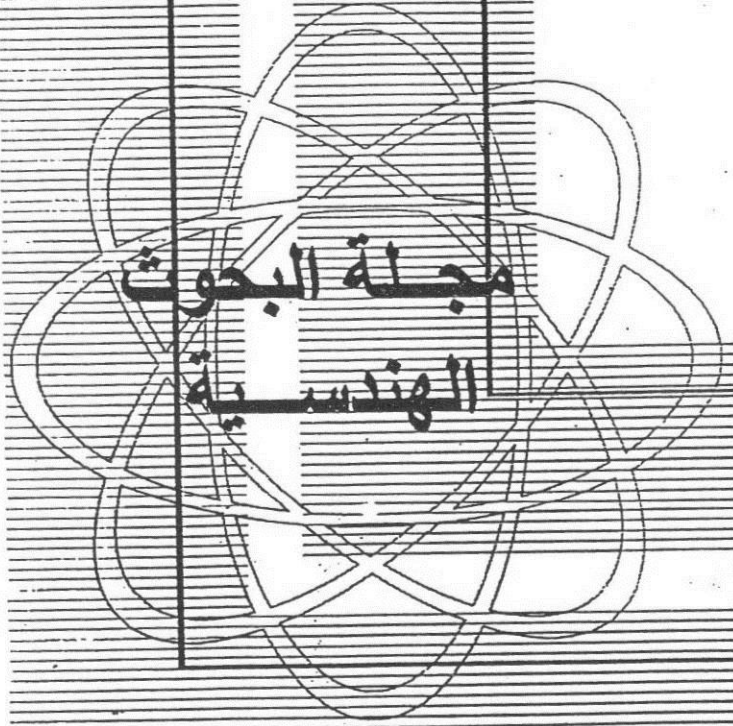
عدم وجود معايير متكاملة للحكم على مدى تدهور المناطق السكنية، وبالتالي صعوبة اتخاذ القرار المناسب في التعامل مع المناطق المتدهورة بصفة خاصة، بل توجد مجموعة غير متكاملة من المعايير ذات أوزان نسبية غير معبرة عن القيمة الحقيقية لكل معيار، مما يؤدي إلى نتائج غير صحيحة وغير واقعية لمدى تدهور منطقة الدراسة.





جامعة أسيوط

جامعة حلوان
كلية الهندسة
المطرية - القاهرة



مجلة البحوث
الهندسية

(ISSN 1110-5615)

سبتمبر ٢٠٠٩

مجلة ١٢٣